University of Sussex

Neuronal oscillations, information dynamics, and behaviour

an Evolutionary Robotics study

Renan Cipriano Moioli

Submitted for the degree of Doctor of Philosophy

University of Sussex

January 2013

Declaration

I hereby declare that this thesis has not been and will not be submitted in whole or in part to another University for the award of any other degree.

Signature:

Renan Cipriano Moioli

Preface

The work reported in this thesis, including the experiments, analyses, and discussions are my own and have been carried out during my doctoral studies. Some of the material have been published before the submission of this thesis in peer-reviewed conference proceedings and in an international journal. Work relating to Chapter 4 appeared in Moioli et al. (2010b), Moioli et al. (2010a), and Moioli et al. (2012). Results from Chapter 5 are in an article currently under review; the genetic algorithm and the adaptations to the simulator used in that chapter have been extended from Moioli et al. (2009).

For convenience, the publications are listed below:

- Moioli, R.C., Husbands, P. (in press) "Neuronal Assembly Dynamics in Supervised and Unsupervised Learning Scenarios." Neural Computation
- Moioli, R. C., Vargas, P. A. and Husbands, P. (2012). "Synchronisation effects on the behavioural performance and information dynamics of a simulated minimally cognitive robotic agent." Biological Cybernetics, 106, 407-427
- Moioli, R. C., Vargas, P. A. and Husbands, P. (2010). "The dynamics of a neural network of coupled phase oscillators with synaptic plasticity controlling a minimally cognitive agent." In: Diamantaras, K., Duch, W. and Iliadis, L.. (Org.). ICANN'10 Proceedings of the 20th international conference on artificial neural networks: Part II. 1ed.: Springer Berlin Heidelberg, 6353, 245-25
- Moioli, R. C., Vargas, P. A. and Husbands, P. (2010). "Exploring the Kuramoto model of coupled oscillators in minimally cognitive evolutionary robotics tasks." In: 2010 IEEE Congress on Evolutionary Computation (CEC), Barcelona, 2483-2490
- Moioli, R. C., Vargas, P. A. and Husbands, P. (2009). "A multiple hormone approach to the homeostatic control of conflicting behaviours in an autonomous mobile robot." In: 2009 IEEE Congress on Evolutionary Computation (CEC), Trondheim, 47-54

UNIVERSITY OF SUSSEX

RENAN CIPRIANO MOIOLI, DOCTOR OF PHILOSOPHY

NEURONAL OSCILLATIONS, INFORMATION DYNAMICS, AND BEHAVIOUR AN EVOLUTIONARY ROBOTICS STUDY

SUMMARY

Oscillatory neural activity is closely related to cognition and behaviour, with synchronisation mechanisms playing a key role in the integration and functional organization of different cortical areas. Nevertheless, its informational content and relationship with behaviour - and hence cognition - are still to be fully understood.

This thesis is concerned with better understanding the role of neuronal oscillations and information dynamics towards the generation of embodied cognitive behaviours and with investigating the efficacy of such systems as practical robot controllers. To this end, we develop a novel model based on the Kuramoto model of coupled phase oscillators and perform three minimally cognitive evolutionary robotics experiments. The analyses focus both on a behavioural level description, investigating the robot's trajectories, and on a mechanism level description, exploring the variables' dynamics and the information transfer properties within and between the agent's body and the environment.

The first experiment demonstrates that in an active categorical perception task under normal and inverted vision, networks with a definite, but not too strong, propensity for synchronisation are more able to reconfigure, to organise themselves functionally, and to adapt to different behavioural conditions. The second experiment relates assembly constitution and phase reorganisation dynamics to performance in supervised and unsupervised learning tasks. We demonstrate that assembly dynamics facilitate the evolutionary process, can account for varying degrees of stimuli modulation of the sensorimotor interactions, and can contribute to solving different tasks leaving aside other plasticity mechanisms. The third experiment explores an associative learning task considering a more realistic connectivity pattern between neurons. We demonstrate that networks with travelling waves as a default solution perform poorly compared to networks that are normally synchronised in the absence of stimuli.

Overall, this thesis shows that neural synchronisation dynamics, when suitably flexible and reconfigurable, produce an asymmetric flow of information and can generate minimally cognitive embodied behaviours.

Acknowledgements

First and foremost, I would like to express my deepest gratitude to my supervisor, Prof. Phil Husbands, for his attention, guidance, and patience during these years. His enthusiasm and inspiring discussions kept me going. Thank you, Phil, this work wouldn't have been possible without your encouragement and constant support.

Special thanks to Dr. Andy Philippides and Dr. Thomas Nowotny for participating in my annual review committees, providing me critical comments and fruitful discussions. Also, I would like to thank Dr. Patricia Vargas for all the opportunities, the constant support, and attention since I was an undergrad student. Additionally, thanks to the University of Sussex and its staff for creating a great environment for learning and working. To Dr. De Bourcier, my sincere gratitude. His generosity made the conclusion of this work possible.

Many thanks to all my colleagues at the CCNR. The conversations, critical comments, laughs, walks in the mud, and French mazurka lessons were of immense pleasure. Thanks also to Fabio Ticconi for helping me with the Evorobot simulator. Thank you all.

I must thank all my colleagues and friends from Brighton and around the world, truly special people. In particular, I would like to thank my housemates along these years, for their patience and friendship; my overseas family at the Mediterranean house, Pedro, Giulio, Joao, Dani, and Eva, and the regular aggregates, in particular Caetano and Ana, for their invaluable company, for tolerating my intermittent stubborn behaviour but unconditionally staying by my side in moments of trouble or fun; the colleagues from Friday football, the most expected moment of the week; Andrea and everyone at the Health Centre; and the colleagues at St. Johns college. All the unlisted friends, I don't need to name you - you surely know how much I appreciate your company and how important you are to me.

To Isabela, thank you for the unlimited patience, love, and support during amazing and difficult times. Being far from you was tough, but now it's time for the next adventure, *together*.

I dedicate this thesis to my family, especially my father Valdir, my mother Iracelis, my brother Bruno, and my grandmother Edna. England is far, but I have always felt you were next to me. Your love and support have been fundamental through all my life, thank you.

Contents

List of Tables

List of Figures

Chapter 1

Introduction

The objective of this thesis is to further understand the relationship between neuronal synchronisation, information dynamics, and behaviour. To this end, we develop a novel model based on the Kuramoto model of coupled phase oscillators and perform three minimally cognitive evolutionary robotics experiments. The analyses focus both on a behavioural level description, investigating the robot's trajectories, and on a mechanism level description, exploring the variables' dynamics and the information transfer properties within and between the agent's body and the environment. This chapter presents the motivation behind this work. It starts with a general description of oscillations and synchronisation, moving on to neuronal oscillations, neuronal synchronisation, and their relationship with cognition and behaviour; finally, we stress the relevance of embodiment and robotics in cognitive science and neuroscience. The chapter closes with an overview of the thesis and a summary of its main contributions.

1.1 Oscillations and synchronisation

Oscillatory phenomena are abundant in nature: the sun rises and sets, tides rise and fall, people sleep and awake, a child's heart and breath accelerate whilst on a playground swing, a musician is greeted with applauses as he hits the final chord in his guitar, powered by alternating current generated thousands of kilometers away. From engineering to social behaviour, they all refer to the same property: a repeating pattern in space or time.

Oscillations have been formally studied since at least the 1650s when Christiaan Huygens invented the pendulum clock ((Huygens, 1673), quoted in Pikovsky et al. (2001)), leading to his analysis of pendulum motion and his later development of the wave theory of light (Figure 1.1). Since then it has been noticed that many events in nature can be understood in terms of their

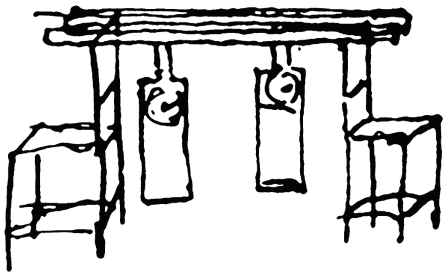

Figure 1.1: Original drawing of Christiaan Huygens showing his experiment with two pendulum clocks fastened to a common beam.

oscillatory properties, with examples ranging from firefly blinking patterns (Ermentrout, 1991) to the synchronisation of multiple laser beams (Hoppensteadt & Izhikevich, 2000).

In mathematical terms, an oscillation can be described in terms of its amplitude, period, and phase. For simplicity, consider a pendulum (Figure 1.2(a)). After an initial displacement (initial phase θ_0), the pendulum displays a periodic oscillation with amplitude A. The time required for a complete oscillation is termed period (T) and the frequency f_0 of oscillation is defined by the relationship $f_0 = 1/T$ (number of complete oscillations per unit of time). This relationship can be represented by the wave in Figure 1.2(b), which illustrates how the angle α of oscillation with respect to the vertical varies in time with period T, amplitude A, and initial phase θ_0. An alternative representation is portrayed by the phase-plane (Figure 1.2(c)), in which the behaviour of the pendulum is described by the time evolution of two given variables, e.g. the angle α of oscillation and the angular velocity ω. The motion of the pendulum is thus

$$\alpha(t) = Asin(\omega_0 t + \theta_0) \tag{1.1}$$

where ω_0 is the angular frequency given by $\omega_0 = 2\pi/T$.

The quantity $\theta(t) = \omega_0 t + \theta_0$ is named **phase** (see Figure 1.2(c)) and is of central importance to this thesis, as will become clear. Notice that the phase monotonically increases by 2π within every oscillatory cycle, but two phases that differ by 2π correspond to the same physical state; importantly, knowing the phase allows one to unambiguously determine the state of the system.

In his experiments with two pendulum clocks placed on a common support (Figure 1.1), Huygens observed that the motion of both pendula, even when momentaneously disturbed, were eventually in agreement. He concluded that this was due to the nearly imperceptible motion of the beam; in other words, he understood that the two physical systems had their rhythms mutually synchronised due to the weak interaction mediated by the common beam.

With the definition of phase given in the previous paragraph, one can classify the behaviour of the two pendula in the following ways: if they move in the same direction and have nearly

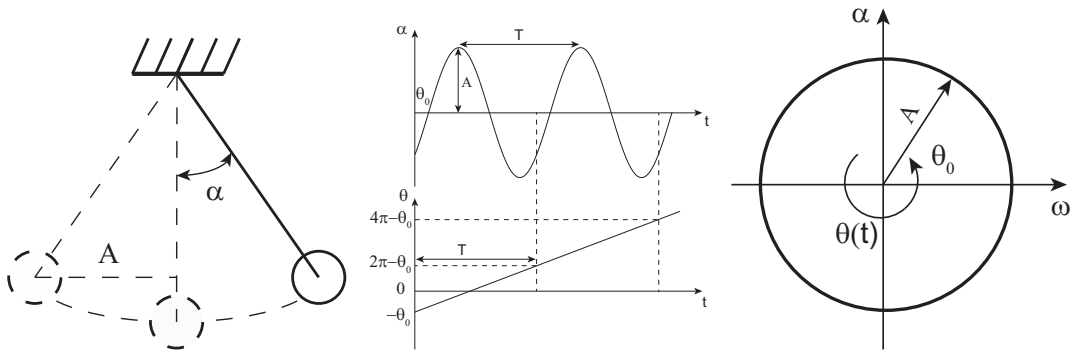

(a) (b) (c)

Figure 1.2: (a) Example of a pendulum's periodic oscillatory behaviour with amplitude A and angle α with respect to the vertical. (b) The angle α varies in time with period T and initial phase θ_0. The bottom plot shows the 2π phase increase at every period. (c) Alternative representation of the pendulum's behaviour (phase-plane), shown as a function of α and the angular velocity ω. Within every oscillatory cycle, the phase $\theta(t)$ monotonically increases by 2π.

the same position at the same time (and hence their phases are almost the same), the two pendula are synchronised in-phase; if by any reason one of the pendula is a bit advanced in relation to the other, we say that there is a phase shift between the two; finally, if they are synchronised but move in different directions, we say that they are in anti-phase. In this sense, synchronisation can be defined as "an adjustment of rhythms of oscillating objects due to their weak interaction" (Pikovsky et al., 2001). Although apparently simple, it is important to stress that synchronisation is a complex dynamical process, and for it to occur the elements of the system have to be weakly coupled and display, autonomously, self-sustained oscillations.

There is a myriad of self-sustained oscillatory systems (the pendulum clock is one example) in nature (Winfree, 1980; Glass & Mackey, 1988). Two subclasses, the harmonic oscillators (Halliday et al., 2004) and the relaxation (*integrate-and-fire*) oscillators (van der Pol, 1926), display features observed in brain dynamics (Winfree, 1980; Glass, 2001). Therefore, following the birth of modern neuroscience at the turn of the last century, it wasn't long before researchers started looking at neuronal dynamics from an oscillatory perspective (Lapicque, 1907; Berger, 1929).

In the next section, we describe how the study of oscillations, synchronisation, and coupled oscillators permeated and changed the course of neuroscience.

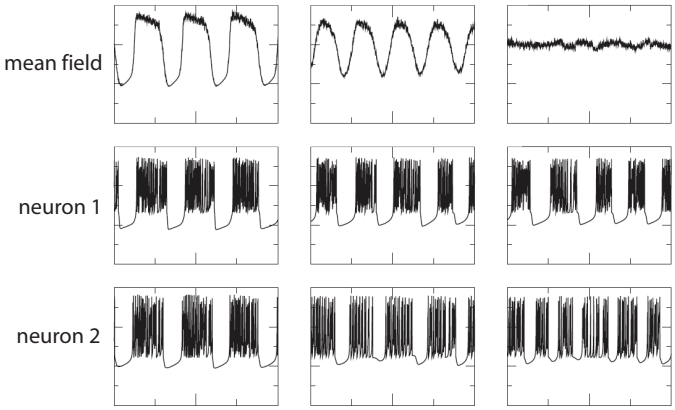

Figure 1.3: The coherent activity (synchronisation) of large groups of spiking neurons generates an electric field which produces a nonzero mean field (leftmost column). With less coherent activity (middle and rightmost columns), the amplitude of the mean field progressively vanishes. Adapted from Viana et al. (2012).

1.2 Neuronal oscillations and neuronal synchronisation

Circa 1907, as a result of his studies of frog nerve stimulation, Lapicque (Lapicque, 1907) developed perhaps the first neuron model using an electric system composed of a capacitor and a resistor, representing the capacitance and the leakage resistance of the cell membrane, respectively. Although he had limited understanding about the biophysical mechanisms of action potentials in neurons, his model captured fundamental oscillatory properties of single neurons and contributed to the study of a broad range of phenomena (Abbott, 1999; Brunel & van Rossum, 2007).

Nearly concurrent, Berger (Berger, 1929) was immersed in the study of electromagnetic forces generated by the brain. Measuring voltage changes from around the skull, he noted the presence of rhythms with different magnitudes. The large amplitude rhythm had a frequency of approximately 10 Hertz, and was later named the "alpha" rhythm, but many other rhythms have been found subsequently (e.g. delta waves, up to 4 Hz, beta waves, from 13 to 30 Hz, and many more, spanning from 0.05 Hz to 500 Hz (Buzsáki, 2006)).

Lapicque's work showed that, at a certain level of abstraction, a neuron can be understood as a self-sustained oscillator (Murray, 1989). As such, and in face of the ideas presented in the previous section, one would expect that groups of weakly connected neurons may synchronise and display collective oscillations. In fact, it is precisely the coherent activity (synchronisation) of large groups of spiking neurons that generates the electric field whose mean field behaviour was observed by Berger in the electroencephalogram (see Figure 1.3).

Therefore, one can approach brain oscillations from a micro scale perspective, which reflects

the microscopic cellular dynamics of neurons, or from a macro scale perspective, which is related to the synchronised activity of large groups of neurons. At the micro scale, models which resemble the behaviour of relaxation oscillators capture many features of a spiking neuron; the most employed ones are the *integrate-and-fire* model (Hill, 1936; Knight, 1972), the Hodgkin-Huxley model (Hodgkin & Huxley, 1952), and the FitzHugh-Nagumo model (FitzHugh, 1961; Nagumo et al., 1962). At the macro scale, dynamics closer to harmonic oscillators are captured by mean-field models as e.g. the Wilson-Cowan model (Wilson & Cowan, 1972, 1973). Models of coupled phase oscillators, under certain assumptions, are able to capture the dynamics of both scales (Winfree, 1980; Kuramoto, 1984; Tass, 1999).

Regardless of the scale, the consensus nowadays is that cognitive processes have a close non-trivial relationship to neuronal rhythms and oscillations (Buzsáki, 2006), with synchronisation mechanisms linking single-neuron activity to behaviour (Engel et al., 2001; Whittington & Traub, 2003; Fries, 2005). In the next section, we discuss some of the key concepts and findings that are most relevant to this thesis.

1.2.1 Relationship with cognition and behaviour

Evidence from animal experiments indicate that oscillatory neural activity is closely related to cognitive processes and behaviour (Eckhorn et al., 1988; Singer & Gray, 1995; Engel et al., 2001; Buzsáki, 2006). More specifically, it has been claimed that the flexible synchronisation of firing neurons is a fundamental brain mechanism (Hebb, 1949; von der Malsburg, 1981; Singer, 1993, 1999; Fries, 2005; Womelsdorf et al., 2007). In fact, there is a growing consensus that groups of neurons, not the single neurons, constitute the basic functional unit of the central nervous system in mammals (Averbeck & Lee, 2004; Nicolelis & Lebedev, 2009).

The brain is a densely connected, distributed system (Singer, 2009; da Rocha et al., 2011), which requires mechanisms for temporal coordination and information integration. Moreover, signaling consumes a significant amount of the total energy used by the brain, suggesting the need for efficient neural codes and axon wirings (Attwell & Laughlin, 2001). In this sense, oscillations and synchronisation are an energy efficient mechanism for temporal coordination of distributed neural activity and provide a substrate for concurrent operations at multiple temporal and spatial scales (Winfree, 1980; Mirollo & Strogatz, 2004; Buzsáki et al., 2004; Uhlhaas et al., 2010; Siegel et al., 2012). Synchronisation may mediate sensitivity to inputs, the interactions between neurons, and be an active mechanism of large-scale integration of neuronal assemblies, impacting on motor control and cognitive performance (Steriade et al., 1990; Hatsopoulos et al., 1998; Engel et al., 2001; Varela et al., 2001; Jackson et al., 2003). Moreover, a range of patholo-

gical states are related to abnormal neuronal synchronisation regimes (Glass, 2001; Brown, 2003; Arthuis et al., 2009). Nevertheless, the way neuronal groups form, synchronise, cooperate, and interact over time remains largely unclear to date (Kopell et al., 2010, 2011).

One hypothesis that has gained considerable supporting experimental evidence states that groups of neurons have their functional interactions mediated by synchronised oscillations, the so-called "binding by synchrony" (BBS) (Singer, 1999; Varela et al., 2001; Uhlhaas et al., 2009). As structural connectivity is relatively static at the time-scale of perception and action, the central idea is that the synchronisation of neuronal activity by phase locking of network oscillations are exploited as a representational coding mechanism to define and encode relations between spatially distributed groups of neurons. A complementary theory, called "communication-through-coherence" (CTC) (Fries, 2005, 2009), proposes that synchronised oscillations constitute more than a representational code, i.e. neuronal coherence is posed as a dynamic selective communication mechanism that serves as the basic neuronal substrate for cognition. In this sense, information dynamics and computations within the neural network largely rely on the timing of individual spikes rather than their rates (although there are certain phenomena, e.g. innervated muscle contraction (Gerstner et al., 1997), which can be better explained simply by the spiking rate, leaving aside more intricate temporal properties).

The importance of considering temporal relations among groups of neurons (temporal coding), either by external influences or sustained by internal mechanisms, has been stressed by various researchers (Singer, 1993; Konig et al., 1996; Singer, 1999; Engel et al., 2001; Fries, 2005; Doesburg et al., 2009; Shanahan, 2010a). According to Varela et al. (2001), it is essential to investigate the temporal dynamics of neural networks in order to understand the emergence and integration of neuronal assemblies by means of synchronisation. These dynamic assemblies, which are related to large-scale neuronal integration, can influence every cognitive act an agent might eventually perform. In studying these temporal dynamics, Varela and collaborators opted to focus on phase relationships of brain signals, mainly because these contain a great deal of information on the temporal structure of neural signals, particularly those relating to the underlying mechanism for brain integration. Other authors have emphasized the relationship between phase information and memory formation and retrieval (Li & Hopfield, 1989; Izhikevich, 1999; Womelsdorf et al., 2007; Masquelier et al., 2009; Kayser et al., 2009; Kunyosi & Monteiro, 2009). Moreover, recent works have shown that specific topological properties of local and distant cortical areas support synchronisation despite the inherent axonal conduction delays, thereby providing a substrate upon which neuronal codes relying on precise interspike time can unfold (Vicente & Pipa, 2008; Pérez & Mirasso, 2011).

Whereas increasingly sophisticated computational and imaging techniques help us to observe and record from different physiological aspects of the nervous system, a great part of the challenge lies in the comprehension of this avalanche of data and its relationship with behaviour (Chialvo, 2010). In addition, the brain presents spontaneous electrochemical activity that is constantly shaped by the body's constraints and time-varying environmental stimuli (Katz, 1999). The brain, therefore, not only processes information but also produces it, and cognitive phenomena are a product of brain-body-environment interactions (Stewart et al., 2010). In the next section, we explore recent findings on the importance of considering the body in neuronal oscillations and synchronisation studies.

1.3 Embodiment and Evolutionary Robotics

In Descartes's Cartesianism, the body and the mind participate differently in cognitive processes. The body is related to experiencing, sensing the world, whereas reasoning and manipulation of basic mental states is done by the mind. In its contemporary guise, cognition was viewed as outcomes of computations over mental states composed of symbolic or sub-symbolic representations of the physical world.

At the turn of the last century, the influence of new theories in psychology, sociology, and linguistics, represented by the work of Heidegger, Husserl, Skinner, Vygotsky, Piaget, among others, originated a series of philosophical doctrines opposed to the Cartesian mind-body dualist view of the world. In particular, Merleau-Ponty (Merleau-Ponty, 1945) focused on the first-person perspective, suggesting that cognitive phenomena are an intricate, intertwined product of brain-body-environment interactions. In this sense, perception is not simply elicited by sensory stimulation but rather a fundamental active process in engaging with the world. This is in accordance with two other very influential concepts, namely von Uexkull's *Umwelt* (von Uexkull, 1940) and Gestalt psychology (von Ehrenfels, 1890). In the first, the mind and the world constitute an inseparable system - the individual's unique Umwelt ("environment", in English) is created and shaped by its interactions with the world, i.e. the world is directly meaningful to the organism, not a static system that is represented as mental states that are later evaluated in order to become meaningful (Colombetti, 2010). In Gestalt psychology, the brain is viewed as a holistic, self-organising system, and perception is an emergent process due to complex, multiple stimuli integration - perception is a product of the whole, not something that can be inferred from the parts in isolation.

From the late 1950's, by the time contemporary cybernetics and artificial intelligence (AI) were established fields, to the mid 1980's and the connectionist revolution, the mainstream approach to cognitive science viewed cognition from an information-processing perspective (cognit-

ivism) (Fodor, 1975). The mind was compared to a computing device, whose main role was to provide appropriate outputs in response to a set of inputs - in this way, detached from the body and the environment.

However, this guiding paradigm struggled in many classes of real-world problems, e.g. the commonsense knowledge problem (Dreyfus, 1991), the frame problem (McCarthy & Hayes, 1969), and the symbol grounding problem (Harnad, 1990). The idea of cognition as abstract symbol manipulation and computers as intelligent machines seemed inappropriate. This motivated the development of an alternative approach towards an embodied-embedded cognitive science, which argues that cognition is best understood if considered as a self-organised dynamic process that emerges out of the brain-body-environment interactions (Varela et al., 1991; Clark, 1997; Nöe, 2004; Gallagher, 2005). In particular, the enactive paradigm of embodied-embedded cognitive science emphasizes that "a living organism enacts the world it lives in; its effective, embodied action in the world actually constitutes its perception and thereby grounds its cognition" (Stewart et al., 2010). In neuroscience, embodiment is related to the recent development of the theory of "sensorimotor contingencies" (O'Regan & Nöe, 2001), which proposes intimate, law-like relations between actions and changes in sensory input. In fact, the embodied action-oriented view of cognitive processing is supported by numerous recent findings (Engel et al., 2001; Pfeifer & Bongard, 2006; Engel, 2010).

The concepts of embodiment influenced a shift in artificial intelligence research with emphasis in robotic agents, with the work of Brooks as a milestone (Brooks, 1991a,b). Pfeifer & Scheier (1999) stress that "The brain does not run "programs"; it does something entirely different. The brain has evolved not to do mathematical proofs but to control our behavior. Intelligence always manifests itself in behavior - thus it is behavior that we must understand. (...) The perspective of embodiment requires working with real world physical systems, i.e. robots. It is its crucial aspect."

It is now well established that robotics models are highly suited to capture essential elements of the brain-body-environment interactions that underlie the generation of behaviour, in a way that studies of disembodied neuronal dynamics cannot achieve (Beer, 2003; Seth et al., 2004; Boden, 2006). A methodology called Evolutionary Robotics (ER) has an important role in this context as it allows the exploration of classes of mechanisms, and the automatic creation of working models when there are insufficient details to fully specify a system in advance. Hence it has been recognized as a useful tool in investigating biological hypotheses (Harvey et al., 2005; Floreano et al., 2008; Floreano & Mattiussi, 2008; Floreano & Keller, 2010). Regarding neural dynamics, there is a rich literature exploring the relationship between neural synchronisation and complex motor

control in embodied (robotic) rhythmical behaviours (Taga, 1994; Ijspeert et al., 2005; Pitti et al., 2009), where synchronisation appears as a more intuitive underlying mechanism; however, to date there has been very little research on the wider issues of neuronal synchronisation in the generation of embodied cognitive behaviours.

The preceding sections highlight that oscillatory activity is ubiquitous in nervous systems, with solid evidence that synchronisation mechanisms underpin cognitive processes. Nevertheless, most of the evidence is only correlative, and there is a lack of studies exploring the informational content and relationship with behaviour when synchronisation is selectively altered. Additionally, cognitive systems cannot be properly appreciated without taking into account brain-body-environment interactions. In the next section, we outline the objectives of this thesis, provide an overview of the following chapters, and state the main contributions of the work.

1.4 Thesis overview

This thesis has two main objectives: first, to explore and shed new light into the role of neuronal synchronization and phase towards the generation of embodied cognitive behaviours; second, to initiate an investigation on the efficacy of such systems as practical robot controllers. To this end, we develop a neural network model based on the Kuramoto model of coupled phase oscillators which is used to control evolved mobile robotic agents following an Evolutionary Robotics methodology. The analyses focus both on a behavioural level description, investigating the robot's trajectories, and on a mechanism level description, exploring the dynamics and the information transfer properties within and between the agent and the environment.

Chapter 2 contains the theoretical basis and a detailed review of neuronal oscillations and neuronal synchronisation that motivated and grounded the development of this thesis. The chapter starts by explaining the physiology of oscillations in the nervous system, followed by a review of the main computational models to study neural oscillations, with special attention to phase oscillators. We proceed by further exploring recent findings regarding neuronal synchronisation, focusing on neuronal assemblies, synchronisation of spatially separate neurons, and the impact of the body and sensorimotor activity in synchronisation; also, a key issue in cognitive science, known as "the superposition catastrophe problem and the binding problem", is detailed. We then comment on different approaches to the neural code, namely the rate code and the temporal code, and on different methods to read each code. In sequence, we present a review of contributions from the field of Information Theory to the study of neuronal oscillations, with a description of "directed information" measures. The chapter closes with a summary and a highlight of its relevance to the thesis.

In Chapter 3, we describe the models and methods employed in the experiments devised in Chapters 4, 5, and 6. First, we outline the broader concepts of Evolutionary Computation and Genetic Algorithms, an optimization technique that is the foundation of Evolutionary Robotics (ER) - the methodology adopted to synthesize systems that exhibit some sort of embodied cognitive behaviour. We describe ER in detail together with examples of experiments in the context of minimally cognitive tasks, i.e. tasks that are simple enough to allow detailed analysis and yet are complex enough to motivate some kind of cognitive interest. Then, we introduce the Kuramoto model of coupled phase oscillators and the framework developed to control a robotic agent. A description of Transfer Entropy, the main information theoretic tool employed here, finishes the chapter.

The next three chapters comprise different experiments, each exploring a particular aspect of neuronal synchronisation (described in Chapter 2). In Chapter 4, for the first time, we apply evolved instances of the Kuramoto model of coupled oscillators to explore the role of synchronisation in the performance of a simulated robotic agent during the execution of two different minimally cognitive tasks: the first, a categorical perception task (Beer, 2003; Izquierdo, 2008; Dale & Husbands, 2010), in which the robot has to discriminate between moving circles and squares; the second, an orientation task, where the robotic agent has to approach moving circles with both normal and inverted vision, adapting to both conditions. These tasks were chosen for being currently regarded as benchmarks in the evolutionary robotics and adaptive behaviour communities, with categorical perception underpinning cognitive systems (Harnad, 1987). We show that there is a statistically significant difference in performance and evolvability depending on the synchronisation regime of the network. In both tasks, a combination of information flow and dynamical analyses show that networks with a definite, but not too strong, propensity for synchronisation are more able to reconfigure, to organise themselves functionally, and to adapt to different behavioural conditions. The results highlight the asymmetry of information flow and its behavioural correspondence. Importantly it also shows that neural synchronisation dynamics, when suitably flexible and reconfigurable, can generate minimally cognitive embodied behaviour.

The dynamic formation of groups of neurons - neuronal assemblies - is believed to mediate cognitive phenomena at many levels, but their detailed operation and mechanisms of interaction are still to be uncovered. In Chapter 5, we investigate neuronal assembly dynamics in two complementary scenarios: the first, a supervised spike pattern classification task, in which noisy variations of a collection of spikes have to be correctly labelled; the second, an unsupervised, minimally cognitive evolutionary robotics task, in which an evolved agent has to cope with multiple, possibly conflicting objectives. In both cases, the more traditional dynamical analysis of the sys-

tem's variables is paired with information theoretic techniques in order to get a broader picture of the ongoing interactions with and within the network. The neural network model allows one to fine tune the network synchronisation dynamics and assembly configuration. The experiments explore the computational power, redundancy, and the generalisation capability of neuronal circuits, demonstrating that performance depends nonlinearly on the number of assemblies and neurons in the network, and showing that the framework can be exploited to generate minimally cognitive behaviours, with dynamic assembly formation accounting for varying degrees of stimuli modulation of the sensorimotor interactions.

In the last chapter of experiments, Chapter 6, we incorporate a wavelet-like spatial kernel to the Kuramoto model to obtain a centre-surround connection pattern between neurons (Breakspear et al., 2010). This extension, in addition to being more biologically plausible than the fully-connected architecture, supports the emergence of both travelling waves and synchronised activity (Heitmann et al., 2012), which are widely present across many regions of the brain and have been linked to a variety of cognitive processes, including motor movement (Ermentrout & Kleinfeld, 2001). However, the functional roles of travelling waves and synchrony are unclear, and there are two opposing proposals in the literature relating them both in the context of sensorimotor processes: one suggests that synchrony is related to the presence of a sensory stimulus and waves are present in the absence of stimulation (Ermentrout & Kleinfeld, 2001); the other, known as the cortical idling hypothesis (Pfurtscheller et al., 1996; Heitmann et al., 2012), posits that synchrony is observed outside periods of sensory stimulation and wave patterns encode motor action states. In face of this dispute, we evolve the extended Kuramoto model to control a simulated robot in a sequential, associative learning task, known as the "light-switching" task (Urzelai & Floreano, 2001), in order to investigate the role of waves and synchrony in a behavioural task. Our results show that agents with higher performance present higher neuronal synchronisation without sensory stimulation and that in the presence of sensory readings the network is less synchronised. Indeed, solutions that present waves as a default state have very poor performance. The analyses include the behavioural and the system's variables dynamics together with the information flow description. Also, we simulate the pseudo local field potential generated by the network and conduct a mutual information analysis to show that sensory and motor information can be extracted from the global dynamics of the system. In this sense, our results agree with the idling hypothesis.

Finally, Chapter 7 presents a broad discussion and a summary of the results obtained, with a highlight of the main contributions of the thesis. We conclude with directions for future work and a brief remark.

Appendix A describe the simulators used in Chapters 5 and 6.

1.5 Summary of Contributions

The main contributions of this thesis can be summarised as follows:

- We develop a novel model to study neuronal synchronisation phenomena in different benchmark evolutionary robotics tasks. We show that, at a certain level of abstraction, the framework is biologically plausible and flexible enough to encompass a variety of open problems in neuroscience and cognitive science.

- We demonstrate that neural synchronisation dynamics, when suitably flexible and reconfigurable, can generate minimally cognitive embodied behaviour and can be used as practical robot controllers. More specifically, we analyse the framework in three different minimally cognitive tasks, focusing on different aspects of neuronal synchronisation dynamics. The first experiment investigates the role of synchronisation in the performance of a simulated robotic agent during the execution of active categorical perception under normal and inverted vision. The second experiment analyses dynamic assembly formation in a supervised spike pattern classification task and in an unsupervised robotics task, in which an evolved robot has to cope with multiple, possibly conflicting objectives. The third experiment evolves a robotic agent in a sequential, associative learning task using a more realistic centre-surround connectivity pattern between neurons to explore the functional roles of travelling waves and neural synchronisation in a behavioural task.

- We demonstrate that performances in the behavioural tasks studied are directly linked with the synchronisation regime of the network. In particular, the results from Chapter 4 indicate that networks with a definite, but not too strong, propensity for synchronisation are more able to reconfigure, to organise themselves functionally, and to adapt to different behavioural conditions. The results from Chapter 5 show that dynamic assembly formation facilitates the evolutionary process and accounts for varying degrees of stimuli modulation of the sensorimotor interactions, i.e. we show that synchronisation selectively modulates the influence of external signals in the current network activity. Finally, in Chapter 6 we show that networks that present travelling waves as a default solution have a far worst performance than networks that are normally synchronised in the absence of stimuli, which further supports the cortical idling hypothesis.

- We demonstrate that neuronal assemblies and phase reorganisation dynamics can play a

significant part in supervised classification tasks and, perhaps most relevant to cognition, can cope with multiple classification tasks without the need for additional adaptive mechanisms. The results show that performance depends nonlinearly on the number of assemblies and neurons in the network, and is predominantly higher in networks with more assemblies, regardless of the number of neurons within each. We also show that redundancy is widely present across different architectures and is directly proportional to the number of neurons in a network with fixed number of assemblies; synergy, on the contrary, is higher in architectures with fewer neurons within each assembly, regardless of the total number of assemblies. All these findings resemble the results obtained in real cortical experiments.

- We pair the more traditional dynamical analysis of the system's variables with information theoretic techniques in order to get a broader picture of the ongoing interactions with and within the network, reinforcing the asymmetry of information flow and its behavioural correspondence. The results systematically show that the combined approach, in the context of evolved robots, provides a complementary form of analyses. For example, in Chapter 5 the dynamical analysis of the phase space formed by the motors' readings and the nodes' phases reveal different orbits that are due to changes in assembly organisation, and an analysis of the information flow in the network reveals that such changes modulate the influence of the inputs in the robot's behaviour (determined by the motor commands).

Chapter 2

Oscillations and Synchronisation - Models and Speculations on its Role for Cognition

---

In this chapter, we present the main concepts of oscillations and synchronisation in the context of this thesis. The interplay between synchronisation, cognition, information dynamics, and behaviour is linked not only with the frequency of the oscillation but also with the underlying physiological properties sustaining that rhythm. Therefore, we start the chapter describing the origins and physiology of neuronal oscillations, together with basic computational models of neural oscillators. We proceed by studying synchronisation phenomena, including neural assemblies, spatially distributed neurons, and the influence of the body on synchronisation and cognition. The chapter continues with a description of different paradigms of the neural code and proposed methods for reading it. The chapter closes by presenting the applications of Information Theory to study neuronal oscillations and synchronisation.

2.1 Neural oscillations

Rhythmic activity in neuronal systems is intuitive if linked to rhythmic muscular activity e.g. walking, galloping, a heart beating, respiration, or even in pathologies such as Parkinsonian tremors and epilepsy; however, there is also a considerable amount of evidence relating cortical rhythms to cognitive processes and complex sensorimotor behaviour (Varela et al., 2001; Buzsáki & Draguhn, 2004; Buzsáki, 2006). In this sense, and following the oscillatory theory presented in Section 1.1, one can label a particular neuronal phenomena as rhythmic if 1) the relevant variable (e.g. the

membrane potentials and currents, or the mean-field activity of a large group of neurons) is quasi-periodic *and* 2) if the oscillatory activity, after a brief perturbation, is brought back to its original magnitude, period, and possibly with a phase-shift (Ermentrout & Carson, 2002).

Dynamical Systems theory states that positive and negative feedback are mandatory for a sustained oscillation to occur. More specific to neuronal systems, oscillations span from single neuron cells to large neuronal networks, thus one may expect that the mechanisms for the production of rhythmic behaviour vary considerably (e.g., in the single cell the membrane properties generate the oscillations whereas at the network level the interactions of excitatory and inhibitory neurons are responsible for the rhythmic behaviour). We now review the basic physiological interactions responsible for cell-scale and network-scale oscillations.

2.1.1 Physiology of neuronal oscillations

The human brain is composed of approximately 10^{12} neurons and more than 10^{15} synapses (a single neuron roughly has thousands of connections with other neurons). It is not an expressive number if compared to the total number of cells in the nervous system or the body as a whole, nevertheless neurons are unique in the sense that they are capable of transmitting electrical signals over long distances.

Electrical activity in neurons is caused by the movement of ions through membrane channels due to electrochemical gradients. More specifically, the extracellular medium, which has a high concentration of Na^+ and Cl^- ions, is conductant, and the difference in concentrations of intra and extracellular ions, mainly calcium (Ca^{2+}), chloride (Cl^-), potassium (K^+), and sodium (Na^+), results in an ionic current.

The ionic current is modulated by the opening and closing of many different membrane channels, a process that is controlled by many factors such as the membrane voltage, neuromodulators, and neurotransmitters. Inputs from other neurons may cause transmembrane currents that influence the membrane potential. When the synaptic currents are large enough, the postsynaptic potentials influence the voltage-sensitive membrane channels, possibly causing a brusque but transient change of membrane voltage - a spike - that is propagated to other neurons.

Until the late 1980's, neurons in the mammalian nervous system were mainly seen as integrate-and-fire units, i.e. a neuron was a silent cell that integrated different input stimulations and, upon reaching a threshold, emitted an action potential propagated to other neurons. This was challenged by Llinás (Llinás, 1988), who paved the way for several works showing the neuron as a much more complex, active unit - a dynamical system on its own. In fact, it is now consensus that spike generation is a product of intricate non-linear interactions between membrane channels,

potentials, and currents (Pinsky & Rinzel, 1994; Buzsáki, 2006). For this reason, neurons respond differently to stimuli e.g. the same stimulus may lead to a sequence of action potentials in one neuron, a bursting activity in another, some neurons won't even fire (Izhikevich, 2007)(see Figure 2.1). Interestingly, it has been shown that the isolated neuron is likely to produce spontaneous oscillatory activity (Cohen & Miles, 2000; Harris et al., 2003), and the network interactions are responsible for keeping them silent most of the time.

The relatively recent approach to neurons as complex dynamical systems may be attributed to the difficulty in accessing, recording, and analysing cellular level fluctuations (Buzsáki, 2010; Lopes dos Santos et al., 2011; Canolty et al., 2012). Recordings of larger scale phenomena obtained from e.g. Local Field Potentials (LFP), which captures the behaviour of dozens of neurons, or electroencephalography (EEG), which is related to the activity of millions of neurons, are far easier to perform. In this sense, macroscale oscillations in the brain are generally attributed to network interactions and synchrony between different neurons (Ermentrout & Carson, 2002). Consider the following example, which illustrates the generation of the pyramidal-interneuron network gamma (PING, $60 - 90$ Hz) rhythm (Kopell et al., 2010): a group of excitatory pyramidal cells stimulate a group of fast spiking interneurons, whose response then inhibits both groups; after a given period of time the inhibition vanishes, which causes the group of pyramidal cells to fire again. Therefore, the $60 - 90$ Hz rhythm detected by a macroscale measurement is directly influenced by the inhibition time and by the excitatory drive of the cells.

However, this is not solely a bottom-up process. Although macroscale rhythms have a straight relationship with the physiological properties of neurons, as highlighted by the example in the previous paragraph, it has been shown that network-scale oscillations modulate neuron-scale activity - the LFP of a certain brain region may interact not only with the proximal cells but also with neurons and other LFPs located in distant areas. Moreover, given that different rhythms are linked with different underlying physiology, neuronal oscillations may assume different roles in brain processes and dynamically modulate distributed functional groups of neurons (Lakatos, 2005; Kopell et al., 2011; Canolty et al., 2012). Mechanisms of synchronisation, neuronal assembly formation, and their relationship with cognition are further detailed in Section 2.2.

To conclude, it is important to stress that the myriad of rhythms are detected by different techniques. A single neuron recording (microscale) reveals a phenomenon that would not be captured by a LFP measurement (mesoscale) or by an EEG (macroscale). Furthermore, here we have only covered the very basic aspects of oscillatory phenomena, leaving aside important factors such as plasticity mechanisms or scenarios where oscillations emerge without interneuron interactions (Magee & Johnston, 1997; Nikonov et al., 2002; Díaz et al., 2007). This reinforces that, regard-

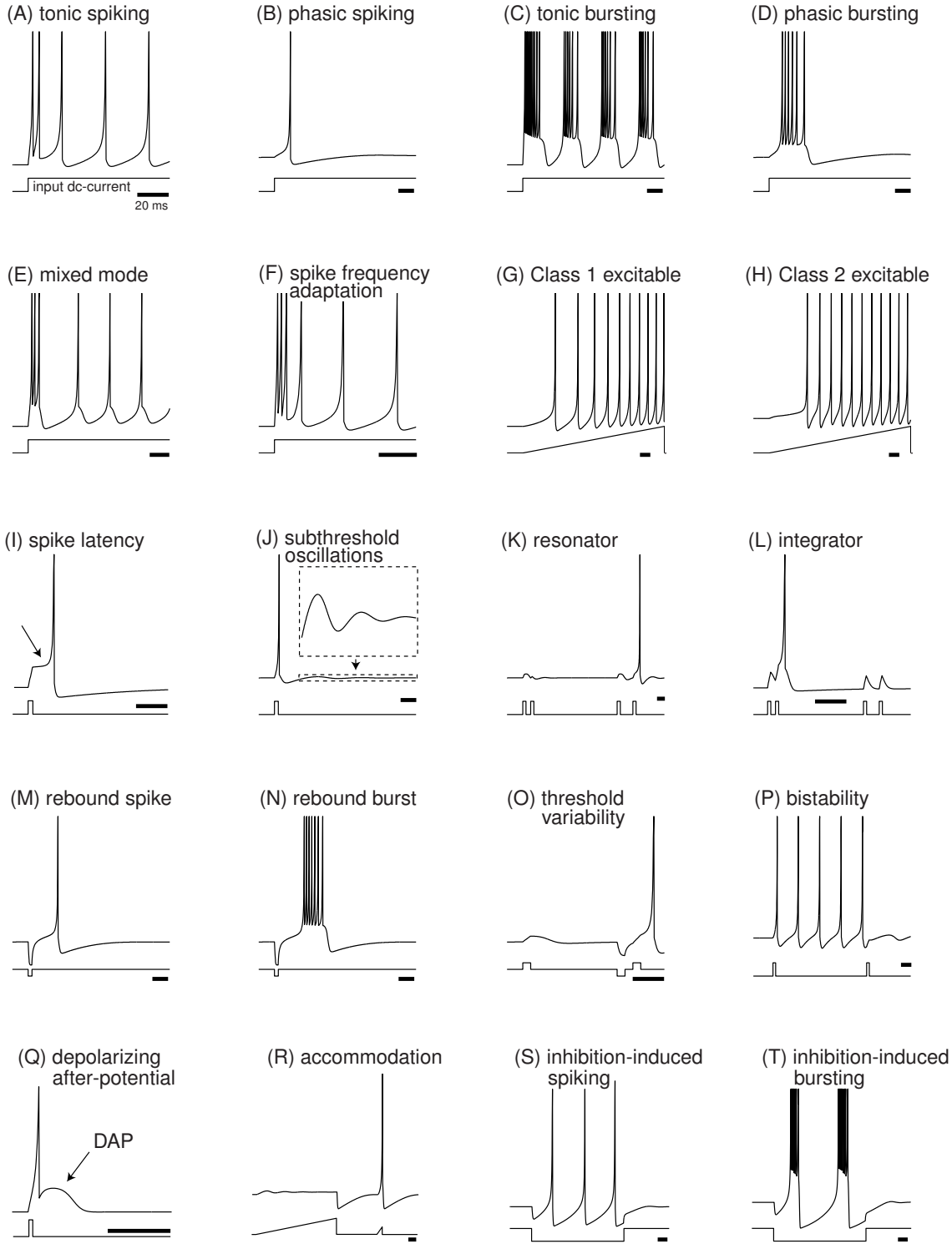

Figure 2.1: 20 different examples of neuronal responses to stimulus. Reproduced from Izhikevich (2004) with author's permission. Electronic version of the figure and reproduction permissions are freely available at www.izhikevich.com

less of the scale, it is still unclear how neuronal groups form, organize, cooperate, and interact over time (Kopell et al., 2010, 2011). Whilst there are numerous physiological mechanisms underlying the generation of oscillations at every scale, at a certain level of abstraction they can be described by a few mathematical principles which simplify their study (Izhikevich, 2007). In the next section, we provide a higher level description of the most used models of neurons and neuronal oscillations and justify our choice for employing a model based on coupled phase oscillators in the experiments.

2.1.2 Computational models of neurons and neuronal oscillators

Ideally, any computational model should aim at reproducing the behaviour of the phenomena of interest with as much detail as possible whilst having a low computational cost; unfortunately, this is rarely the case. The following models of neurons and neuronal oscillators have both biological plausibility and computational cost differences, nevertheless they have all been extensively employed in the literature.

Independently of the model, the physiological features of neurons and networks are better grasped by nonlinear equations (Glass, 2001). As a consequence, analytical solutions are hard or even impossible to obtain. The solution, therefore, is to rely on numerical simulations. Hodgkin (1948) proposed a classification of neuronal models regarding their dynamical properties in response to a step input current which is particularly useful for it helps to predict the global behaviour of neurons when coupled in networks. Also, there are models with varying levels of complexity within the same class and different neurocomputational properties when compared to other classes; if some interesting property is observed in one model, it is possible to extend the findings to other models of the associated class. Simply put, the Hodgkin classification is as follows:

- Class 1 excitable: the frequency of spikes can be arbitrarily low, or in equivalent terms oscillations can have arbitrarily long periods; the frequency of fire $\times$ injected current curve scales with the square root of the bifurcation parameter. Therefore, the firing rate of this neuron contains information about the magnitude of the stimulation.

- Class 2 excitable: spikes are generated in a limited range of frequencies; the frequency of fire $\times$ injected current curve has a discontinuity. Therefore, the magnitude of the stimulation cannot be retrieved from the firing rate of this neuron.

- Class 3 excitable: the neuron produces a spike in response to an abrupt current increase and remains silent unless an extremely strong current is injected. Therefore, this neuron can rarely sustain any spiking activity.

We now have a deeper look into different examples of Class 1 and Class 2 models.

Integrate-and-fire model

The integrate-and-fire (IF) model has its origins in the work of Louis Lapicque (Lapicque, 1907), in which the neuron membrane capacitance and the leakage current are represented by a capacitor and a resistor, respectively, but the traditional formulation was proposed by Richard Stein (Stein, 1965; Brunel & van Rossum, 2007), with the term coined later by Bruce Knight (Knight, 1972). It can be written in a simplified manner according to Equation 2.1 (Izhikevich, 2004).

$$\dot{v} = I + a - bv,\ if\ v \geq v_{thresh},\ then\ v \leftarrow c \tag{2.1}$$

where v is the membrane potential, I is the input current, and a, b, c, and v_{thresh} are the parameters. A spike is produced whenever the membrane potential reaches the threshold v_{thresh}.

The leaky IF model can be classified as a simple Class 1 excitable model. It is computationally cheap, easy to implement, and linear, which facilitates analytical studies. As a drawback, notice that the action potentials (spikes) that are produced all have the same shape and duration; it is also common to manually draw a spike whenever $v \geq v_{thresh}$ just to improve the visualisation. Therefore, the model does not capture in details the voltage trajectory of an action potential, and it is not capable of reproducing a variety of real-neuron dynamics such as bursting, phasic spiking, among others. Finally, the input I can facilitate or suppress spike generation, depending on whether $I > 0$ (excitatory) or $I < 0$ (inhibitory), respectively. In this way, the spiking rate encodes the magnitude of the input, and the neuron resembles an integrator.

Despite the limitations mentioned above, the IF model has been used in a variety of studies, from single neurons to networks of thousands of neurons. Several extensions have been proposed to overcome the limitations of the original IF model and make it more biophysically plausible, e.g. the adaptive IF (aIF), the IF-or-Burst (bIF), and resonate-and-Fire (rIF), many of them simply by incorporating a second linear equation to the model. A model named quadratic IF (qIF), closely related to the theta-neuron or the Ermentrout-Kopell canonical model, is specially useful because it is fast, simple, and yet captures many dynamical properties of real neurons such as latencies, activity-dependent threshold, among others, which make it a suitable choice to simulate large-scale networks. It is described by Equation 2.2.

$$\dot{v} = I + a(v - v_{rest})(v - v_{thresh}),\ if\ v \geq v_{peak},\ then\ v \leftarrow v_{reset} \tag{2.2}$$

where v_{rest} and v_{thresh} are the resting and the instantaneous threshold values of the membrane potential, and v_{peak} is a sufficiently large constant above which a spike is produced. After the

peak of the spike is reached, $v(t)$ is reset to the value of v_{reset}.

Hodgkin-Huxley model

The Hodgkin-Huxley model (HH) (Hodgkin & Huxley, 1952) presents both Class 1 and Class 2 excitability - it is perhaps the most used and one of the most important neuron models in computational neuroscience, commonly referred to as the basis of any conductance-based model. The model was based on the physiology of action potentials in the squid giant axon; it is composed of four equations and several parameters (whose description we omit here for brevity) which describe the membrane potential v as a function of the membrane capacitance C, the sodium (I_{Na^+}), potassium (I_{K^+}), leakage (I_{leak}), and stimulating (I_{input}) currents.

$$\begin{aligned} C\dot{V} &= -g_{Na}m^3h(v - E_{Na}) - g_K n^4(v - E_K) - g_{leak}(v - E_{leak}) + I_{input} \\ \dot{m} &= \frac{1}{\tau_m(V)}(-m + M(V)) \\ \dot{h} &= \frac{1}{\tau_h(V)}(-h + H(V)) \\ \dot{n} &= \frac{1}{\tau_n(V)}(-n + N(V)) \end{aligned} \tag{2.3}$$

One of the key findings of Hodgkin and Huxley was that the conductances g were not constant but a function of the membrane potential V. Also, the parameters and the shape of the functions $\tau_m(V)$, $\tau_n(V)$, $\tau_h(V)$, $M(V)$, $H(V)$, and $N(V)$, were obtained from real data. Thus, the model has a great level of biophysical plausibility, which allows for detailed investigations about action potentials and ionic currents generation and propagation, and many other properties of the single neuron dynamics. However, there is no free lunch: the model has a huge computational cost associated to its execution (roughly it is 250 times slower than the traditional IF model), therefore only simulations of a few neurons are feasible.

After considerable effort to attempt to simulate the HH model in an analog computer, John FitzHugh suggested a simpler model of action potential generation (FitzHugh, 1961), and an equivalent circuit model was shortly later devised by Nagumo et al. (1962). The FitzHugh-Nagumo model (FN) reduces the four-dimensional HH model to a two-dimensional model by taking into account the different temporal dynamics of the variables in Equation 2.3 and by introducing a recovery variable W that can be associated to the outward current of ions K^+ (which in turn is responsible for the hyperpolarization of the axon after a spike) (FitzHugh & Izhikevich, 2006):

$$\begin{aligned} \dot{V} &= V - V^3/3 - W + I \\ \dot{W} &= 0.08(V + 0.7 - 0.8W) \end{aligned} \tag{2.4}$$

The FN model is widely used because first, it can reproduce many of the biophysical properties of neurons with a computational cost more than 10 times smaller than the cost of simulating the HH model (Izhikevich, 2004), and second, it is a model with non-trivial dynamics that admits a phase plane analysis of its behaviour.

Wilson-Cowan model

So far, the explored models concerned the dynamics of single neurons, with detailed description of the generation and transmission of action potentials and ionic currents. In a different approach, Hugh Wilson and Jack Cowan (Wilson & Cowan, 1972, 1973) shifted the focus on the microscale properties of nerve cells to analyse the collective properties of populations of neurons. Their study employed mean-field methods from statistical mechanics, resulting in coupled nonlinear differential equations for the dynamics of two types of cells, excitatory neurons (E) and inhibitory neurons (I), which are distributed in space and follow a variety of connection schemes (extensions to the original model incorporate more complex behaviours e.g. bursting or intricate connectivity patterns). In this sense, the model captures the dynamics of a cortical column instead of a single neuron, which simplifies analytical studies and make simulations of large networks more feasible. Moreover, new methods for analysing population-level activity contribute to testing the model (Destexhe & Sejnowski, 2009). The Wilson-Cowan (WC) model has the form of Equation 2.5:

$$\begin{aligned} \tau_e \dot{A}_e &= -A_e + h_e(w_{ee}A_e - w_{ie}A_i + I_e) \\ \tau_i \dot{A}_i &= -A_i + h_i(w_{ei}A_e - w_{ii}A_i + I_i) \end{aligned} \tag{2.5}$$

where A_e and A_i denote the activity of the excitatory and inhibitory populations, respectively, τ is a time constant, I is the synaptic input, h is a function that models the synaptic input activity-dependence of a population, and w_{ee}, w_{ie}, w_{ei}, and w_{ii}, are the connection weights between the populations.

By manipulating the function h, one can obtain different dynamics from the model (Ernst & Eurich, 2002). For instance, if (as in the original work) h is a sigmoid function that saturates at 1, the population activity A represents the proportion of active neurons; instead, if one chooses h as a function that is 0 up to some threshold and then linearly increases, then the population activity A represents the firing rate of the population.

To sum up, the WC model presents both Class 1 and Class 2 excitability and can be used to investigate a variety of physiological phenomena corresponding to the dynamics from hundreds to thousands of cortical neurons (Jirsa & Haken, 1997; Tsodyks et al., 1997;

Hoppensteadt & Izhikevich, 1998). Furthermore, the model is simple enough to motivate analytical studies but also admits investigations using phase plane methods and numerical simulations.

Phase models

In the previous sections, we explored models with different levels of abstraction, starting from simple integrate-and-fire single neuron models, moving to highly detailed models such as the Hodgkin-Huxley model, up to models e.g. the Wilson-Cowan model that capture the behaviour of populations of neurons. To conclude, we present a class of models that up to some level of abstraction can account for the dynamics portrayed by any of the previous models.

Many neurons are thought of generating sequences of action potentials upon constant stimulation. Following a dynamical systems approach, this is equivalent to say that such neurons generate a limit cycle oscillation in response to constant stimulation - in other words, neurons are modelled as oscillators. If neuronal oscillators are connected, the theory developed by the field of nonlinear coupled oscillators indicate that the resulting system may lead to extremely intricate, hard to analyse mechanisms (Pikovsky et al., 2001; Izhikevich, 2007). However, a seminal work from Avis Cohen and collaborators (Cohen et al., 1982), and many others that followed (Ermentrout & Kopell, 1984; Ermentrout, 1985; Kopell, 1995; Hansel et al., 1995; Hoppensteadt & Izhikevich, 1997), showed that the dynamics of coupled neuronal oscillators can undergo powerful mathematical simplifications if one assumes that the coupling is weak. In such scenarios, the shapes and amplitudes of the action potentials do not change significantly due to interactions, but their timings, phase relations, and frequencies may change. In this case, only the phase dynamics of each oscillator need to be considered (Wilson, 1999).

A phase oscillator is modelled according to Equation 2.6:

$$\dot{\theta} = \omega \tag{2.6}$$

where θ is the oscillator phase and ω is the natural frequency of the limit cycle oscillation. Recall from Section 1.1 that the phase increases by 2π with every period of oscillation.

If two neurons are coupled, the resulting system is described by Equation 2.7:

$$\begin{aligned} \dot{\theta_1} &= \omega_1 + H_1(\theta_2 - \theta_1) \\ \dot{\theta_2} &= \omega_2 + H_2(\theta_1 - \theta_2) \end{aligned} \tag{2.7}$$

where H is a 2π periodic coupling function that characterizes the interactions between the different oscillators. Different H functions, also known as phase interaction function (PIF), lead to models that capture different properties of neuronal interactions, ranging from models

that resemble the behaviour of Hodgkin-Huxley models to systems similar to Wilson-Cowan models (Ermentrout & Kopell, 1994; Wilson, 1999). In fact, H is basically the average of the response of the postsynaptic neuron to the incoming current from the presynaptic neuron (Ermentrout & Carson, 2002).

If the phase difference between the two oscillators is constant and invariant with time, the oscillators are said to be phase-locked. If the oscillators are phase locked with zero phase difference, then the oscillators are synchronised. In the analogy with real neurons, consider two neurons, each producing an independent sequence of action potentials. The relative phase between the neurons is then defined as the time difference between two action potentials, one from each neuron, divided by the period. If the waveforms are not identical, one possible solution is to choose a single feature present in both waveforms and then measure the time differences relative to that feature (Ermentrout & Carson, 2002). If one arbitrarily chooses one neuron to fire at zero phase, then all the relative phases to all the other neurons can be estimated.

Hence, phase models offer a direct way of studying neuronal synchronisation, focusing on temporal relations, whilst avoiding any problems in obtaining the phase information (which, as seen from above, can be an issue in other models which consider frequency and amplitude dynamics (Pikovsky et al., 2001)). Moreover, phase models simplify the study of multiple-variables conductance-based models simply by assuming that the amplitude and shape of spikes do not change because of interneuron interactions. In this way, findings from simulations using phase models are directly applicable to whole classes of models. To further support this approach, some researchers have argued that the amplitudes of action potentials carry little information whilst a perturbation in systems of coupled oscillators results in phase-shifts throughout the network.

Given all the simplicity and advantages mentioned above, we opted to use a model inspired by the Kuramoto model of coupled phase oscillators in the experiments of this thesis. In the next chapter, Section 3.3 presents the details of the model, but first we explore the findings relating neuronal synchronisation, information dynamics, and cognition.

2.2 Synchronisation

As briefly mentioned in Section 1.2, EEG, MEG, and LFP recordings have revealed a great number of rhythms in the brain. Neurons fire and display oscillating membrane potentials upon stimulation or as a result of complex physiological dynamics; some cells such as the pacemaker cells or the circadian oscillators even exhibit an astonishing periodic behaviour sustained by intricate molecular mechanisms.

The collective behaviour of neurons, which can be recorded with the techniques above, result

in a whole collection of rhythms. The frequencies of these rhythms in the mammalian brain span from 0.05 Hz to 500 Hz and form an arithmetic progression on a natural logarithmic scale, which originate the separated frequency bands (Penttonen & Buzsáki, 2003; Buzsáki & Draguhn, 2004). In this way, neuronal oscillators that belong to adjacent frequency bands cannot phase-lock with each other because the ratios of the mean frequencies of neighbouring oscillators are not integers. This results in transient metastable dynamics of neuronal oscillators that continuously engage and disengage with oscillators from another band. Also, due to biophysical properties such as connectivity pattern, axon length, and limited speed of synaptic transmission, higher frequency oscillations are more observed in reduced neuronal spaces whereas slow frequency oscillations occur in broader areas of the neuronal tissue (Csicsvari et al., 2003). Adding to that, there is an inversely proportional relationship between the power density of an EEG or a LFP recording and the frequency ($EEG \propto 1/f$), which is a signature of complex dynamical interactions and means that perturbations at slow frequencies can lead to a cascade of energy dissipation at higher frequencies (Bak et al., 1987). In summary, there are multiple metastable rhythms, superposed in different frequency bands, mediating a wide range of spatio-temporal neuronal interactions.

Researchers were intrigued facing this myriad of rhythms: how do the distributed activity of functionally specialised brain regions and the transient activity of many neuronal groups that are constantly shaped by sensorimotor interactions bind together and communicate in order to support cognitive events?

Since the work of Adrian (Adrian, 1950), it is known that there is a relationship between brain rhythms and cognitive processes; however, the detailed mechanisms and functional roles remain largely obscure. Decades later, work in the cat visual cortex (Eckhorn et al., 1988; Gray et al., 1989; Engel et al., 1991) found that oscillations in the 20-80 Hz range influence the action potential activity in cortical neurons by showing that the oscillatory rhythm caused groups of cells to fire synchronously with higher precision. This highlighted the modulation in neuronal excitability, i.e. the probability that a neuron generates an action potential or its sensitivity to a synaptic input, caused by oscillatory activity. Also, many cognitive events last no more than a few hundreds of milliseconds, time enough for a neuron to fire just a few spikes. A neuron receiving inputs from many other neurons will not fire in response to a few spikes arriving in sparse intervals, but if the stimulating neurons all spike together, then the target neuron will fire consistently (Eckhorn, 1992; Tononi et al., 1992). This is in line with Hoppensteadt & Izhikevich (1998), who have shown in simulations that synaptic interactions do not suffice to establish successful cortical communication, a resonance frequency is also needed. Therefore, considering that oscillatory rhythms stimulate groups of neurons to synchronously fire, and bearing in mind that the coordinated activity of

a group of neurons effectively stimulates target neurons, one can expect that groups of coherently oscillating neurons can communicate effectively because their excitability time frames for input and for output become aligned. This is known as the "communication-through-coherence" (CTC) hypothesis (Fries, 2005).

Following the works in the cat visual cortex, several studies explored the mechanisms and functional roles of neuronal synchronisation in other animals (Kreiter & Singer, 1996; Neuenschwander et al., 1996; Tallon-Baudry, 2009), finding it a ubiquitous phenomena linked to a variety of different functions. Although the cellular basis of synchronisation phenomena as well as the mechanisms of large-scale integration of neuronal groups are not fully understood (synchronisation may occur e.g. as a result of diffused chemical substances (Viana et al., 2012), stimulus onset (Churchland et al., 2010; Ledberg et al., 2012), and attention (Cohen & Maunsell, 2009)), the consensus nowadays is that synchronisation underpins cognitive processes such as memory, attention, and consciousness (Engel et al., 2001; Kahana et al., 2001; Varela et al., 2001; Ward, 2003; Melloni et al., 2007; Uhlhaas et al., 2009). Furthermore, in agreement with that, disruptions in synchronisation mechanisms result in a series of pathological conditions such as epilepsy, schizophrenia, and Parkinsonian tremors (Tass, 1999; Uhlhaas et al., 2009).

In the sections that follow, we explore important concepts within the topic of neuronal synchronisation that will be approached by the experiments in the next chapters: neuronal assemblies, the influence of space in neuronal synchronisation, synchronisation and cognition, concluding with an overview of the superposition catastrophe problem.

2.2.1 Neuronal assemblies

Charles Sherrington was among the first to appreciate the role of groups of nervous cells in comparison to single neurons in his works discussing the formation and cooperation of pools of motor neurons, but it was probably Donald Hebb's *The organization of behavior* (Hebb, 1949) who was the first to emphasise the relationship between the formation of cell assemblies and the mechanisms of perception and learning (Gerstein et al., 1989; Nicolelis et al., 1997). They challenged the idea that the properties of single neurons alone could account for all the computational processes in the brain.

Single neurons are unstable due to the large fluctuations caused by the thousands of inputs per second it receives (Paisley & Summerlee, 1984; Steriade et al., 1993). This large amount of incoming signals also means that a single neuron has little influence in the activity of another (Toyama et al., 1981; Abeles, 1988), hence a given stimulus is unlikely to have a corresponding single neuron activation. If that were the case, there wouldn't be enough neurons in the brain

to deal with all the information content one is presented with during they lifetime, and some characteristic brain phenomena such as redundancy or functional plasticity upon e.g. a lesion could not occur (Sakurai, 1999).

Importantly, in the previous section we stated that neuronal assemblies are formed through the synchronised activity of oscillatory groups of neurons, but this is not to say that the properties of a neuronal assembly result simply from averaging out the instabilities of a single neuron (outlined above) by summing the neuronal activity within the group. In fact, this approach would still present some problems that are observed in single neurons (Wickelgren, 1992). Intra and inter-assembly neurons have much more complex interactions; although still a point of much debate, the most accepted hypothesis is that the temporally correlated spiking activity among neurons facilitate the cooperation and form the dynamic functional circuits (Singer, 1999; Fries, 2005; Singer, 2009). In this way, the transient synchronisation between different groups of neurons would mediate the establishment of functional connections, producing coalitions of neurons able to rapidly form or break apart (Shanahan, 2012).

One of the key properties relating cell assemblies and cognitive processes is the difference in time scales when one looks at single neuron level and at network level. For a single neuron, the integration time window for synchrony, i.e. the time period within which an earlier input affects a later response and above which the earlier event has no influence on the response, is of the order of tens to a few hundreds of milliseconds (Buzsáki, 2006). Experimental evidence, however, suggests that the time scale of elementary cognitive acts is of the order of a few hundreds of milliseconds up to seconds (Dennett & Kinsbourne, 1991; Varela, 1995). Due to biophysical interactions, neuronal assemblies, as opposed to single neurons, have a far wider integration time window ranging from hundreds of milliseconds to many seconds (Varela et al., 2001; Buzsáki, 2006). Therefore, the time scale of transient assembly formation and existence coincides with that of cognitive processes, further supporting the view of neuronal assemblies, not the single neuron, as the fundamental unit of brain operation (Averbeck & Lee, 2004; Nicolelis & Lebedev, 2009).

When considering transient assembly formation, it is important to stress that there is an overlap of neurons among assemblies, i.e. neurons or groups of neurons can participate concurrently in more than one assembly. Therefore, higher rates of activation are not enough to determine if a given neuron belongs to an assembly, instead one has to take into account the temporal correlations of firing (von der Malsburg, 1981; Burwick, 2008). We further explore this topic in the section that follows.

To conclude, labelling a certain group of neurons as constituting an assembly is a challenging task that only recently has been alleviated by more advanced recording techniques and analysis

tools (Buzsáki, 2010; Lopes dos Santos et al., 2011; Canolty et al., 2012). Also, it is still unclear how neuronal groups form, organize, cooperate, and interact over time (Kopell et al., 2010, 2011).

The role of connectivity and space

Hebb postulated that neurons are brought together in assemblies according to a temporal relationship and a plasticity rule: the synaptic efficiency of a certain neuron A that persistently takes part in firing a neuron B is enhanced, thus the structural connectivity between the two neurons gets stronger than with other neurons that were not part of the assembly. In this way, an assembly would comprise neurons that are wired together and that fire together.

The weak point of the theory is that it does not properly take into account the temporal aspect of assembly dynamics. The postulate may provide a sensible mechanism for assembly formation as a consequence of excitatory synapses, however it does not explain how the assemblies would vanish or what would avoid an eventual state of global synchronisation (Buzsáki, 2006).

This problem is attenuated if one also considers the temporal correlations among neurons, i.e. an assembly is comprised by neurons that present a correlated firing activity that goes beyond chance - whether or not they have a direct synaptic connection is irrelevant. Of course, the mechanisms of synaptic plasticity suggested by Hebb still operate, but with this approach the theory of cell assemblies is more comprehensive for it includes anatomically dispersed but functionally integrated parts of the brain as well as distant neurons that fire together e.g. due to inhibitory circuits or because they share common inputs. By distant, one may assume that neurons lying within one centimeter (with an average transmission delay of 4-6ms) compose local assemblies; above that, neurons compose large scale assemblies (with an average transmission delay greater than 8ms) (Girard et al., 2001; Varela et al., 2001).

Considering that neuronal assemblies occur both in local and large scales, temporal delays between neurons that comprise the same assembly are inevitable. For this reason, it is important to stress that neuronal assemblies are formed by neurons that present temporal correlation in their firing, but are not strictly synchronous - synchrony in the sense of simultaneous firing may occur locally, in nearby neurons, but generally neurons that belong to the same assembly are synchronous in the sense that their activity presents synchronous response episodes (Tsukada et al., 1996).

The above definition reinforces the role of time in establishing functional networks, regardless of spatial connectivity. More precisely, anatomical connections constrain and provide a substrate upon which functional networks unfold, but only the emergent dynamics of the whole system determine the assembly functionality. However, the whole process is much more complicated - although maps of brain connectivity have been established and are continuously improved

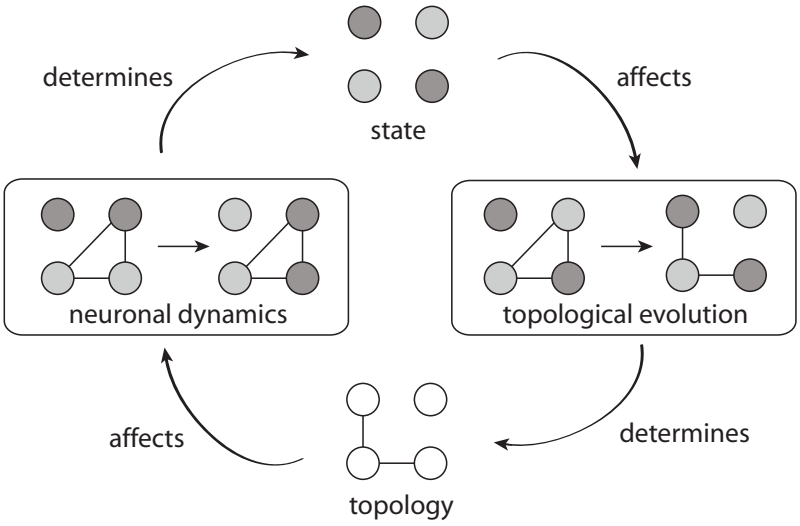

Figure 2.2: Interplay between structural and functional connectivity dynamics. Figure adapted from Gross & Blasius (2008).

(Hagmann et al., 2007, 2008), the dynamics of synaptic modification in the adult brain are still a point of controversy (Bullmore & Sporns, 2009). In the same manner that structural connectivity shapes the formation of functional networks, functional assemblies can modify the synaptic connections via activity-dependent mechanisms (Passingham et al., 2002; Sporns, 2011). The main difference is that functional connectivity is observed on fast as well as slower time scales whereas structural connectivity have a much slower plasticity dynamics (Sporns, 2011). Figure 2.2 illustrates the interplay between structural and functional connectivity.

In the next section, we explore an important problem that emphasises how synchronisation mechanisms bind structural and functional networks (assemblies) which underlie cognitive processes.

The Superposition Catastrophe problem

The theory devised by Hebb states that the basic functional unit of the brain is the cell assembly, which is formed by neurons with coherent firing activity and that have their anatomical connections reinforced by a plasticity rule. The previous section highlighted some problems with this approach, with focus on the spatial pattern of functional connectivity and the temporal properties of cell assemblies; however, another problem becomes evident.

According to the above theory, upon the onset of e.g. a visual stimulus a given group X of neurons would present an increase in the mean firing rate and thereby one could associate that neuronal group to the stimulus processing (Figure 2.3). A different stimulus would also elicit the formation of a possibly different neuronal group Y (detected by an increase in the firing rate

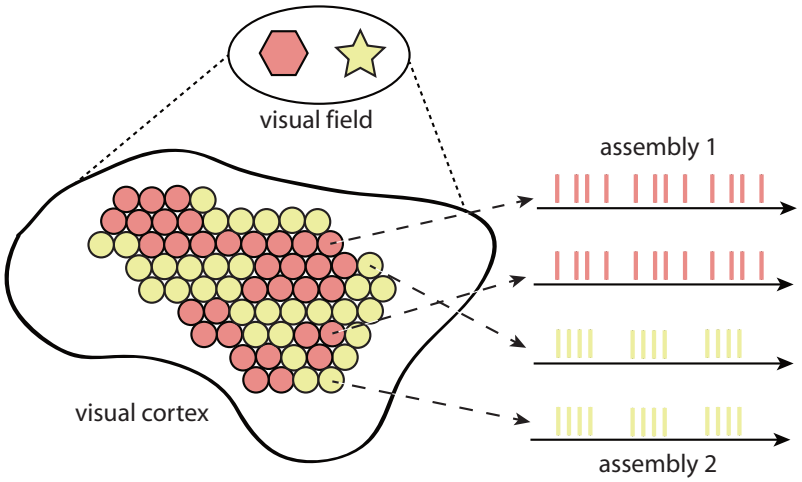

Figure 2.3: Illustration of the superposition catastrophe problem. The presentation of two different visual stimuli increase the firing rate of neurons and elicit the formation of two assemblies, each corresponding to the recognition of one object. If objects are presented concurrently, it is impossible to distinguish between the two assemblies in terms of their increase in firing rate. If, instead, one considers the temporal correlation of neuronal activity as the basic mechanism in the formation of neuronal assemblies, the superposition catastrophe is suppressed. Figure adapted from Engel (2010).

of some neurons). In this way, both patterns could be identified without problems. However, if the stimuli are concurrent, the neuronal responses corresponding to each pattern superpose and it becomes impossible to distinguish between the two assemblies in terms of their increase in firing rate. This is known as the *superposition catastrophe problem* (von der Malsburg, 1981, 1986).

To overcome this issue, von der Malsburg proposed the temporal correlation of neuronal activity as the basic mechanism in the formation of neuronal assemblies, as opposed to the firing rate approach. Therefore, in the scenario above, assembly X (comprised of neurons firing in synchrony) could be distinguished from assembly Y (also comprised of synchronised neurons) because the temporal properties of these two groups are different. Even if both assemblies are firing synchronously with the same frequency, they would still be separable e.g. due to different phase relationships (Burwick, 2006, 2008).

"Binding by synchrony" solves not only the superposition catastrophe problem but is also a widely accepted solution for the *binding problem* (Singer, 1999), explained as follows: there is plenty of evidence, especially in the visual system, that the brain responds to stimuli in a distributed way i.e. different features of the stimuli are processed by different spatially distributed assemblies. Two objects with different features (shapes and colours, for example) elicit a distributed neuronal activity related to different properties of each feature (square and circle, black and

white, for example). Upon the simultaneous presentation of the objects, the region related to shape processing would fire for both square and circle in the same manner that the colour-related region would fire for both black and white, thus posing a challenge of how the independent integration of the global properties of each object may happen.

If instead of the firing rates one considers the temporal relations between the neurons of the assembly, then each region can unambiguously encode for different properties of the same feature of the objects because the same neuron that participates in the processing of a given feature can be recruited by different coexisting assemblies which correspond to different properties of the same feature. Note that this would represent a temporal code but also a relational code, as the activity of each neuron depends on the emerging dynamics of the other neurons within the assembly (Singer, 1993).

A variety of computational models have implemented the concepts of temporal coding and succeeded in solving the above problems and others that share related issues. In this context, phase models are well suited to capture the dynamics of temporal correlations because they explicitly represent the time evolution of each unit in the network and have emergent synchronisation dynamics (Tononi et al., 1992; Burwick, 2006, 2009).

In summary, all of the above reinforce that normal brain function, more specifically the selective processing of information, perception, and stimuli integration, rely on functional, transient, and spatially distributed networks, brought about by synchronised interactions of neuronal assemblies. Nevertheless, mainly due to technical difficulties, it is still challenging to identify, characterise, and record the activity of neuronal assemblies and their multi-scale spatiotemporal interactions (Akam & Kullmann, 2010; Hipp et al., 2011).

The rate code, the temporal code, and other coding paradigms associated to the so-called neural code will be further detailed in Section 2.3. The next section explores the findings relating synchronisation of brain activity and cognition, with special attention to embodiment and enactive behaviour.

2.2.2 Synchronisation and cognition

Neuronal synchronisation is considered the mechanism linking brain processes to cognitive processes. As mentioned previously in this chapter, cognitive processes are grounded on fast-changing spatiotemporal functional networks that emerge on top of slow-changing structural networks by means of flexible synchronisation mechanisms.

Cognition is closely related to the guidance of behaviour. In this sense, the traditional approach for investigating neuronal correlates of cognitive processes is to perform electroencephalogram

(EEG) and magnetoencephalogram (MEG) recordings, or more invasive recordings, whilst the animal is engaged in a behavioural act. Despite the differences in neuroanatomy, there is evidence that functional-structural interactions mediated by synchronisation activity are conserved between and within species throughout mammalian evolution (Cantero & Atienza, 2005). The interactions comprise oscillations and transient neuronal assemblies with a strong temporal correlation with external stimuli as well as rhythms that have no direct link to sensory events but are thought to mediate higher cognitive functions; in other words, different behavioural tasks correspond to diverse functional networks and are associated with distinct synchronisation patterns between functionally specialised brain regions.

Alpha waves (8-12 Hz), the first to be observed in EEG recordings (see Section 1.2), are associated to attention and states of alert (Klimesch, 1999). Alpha oscillations increase when an awake relaxed adult closes its eyes, and decrease with eyes opened or during REM sleep periods. The adult brain, during a resting state, presents a considerably higher alpha power in comparison to the children, elderly, or unhealthy brain; also, a larger decrease (desynchronisation) in the alpha power of a healthy adult brain relates to good memory and cognitive performance.

On the other hand, theta waves (4-7 Hz) have an almost opposite behaviour, decreasing during resting states and increasing during memory and cognitive tasks. Interestingly, theta waves are very prominent in rodents, mediating neural plasticity, locomotion, and other exploratory behaviours, but they are harder to detect in the human EEG. However, recent intracranial EEG techniques enabled the recording of much smaller networks in the human brain, revealing that theta is involved in verbal and spatial memory tasks (Kahana et al., 2001).

One of the most studied rhythms is the gamma rhythm (25-100 Hz), considered to be directly linked to the creation and maintenance of neuronal assemblies, memory, and attentional processes (Ward, 2003; Buzsáki, 2006; Kopell et al., 2010). It is also present during REM sleep (Llinas & Ribary, 1993), which originates speculations on its role in the establishment of consciousness states (Cantero & Atienza, 2005; Melloni et al., 2007).

Finally, beta waves (12-30 Hz) are mainly associated to movement preparation, muscle contractions, and movement onset (Zhang et al., 2008), but recent results indicate that this rhythm is related to the maintenance of the current sensorimotor or cognitive state (Engel & Fries, 2010).

In general, there is no specific neuronal rhythm during the execution of a given cognitive task, but a collection of different waves spanning the frequency spectrum, which vary depending on the recording technique and the point of measurement. The important observation is that there is a substantial amount of studies showing that local and large scale integration in the brain, which underpin sensorimotor coordination, memory formation and retrieval, perception, emotion, etc., is

reflected in the interplay of multiple neuronal rhythms (Siegel et al., 2012). Also, there is evidence that synchronisation phenomena are influenced by the context-dependent sensory stimuli configuration and top-down attentional processes. We close this section exploring the influence of the body, action, and active action planning in neuronal synchronisation and cognition.

The body's influence on synchronisation and cognition

Based on some of last century's the most influential philosophers, such as Heidegger, Dewey, and Merleau-Ponty, a paradigm shift towards an embodied situated approach to cognition has taken place in cognitive science, neuroscience, and artificial intelligence (Varela et al., 1991; Brooks, 1991a; Clark, 1997; O'Regan & Nöe, 2001; Pfeifer & Bongard, 2006; Kurthen, 2007; Stewart et al., 2010). Before describing the neurodynamical implications, let us first highlight some of its most relevant concepts.

We mentioned that cognition is strictly related to behaviour, but the latter is not programmed in the animal, it is rather an emergent process resulting from sensorimotor interactions in the environment. Therefore, a situated body is a mandatory component of a cognitive system, and as a consequence cognition and brain functioning cannot be properly appreciated without taking into account brain-body-environment interactions. The more radical, less intuitive claim that has been posed by this approach is that a complex intelligent behaviour may emerge out of simple, sometimes spontaneous mechanisms, which would naturally arise from sensorimotor interactions, morphological and environmental computations (Pfeifer & Scheier, 1999). In the words of Pfeifer & Bongard (2006), "intelligent behavior comes about without the need for rational thought".

Imagine yourself engaged in a "simple" behaviour such as walking downhill. According to the classical view, your brain receives external sensory information from e.g. your feet, skin, and eyes, integrate them all with the existent memory (you probably want to avoid a banana peel more than a shredded newspaper), and generates an appropriate motor response. In this task, the walking control alone is extremely hard - the body has many degrees of freedom, the environmental conditions (ground friction, wind speed, etc.) are diverse - and would constitute a challenging problem for a central control system (brain). Conversely, in the embodied situated approach, the brain 1) exploits a body that is constrained by its morphological constitution and 2) exploits the environment and the forces of gravity, viscosity, and friction, thus drastically reducing the number of possible actions through the establishment of sensorimotor synergies. In this way, walking is a much easier task to accomplish considering the joints of the legs, the flexible tendons, the gravity, and the slope of the terrain. If the brain, for example, changes the angles between the feet and

the ground, a tendon's stiffness or a muscle contraction, walking can turn into running as a result of the morphological properties of the body and the environment. Also, more than simply tuning the body, active sensorimotor interactions can induce sensory correlations which reduce the complexity of an otherwise independent sensory stimulation - action shapes perception.

Work in robotics deeply contributed to developing and incorporating the situated embodied approach to the study of cognition. Brooks initiated the criticism of cognitivism and symbolic reasoning by showing with autonomous robots that complex behaviours emerge out of simpler structures due to interactions with the body and the environment. Studies that followed demonstrated, with robots, the dependence of behaviour on the coupling between brain, body, and environment (Ijspeert et al., 2005; Fleischer et al., 2007; Izquierdo, 2008; Pitti et al., 2010; Bigge & Harvey, 2010; Hoffmann & Pfeifer, 2011), also showing that an enactive agent induces regularities in the sensory information acquired and actively modulates the flow of information between the system's components (Lungarella & Sporns, 2006; Pitti, 2007; Pitti et al., 2009). Importantly, the robotics approach facilitated studies about the influence of social interactions in learning, memory, and cognitive performance of both grouped and individual agents (Marocco et al., 2002; Quinn et al., 2003; Mitri et al., 2012; Wischmann et al., 2012). Finally, the incorporation of evolutionary techniques in robotics, Evolutionary Robotics, was fundamental for the development of more advanced robotic controllers as well as for the formulation and testing of biological hypotheses using artificial agents (Husbands et al., 1998; Reil & Husbands, 2002; Philippides et al., 2005; Floreano et al., 2008; Dale & Husbands, 2010), helping to bridge the gap between artificial and biological systems.

With plenty of evidence from works in robotics, the embodied enactive approach slowly permeated neuroscience. Similarly to what have been found with artificial agents, neurobiological studies reinforced the role of the enactive body in perception and cognition (Engel, 2010). This is clearly seen in the developmental process, where action-dependent plasticity mechanisms together with sensorimotor interactions continuously shape the structural and functional neuronal circuits, affecting learning and behaviour (Munte et al., 2002; Majewska & Sur, 2006; Eagleman & Dragoi, 2012). Moreover, top-down attentional processes and predictions about sensory stimuli and outcomes of actions modulate cortical dynamics in such a way that behaviour becomes a product of interactions between the active brain, the morphological structures of the body, and the dynamic environment (Engel et al., 2001).

Synchronisation of neuronal groups is considered a plausible mechanism to account for the processes described above. The hypothesis is that ongoing brain activity, represented by intrinsic dynamic patterns of synchronisation, is modulated by a variety of neuronal processes such as

memory, attention, and action planning (Fries et al., 1996; Riehle et al., 1997; Von Stein et al., 2000; Ward, 2003; Van Der Werf et al., 2010; Landau & Fries, 2012). Instead of simply processed, incoming sensory stimuli interact with ongoing brain activity, thus the temporal properties of both internally/externally generated signals contribute to the formation of functional networks which in turn are associated with cognitive processes and behaviour (Engel et al., 2001; Tort et al., 2008). For example, it has been shown that selective attention can modulate neuronal synchronisation to attend to different modalities of stimuli, resulting in the formation of different transient neuronal assemblies which enhance the processing of the attended modality whilst suppressing the unrelated stimuli (Steinmetz et al., 2000). Also, Churchland et al. (2010) and Deco & Hugues (2012) describe that the variability of neuronal activity across trials, which hinder neuronal processing from an information theoretic point of view, is reduced as a result of stimulus onset and attention, thus improving information encoding. Finally, brain activity patterns elicited by anticipation or prediction of incoming stimuli were found to correlate with that of subsequent activity observed during behavioural acts (Riehle et al., 1997; De Oliveira et al., 1997; Lima et al., 2011); this is also the case in motor action planning (Andersen & Cui, 2009; Saleh et al., 2010; Rosenberg-Katz et al., 2012) and in passive versus active sensory stimuli acquisition (Krupa et al., 2004; Stapleton et al., 2007). The main advantage of preceding neuronal activity is in improving the reliability and reducing the time for the establishment of correlated temporal responses (assemblies), thus enhancing cognitive performance and behaviour.

The previous sections emphasised that cognition is mediated by a variety of neuronal activity. In the next section, we explore which aspects of this activity may convey more information about stimuli and hence be a good candidate to integrate what has been known as the neuronal code.

2.3 The neuronal code

Neuronal activity is characterised by the build-up and decay of membrane voltages or action potentials. In this sense, neurons communicate through excitatory or inhibitory spike trains. Investigations on the essence of the neuronal code are concerned with which aspects of this train are more relevant from an information theoretic point of view, i.e., which properties of the action potential activity, e.g. the number of spikes per second, the time between spikes, or the phase of firing in relation with ongoing activity, contains information about sensory stimuli that may be used by downstream neurons to produce appropriate behavioural response. For that reason, when studying different hypotheses regarding neuronal codes it is equally important to consider which mechanisms would be needed to read the proposed code, and test for its biological feasibility.

Figure 2.4(a) shows the basic concepts regarding neuronal codes, which are characterised

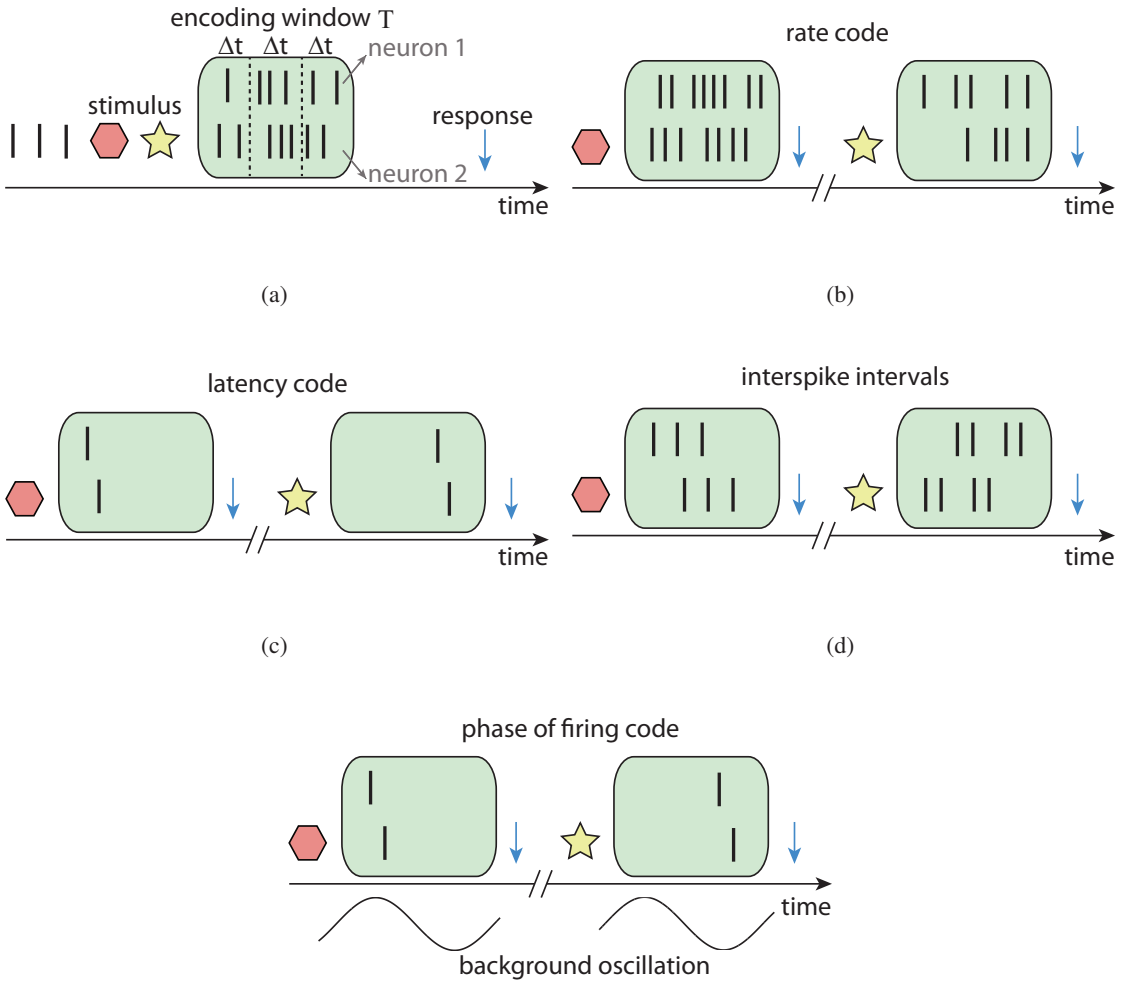

Figure 2.4: Different neural code paradigms. **(a)** Representation of the basic concepts of analysis: the encoding time window T and the temporal precision Δt, different stimuli, response, and the spike train (denoted by short vertical lines). Upon stimuli onset, the spikes from one or more neurons within the encoding time window form the basic elements of the code, which could then be exploited to produce stimulus-specific responses. **(b)** Rate code, in which different stimuli correspond to different spike firing rates. **(c)** Temporal latency code, in which information is conveyed by the time between stimulus onset and the corresponding first neuronal spike response. The time reference frame is externally defined by stimulus onset. **(d)** Interspike temporal code, in which information is conveyed by the time between consecutive spikes. The time reference frame is independent from external stimulus onset. **(e)** Phase of firing code, in which information is conveyed by the spike time relative to an internally generated rhythm that serves as the time reference frame. Adapted from Panzeri et al. (2010).

empirically by two main properties (Panzeri et al., 2010): the encoding time window T and the temporal precision Δt. The first is defined as the time window of duration long enough to encompass the neuronal activity that forms the basic elements of the code but shorter than change in stimulus features and behavioural acts; the latter consists of sampling time scale with which action potentials have to be sampled to guarantee no information is lost. Notice that, by definition, the temporal precision has to be shorter than the encoding time window.

In the subsections that follow, we explore two of the most relevant neuronal code paradigms, namely the rate code and the temporal code. Following the key described in Figure 2.4(a), Figures 2.4(b) to 2.4(e) highlight the properties of each of the above codes upon stimuli presentation. Finally, we conclude with approaches to read the code.

2.3.1 Rate code

In rate coding (Figure 2.4(b)), the assumption is that stimulus information is contained in the firing rate of the neuron, i.e. properties of the stimulus being processed are reflected by the number of action potentials within an encoding time window. This approach dates back to the work of Adrian and collaborators (Adrian & Zotterman, 1926; Adrian, 1928), who showed that the flexion force in a muscle is directly proportional to the firing rate of neurons projecting to that muscle.

There are mainly two forms of defining a rate code (Rieke et al., 1997; Gerstner & Kistler, 2002): spike count average over time and spike count average over runs (see Figure 2.4(b)). The first is simply the number of spikes occurring in the duration of a time window T divided by T. In the second, the number of spikes occurring every T seconds is recorded at every run and then averaged over the total number of runs; one can also average by counting the spikes occurring at every Δt seconds in all runs and then divide by the total number of runs, which results in a spike density measurement.

A possible application of rate codes is in the transmission of an analog stimulus over long distances. Although only two consecutive spikes suffice to estimate the rate, using a larger number of spikes could alleviate spurious effects caused by spike irregularities and noise. However, this strategy is also a strong point against practical rate codes because behavioural acts typically occur in a faster time scale than the one required to average a sufficient number of spikes. Notwithstanding, some of the experimental evidence of rate codes do not present this problem exactly because the studies are performed in a scenario where the stimulus and the behavioural responses vary slowly (Gerstner & Kistler, 2002). Additionally, if one considers averaging across many trials as an alternative strategy of reliable rate codes, a similar problem arises: behavioural decisions are commonly based on single events, therefore a code that demands a certain number of reoccurring

events prior to any decision is not likely to account for any brain process. Finally, as described in Section 2.2.1, rate codes suffer from the superposition catastrophe problem.

2.3.2 Temporal code

Temporal codes are defined when the information within the encoding time window is other than solely the number of spikes, that is, the temporal structure of spikes carry information. In fact, it has been shown that temporal patterns of spikes can encode much more information about the stimulus and be more reliable than rate codes (Gerstner & Kistler, 2002; Kayser et al., 2009; Jacobs et al., 2009; Panzeri et al., 2010). For example, consider an encoding time window T divided in 5 time bins Δt. In a rate code, the information capacity is $log_2(6) = 2.6$ bits whilst in a temporal code the information capacity is 5 bits.

There are many forms of exploiting a temporal code, and here we analyse three (see Figures 2.4(c), 2.4(d), and 2.4(e)):

- latency code (Gawne et al., 1996): sometimes referred to as time-to-first-spike code, the information is conveyed by the time between stimulus onset and the corresponding first neuronal spike response. Some researchers argue that in addition to being a simple and energetically cheap code, most of the relevant information is in the first spikes after stimulus onset (Tovee & Rolls, 1995; Thorpe et al., 1996), which supports latency codes. Its main limitation is the dependence on the precise knowledge of the external stimulus time, used as a reference frame; the brain, however, does not always have a reliable access to such precise knowledge (Panzeri et al., 2010), therefore this type of code might not be relevant within the brain.

- interspike interval code (Reich et al., 2000): information is conveyed by the time between consecutive spikes. Therefore, the time frame of reference is internally generated and independent from the external stimulus. This form of coding is considered to be more effective than the latency code because 1) it does not need the external stimulus as a time reference frame, 2) the relative timing between spikes presents less trial-to-trial variability than the latency code, and 3) it has an enhanced capability of encoding information compared to both latency and rate codes (Lundstrom & Fairhall, 2006).

- phase of firing code (Kayser et al., 2009; Nadasdy, 2009, 2010): information is conveyed by the spike time relative to an internally generated rhythm that serves as the time reference frame, hence the name phase code. This code has many advantages such as high spatial and temporal information resolution, robustness to noise and delays, and the possibility of

encoding diverse types of sensory data. In this sense, a possible function for the rhythms explored in Section 2.2.2 is to provide a time frame of reference relative to which neuronal activity could encode information without having to rely on externally generated timing.

Despite all the different hypotheses on how the brain exploits the neuronal action potentials to encode, transfer, and recollect information about stimulus, most likely the neuronal code is a combination or a synergistic cooperation of multiple codes, each providing complementary information (Jacobs et al., 2009; Panzeri et al., 2010). Moreover, although we focused on a few groups of neurons to explain the different coding paradigms, evidence points at stimuli coding and processing depending on the response of a large number of neurons, therefore the theory presented above should be considered at a population level (Singer, 1999; Pouget et al., 2008). Additionally, it is fundamental to further understand the essence of the neuronal code and what the basic unit of information is for it influences data analysis and the understanding of neuronal mechanisms of computation.

Finally, even if we record spiking activity and demonstrate that a given coding paradigm encodes all the information to disambiguate between stimuli, that does not imply that the brain is actually using this code - mechanisms to extract the information are necessary. In the next section, we investigate some approaches for reading the neuronal code.

2.3.3 Reading the neuronal code

The basic assumption when investigating mechanisms capable of reading the neuronal code is that downstream neurons are sensitive to the characteristics of the code employed by upstream neurons. Whilst there is evidence for a great number of mechanisms employed by such neurons (Buzsáki, 2010), the physiological details are beyond the scope of this thesis; furthermore, according to the embodied enactive approach presented in Section 2.2.2, there may not even be an explicit decoding system. Rather, we will focus on algorithms and techniques of decoding (i.e. predict the stimulus or behaviour) based on measured neuronal activity.

Given a neuronal population activity (e.g. a collection of spike trains or local field potentials), the problem is to find a relationship between different properties of the physiological measurements and the stimulus presented or the behaviour observed. The goal is to have a system that produces an output, easy to understand, that predicts the stimulus or behaviour.

A common approach is to use a Bayesian decoder (Oram et al., 1998). Based on Bayes' rule, it is a method that estimates the stimulus probability given the observed neuronal response, based on probabilities estimated previously from neuronal responses elicited by a known set of stimulus. Equation 2.8 describes the method.

$$P(s|r) = \frac{P(r|s) \cdot P(s)}{P(r)} \tag{2.8}$$

where $P(s|r)$ is the conditional probability of a stimulus s given a response r, $P(r|s)$ is the probability of observing the neuronal response r upon presentation of stimulus s, $P(s)$ is the probability of presenting a stimulus s, and $P(r) = \sum_s P(r|s) \cdot P(s)$.

The Bayesian decoder is widely used because, apart from limitations in estimating the probabilities from data, it is an optimal decoding method which is independent of the intrinsic properties of the relationship between the neural response and the stimulus. For instance, Jacobs et al. (2009) used a Bayesian decoder to calculate upper bounds in the information encoded by different coding paradigms - any method to decode the neuronal activity, including the one the animal actually employs, cannot have a performance greater than the Bayesian decoder.

Other methods such as support vector machines and artificial neural networks have been developed. An interesting strategy has been developed by brain-machine interface (BMI) studies, where robotic tools are controlled by a relatively simple linear model that predicts in real time the velocities of different actuators based on the neuronal activity. The approach was developed after findings relating the neuronal firing rate with movement velocity in primate's cortex (Carmena et al., 2003). For example, Lebedev et al. (2005) and Héliot et al. (2010) used a weighted linear combination of neuronal firing rates to predict the velocity of a robotic hand. See Equation 2.9.

$$V(t) = b + \sum_{\tau=0}^{L} w(\tau) n(t-\tau) + \epsilon(t) \tag{2.9}$$

where $n(t-\tau)$ is a vector of neuronal firing rates at time t and time lag τ, $V(t)$ is the velocity command at time t, $w(\tau)$ are the weights for each neuron at time lag τ, b is a constant, L is the number of time lags, and $\epsilon(t)$ is the residual error.

Other linear and non-linear readers have been proposed in addition to the strategy described above (Kim et al., 2006; Donoghue et al., 2007; Hatsopoulos & Donoghue, 2009). To assess the performance of different readers, a possible method is to build a "confusion matrix" (Quiroga & Panzeri, 2009), whose rows and columns correspond to different stimuli presentation and stimuli prediction by the decoder, respectively. The better the decoder, the more the matrix resembles the identity matrix; if the reader performs at chance levels, each entry in the matrix has a uniform probability determined by the number of stimuli.

The last section of this chapter explores a complementary approach, based on information theory, to study neuronal activity.

2.4 Information Theory and Neuronal Oscillations

Information theory (IT) has its origins in the work of Shannon, entitled "A Mathematical Theory of Communication" (Shannon, 1948). The work tackled problems of data storage and transmission in noisy channels, but was soon extended to a myriad of research fields. In neuroscience, the first applications of information theory focused on information transmission capacity of nerve cells (MacKay & McCulloch, 1952; Rapoport & Horvath, 1960) and information transmission constraints linking the formation of neural structures and perception to statistical properties of external sensory stimuli (Attneave, 1954; Barlow, 1961).

Information theory, in the context of neuronal oscillations, focuses on quantifying the amount of information encoded in neuronal signals rather than extracting and producing an output related to stimulus or behaviour prediction. Generally, the methods estimate how much the uncertainty about a given neuronal or behavioural phenomenon is reduced upon knowledge of other variables, or, alternatively, how much information is gained about neuronal or behavioural activity upon the observation of other variables. The appealing aspect of information theory is its mathematical rigour in establishing which features of the stimulus may be encoded in the neuronal activity as well as the reliability, dynamics, and influence of this activity in relation to behaviour. Below, we highlight some applications of information theoretic approaches in neuroscience (Borst & Theunissen, 1999):

- IT can estimate and provide upper-bounds for the efficiency and capability of different coding paradigms; in this way, one can e.g. estimate whether a rate code carries enough information about a sensory stimulus, or establish the appropriate time window to investigate temporal neuronal responses. For instance, IT studies showed that phase codes encode much more information than rate codes (Jacobs et al., 2009; Schyns et al., 2011).

- IT can estimate information dynamics without making any a priori assumptions about the underlying mechanisms that generated the stimulus or the response.

- IT can estimate how much information about a single stimulus feature or combinations of different stimulus or features is encoded by the neuronal response.

Nowadays, information theoretic tools are widespread in neuroscience research (Milenkovic et al., 2010; Dimitrov et al., 2011), but they have also been used to explore the relationship between information dynamics and behaviour in real and simulated artificial systems. For example, using a chaotic oscillator coupled to different robotic architectures, Pitti and collaborators (Pitti et al., 2009, 2010) explored the mechanisms underlying the control of

motor synergies and showed a correspondence between synchronisation and robust behaviour; Lungarella & Sporns (2006) used different information theoretic tools to analyse the information flow in sensorimotor networks of various robotics systems, stressing the relationship between body, environment, and information processing; in the same sense, Williams & Beer (2010) used an evolved agent in a relational categorization task to introduce a new information-theoretic approach to study the dynamics of information flow in embodied systems, complementing the more established dynamical systems analysis.

According to the definition, information is not an absolute value obtained from a measurement but rather a relative estimation of how much you can still improve in your current knowledge about a variable. Commonly, transmitter-receiver modelling involves random variables and the inherent uncertainty in trying to describe them is termed *entropy* (Shannon, 1948; Cover & Thomas, 1991). It is an intuitive notion of a measure of information, described by Equation 2.10:

$$H(X) = -\sum_{x \in A} p(x) \log_2 p(x) \tag{2.10}$$

where X is a discrete random variable defined for an alphabet A of symbols and probability mass function $p(x)$. The logarithm base defines the unit of information - for a base 2, entropy is given in bits.

For example, the entropy of a single toss of an unbiased coin is 1 bit because the uncertainty regarding the result of the coin toss can be resolved with a 1 bit message (e.g., 0 if the outcome of the toss is head, 1 if it is tail), which can be easily verified by $H(coin\ toss) = -(p(head) \log_2 p(head) + p(tail) \log_2 p(tail)) = -(0.5 \cdot -1 + 0.5 \cdot -1) = 1$ bit.

From the definition of entropy, many other quantities that reveal different aspects of the relationship between variables can be measured. For example, a quantity named mutual information (Equation 2.11) measures the mutual dependence between two random variables, that is, it measures the reduction in uncertainty about one random variable given knowledge of another. The higher the mutual information value (in bits), the more the uncertainty is reduced (notice that a value of zero indicates that the variables are independent).

$$I(X, Y) = H(X) - H(X|Y). \tag{2.11}$$

where $I(X, Y)$ denotes the mutual information between the random variables X and Y, $H(X)$ is the entropy of X and $H(X|Y)$ is the conditional entropy of X given Y.

Mutual information has been vastly employed in neuroscience, uncovering aspects of neuronal dynamics such as synchronisation dynamics and behavioural correlates (Hatsopoulos et al., 1998; Manyakov & Van Hulle, 2008), neuronal communication (Rolls et al., 2003; Szczepanski et al.,

2011), neuronal encoding of sensory stimuli (Mazzoni et al., 2008), and many others (Borst & Theunissen, 1999; Quiroga & Panzeri, 2009; Dimitrov et al., 2011). However, the theory originally developed by Shannon is not always adequate outside communication theory, specially in neuroscience, because of its nonstationary, nonergodic, and time-varying properties (Milenkovic et al., 2010). Some tools based on information theory attempt to extend the original formulation whilst alleviating the limitations to make them more feasible to study information dynamics in real and artificial systems. In the paragraphs that follow, we review a class of such tools, named "directed information" tools.

Directed information measures (Massey, 1990) are variants from the work of Granger on causal interactions (Granger, 1969). As a common feature, they provide a notion of exchange and directivity to the information flow through a communication channel, thus improving on symmetric correlative methods (such as mutual information) that are only capable of finding shared, directionless relationships between variables. This is interesting for neuronal studies for it allows the identification of functional networks in terms of the type of relationship between different brain regions or neuronal ensembles - it is possible to determine whether neuronal interactions are mutual or unidirectional.

In essence, Granger causality is inspired by the concepts of causality developed by Wiener (Wiener, 1956) and is used to determine whether one time series is useful in predicting another (Seth, 2007). Consider three time series: X_t, Y_t, and W_t. If, according to some performance criteria, the forecast of X_{t+1} given X_t and W_t is worst than the forecast of X_{t+1} given X_t, W_t, and Y_t, then we say that Y_t *Granger cause* X_{t+1}; in other words, past values of Y contains information above and beyond the information contained in past values of X for predicting future values of X.

The original formulation of Granger causality supposes that 1) the signals can be approximated by a linear description, 2) the signals are covariance stationary, and 3) the noise levels and interferences in measurements are minimum. These requirements are rarely fulfilled in neuronal studies, where interactions tend to be non-linear, subject to transmission delays, and prone to interferences in measurements such as EEG or MEG.

A technique called Transfer Entropy (Schreiber, 2000) incorporates the concepts of Granger causality in an information-theoretic measure (in fact, Granger causality and transfer entropy are equivalent for Gaussian variables (Barnett et al., 2009)) and defines a quantity more suitable to the study of neuronal phenomena for it is model-free, supports linear and non-linear processes as well as processes with delays, and is asymmetric (thus it can detect directional flow of information) (Vicente et al., 2011). Simply put, given two time series X and Y, transfer entropy can estimate the information about a future observation y_{t+1} given the available observations x_t^m and y_t^n that

goes beyond the information of the future state y_{t+1} provided by y_t^n alone. Importantly, parameters m and n define a "causality time window" or how far in the past one wishes to look for causal influences in the present; this can be very useful in determining the temporal properties of neuronal integrative properties (Gourévitch & Eggermont, 2007). In the next chapter, Section 3.4, we provide a complete description of the method.

For all of its properties, transfer entropy is increasingly being applied in neuronal studies in real and artificial systems (Lungarella & Sporns, 2006; Gourévitch & Eggermont, 2007; Honey et al., 2007; Honey & Sporns, 2008; Buehlmann & Deco, 2010; Neymotin et al., 2010; Williams & Beer, 2010; Vicente et al., 2011; Moioli et al., 2012), but many extensions have been developed to make it more adequate to diverse contexts (Staniek & Lehnertz, 2008; Ito et al., 2011). For instance, Williams & Beer (2011) developed two extensions to TE: the first aims at identifying state-dependent and state-independent transfers, i.e., whether the information transfer from the source to the target depends or not on the state of the target; the second quantifies the type of influence of multiple sources to the target, i.e., it determines for each source whether the influence on the target is unique, redundant, or synergistic. However, transfer entropy, likewise Granger causality, is still limited when applied to neuronal data, specially due to nonstationarities, interferences caused by preprocessing filtering, delayed interactions, and its restriction to bivariate time-series. Recent methods attempt to tackle some of these issues (Barrett et al., 2012; Runge et al., 2012), but given all of the above, results should be taken with care.

The next section provides a summary of all the topics presented in this chapter, highlighting the relevance to the thesis.

2.5 Summary

This chapter provided the theoretical basis for the development of the thesis. We started with a physiological description of the mechanisms underlying neuronal oscillations at both neuron-level and network-level scales, emphasizing the difference between oscillatory phenomena generated by ionic membrane currents and those generated by the electromagnetic field produced by the collective behaviour of neurons. Then, we described the four (arguably) most important computational models of neuronal activity - the integrate-and-fire model, Hodgkin-Huxley model, Wilson-Cowan model, and phase models - focusing on basic dynamic properties and applications.

The next section was devoted to synchronisation, an ubiquitous phenomena in natural and artificial systems. We showed how synchronisation facilitates neuronal communication and mediates the formation of neuronal assemblies, the basic unit of information processing in the mammalian brain. We put special effort in describing the spatiotemporal nature of transient assembly

formation and how it constitutes a sensible framework for tackling many cognitive neuroscience problems, such as the superposition catastrophe problem and the binding problem. The chapter concluded with an analysis of the situated body influence in neuronal activity, reinforcing that synchronisation of brain rhythms and cognition are intertwined with the morphology of the body and the physical environment; additionally, attentional processes, intentionality, and action planning, all modulate the neuronal activity and, ultimately, behaviour.

The next section explored different approaches to determining which aspects of a neuronal spike train - the number of spikes per second, the time between spikes, or the phase of firing in relation with ongoing activity - contain more information about sensory stimuli that may be used by downstream neurons to produce an appropriate behavioural responses. In other words, the chapter covered approaches to better understand the essence of the neuronal code. Also, we described methods and techniques for reading this code, and how they have been used in animal studies and in the development of brain-machine interface devices.

The last section focused on information theoretic approaches to study neuronal oscillations and cognition. More specifically, we explored the basic concepts of information theory and how its original formulation, together with recent extensions, is contributing to further understand the relationship between brain-body-environment interactions in natural and artificial systems. The emphasis was on "directed information" tools, specially transfer entropy, which enhance the traditional information theoretic tools by providing a measurement that is model-free, support linear and non-linear processes as well as processes with delays, and can detect the directional flow of information.

We now highlight how all these concepts are of relevance to the thesis.

2.5.1 Relevance to the thesis

Sections 2.1 and 2.2 described many open questions regarding the role of neuronal oscillations and neuronal synchronisation in cognition and behaviour. The two main objectives of this thesis are 1) to explore and shed new light into the role of neuronal synchronization and phase towards the generation of embodied cognitive behaviours and 2) to initiate an investigation on the efficacy of such systems as practical robot controllers; in this sense, we extracted research guidelines from the theory presented above.

According to Sections 2.2 and 2.3, the temporal properties of neuronal activity are fundamental in cognitive processes and behaviour, and carry much more information than frequency or amplitude alone. In this way, a model to study neuronal synchronisation, cognition, and behaviour should, foremost, include temporal dynamics. After reviewing computational models of neurons

and neuronal oscillators in Section 2.1.2, the clear candidates are phase models, given their relative simplicity and explicit focus on temporal interactions - hence our choice for the Kuramoto model of coupled phase oscillators in the experiments.

Also, Section 2.2.2 emphasised that cognitive systems cannot be fully understood without taking into account brain-body-environment interactions. To explore the synchronisation and oscillatory properties underlying behaviour, we chose to use simulated evolved robots engaged in minimally cognitive tasks. The control system of these agents, based on the Kuramoto model, takes into account the temporal properties of the neuronal network model, following the advantages of using a temporal code (Section 2.3.2), whose activity is read by a mechanism inspired by the method successfully employed in brain-machine interface studies, described in Section 2.3.3.

We perform three sets of experiments, focusing on topics of much controversy and with plenty of clarifications needed: the relationship of synchronisation properties with information dynamics and behaviour (described in Section 2.2 and explored by the experiments of Chapter 4), the influence of transient neuronal assemblies in information processing and behaviour (described in Section 2.2.1 and explored by the experiments of Chapter 5), and the synchronisation properties and information dynamics of spatially-embedded neurons with transmission delays (described in Section 2.2.1 and explored by the experiments of Chapter 6).

To investigate the results, in addition to the more traditional dynamical analysis, we explore the information transfer properties within and between the agent and the environment, as described in Section 2.4.

The next chapter describes with further details the models and methods employed in the experiments.

Chapter 3

Models and methods

This chapter describes the computational techniques used to perform the experiments developed in the following chapters. First, we provide the basics of Evolutionary Computation, focusing on Genetic Algorithms; then, we explain the paradigm adopted to synthesize systems with minimally cognitive behaviours, named Evolutionary Robotics, followed by a description of the Kuramoto model of coupled phase oscillators, used as an artificial neural system to model the internal dynamics of the simulated robots; the chapter concludes with a description of an information theoretic tool named Transfer Entropy.

3.1 Evolutionary Computation and Genetic Algorithms

Based on Charles Darwin's studies and his work on evolution and natural selection (Darwin, 1859), the biological sciences found alternatives to explain how populations interact, reproduce, and adapt to the environment. According to the theory, an individual better adapted to the environment is likely to have reproductive and survival advantages, thus propagating its genes to the next generation. This inspired the development of computational algorithms based on the Darwinian principles of evolution and natural selection.

Evolutionary Computation (EC) (Holland, 1975; Schwefel, 1981; Goldberg, 1989; Michalewicz, 1996) incorporates several proposals of evolutionary algorithms and is characterised basically by a manipulation of a population of possible solutions, which generates new possible solutions based on variations of the current set (reproduction). The environmental pressure on the individuals is associated to the problem to be solved; in this sense, each individual has a fitness score according to its performance in solving the task. In the presence of individuals with different fitnesses and a population with a limited size, with selection mechanisms operating in favour of

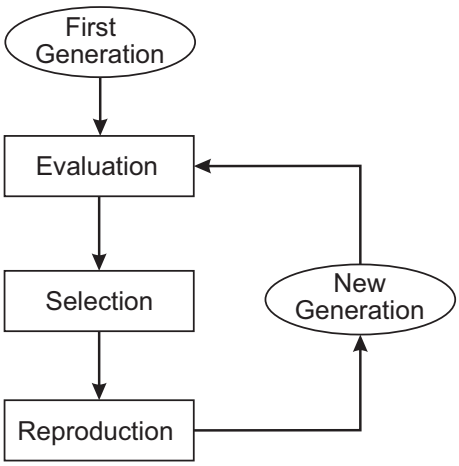

Figure 3.1: Main steps of a genetic algorithm.

the more adapted and reproduction operators causing aleatory variations, the average fitness of the population tends to increase over generations as a result of competition under limited resources.

In this way, EC is a biologically inspired iterative and parallel search tool, easy to hybridize, capable of dealing with multimodal problems, and appropriate to problems where the number of possible solutions to explore is computationally unfeasible to more traditional search and optimization techniques (Michalewicz & Fogel, 2000).

The most common evolutionary algorithms are the Genetic Algorithms (GA) (Holland, 1975), the Evolutionary Strategies (Schwefel, 1965; Rechenberg, 1973), Evolutionary Programming (Fogel, 1962), and Genetic Programming (Koza, 1992). Our focus will be on GA.

Figure 3.1 illustrates the main steps of a GA: initialization of the first generation, evaluation, selection, and reproduction with genetic variation.

The GA starts with an initial population of possible solutions to the problem (individuals). Every execution of the algorithm results in a new population, named new generation. Each individual has a genotype that encodes a candidate solution specific for the problem being solved. The genotype can be represented by a string or vector of attributes (chromosome) where each position of this vector (locus) has a value (allele) according to the coding format adopted (binary, integer, floating point, etc.); importantly, the coding format influences directly the search space and complexity. Then, the individual's genotype is mapped into the individual's phenotype (set of observable properties and characteristics of this solution) according to the problem under consideration. For example, in an aerodynamic shape optimization problem that employs binary coding, the value "1" in a certain position of the genotype may be mapped into the phenotype "round shaped", whereas a value of "0" may indicate "square shaped".

Next, each individual is evaluated in the task, attaining a performance (fitness) according to

its phenotypic characteristics and the problem. Fitness is determined by a fitness function, which measures the individual's suitability for solving the problem; it should guide the evolutionary process towards the expected solution and discriminate each solution in a relative way, thus creating a performance gradient among solutions. For example, in the "Travelling Salesman Problem" (Applegate et al., 2006), where one aims at finding the shortest route that visits a set of cities, returning to the departing point without visiting the same city twice, the fitness function could be defined as the inverse of the distance travelled.

The following step is the selection for reproduction based on the fitness value of each individual. The most common methods are (Fogel, 1994; Michalewicz, 1996; Miller & Goldberg, 1996):

- roulette wheel: the probability of choosing an individual is proportional to the value of its fitness in relation to the sum of the fitness of all individuals in the population;
- elitist: the individual with the highest fitness is chosen, together with another individual of the population (the criteria for this latter choice may vary and depends on the problem). The highest fitness individual is kept in the next generation to avoid that good individuals disappear from the population due to the reproduction process;
- tournament: a few individuals are randomly selected, and the one or two with highest fitness are selected to take part in the reproduction process. This method is more robust in avoiding premature convergence (loss of diversity) in the population;
- diversity-based selection: the most diverse individuals in the population are chosen;
- bi-classist: the $P\%$ best individuals are chosen together with the worse $(100 - P)\%$.

After selection, in the reproduction stage, the offspring is generated as a result of mutation and crossover operators applied in copies of the parents. The aim is to produce new, better adapted individuals that inherit characteristics that make their parents good solutions for the problem.

The crossover operator combines the genotype of two parents to generate one or more new individuals. The most usual operators are (Holland, 1975; Bäck et al., 2000a,b): single point, in which the parent's chromosome is cut at a given point and the new individuals are generated by swapping the segments; multiple points, similar to the previous operator but with two or more cutting points; uniform, in which each position in the genotype of the new individual is determined by the corresponding field in the genotype of one of the parents, randomly chosen.

The mutation operator produces a change at a randomly chosen position in the genotype. This can be a perturbation in the current value of the gene (following, e.g., a Gaussian or uniform

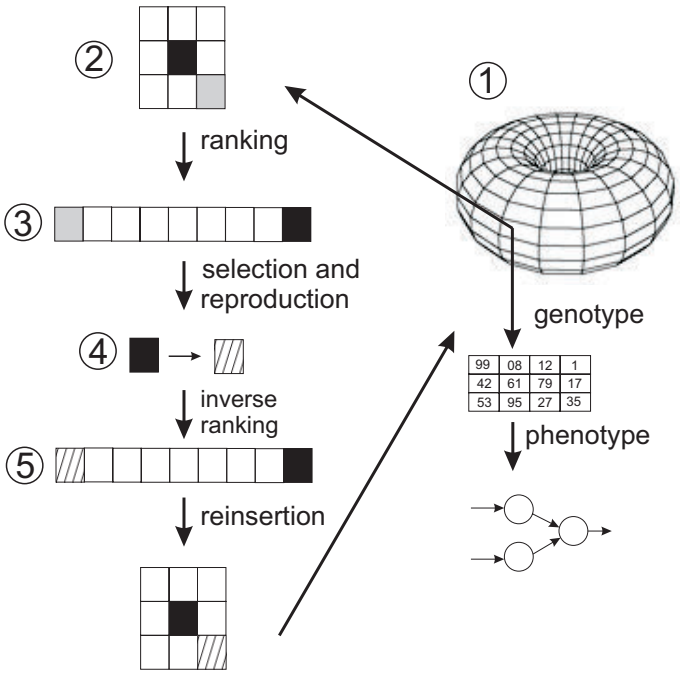

Figure 3.2: Distributed genetic algorithm operation. At every generation, a randomly chosen individual, together with its 8 neighbours, are selected from the toroidal grid. These individuals are ranked according to fitness, and the one with highest fitness (black) has a higher chance of reproducing. The lowest fitness individual, in turn, has a higher chance of substitution. The new individual is represented by the hachured square.

distribution) or it can be a new randomly chosen value within the maximum range permitted. Mutation operators aim at maintaining the diversity of the population and help to fine tune a solution (Holland, 1975), taking into account that crossover operators are not very effective in local search. In fact, Harvey (2001) argues that mutation alone can be a driving force in artificial evolution and that the lack of population diversity is not necessarily bad for the search.

After reproduction, the new individuals are reinserted into the population, substituting or not their parents, forming the new generation. Finally, the algorithm reinitiates until a stopping criterion is reached. There are several methods to terminate the algorithm (Bäck et al., 2000a,b), e.g. when the highest fitness in the population is above a certain threshold (and then the solution for the problem is given by the individual with the highest fitness), or after a maximum number of generations.

Two variations of GAs are used in the experiments in this thesis, and are detailed as follows.

Geographically distributed genetic algorithm

In the experiments of Chapters 4 and 5, a variation of the traditional GA, named geographically distributed genetic algorithm with local selection and replacement (Husbands et al., 1998), is used to determine the parameters of the systems. The genotype and the phenotype of individuals, the fitness function, and the maximum number of generations (stopping criterion) are specific to each experiment and are detailed in the corresponding chapters; nevertheless the structure of the algorithm is the same.

See Figure 3.2. The genotype of each individual consists of an array of integer variables lying in the range $[0, 999]$ (each variable occupies a gene locus), which are mapped to values determined by the range of their respective parameters. The population size is 49, arranged in a 7×7 toroidal grid (step 1). In a breeding event, a mating pool is formed by choosing a random point in the grid together with its 8 neighbours (step 2). The set is ordered according to the fitness of each individual and a single parent is chosen through rank-based roulette selection (step 3), according to Equation 3.1:

$$P(i) = \frac{i}{\sum_{j=1}^{j=N} j} = \frac{2i}{N(N+1)} \tag{3.1}$$

where $P(i)$ is the probability of an element i in a vector of size N being chosen, considering that the vector is ordered (0 to $N-1$) according to an increasing value of fitness.

Then, two mutation operators are applied (step 4): the first operator is applied to 20% of the genes and produces a change at each locus by an amount within the $[-10, +10]$ range according to a normal distribution. The second mutation operator has a probability of 10% and is applied to 40% of the genotype, replacing a randomly chosen gene locus with a new value within the $[0, 999]$ range in a uniform distribution. There is no crossover. The mutation produces a new individual, which is evaluated and placed back in the mating pool in a position determined by inverse rank-based roulette selection (step 5). In this way, the individual with the highest fitness can not be replaced by the offspring. The values adopted for the parameters of the GA were empirically defined, with similar results obtained with different grid sizes and mutation rates.

Steady-state Genetic Algorithm

The genetic algorithm described in this subsection is the one used in the experiments of Chapter 6. The algorithm, inbuilt in the robotic simulator used, is a variation of the steady-state genetic algorithm (Whitley & Kauth, 1988), in which there is no complete replacement of the older population by its offspring, but a substitution of a subset of the entire older population by newly generated individuals.

More specifically, this GA first generates a random population of 100 individuals. The genotype of each individual consists of an array of integer variables lying in the range $[0, 255]$ (each variable occupies a gene locus), which are mapped to values determined by the range of their respective parameters. At every generation, the 20 best (highest fitness) individuals are selected for reproduction, creating 5 new individuals each. The new individuals that outperform their parents in solving the task replace the worst individuals of the population. Also, the best individual from each of the 20 subpopulations is kept at every step of evolution (elitism). The mutation operator consists of replacing 2% of the genotype by randomly chosen values within the range $[0, 255]$. The algorithm runs for a maximum of 300 generations, and the highest fitness individual at the last generation is chosen as solution.

In Chapter 6 we provide more details about the GA and the fitness function used. The next section explains how genetic algorithms are used together with robotics to optimize the performance of agents in minimally cognitive tasks.

3.2 Evolutionary Robotics and Minimally Cognitive Tasks

Evolutionary Robotics (ER) is a relatively new field of interdisciplinary research grounded in concepts from Computer Science and Evolutionary Biology (Harvey et al., 2005; Floreano et al., 2008; Floreano & Mattiussi, 2008; Floreano & Keller, 2010). Originally devised as an engineering approach to automatically generate efficient robot controllers in challenging scenarios, where traditional control techniques have limited performance, ER is now well regarded among biologists, cognitive scientists and neuroscientists, as it provides means to simulate and investigate brain-body-environment interactions that underlie the generation of behaviour in a relatively unconstrained way, thus penetrating areas that disembodied studies cannot reach (Nöe, 2004; Pfeifer et al., 2007; Engel, 2010).

Consider a real or simulated robot, with sensors and actuators, situated in an environment with a certain task to accomplish. Each solution candidate (individual) is represented by a genotype, which contains the basic information of the agent's body and/or its controller's parameters (e.g. the number of wheels the robot has and/or the values of the weights of an artificial neural network acting as its controller). According to some criteria, normally the previous performance of that individual in solving the task (fitness), parents are selected and undergo a process of mutation and recombination, generating new individuals which are then evaluated in the task. This process is repeated through the generations, eventually obtaining individuals with a higher performance in the given task. In this sense, ER is a reasonable approach to studying embodied and situated behaviour generation, because it can be used as a powerful model synthesis technique (Beer, 2003;

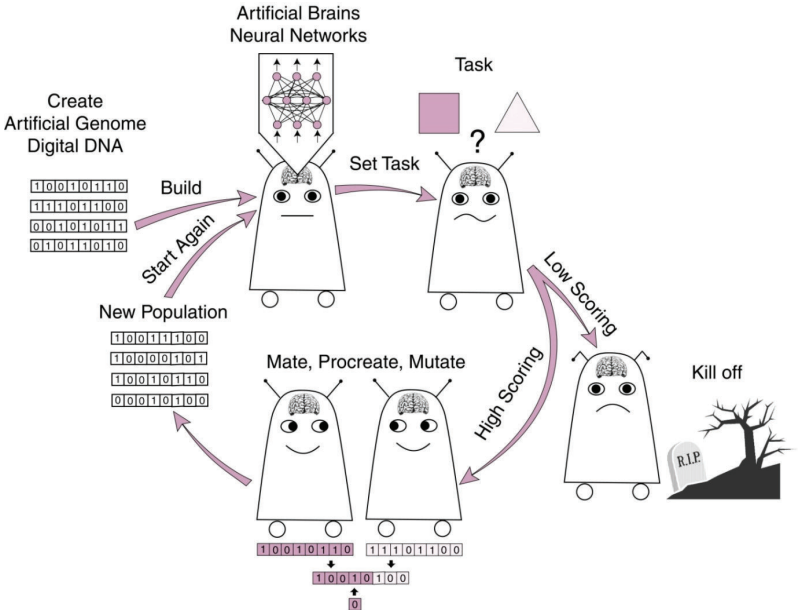

Figure 3.3: Main steps in Evolutionary Robotics (adapted from Rohde (2008)).

Husbands, 2009). Figure 3.3 illustrates the process.

Relatively simple, tractable models can be produced and studied in the context of what have been called Minimally Cognitive Tasks (Beer, 2003), which are tasks that are simple enough to allow detailed analysis and yet are complex enough to motivate some kind of cognitive interest. To name but just a few: Di Paolo (2003) used a simulated agent in a simple phototaxis task to show that the firing patterns and synaptic plasticity in an artificial neural network provide substrate for memory and learning of complex sensorimotor behaviours; Quinn et al. (2003) studied a formation-movement task, showing the emergence of collective behaviour, functionally distinct roles, and coordination in evolved teams of robots; Izquierdo (2008) and Gigliotta & Nolfi (2008) provided a series of examples demonstrating the need to consider the body and the environment, together with the agent's control system dynamics, to approach and understand learning and behaviour; Egbert et al. (2010) used a minimally cognitive model based on bacteria chemotaxis to investigate the relationship between metabolism and behaviour.

In the following chapters, a simulated robotic agent is evolved following the ER approach to solve different minimally cognitive tasks, each detailed in the corresponding chapter. The next section presents the Kuramoto model, the basis of the control system architecture, together with the implementation details of the evolutionary robotics framework.

3.3 The Kuramoto Model

In a study pioneered by Winfree (Winfree, 1980), the dynamics of a population of interacting limit-cycle oscillators have been approximated by a population of interacting phase oscillators, leading to a mean-field approximation model extensively explored by Kuramoto (Kuramoto, 1984). In his approach, the phase of each oscillator is determined by its natural frequency (drawn from some distribution) modulated according to a function that represents its sensitivity to the phase in every other node. See Equation 3.2:

$$\frac{d\theta_i}{dt} = \omega_i + \sum_{j=1}^{N} \Gamma_{ij}(\theta_j - \theta_i), i = 1, \ldots, N. \tag{3.2}$$

where θ_i is the phase of the *i*th oscillator, ω_i is the natural frequency of the *i*th oscillator, Γ is the phase interaction function (PIF) and represents the interaction between nodes, and N is the total number of oscillators.

If one considers the PIF to be periodic, i.e. $\Gamma_{ij}(x + 2\pi) = \Gamma_{ij}(x)$, it can then be expanded into a Fourier series. Considering only the first term of this series, and specifying that the network is symmetrically coupled with strength K, the previous model reduces to Equation 3.3, which is known as the Kuramoto model (see Figure 3.4(a)):

$$\frac{d\theta_i}{dt} = \omega_i + \frac{K}{N} \sum_{j=1}^{N} sin(\theta_j - \theta_i), i = 1, \ldots, N. \tag{3.3}$$

Notice that if nodes are uncoupled ($K = 0$), each oscillator has a self-sustained dynamics, and the individual phases increment by 2π in every period of oscillation (determined by the natural frequencies). Although not mandatory, it is common to define a phase reset threshold (normally 2π), above which the phase value of that node is reset to 0. Figure 3.4(b) illustrates this effect.

Basically, if the frequency of all possible pairs of nodes i and j ($i, j = 1, 2...n$) are equal, i.e. $d\theta_i - d\theta_j = 0$ or $\theta_i - \theta_j = constant$, the model is said to be globally synchronised. It is possible to calculate a synchronisation index, which gives a good idea of how synchronised the set of oscillators are (Kuramoto, 1984). Consider Equation 3.4, where r is the synchronisation index (1 meaning high synchronisation, 0 meaning incoherent oscillatory behaviour) and Ψ is the mean phase of the system.

$$re^{i\Psi} = \frac{1}{N} \sum_{j=1}^{N} e^{i\theta_j} \tag{3.4}$$

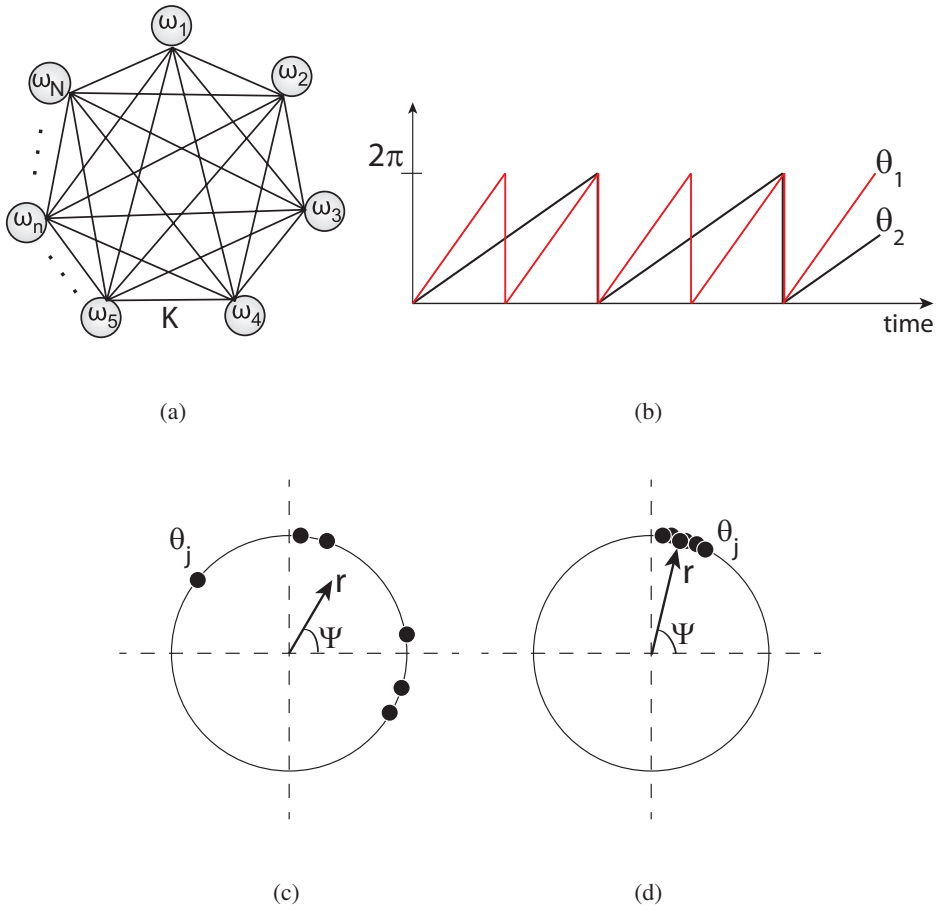

Figure 3.4: (a) Schematic representation of the Kuramoto model: a population of N interacting phase oscillators symmetrically coupled with strength K and natural frequencies $\omega_1, \omega_2, \ldots, \omega_N$. The activity of each node is modulated by all other nodes according to a phase interaction function (in the original formulation, the sin function is used). (b) Example of the phase dynamics θ_1 and θ_2 of two uncoupled oscillators with $w_1 = 2w_2$. (c) In an alternative representation, each oscillator (small black circle) is placed in the unit circle according to its phase θ_j. The complex number $re^{i\Psi}$ (Equation 3.4) is the centroid vector of the phase distribution in which r is the synchronisation index and Ψ is the mean phase of the system. In this particular example, the phases are widespread and the system is not synchronised. (d) Same as (b), but for a fully synchronised system.

The rationale for the above equation is as follows: each oscillator can be represented as a vector of magnitude 1 and angle corresponding to its phase $\theta_j \in [0, 2\pi)$, placed in the unit circle; the averaged sum of all vectors is the centroid vector of the phase distribution. Its magnitude $r(t)$ is a measure of phase coherence, and its angle Ψ is the average phase. See Figures 3.4(c) and 3.4(d).

One of the most interesting properties of the Kuramoto model is that by varying the value of the coupling between units the network can be tuned in subcritical, critical or supercritical regions

(Figure 3.5(a)) (Strogatz, 2000). In the subcritical region, the interactions between oscillators are very weak, leading to an almost total lack of any collective behaviour. In the supercritical region, the coupling is so strong that the whole system synchronises and behaves like a single giant oscillator. The critical region is characterized by a second-order phase transition region between the subcritical and the supercritical regions; it tends to exhibit complex, unstable dynamics. It has been claimed in recent years that systems operating in this critical region - and there is some evidence to suggest this includes biological neuronal networks - have better performance on a variety of tasks and process information in a highly efficient way (Beggs, 2008; Kitzbichler et al., 2009).

In the Kuramoto Model, the critical coupling value i.e. the value of the coupling between units that will induce the network to remain in this critical region is given by Equation 3.5:

$$K_c = \frac{2}{\pi g(w_0)} \tag{3.5}$$

where $g(w_0)$ is the value of the distribution of natural frequencies $g(\omega)$ formed by each oscillator's natural frequency ω calculated at the central frequency ω_0. See Figure 3.5(c).

The probability densities of the discrete frequency distributions are estimated using a smoothing kernel approach with automatic choice of window width, but other techniques may be used (Silverman, 1998). See Equation 3.6:

$$\hat{f}(\boldsymbol{x}) = \frac{1}{nh^d} \sum_{n}^{i=1} K \left\{ \frac{1}{h}(\boldsymbol{x} - \boldsymbol{X_i}) \right\} \tag{3.6}$$

where $\hat{f}$ is the estimate density, $X_1, \ldots X_n$ is the given multivariate data set whose underlying density is to be estimated, h is the window width, d is the dimension of $\boldsymbol{x}$, and $K(\boldsymbol{x}) = (2\pi)^{-d/2} exp(-1/2\boldsymbol{x}^T\boldsymbol{x})$ is the kernel function.

The optimum window width h_{opt}, assuming that the underlying distribution is Gaussian, is given by Equation 3.7:

$$h_{opt} = \{4/(d+2)\}^{1/(d+4)} \, n^{-1/(d+4)} \tag{3.7}$$

The Kuramoto model presents a series of properties that makes it suitable for the study of different types of synchronisation problems. A particularly interesting property is known as partial synchronism. Consider a network composed of 4 nodes (Figure 3.5(b)), where each node is connected to its immediate two neighbours in a shape similar to a ring. Depending on the coupling factor K and the natural frequency w_i of each node, the network can present a global synchronous behaviour, but Monteiro et al. (2003) showed that by changing the frequency of one node the

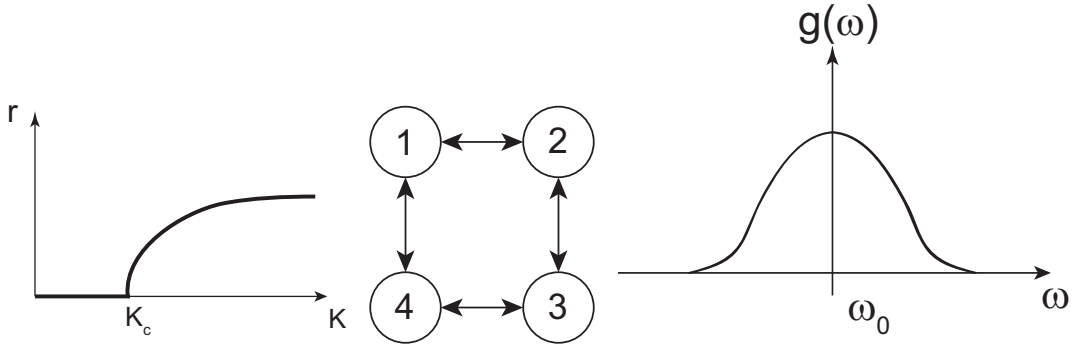

(a) (b) (c)

Figure 3.5: (a) Synchronisation behaviour obtained in the Kuramoto model, represented by the subcritical ($K < K_c$), critical ($K = K_c$), and supercritical ($K > K_c$) regions. (b) Example of a partially connected network with four nodes. (c) Representation of the distribution of natural frequencies $g(\omega)$ around a central frequency ω_0.

resultant network may exhibit partial synchronism, i.e., some of the nodes become synchronized while other nodes are not. Moreover, the oscillatory behaviour of one node can be influenced by another node in the network not necessarily connected to it: Tessone & Zanette (2012) showed that by manipulating the dynamics of highly disconnected systems (i.e. manipulating the interactions patterns between nodes) one can obtain different synchronisation patterns, including full synchronisation, resembling the behaviour obtained in densely connected architectures.

The importance of this property in mimicking brain related dynamics relies in the fact that different neuronal blocks could synchronise and influence other blocks, and in consequence different cortical areas could flexibly establish communication channels depending on their temporal activity. This is in agreement with some recent findings in neuroscience (Buzsáki, 2006), reinforcing the feasibility of applying the Kuramoto model to study cognitive processes.

Additionally, it has been shown that if the PIF Γ (Equation 3.2) incorporates more complex interactions between the nodes rather than the first harmonic only, the model displays a more complex spatio-temporal behaviour and the synchronisation patterns observed are closer to the ones measured in real brains (Hansel et al., 1995; Kitzbichler et al., 2009; Breakspear et al., 2010). Therefore, the Kuramoto model is highly relevant, at a certain level of abstraction, to modelling neural mechanisms underlying adaptive and cognitive behaviours (Bhowmik & Shanahan, 2012).

In the following chapters, the experiments will explore different aspects of the rich dynamics observed in the Kuramoto model to investigate the relationship between synchronisation, information dynamics, and behaviour. In the next section, we describe how the Kuramoto model is

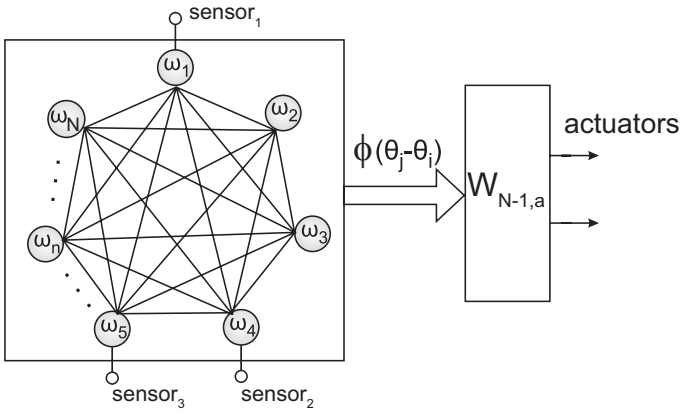

Figure 3.6: Framework for application in evolutionary robotics. This is the basic set-up used in all the experiments reported in this thesis; minor task- and model-related adjustments are made and explained in chapters 4, 5, and 6. The oscillatory network is composed of N fully connected oscillators, with some nodes connected to the robot's A sensors (each sensor is attached to a single node and no more than one sensor is attached to any given node). A phase-sensitivity function $\phi(\gamma)$ is applied to each of the phase differences $\gamma_{i,i-1}, i = 2 \ldots N$, then linearly combined by an output weight matrix, $W_{N-1,a}$, resulting in a signals that will command the a actuators of the agent.

incorporated into the framework for application in ER.

3.3.1 Framework for application in evolutionary robotics

The model developed here is inspired by the Kuramoto model, adapted so that it could be applied to control a simulated robotic agent. In this section we describe the basic framework, used in all of the experiments in Chapters 4, 5, and 6; there are minor, experiment-dependent variations to the model, which are described in the corresponding section of the following chapters.

Consider a robotic agent with A sensors and a actuators. The control system framework, illustrated in Figure 3.6, is composed of N fully connected oscillators, with some nodes connected to the robot's sensors (each sensor is attached to a single node and no more than one sensor is attached to any given node). The frequency of each node is the sum of its natural frequency of oscillation, w_i, and the value of the sensory input $I_i(t)$ related to that node (0 if there is no input), scaled by a factor z_i (Equation 3.8).

$$\frac{d\theta_i}{dt} = (\omega_i + z_i I_i(t)) + \frac{K}{N} \sum_{j=1}^{N} \Gamma(\theta_j - \theta_i) \tag{3.8}$$

The natural frequency w_i can be associated with the natural firing rate of a neuron or a group of neurons, and the sensory inputs mediated by z_i alters its oscillatory behaviour according to

environmental interactions, thus improving the flexibility of the model to study neuronal synchronisation (Cumin & Unsworth, 2007) within a behavioural context.

To control a robotic agent, a readout unit that captures the dynamics of the network and generates an output for the robot's actuators is necessary. An intuitive approach would be to use the dynamics of all the possible combinations of phase differences, and indeed that has been successfully done in Moioli et al. (2010b,a). However, as the system scales up in number of nodes, the number of phase differences grows exponentially, therefore a different strategy is recommended. The alternative adopted in this thesis is based on Maistrenko et al. (2005) and Popovych et al. (2005), who studied conditions for the emergence of chaotic behaviour in the Kuramoto model and showed that the phase differences $\gamma_{i,i-1}$ from a node i to preceding nodes $i-1$, $i = 2 \dots N$, are sufficient to capture all the effective dynamics of the system, i.e., by choosing a reference phase and an arbitrary ordering the N-dimensional Kuramoto model can be studied by inspecting $N-1$ variables.

In this way, the rationale for the readout unit used here is as follows: at each iteration of the task, a phase-sensitivity function $\phi(\gamma)$ is applied to each of the phase differences $\gamma_{i,i-1}$, $i = 2 \dots N$, and the result is linearly combined by an output weight matrix, $W_{N-1,a}$, resulting in a signals that will command the actuators of the robot (Equation 3.9).

$$\boldsymbol{M} = \boldsymbol{W}^{'} \phi(\boldsymbol{\gamma}) \tag{3.9}$$

where $\boldsymbol{M} = [M_1, \dots M_a]^T$ is the actuators' state space, with M_1 corresponding to the first actuator, M_2 to the second, and so forth.

As a consequence, the phase dynamics and the environmental input to the robotic agent will determine its behaviour. It is important to stress that nodes that receive no input participate in the overall dynamics of the network, hence their natural activity can modulate the global activity of the network. Furthermore, literature in brain-machine interface studies has shown that a relatively simple linear readout unit from a reduced number of neurons is able to extract the relevant neuronal activity that relates to the action being performed (Carmena et al., 2003; Lebedev et al., 2005; Kim et al., 2006).

The framework above is general in the sense that it shows the basic set-up used in all the experiments in this thesis. However, because we explore different aspects of synchronisation, the framework is adjusted in each chapter. In special, the Kuramoto model will be structured in different ways in order to support the occurrence of different neural phenomena. In Chapter 4, we opt for a fully connected network because we want to tune the network in specific synchronisation regions, and the conditions to guarantee that (Equation 3.5) only hold for fully connected

networks; in Chapter 5, the focus will be on assembly dynamics, but the Kuramoto model in its original formulation does not support the occurrence of stable assemblies, thus we use a different PIF, one that guarantees the emergence of neuronal groups. Finally, in Chapter 6, we investigate synchronisation and traveling waves, but in order to have both phenomena occurring in the network, a PIF different than that of the original model has to be used. The details of each adjustment are explained in depth in the respective chapters.

The next section describes the methods for Transfer Entropy analysis, the information theoretic tool used to investigate information transfer dynamics between variables of the system.

3.4 Information Theory and Transfer Entropy

Transfer Entropy (TE) (Schreiber, 2000) is based on classical Information Theory (IT) and allows one to estimate the directional exchange of information between two given systems. The choice of TE in this thesis is based on a study conducted by Lungarella et al. (2007a), who compared the performance of different IT tools in bivariate time-series analysis, which will be the case here, and concluded that TE is in general more stable and robust than the other tools explored. Moreover, agent-environment systems pose extra challenges in devising and interpreting a sensible measurement of information flow, for they normally have noisy and limited data samples, asymmetrical relationships among elements of the system and temporal variance (i.e. sensory and motor patterns may vary over time). Transfer Entropy, in this scenario, is suggested as a suitable and robust information theoretic tool (Lungarella et al., 2007b,a), and has also been applied to investigate real neural assemblies and other neuroscience problems (Borst & Theunissen, 1999; Gourévitch & Eggermont, 2007; Buehlmann & Deco, 2010; McDonnell et al., 2011; Vicente et al., 2011); it will, thus, be used in our analysis. The next paragraphs describe the technique.

Let I be a stationary higher-order Markov process (with memory) with transition probability p from one state to another i.e. $p(i_{t+1}|i_t, \ldots, i_{t-k+1}) = p(i_{t+1}|i_t, \ldots, i_{t-k})$ where i is a state from I at a given time t and k is the order of the process. Using Shannon Entropy, the optimal number of bits necessary to encode one more observation in the above time series is given by $H_I(k) = -\sum p(i_{t+1}, i_t^k) \log p(i_{t+1}|i_t^k)$. If, instead of the optimal probability function $p(i)$, we had a different function $q(i)$, using the Kullback Entropy (Kullback, 1959) one can obtain the number of bits in excess when encoding one more observation, given by $K_I(k) = -\sum p(i_{t+1}, i_t^k) \log \frac{p(i_{t+1}|i_t^k}{q(i_{t+1}|i_t^k)}$.

Consider now two time series, $X = x_t$ and $Y = y_t$, and assume they can be represented as a stationary higher-order Markov process. Transfer Entropy calculates the deviation from the gen-

eralised Markov property $p(y_{t+1}|y_t^n, x_t^m) = p(y_{t+1}|y_t^n)$ where $x_t^m \equiv (x_t, x_{t-1}, \ldots, x_{t-m+1})^T$, $y_t^n \equiv (y_t, y_{t-1}, \ldots, y_{t-n+1})^T$ and m and n are the orders of the higher-order Markov process (note that the above property holds only if there is no causal link between the time series). Based on the concepts described in the previous paragraph, Schreiber (Schreiber, 2000) defines Transfer Entropy as:

$$TE(X \to Y) = \sum_{y_{t+1}} \sum_{x_t} \sum_{y_t} p(y_{t+1}, x_t^m, y_t^n) \log \frac{p(y_{t+1}|y_t^n, x_t^m)}{p(y_{t+1}|y_t^n)} \tag{3.10}$$

Therefore, from Equation 3.10 one can estimate the information about a future observation y_{t+1} given the available observations x_t^m and y_t^n that goes beyond the information of the future state y_{t+1} provided by y_t^n alone. It is thus a directional, non-symmetrical estimate of the influence of one time series on another.

The original formulation of Transfer Entropy suffers from finite sample effects when the available data is limited, and the results obtained may not be correctly estimated. To attenuate these limitations, Marschinski & Kantz (2002) introduced an improved estimator, "Effective Transfer Entropy" (ETE), which is calculated as the difference between the usual Transfer Entropy (Equation 3.10) and the Transfer Entropy calculated after shuffling the elements of the time series X, resulting in the following equation:

$$ETE(X \to Y) \equiv TE(X \to Y) - TE(X_{shuffled} \to Y) \tag{3.11}$$

The ETE formulation is the one used in this thesis. Also, the conditional probabilities are calculated by rewriting them as joint probabilities which are then estimated using histograms.

To illustrate the properties of the tool, we now provide an example (also described in Lungarella et al. (2007a)). Consider two unidirectionally coupled autoregressive processes of first order given by Equations 3.12 and 3.13:

$$x_i = 0.8x_{i-1} + n_i^{(x)}(\sigma_x^2) + ey_{i-1} \tag{3.12}$$

$$y_i = 0.4y_{i-1} + n_i^{(y)}(\sigma_y^2) \tag{3.13}$$

where $n_i^{(x)}$ and $n_i^{(y)}$ are independent Gaussian random processes with zero mean and variance $\sigma_x^2 = \sigma_y^2 = 0.2$, and $e \in [0, 1]$ is a parameter that controls the coupling between the two processes.

Note that if $e = 0$, the two processes are independent, but as e increases, the time series y_i unidirectionally influences the time series x_i. Therefore, one would expect that the transfer entropy from y_i to x_i ($ETE_{Y \to X}$) increases with e whereas $ETE_{X \to Y}$ remains inexpressive. Figure 3.7 shows the results.

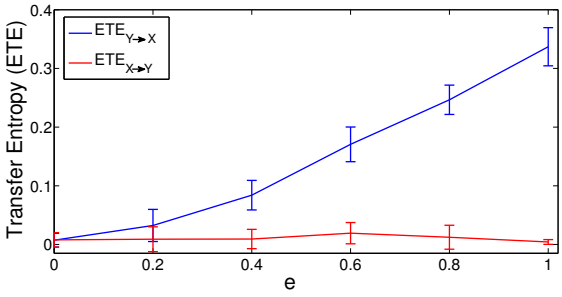

Figure 3.7: Transfer Entropy between two unidirectionally coupled autoregressive processes X and Y, with coupling parameterized by e. Note that $ETE_{Y\to X}$ increases with e (see Equations 3.12 and 3.13), whereas $ETE_{X\to Y}$ is not affected. The plot shows the mean over 20 runs of 1000 samples each with different initial conditions (the first 1000 samples were discarded in every run), with parameters $m = n = 1$ (Equation 3.10). Both time series were discretised in 8 equiprobable states, which improves the robustness of the statistics (Marschinski & Kantz, 2002; Lungarella et al., 2005)

.

3.5 Summary

In this chapter, we described the main models and methods that are going to be used in the remaining of the thesis: Genetic Algorithms (GA), used to optimize the parameters of the system, evolved according to the Evolutionary Robotics (ER) paradigm, in which a robotic agent controlled by an oscillatory neural network model inspired by the Kuramoto model of coupled phase oscillator has to accomplish a minimally cognitive task. Among other analysis, particular to each experiment, Transfer Entropy (TE) will be used to explore the information dynamics between different variables of the system. We stress that each experiment will have its specific set of parameters and minor adjustments to the models depending on what is under investigation, but they all employ the basic structure of the techniques mentioned above.

The next chapter presents the first experiment of this thesis, where we investigate synchronisation effects on the behavioural performance and information dynamics of a simulated minimally cognitive robotic agent whilst performing a categorical perception task under normal and inverted vision.

Chapter 4

Synchronisation effects on the behavioural performance and information dynamics in a categorical perception task

---

In this chapter, we explore the role of neural synchronisation in the performance of a simulated robotic agent in two different minimally cognitive tasks. We show that there is a statistically significant difference in performance and evolvability depending on the synchronisation regime of the network. In both tasks, a combination of information flow and dynamical analyses show that networks with a definite, but not too strong, propensity for synchronisation are more able to reconfigure, to organise themselves functionally, and to adapt to different behavioural conditions. The results highlight the asymmetry of information flow and its behavioural correspondence. Importantly it also shows that neural synchronisation dynamics, when suitably flexible and reconfigurable, can generate minimally cognitive embodied behaviour.

4.1 Introduction

In this chapter, we explore the role of synchronisation in the performance of a simulated robotic agent during the execution of two different minimally cognitive tasks: the first, a categorical perception task (Beer, 2003; Izquierdo, 2008; Dale & Husbands, 2010), in which the robot has to discriminate between moving circles and squares; the second, an orientation task, where the robotic agent has to approach moving circles with both normal and inverted vision, adapting to both

conditions. These tasks were chosen for being currently regarded as benchmarks in the evolutionary robotics and adaptive behaviour communities, with categorical perception underpinning cognitive systems (Harnad, 1987).

The objective of the chapter is to shed some light on the role of neural synchronisation in simple embodied cognitive behaviours. More specifically it aims to $1)$ test whether different degrees of coupling in the agent's oscillatory neural network, which will encourage more or less synchrony in the network dynamics, have an effect on the performance of the agent and $2)$ determine if there are circumstances in which more (or less) synchrony is better suited to the generation of adaptive behaviour in the context of the tasks studied.

The model is based on the framework described in Section 3.3, which explicitly captures the phase dynamics of units that alone have spontaneous oscillatory activity and once connected can generate emergent rhythmic patterns. Its synchronisation regime can be adjusted by one parameter (Equation 3.5), suiting our study, whilst also avoiding any problems in obtaining phase information.

Analysis of results is centred on how the information dynamics (more specific, transfer entropy) between the nodes of the network, the agent's body and the environment vary depending on the current synchronisation status of the system and how this is reflected in the behaviour being displayed.

The chapter is organised as follows: the next section presents the methods adopted to develop the experiments and analysis, covering the ER framework, the details of the active categorical perception and orientation under normal and inverted vision tasks, the details of the genetic algorithm used to optimise the parameters of the system (based on the algorithm described in Section 3.1), and concluding with details of the time-series analysis using Transfer Entropy. Following this, we present the results, which show a difference in performance and behaviour depending on the synchronisation regime of the network, relating the observed sensorimotor strategies with the dynamics and the information flow of the system. The chapter closes with a discussion on the results obtained.

4.2 Methods

4.2.1 Active Categorical Perception

The active categorical perception task studied here consists of a circular robotic agent, able to move horizontally along the bottom of a 250×200 rectangular environment (Figure 4.1), which has to discriminate between circles and squares as they move from the top of the arena to the

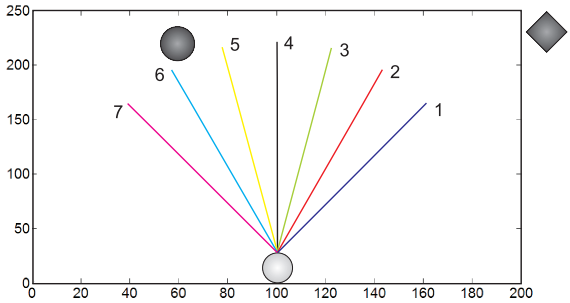

Figure 4.1: Experiments 1 and 2 scenario. The agent (grey circle at the bottom) has to catch falling circles and avoid squares in Task 1 and catch falling circles with normal and inverted vision in Task 2. The robotic agent has 7 ray sensors, symmetrically displaced with relation to the central ray in intervals of $\pm\pi/12$ radians, and two motors that can move it horizontally.

bottom (only one object on each trial) (Beer, 2003; Izquierdo, 2008). The robotic agent's body has 7 ray sensors, symmetrically displaced in relation to the central ray in intervals of $\pm\pi/12$ radians, and two motors to move it left and right along a straight line. Sensory inputs $I_i(t)$ for each distance sensor i at a given time t are calculated following Equation 4.1:

$$I_i(t) = \begin{cases} 10(1 - \frac{l_i(t)}{200}), & \text{if } l_i(t) < 200 \\ 0, & \text{otherwise.} \end{cases} \tag{4.1}$$

where l_i is the length of the ith ray between the robot's body and the object, $i = 1, \ldots, 7$.

The diagonal of the square, and the radii of both the robotic agent and the circle all measure 15 units. Each sensor is attached to an even-numbered node of the network (Figure 4.2). The velocity adjustment V (Equation 4.2) is obtained subtracting the left motor command value from the right (a positive value drives the robot to the right, a negative value to the left).

$$V = s(M_2 - M_1) \tag{4.2}$$

where s is a motor output weight, M_1 is the left motor command and M_2 is the right motor command (Equation 4.4).

At the beginning of each trial, a circle or a square is dropped from the top of the environment at a random horizontal position within a maximum of 50 units from the robotic agent, and moves vertically with a velocity of 3 units per timestep. The robotic agent has to approach the circles and avoid the squares, adjusting its horizontal velocity accordingly (limited to 5 units per timestep).

A variation on this experiment consists of an orientation task. In the same environmental set-up, the robotic agent has to adjust its horizontal position and catch circles with normal and inverted vision (catching is considered to occur automatically when the object is within the agent's body

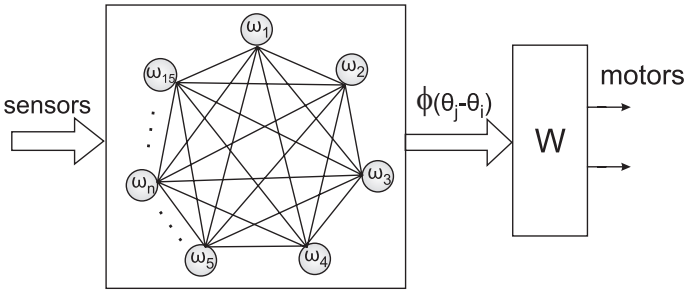

Figure 4.2: Framework for application in evolutionary robotics. The oscillatory network is composed of 15 fully connected oscillators, with even nodes connected to the robot's sensors (1 sensor per node). A phase-sensitivity function $\phi(\gamma)$ is applied to each of the phase differences $\gamma_{i,i-1}, i = 2 \ldots 15$, then linearly combined by an output weight matrix, W, resulting in two signals that will command the left and right motors of the agent.

radius). A task, comprised of many trials, is composed of an equal number of trials under normal and inverted vision. When submitted to visual inversion, sensory readings from an object on the right side of the agent are perceived by the agent's left set of sensors, and vice-versa. Therefore, to successfully execute this task the agent has to devise a context-dependent strategy to cope with the ambiguity of having equal stimuli in different scenario and vision configurations.

Taken together, the two tasks present challenging and important scenarios for a cognitive agent (Di Paolo, 2000; Izquierdo, 2008), justifying their choice as an experimental scenario: the first task requires the engagement of, and discrimination between, two different objects whereas in the second task the robotic agent has to develop a strategy to overcome the disruption caused by the inversion of the visual field.

4.2.2 Framework for application in evolutionary robotics

The framework, illustrated in Figure 4.2, is based on the model described in Section 3.3.1. It is composed of 15 fully connected oscillators, with even-numbered nodes connected to the robot's sensors (1 sensor per node). The frequency of each node is the sum of its natural frequency of oscillation, w_i, and the value of the sensory input $I_i(t)$ (calculated according to Equation 4.1) related to that node (0 if there is no input), scaled by a factor z_i (Equation 4.3).

$$\frac{d\theta_i}{dt} = (\omega_i + z_i I_i(t)) + \frac{K}{N} \sum_{j=1}^{N} sin(\theta_j - \theta_i) \tag{4.3}$$

Notice that we employ the same phase interaction function (PIF) that is used in the original formulation of the Kuramoto model, i.e. $\Gamma(\theta_j - \theta_i) = sin(\theta_j - \theta_i)$ (see Equation 3.2).

At each iteration the phase differences $\gamma_{i,i-1}$ from a node i to nodes $i-1$,$i = 2 \ldots 15$, are

calculated following Equation 4.3. The rationale for a network with 15 nodes relates to richer dynamical behaviour in the Kuramoto model with this number of nodes (Maistrenko et al., 2005; Popovych et al., 2005). In this chapter, we use the $\sin$ function as the phase-sensitivity function $\phi(\gamma)$, applied to each of the phase differences $\gamma_{i,i-1}$ in order to reduce instabilities in the phase differences caused by the resetting of the phase of each oscillator when it exceeds 2π. The modified phase differences are then linearly combined by an output weight matrix, W, resulting in two signals that will command the left and right motors of the agent (Equation 4.4).

$$\boldsymbol{M} = \boldsymbol{W}^{'} sin(\boldsymbol{\phi}) \tag{4.4}$$

where $\boldsymbol{M} = [M_1, M_2]^T$ is the motor state space, with M_1 corresponding to the left motor command and M_2 to the right motor command.

The experiments reported later explore the relationship between the network synchronisation state and the agent's behaviour. Different synchronisation regimes in the network are obtained by varying the coupling strength between units (K). During a given simulation, the value of the coupling is set by multiplying the value of K_c (calculated according to Equation 3.5) by a scaling factor to tune the nodes in a subcritical ($K < K_c$), supercritical ($K > K_c$) or critical zone ($K = K_c$).

The next section presents the details of the evolutionary process.

4.2.3 Genetic Algorithm

A geographically distributed genetic algorithm with local selection and replacement (described in Section 3.1) is used to determine the parameters of the system: the frequency of each of the 15 nodes, $w_i \in [0, 10]$, the 7 input weights $z_i \in [-5, 5]$ to even nodes (0 otherwise), the matrix $W_{N-1,a}$ with $14 \times 2 = 28$ elements in the interval $[-1, 1]$, a motor output weight $s \in [0, 100]$ and the network update time $t_u \in [0, 50]$ (the number of time steps Equation 4.3 is updated before the phase-differences are used to calculate the motor output), resulting in a genotype of length 52 for a network with $N = 15$. The population size was 49, arranged in a 7×7 toroidal grid. A generation is defined as 100 breeding events and the evolutionary algorithm runs for a maximum of 100 generations.

In the active categorical perception task, fitness is evaluated from a set of 34 trials with randomly chosen objects (circles or squares), starting at an uniformly distributed horizontal offset in the interval of ± 50 units from the robotic agent. Fitness is defined as the robotic agent's ability to catch circles and avoid squares, and is calculated according to the following equation: $fitness = \sum_{i=1}^{N} i f_i / \sum_{i=1}^{N} i$, where f_i is the ith value in a descending ordered vector $F_{1,N}$, and

is given by $1 - d_i$, in the case of a circle, or by d_i in the case of a square. d_i is the horizontal distance from the robotic agent to the object at the end of the ith trial (when the object reaches the bottom of the environment), limited to 50 and normalized between 0 and 1. Therefore, a robotic agent with good fitness maximizes its distance from squares and minimizes its distance from circles. Notice that the form of the fitness function creates pressure for good performance in *all* trials in a given fitness evaluation, instead of just averaging the performance across the trials, which could bias the mean fitness of a given robotic agent leading to poor generalisation behaviour.

In the orientation task under normal and inverted vision, fitness is evaluated from 17 trials with the normal vision scheme followed by 17 trials with inverted vision. The circles are dropped at an uniformly distributed horizontal offset in the interval of ± 50 units from the robotic agent. Fitness for each part of the evaluation is defined as in the previous paragraph, but considering just the circle catching scenario. Therefore, a robotic agent with good fitness minimizes its distance from circles, in both normal and inverted vision situations.

The next section describes the methods for Transfer Entropy analysis.

4.2.4 Transfer Entropy

Following the notation and the theoretical background presented in Section 3.4, the analysis will focus on the information transfer between pairs of variables of the system. For all experiments, we adopt the orders of the higher-order Markov processes as $m = n = 1$ (Equation 3.10), but see Section 7.3 for further comments.

To collect the data, the evolved agent under analysis was evaluated on a single trial, from a predetermined initial position (equal for every test), having its sensory information, its motor commands and the phase dynamics of each node recorded. Details of agent selection are presented in the next section. Each data point interval (obtained according to an Euler integration time-step of $15ms$) is then linearly interpolated (in $1.5ms$ time intervals) resulting in a coarse grained time-series, which facilitates a more robust ETE analysis. If the data were collected in shorter time intervals instead, the computational time needed for the evolutionary process to complete would be prohibitive. Moreover, given the structure of the data observed in the experiments, the changes in the qualitative aspects of the original time series after interpolation were minimal.

Recall that the objective is to investigate the flow of information between the nodes of the network, and between the agent's body (motors) and the environment (distance sensors). However, the methods to calculate Transfer Entropy, as described in Section 3.4, require bivariate time series. To analyse the flow between pairs of nodes, the bivariate time series that correspond to their respective phase dynamics suffice, but to investigate the flow between the 7 sensors and the 2 mo-

tors, a representative single time series has to be generated for each sensor modality, i.e., we need to reduce the 7-dimensional sensor space to a single dimension time series and the 2-dimensional motor space to a single time series in order to construct a bivariate time series over which TE can be calculated.

In this sense, the time series for the seven sensors (one time series for each sensor), obtained as described above, are submitted to a dimension reduction using a principal component analysis (PCA) (Jolliffe, 2002). First, the mean of each sensor's data vector is subtracted from its correspondent data set to ensure that the dynamics of the first component describes the direction of maximum variance in the data. We then calculate the principal components and project the original seven time series data onto the first principal component, reducing the original data to a single time series that captures the most significant features of the multidimensional input space. The motor commands are also combined to generate a single time series by subtracting the value of the left wheel command from the right wheel command. The phase dynamics are recorded directly from the nodes. Finally, the time series used in the calculations of Effective Transfer Entropy are obtained from the first derivative of each of the above described time series, discretised in 6 equiprobable states, which improves the robustness of the statistics (Marschinski & Kantz, 2002; Lungarella et al., 2005).

Two ETE analyses are conducted across the experiments: one considering the information flow between the agent's sensors and motors, and another considering the information flow between the nodes of the network (represented by the phase dynamics). We are mainly interested in studying how ETE between these variables vary as the task progresses, given that the agent continually engages with the object during the discrimination and orientation processes. For this purpose, a sliding window technique is used (Staniek & Lehnertz, 2008; Szczepanski et al., 2011), with a window size of 200 data points. Therefore, at every time step of the task, the ETE is estimated (according to Equations 3.10 and 3.11) considering the time series contained in that window.

4.3 Results

In the first experiment, individuals are evolved to perform categorical perception under different coupling configurations, calculated by re-scaling the current value of K_c (see the $Methods$ section for details). Figure 4.3(a) presents the fitness statistics for the best evolved agents obtained in 100 evolutionary runs at different coupling configurations. Notice that the agent's overall performance is poor in the no coupling case ($0K_c$), smoothly increases as the coupling strengthens (peaking at $K = K_c$) and then sharply falls for strong coupling ($3K_c$ onwards).

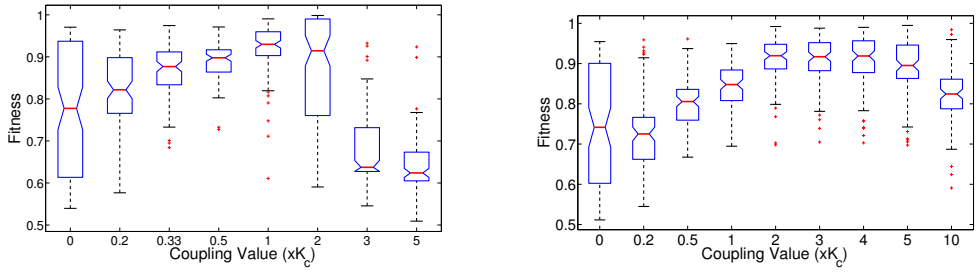

(a) (b)

Figure 4.3: Fitness statistics for the best evolved agent obtained in 100 evolutionary runs at different coupling configurations for a categorical perception task (a) and an orientation under normal and inverted vision task (b). The boxes represent the lower, median and upper quartile. The central mark is the median and whiskers (dashed lines emerging from the boxes) extend to the most extreme data points not considered outliers (outliers are shown as red crosses).

These results indicate that tuning the oscillatory networks in a certain region of their synchronisation regime may have a direct impact on the performance and evolvability of the agent, but would this result hold had we had a different task? We therefore performed a second set of experiments by changing from categorical perception to the circle catching (orientation) task under normal and inverted vision, as described in Section 4.2. Figure 4.3(b) presents the fitness statistics for the best evolved agents obtained in 100 evolutionary runs at different coupling configurations. Notice that the performance increases with the coupling and reaches its peak with values of K around $2K_c$, whilst in the previous experiments we observed a decrease in fitness with coupling values larger than K_c.

It is clear from these two figures that the synchronisation regime the network is tuned to influences the behavioural performance of the agent. In order to clarifying why this happens and to explore the underlying mechanisms, we investigate the performance, system dynamics, and information flow properties of three evolved agents with different couplings strengths, which encourage different degrees of synchronisation, within each of the above experiments (agents are no longer under the influence of the evolutionary process during these analyses). These were chosen to be $0K_c$, K_c and $5K_c$ for Analysis 1 (categorical perception) and $0K_c$, $2K_c$ and $10K_c$ for Analysis 2 (orientation), to represent weak, 'optimal' and strong coupling for those behaviours. All experiments are carried out with agents chosen to have similar t_u (network update time, see Section 4.2.3) and with final fitness values as close as possible to the median of the fitnesses obtained in the evolutionary process for the given coupling scenario. The rationale for that is because there is a statistically significant difference in evolvability for different coupling strengths, but this dif-

ference is less noticeable if only the fittest individual of each coupling scenario is considered. Therefore, considering the interquartile intervals in Figure 4.3, choosing an individual based on the median of the population fitness, and not on the highest fitness obtained, help to elucidate why specific synchronisation regimes facilitate or impair most agents from a given architecture to succeed in the task. Also, it is important to stress that agents with similar fitnesses within a given population may present different behaviours to solve the task, but for the vast majority the strategies were found to be similar, e.g. a certain agent may start the task by moving towards the left part of the scenario whilst another agent might move towards the opposite direction, but both agents present the behaviour "move towards one side of the scenario". In this sense, the results found for the agents analysed herein hold for other possible choices of agents.

4.3.1 Analysis 1: Categorical Perception Task

Figures 4.4(a), 4.4(c) and 4.4(e) present the generalisation performance (performance in 100 aleatory trials after evolution) of three agents evolved in the $0K_c$, K_c and $5K_c$ conditions, respectively. The plots illustrate the agent-object horizontal separation.

Notice that all agents present some level of discrimination between circles and squares, characterized by the different trajectories adopted by the agent as the task progresses; however, their accuracies differ which seems to be the main factor responsible for the variations in fitness scores. Additionally, both $0K_c$ and $5K_c$ agents present a high proportion of trajectories similar to the ones observed with intrinsic autonomous network dynamics (i.e. sensory inputs fixed at 0), whilst in the K_c agent this is only observed when the object is a square and has its initial positioning far from the agent - the general strategy elsewhere is to initially move to centralize the object and then, approximately half way through the task, orient with the circles and move away from the squares.

Figure 4.5 presents, for each of the three agents, the time course of various system variables from a particular scenario where the agent (object) starts at the horizontal coordinate 100 (60). The agent-object trajectory, the frequency of each node and the synchronisation index are shown. Recall that in our model the sensory inputs, proportional to the agent-object distance, impact on the natural frequency of some nodes. That, in turn, affects the phase dynamics of the network, producing the different motor outputs that determine the agent's position and hence its performance on the task.

For the $0K_c$ agent, the frequency plot shows that the oscillatory behaviour of each node is only influenced by its natural frequency and the sensory input. For this reason, nodes without sensory connections don't change their frequency as the task progresses and the network does not present

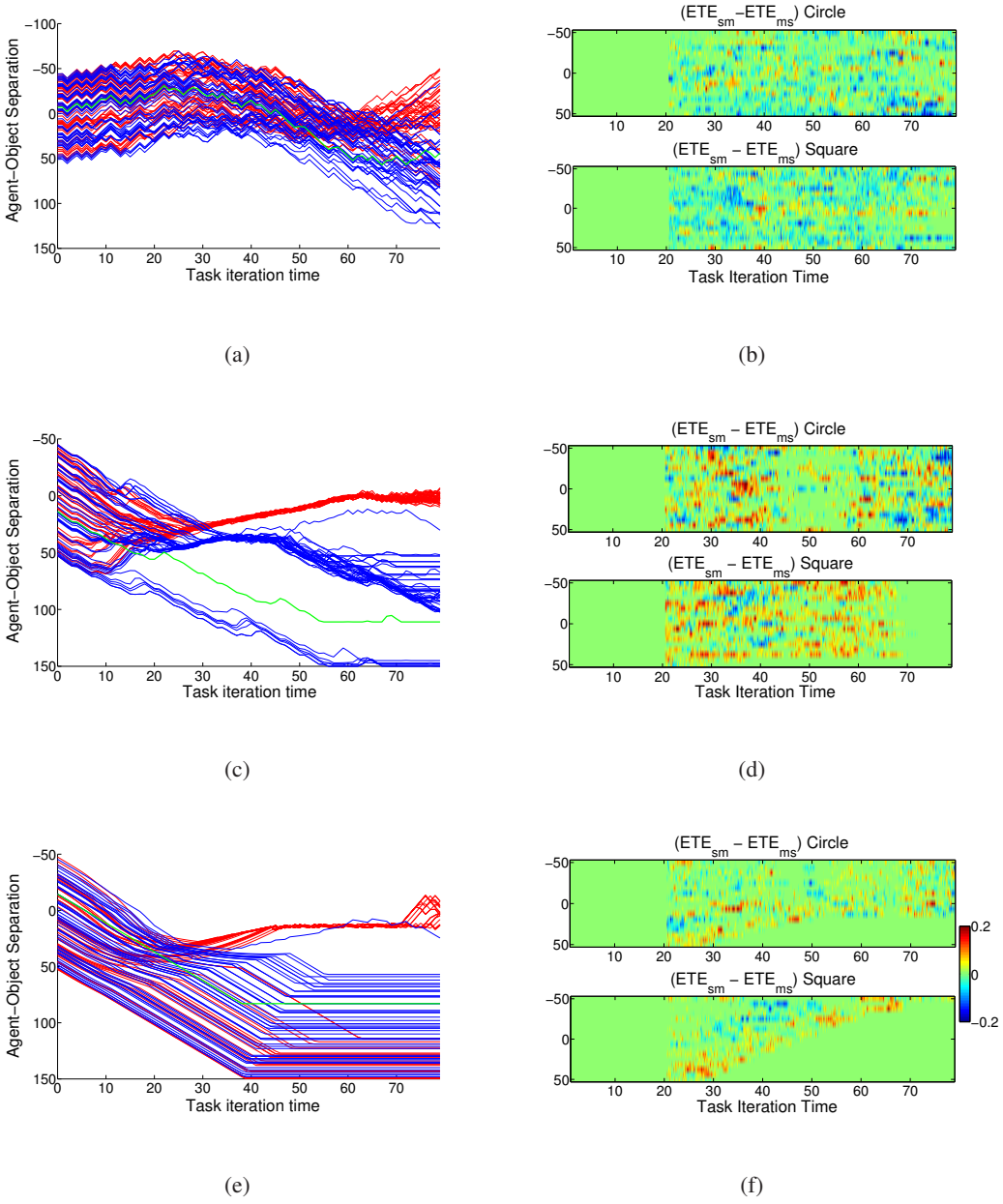

Figure 4.4: Left column plots: generalisation performance of the agent over 100 aleatory runs. The red colour is related to the circle catching behaviour and the blue colour to the square avoidance behaviour. Green lines reflect the behaviour under autonomous network dynamics. The plots illustrate the value of the horizontal separation of the agent and the object. Right column plots: difference between Effective Transfer Entropy from sensors to motors, ETE_{sm}, and from motors to sensors, ETE_{ms}, for each of the 17 different initial horizontal displacements ($[-50, 50]$) that the agent is evaluated during evolution (Section 4.2). ETE is calculated according to Equation 3.11. Figures refer to (a)(b)$0K_c$, (c)(d)K_c and (e)(f) $5K_c$.

any kind of internal coupled dynamics. The synchronisation index remains low, below 0.4, and its amplitude variation can be explained by observing Equation 3.4: the index reflects a sum of vectors, each representing the phase of an oscillator; with different evolved natural phase speeds (frequencies), the total sum varies over time, unless these frequencies maintain a constant relation, reflecting synchronisation.

In the K_c coupling condition, the frequency of each node presents a rich dynamics due to the critical internal coupling and the external sensory stimulus. With the agent approaching the object, the sensory inputs cause a large variation in the nodes' frequencies and as a consequence different node clusters emerge (see the black arrow in the circle catching row of plots). Conversely, moving away from the squares diminishes the external stimulus, and most of the network's nodes synchronise. This can be further observed by the synchronisation index plot, which approaches the dynamics observed in the autonomous condition in the square avoidance scenario (see the black arrow in the corresponding plot) but diverges from it in the circle catching sequence. Yet, the dynamics of both indexes reflect a higher synchronisation level (around 0.7 throughout the task).

The last figure of the set shows the results for the $5K_c$ network. The agent's behaviour is practically the same for both circle and square scenarios: the agent moves away from the object towards one side of the environment at constant speed, failing to discriminate. Inspecting the frequency plot, we notice that the network rapidly entrains with the synchronisation index remaining high throughout the task (in contrast to the K_c coupling condition). The small variations in the frequency dynamics (marked by a black arrow on the plot) relate to the phase resetting phenomena, where some nodes, although synchronised, reset at slightly different times, perturbing the ongoing synchronisation status. With these plots in mind, the agent's behaviour can thus be explained by a specific property of the model (Figure 4.2), where the synchronised phase dynamics result in stable phase differences, which culminate in constant motor speeds that cause a linear movement of the agent. Therefore, looking back at Figures 4.4(c) and 4.4(e), one can speculate why the $5K_c$ network does not achieve a high fitness: the tendency to fully synchronise reduces the sensitivity of the system in discriminating objects when the stimulus is not strong enough to modulate the ongoing phase dynamics, whereas the K_c network, although synchronising at some stages, is still flexible enough to escape the entrained state and adapt its phase dynamics in order to generate the appropriate motor commands.

In the above paragraphs and in the analyses to follow, the behaviour being displayed by the agent is compared to the one observed in the absence of inputs (behaviour under autonomous network dynamics - henceforth often referred to as the autonomous trajectory for short). This is to emphasize that the behaviour being displayed by the agent is not simply a response to its sensory

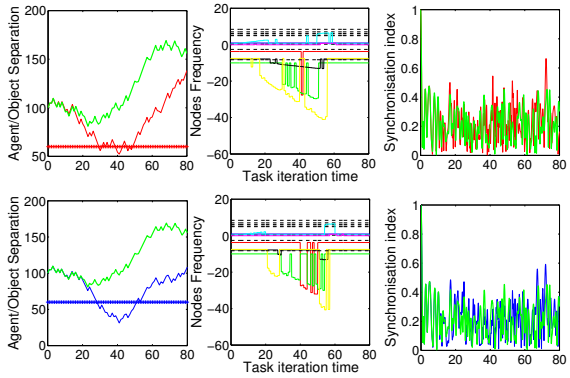

(a)

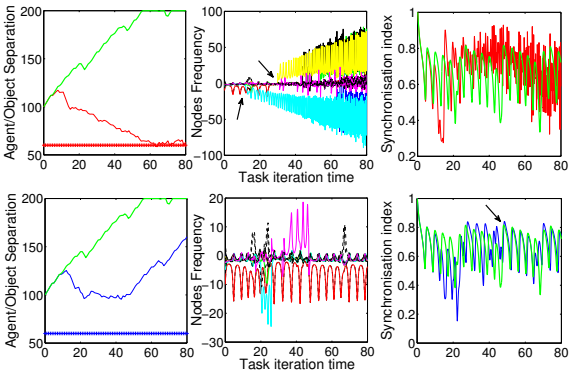

(b)

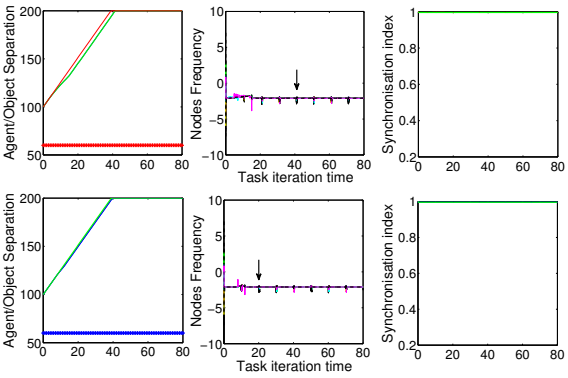

(c)

Figure 4.5: Detailed behaviour of the agent's internal and external dynamics for a given starting position. The top three graphics of each figure refer to the circle catching behaviour and the bottom ones to the square avoidance behaviour. The leftmost column illustrates the horizontal coordinate of the agent and the object (straight horizontal lines), the middle one shows the frequency of each node of the network as the task progresses (colour lines for nodes with inputs, dashed lines otherwise) and the rightmost ones present the synchronisation index. Green lines reflect the autonomous behaviour dynamics (clamped sensors). (a) $0K_c$, (b) K_c and (c) $5K_c$

readings or to the ongoing network dynamics alone, but a more intricate interplay between the two. The actions taken by the robot at the beginning of the task, when the sensory readings are small, are mainly a result of the intrinsic network dynamics, but they will modulate and affect the sensory readings that the robot will face in the future, which will also affect and shape the sequence of actions.

The previous results stress the relationship between the sensory inputs (environmental context) and the internal dynamics of the network. From these plots alone, however, it is not easy to determine to what extent the behaviour displayed by the robot is influenced by the network's internal dynamics or a response to the sensory readings. The Transfer Entropy analysis, as described in Section 4.2.4, may offer some insights into the temporal flow of information within the brain-body-environment system.

Consider Figures 4.4(b), 4.4(d) and 4.4(f). For each of the 17 different initial positions that the agent is evaluated on during evolution (Section 4.2), we calculate the flow of information from sensors to motors, ETE_{sm}, and from motors to sensors, ETE_{ms}. The first corresponds to the influence of the sensors in determining the behaviour of the agent whereas the latter corresponds to the changes in sensory inputs brought about by the agent's motion. Notice that we are not primarily concerned with the magnitudes of the information flows but rather on their form of interaction (causal influence); therefore, we depict the difference between ETE_{sm} and ETE_{ms} (positive values indicate a higher information flow from sensors to motors than from motors to sensors, negative values indicate the opposite). The plots show the difference between the results obtained for the circle catching and the square avoidance scenarios, and, together with the respective Figures 4.4(a), 4.4(c) and 4.4(e), allow for a wider perspective on how the information flow develops given different scenario configurations.

Figure 4.4(b) presents the ETE for the $0K_c$ coupling condition. Notice the widespread (wide deviations from zero) flow of information in both circle and square scenarios, with measurements being recorded in both directions (motors to sensors and sensors to motors) at all times, which may relate to a constant interaction between the agent and the object - indeed, the lack of internal coupling between nodes would promote a highly reactive agent resulting in a constant mutual interaction with the environment to perform the categorization. The performance, however, is poor.

Figure 4.4(d) presents the corresponding analysis for the K_c agent. The first observation, contrasting with the uncoupled network, is the higher magnitude of the difference between the ETE from sensors to motors and the ETE from motors to sensors during diverse moments of the task execution for both objects. Following the argument in the previous paragraph, we would there-

fore expect that in the current coupling condition the agent is more able than with the uncoupled architecture to convey sensory information into motor responses, adjusting the agent's position in order to maximize its performance. In the circle catching sequence, there are mainly two intervals of high difference in ETE, coinciding with major adjustments in the agent's trajectory when compared with the autonomous trajectory. Between iterations 20 and 40, the flow from sensors to motors is more noticeable for most initial conditions, which may relate to the scanning behaviour and identification that the object is a circle and should be captured. At the end of the task, after iteration 60, however, the difference in the flow increases towards a greater ETE from motors to sensors for many initial conditions, while at a behavioural level we observe that the agent is centred on the circle and stays relatively still keeping the horizontal separation near 0. In the square scenario, the ETE from sensors to motors is higher than the ETE from motors to sensors through most of the task for most initial conditions, while we observe the agent moving away from the object. At the end of the task, when the object is out of sensory reach, the ETE_{sm} and consequently the ETE_{ms} tend to 0, which explain the lack of information flow after iteration 70.

Turning to the $5K_c$ plot (Figure 4.4(f)), the immediate observation is the sparse and reduced amount of ETE throughout the task when compared to the K_c condition. Although some significant values occur, there is no consistency in the flow with many null values recorded. Observing the behavioural strategy, this is easily explained: the agent succeeds in discriminating between the objects in just a few situations, which have a corresponding reading in the ETE plot, whereas from most of the initial displacements the agent moves to a far side of the environment, where all sensory readings are absent. In this sense, the poor performance can be associated with a lack of sensitivity to sensory readings, explained by the high synchronisation level of the network despite the external perturbation to its nodes' frequencies. The external perturbations are not able to modulate the highly synchronised network dynamics.

The analysis of the flow of sensorimotor information provides insights into how the brain-body-environment system interacts over time and engages in determining the observed behaviour of the agent for different objects; insights which may not be evident solely from the system variables' time series. In order to add further depth, the next set of results explore the information flow between the nodes of the network, as described in Section 4.2.

Consider Figure 4.6(a), which presents in its first row the average over time of the information flow between the oscillatory nodes of the uncoupled network for the circle catching (first column) and square avoidance (second column) scenarios, respectively, according to Equation 4.5:

$$\bar{T}(n,n') = \frac{1}{T_w}\sum_{w=1}^{T_w}[ETE_w(n,n') - ETE_w^A(n,n')] \tag{4.5}$$

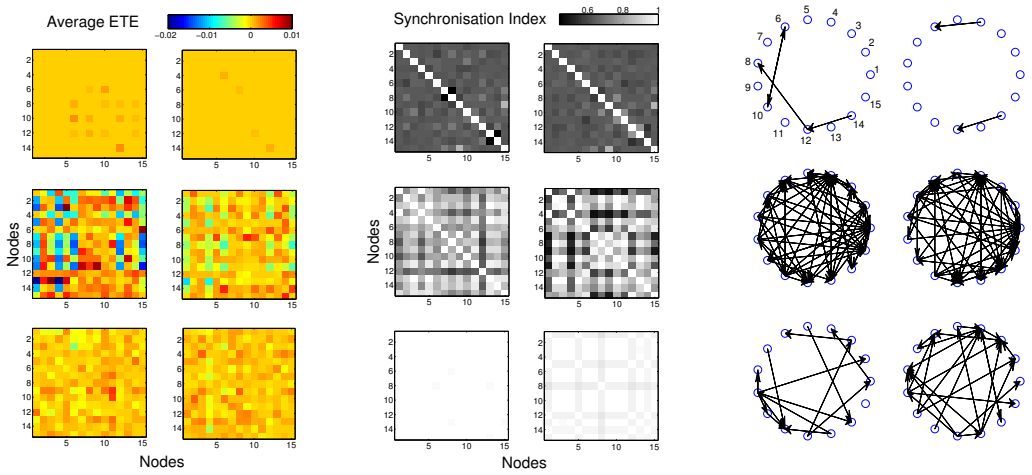

(a) (b) (c)

Figure 4.6: (a) Averaged information flow between the oscillatory nodes of the network (Equation 4.5). The autonomous flow is subtracted in all plots to highlight the task-specific activity. (b) Same as (a) but for the synchronisation index. (c) functional network - a directed arrow is drawn whenever the Transfer Entropy between two given nodes exceeds 50% of the maximum ETE value obtained in the whole task. The rows correspond to the $0K_c$, K_c and $5K_c$ agents, the left side of each column corresponds to circle catching and the right side to square avoidance.

where $\bar{T}(n, n')$ is the average Effective Transfer Entropy ETE between the pair of nodes (n, n'), estimated according to Equation 3.11, w is the time window and T_w is total number of windows. The superscript A stands for the ETE calculated in the autonomous case.

As expected, the uncoupled network has almost no ETE between nodes during most of the task, except when sensory readings modulate the ongoing phase activity, which explains why the few deviations from zero that occur are with relation to nodes that have sensory inputs (recall that only even nodes receive sensory inputs, see Figure 4.2.2 for details). Observe that the flow between any two given nodes is not necessarily symmetric (e.g. there is a flow from node 14 to 12 but the opposite is not true), as explained in Section 3.4.

In the K_c condition (Figure 4.6(a), second row), however, the coupling elicits a much broader modulation of the nodes' phase activity by the sensory inputs, stressing the internal communication between oscillators. The network is fully connected but nodes do not interact in the same way: the ETE values between pairs of nodes vary according to the corresponding sensory stimulus, the previous phase activity of the nodes and its natural frequency. Also, notice that the sensory inputs not only increase the information flow within the network but also decrease it, reflecting a mod-

ulation of the spontaneous network phase activity (the activity the network would have without sensory inputs). Although Transfer Entropy always results in a positive measurement, recall from Section 4.2 that to highlight the sensory influence the above results are obtained by subtracting the ETE calculated for the autonomous condition, hence the negative readings in the plots.

Compare the previous analysis with the $5K_c$ condition (Figure 4.6(a), third row). As the network is strongly coupled and acts as a single giant oscillator, weak sensory stimuli of one or more nodes cannot promote a significant perturbation or change in the ongoing dynamics; in other words, the sensory readings do not contribute to the discrimination of the object given that different incoming stimuli through other nodes would have little impact on the entrained network. Even though the system is able to detect the object and generate a motor response to it, the categorization performance is impaired.

This diversity of information flow between the different coupling configurations follows the variation in the synchronisation index between nodes of the network, portrayed in Figure 4.6(b). The small level of synchronisation in the $0K_c$ network has a corresponding small flow of information between nodes, and the large level of synchronisation in the $5K_c$ network is accompanied by a reduced flow of ETE between its nodes. The intermediate point, the K_c network, has both a synchronisation regime and diverse and highly asymmetric information dynamics.

In summary, although all configurations are fully connected, the K_c network is able to use a great variety of flexible, reconfigurable functional connections. Figure 4.6(c) illustrate this fact by redrawing the connection scheme according to the magnitude of the ETE between nodes - only nodes with mean information flow 50% above the global average are connected. Notice the much richer connectivity in the K_c condition than in the other two. The higher performance and evolvability achieved by this configuration can thus be attributed to its nodes' superior ability to communicate and organise themselves functionally, resulting in a more efficient information flow between the ongoing network activity, the agent's body and the environmental context.

Figure 4.7 shows the temporal evolution of the net Transfer Entropy from a given node to all remaining nodes of the network in 50 equally spaced time windows, defined as the preferred direction of information flow (Staniek & Lehnertz, 2008):

$$T(n, n', w) = \frac{1}{N-1} \sum_{n \neq n'} [ETE_{n,n'}(w) - ETE_{n',n}(w)] \tag{4.6}$$

where ETE is the Effective Transfer Entropy between the pair of nodes (n, n') estimated according to Equation 3.11, w is the time window and N is the total number of nodes in the network.

The first configuration (top row), the $0K_c$ network, shows almost no information flow between nodes, whereas in the K_c network (middle row) there is a widespread activity, with driving nodes

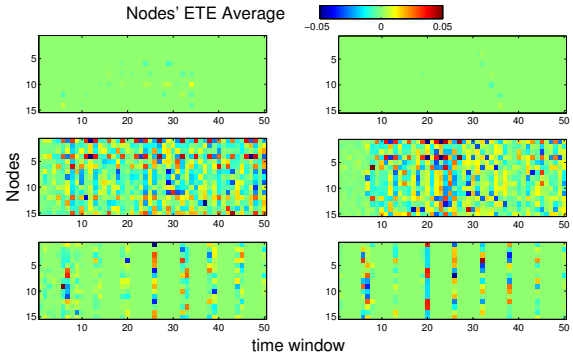

Figure 4.7: Net Transfer Entropy from a given node to all remaining nodes of the network in 50 equally spaced time windows (Equation 4.6). The autonomous flow is subtracted in all plots to highlight the task-specific activity. Top row: $0K_c$ agent, middle: K_c, bottom: $5K_c$.

(nodes with higher information flow) alternating in time. Notice, however, the increased activity in the square avoidance scenario between time windows 20 and 35. Observing Figure 4.4(c), this iteration interval corresponds exactly to major adjustments in the agent's trajectory when compared with the autonomous trajectory. This could help explain the more widespread activity observed in the circle catching scenario, as the agent constantly adjusts its trajectory in order to capture the approaching object. The $5K_c$ network (bottom row), as with the $0K_c$, presents a reduced flow in both scenarios, with few exceptions which correspond to the phase resetting behaviour of the model described earlier.

The experiments analysed in this section show that tuning the networks in a certain region of their synchronisation regime appears to have a direct impact on the performance and evolvability of the agent. The information flow analysis together with that of the system variables' dynamics indicate that extreme scenarios, e.g. no coupling or strong coupling, are not suitable for the categorical perception task. Importantly it also shows that neural synchronisation dynamics, when suitably flexible and reconfigurable, can generate minimally cognitive embodied behaviour.

In order to test the generality of these results, following the same methodology as above, the next set of experiments explores the performance of different coupling configurations on a different minimally cognitive task where the agent has to orient itself to an approaching object (circle) under normal and inverted vision (see Section 4.2 for experimental procedures).

4.3.2 Analysis 2: Orientation under Normal and Inverted Vision

Recall Figure 4.3(b), which presents the fitness statistics for the best evolved agents obtained in 100 evolutionary runs at different coupling configurations for task 2 (circle catching with normal and inverted vision). The performance increases with the coupling and peaks at $K = 2K_c$,

presenting a noticeable fall in performance for couplings greater than $5K_c$. The following analysis will therefore consider three individuals: one drawn from the $0K_c$ scenario, one from the $2K_c$ and one from the $10K_c$ scenario, all with fitness values close to the fitness median obtained on each respective coupling scenario set of results.

Observe Figures 4.8(a), 4.8(c) and 4.8(e), which present the generalisation performance of the agents (performance in 100 aleatory trials after evolution). The agent controlled by the uncoupled network ($0K_c$) cannot succeed in catching circles with either normal or inverted vision and all trajectories seem to be a variation of the autonomous trajectory (illustrated by the green line in the plot) - there is almost no influence from the sensory readings. The $2K_c$ agent, however, has good performance in both sensory modes, centring on the object in slightly different ways as the task progresses, depending on whether it has normal or inverted vision, making fine adjustments to the trajectory towards the end. A similar strategy is employed by the very strongly coupled agent ($10K_c$), however the accuracy with which the agent centres on the object towards the end of the task is poor and this divergence explains the lower fitnesses obtained. Nevertheless, both $2K_c$ and $10K_c$ agents display different behaviours from their autonomous trajectories, in contrast with the uncoupled network, indicating that they make use of the sensory information to solve the task.

An inspection of the dynamics of some of the system variables reveals that, as expected, the uncoupled network has some node activity varying directly with the sensory readings, with nodes without inputs keeping their natural frequency throughout the task (see Figure 4.9(a)). The synchronisation index remains low but has a significant variance. The lack of internal coupling results in the absence of any internal communication or flow of information as well as any influence caused by acting on the environment. As the task is intrinsically ambiguous, the agent cannot perform well.

The $2K_c$ network (Figure 4.9(b)), in contrast, remains synchronised for most of the time and the nodes can only "escape" this state when sensory readings rapidly change their natural frequency. The agent's trajectories in both vision conditions are similar, but the synchronisation index plot reveals a diverse phase dynamics. Therefore, even though the network has a fixed, all-to-all pre-established coupling configuration, with no explicit plasticity mechanisms, it can respond and adapt to conflicting sensory conditions and obtain a good performance in the task. This behaviour is also observed in the $10K_c$ network (Figure 4.9(c)), but as the task approaches its end and the magnitude of the sensory readings increase, the frequency behaviour changes drastically, partly because of the high inputs, partly because of some instabilities inherent in the model (high coupling values, associated with properties of the nodes' frequencies distribution, may lead to unstable behaviour in the Kuramoto model (Acebrón et al., 2005)). Taken together, these results

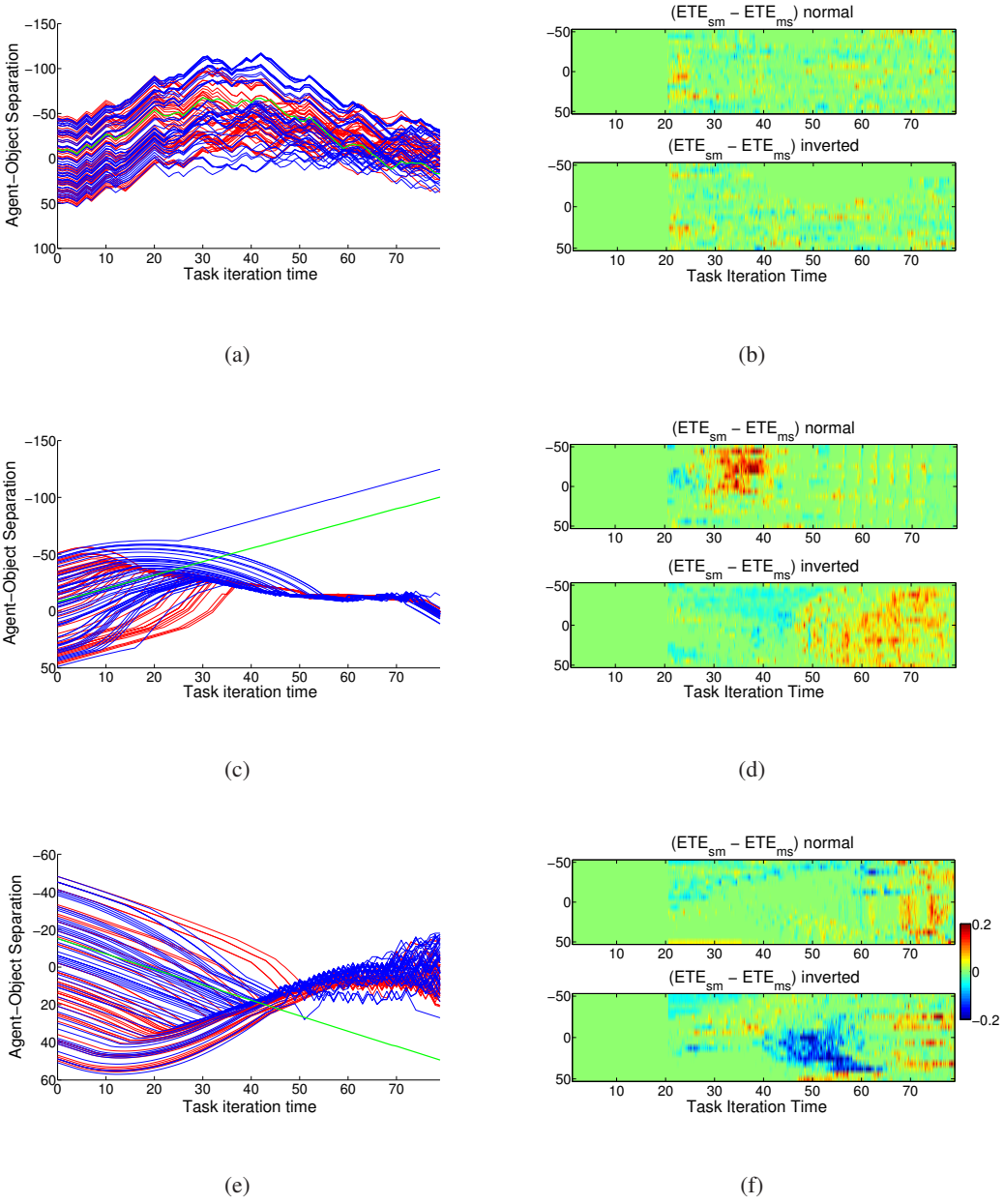

Figure 4.8: Left column plots: generalisation performance of the agent over 100 aleatory runs. The red colour is related to circle catching under normal vision and the blue colour to the inverted vision scenario. Green lines reflect the behaviour under autonomous network dynamics (clamped sensors). The plots illustrate the value of the horizontal separation of the agent and the object. Right column plots: difference between Effective Transfer Entropy from sensors to motors, ETE_{sm}, and from motors to sensors, ETE_{ms}, for each of the 17 different initial horizontal displacements ($[-50, 50]$) that the agent is evaluated on during evolution (Section 4.2). ETE is calculated according to Equation 3.11. Figures refer to (a)(b)$0K_c$, (c)(d)$2K_c$ and (e)(f) $10K_c$.

suggest that more synchronised networks are more flexible in adapting to sensory ambiguity, but the variables' dynamics alone cannot provide a broader insight into the processes underlying this adaptation. In order to do that, we conduct an information flow analysis of different parts of the system.

A Transfer Entropy analysis between the agent's sensors and motors (environment and body) across all possible starting positions used during evolution for the $0K_c$ network (Figure 4.8(b)) reveals almost no information flow between the agent's body and the environment. As noted before, the lack of internal coupling prevents the agent from properly responding to the ambiguity of the task. The same analysis, carried out on the more strongly coupled networks (Figures 4.8(d) and 4.8(f)), shows that the normal and inverted vision conditions elicit different information flows at specific points of the agent's trajectory, reflecting its ability to successfully catch circles in both scenarios. For the $2K_c$ network, especially, starting positions that require a very different behaviour from that observed in the autonomous trajectory (e.g. agent-object separation between $[-50, 0]$, where the agent has to move against the straight autonomous trajectory) correspond to a higher (smaller) flow from sensors to motors in the normal (inverted) vision scenario in some parts of the task (between iterations 30 and 40), with the opposite happening from iteration 50 onwards. The same happens for the $10K_c$ network, although in this case there is a higher flow from motors to sensors in the inverted vision case between iterations 40 and 60 (again, corresponding to points where the agent has to actively move against its autonomous trajectory), and a higher flow from sensors to motors towards the end in both vision configurations. In summary, the point to stress here is the asymmetry of information flow and its behavioural correspondence obtained in fully connected oscillatory networks only by changing their level of synchronisation.

Looking at the average node activity for these coupling configurations (Figure 4.10(a)), one can see that the information flow under normal and inverted vision is similar, with very little activity for the uncoupled network, whereas the more strongly coupled agents ($2K_c$ and $10K_c$), although having a nearly identical trajectory when catching the circles with normal and inverted vision in each corresponding scenario, show variation in their internal nodes' information flow. Having only the environmental feedback to shape its behaviour, the $0K_c$ network fails to detect and respond properly to this conflicting situation because the phase dynamics of each node can only be altered by the external stimulus, which in this case is made ambiguous, while the internal activity of the $2K_c$ and the $10K_c$ networks is modulated by the environmental context - the conflicting readings result in different phase dynamics that are exploited to generate fit behaviour. The synchronisation index adds to that perspective by showing that although highly synchronised, the $2K_c$ network is still flexible enough to escape the nearly entrained state of the $10K_c$ network or

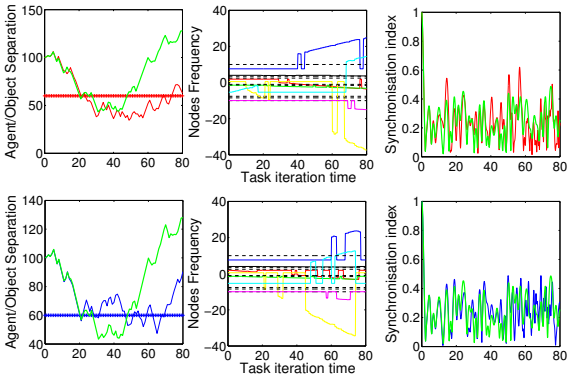

(a)

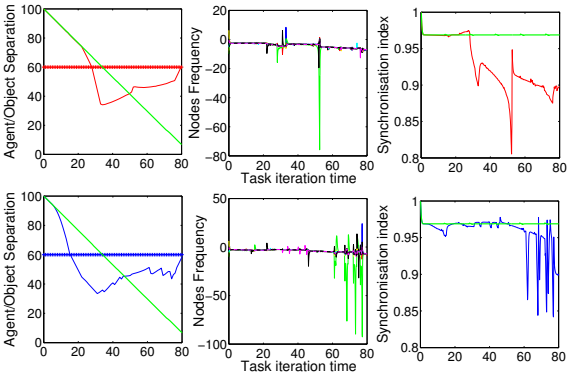

(b)

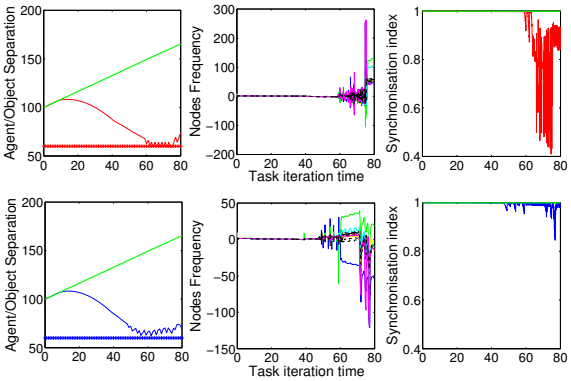

(c)

Figure 4.9: Detailed behaviour of the internal and external dynamics for the orientation task agents. The top (bottom) three graphics of each figure refer to the circle catching under normal (inverted) vision behaviour. The leftmost column illustrates the horizontal coordinate of the agent and the object (straight horizontal lines), the middle one shows the frequency of each node of the network as the task progresses (colour lines for nodes with inputs, dashed lines otherwise) and the rightmost ones present the synchronisation index. Green lines reflect the autonomous trajectory. (a) $0K_c$, (b) $2K_c$ and (c) $10K_c$.

the incoherent behaviour of the uncoupled framework, producing the fittest agent.

With these two plots in mind, observe the picture of the equivalent functional network for the chosen agents in this task (Figure 4.10(c)). There are richer functional connections between nodes in the $2K_c$ network not only when comparing across different coupling configurations but also between the two vision conditions (inverted vision uses a denser set of functional connections than normal vision). This higher performing network is more able to reconfigure its internal functional architecture than its counterparts, allowing it to cope well with both conditions.

Figure 4.11 shows the temporal evolution of the net Transfer Entropy between nodes (Equation 4.6). It reveals the absence of significant readings in the uncoupled network but shows much higher levels in the $2K_c$ network as the task progresses, with the $10K_c$ network having alternating moments of high and low readings. This plot provides a different angle of analysis on our system by making evident the differences in the flow of information within the different networks and hence in the relationships between the nodes in the various contexts. Given that the phase difference dynamics captures all the effective dynamics of the Kuramoto model (Maistrenko et al., 2005), it's possible to see how different functional networks emerge from the interaction with the environment within the same coupling condition, stressing adaptability, or across different coupling conditions, revealing aspects of functional structure dependent on degree of coupling.

Comparing Figures 4.8(d) and 4.8(f) with Figure 4.11, notice how the magnitude of the ETE_{sm} and ETE_{ms} flows are high at particular moments of the task in the $2K_c$ agent, whilst the ETE between nodes has noticeable deviations from zero across the trial. There is, therefore, no clear similarity between the sensorimotor and the network's nodes phase activity information flow. In the $10K_c$ network, however, the higher variability of the flow between nodes have a correspondence in the ETE_{sm} and ETE_{ms} flow. This correspondence can be explained by the higher value of coupling between nodes in the sense that the sensorimotor activity perturbs a much more rigid framework, driving all nodes' behaviour. The $2K_c$ network is more loosely coupled so that the perturbations modulate and influence the nodes' behaviour, but do not ultimately determine it.

In summary, the previous experiments with categorical perception revealed a limitation of both weakly and strongly coupled networks in achieving good performance in discriminating objects with different shapes. The second experiment with orientation in normal and inverted vision conditions shows that the weakly coupled network continues to fail in a conflicting scenario, but the more strongly coupled networks succeed. The conclusion is that, for our framework, networks with high synchronisation levels are able to detect and respond to visual stimuli but struggle to exploit the environmental context. In other words, the highly synchronised structures evolved here can detect (even with altered vision) but not discriminate among different external stimuli. In

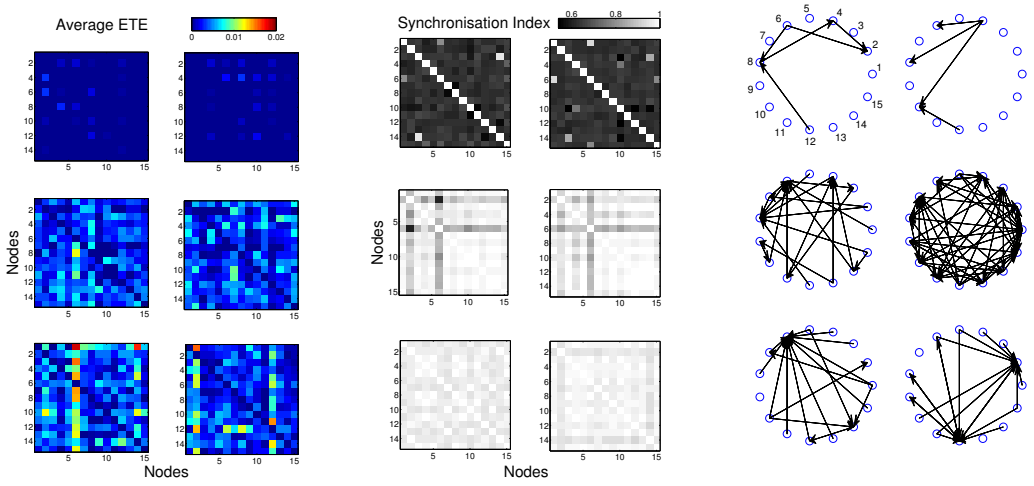

(a) (b) (c)

Figure 4.10: (a) Averaged information flow between the oscillatory nodes of the network (Equation 4.5). The autonomous flow is subtracted in all plots to highlight the task-specific activity. (b) Same as (a) but for the synchronisation index. (c) functional network - a directed arrow is drawn whenever the Transfer Entropy between two given nodes exceeds 50% of the maximum ETE value obtained in the whole task. The rows correspond (top to bottom) to the $0K_c$, $2K_c$ and $10K_c$ agents. The left side of each column refers to orientation with normal vision, the right to inverted vision.

both tasks, networks with 'intermediate' levels of coupling (and hence propensity for synchronisation) perform best as this provides a more fluid, flexible network able to reconfigure and adapt to different behavioural conditions. However, as we have seen, this optimal 'intermediate' level is significantly different for the two tasks.

4.4 Discussion

Current research on neurophysiological processes shows that oscillatory neural activity is closely related to cognition and behaviour, with synchronisation mechanisms playing a key role in the integration and functional organization of different cortical areas (Varela et al., 2001; Engel et al., 2001; Womelsdorf et al., 2007). Nevertheless, its informational content and relationship with behaviour - and hence cognition - are still to be fully understood (Rieke et al., 1997; Mazzoni et al., 2008; Deco et al., 2011; Flanders, 2011).

In this context, following an Evolutionary Robotics approach, we evolved simulated robotic agents controlled by a spontaneously rhythmic network of coupled phase oscillators, showing that

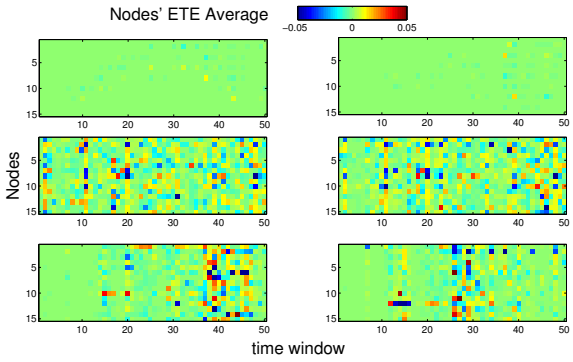

Figure 4.11: Net Transfer Entropy from a given node to all remaining nodes of the network in 50 equally spaced time windows (Equation 4.6). The autonomous flow is subtracted in all plots to highlight the task-specific activity. The rows correspond (top to bottom) to K_c, $2K_c$ and $10K_c$ agents. The left column is for normal vision and the right for inverted vision.

their performances in variations of a categorical perception task depend on the synchronisation regime of the network. This was also shown to be the case for an orientation task under normal and inverted vision, but the dependence on the synchronisation regime was quite different from the first task. The analysis focused both on a behavioural level description, investigating the agent/object trajectories, and on a mechanism level description, exploring the dynamics and the information transfer properties within and between the agent and the environment.

The design of the experimental framework attempted to capture relevant properties of its biological counterparts that would suit the aims of our study. The network model is inspired by the Kuramoto model of coupled phase oscillators whilst the robotics approach explores the enactive nature of sensory and cognitive processes. Our focus is on three aspects: the information flow between sensors and motors, capturing the body/environment interaction; the average flow between nodes of the network, stressing the internal communication; and the evolution in time of the average net flow from a given node to all its counterparts, revealing at various moments of the task a higher/lower participation in the overall information dynamics.

The first experiment explored the fitness variation of evolved individuals under different network couplings K for a categorical perception task. The results showed that there is a statistically significant difference in performance for different strengths of coupling, with the best fitness evolution performance obtained when $K = K_c$, the critical value. Although the term "critical" here is not directly related to its meaning for self-organised criticality (Beggs, 2008), previous work (Kitzbichler et al., 2009) showed that the Kuramoto model presents properties of critical systems (e.g. greater information transmission, storage, sensitivity to external stimulus) when its coupling is tuned to the critical value (Equation 3.5). Our results confirm this for the categorical perception

task.

For the agent with best performance ($K = K_c$), the dynamical analysis shows that there is a very rich phase behaviour in the critical coupled network, with nodes oscillating at a variety of frequencies, occasionally synchronising and forming independent functionally connected clusters. In the Effective Transfer Entropy (ETE) analysis, we notice a higher flow magnitude in the sensorimotor loop time series (ETE_{sm} and ETE_{ms}), which has a behavioural correspondence and relates to sharper adjustments in the agent's trajectory, suggesting that the agent is more able to convert sensory information into motor responses to maximize its performance; we also observe a much broader internal communication between oscillators, with a great variety of functional connections in comparison with other coupling configurations. Remarkably, even though the network is fully connected, the flow is not symmetric, and the higher performance of the critical coupled network can be linked to its flexible ongoing dynamics which can be modulated by the environmental context.

The second experiment studied orientation to falling circles under normal and inverted vision, particularly interesting for presenting to the agent an ambiguous and conflicting scenario.

We found that the performance increases with the degree of coupling, but this time reaches its peak between 2 and $4K_c$, decreasing for the very strong coupling values greater than that. We compared three evolved individuals, one with no coupling ($0K_c$), one with strong coupling ($2K_c$) and the other with very strong coupling ($10K_c$) between oscillators. The first is unable to succeed on the task whilst the 2 and $10K_c$ agents produce good performance in both sensory modes, with the $2K_c$ agent outperforming the very strongly coupled one.

Dynamical analysis shows that the $2K_c$ network rapidly synchronises, with some nodes escaping the entrained state only when the corresponding sensory input is large. However, there is a diverse phase dynamics, with conflicting values resulting in different phase dynamics that are exploited to generate fit behaviour that can cope with the different visual conditions. Therefore, even though the network has a fixed, all-to-all pre-established coupling configuration, with no explicit plasticity mechanisms, it can respond and adapt to conflicting sensory conditions and obtain good performance on the task. This is further stressed by the Transfer Entropy analysis which shows that the normal and inverted vision conditions elicit a difference in the information flow at specific points of the agent's trajectory. The results highlight the asymmetry of information flow and its behavioural correspondence obtained in fully connected oscillatory networks only by changing their level of synchronisation. Hence, the results suggest that synchronised networks with an 'intermediate' level of coupling are more able to reconfigure functional connections not only when comparing across different coupling configurations but also between the two vision conditions,

reflecting its superior performance on the task.

Concluding our analysis for both experiments, consider Figures 4.12(a) and 4.12(b), which display the formation of groups of oscillators during the execution of the task for the selected coupling conditions for Experiments 1 and 2, respectively. The network has initially 15 single-node "clusters", each corresponding to an oscillator. A group (cluster) is merged whenever the phase difference between two given nodes is below a certain threshold (chosen to be 1 here) and the frequencies are similar (less than $1Hz$ apart). Hence values vary from 1 (single, giant cluster containing all the oscillators) to 15 (single-node clusters).

In the first experiment, the uncoupled network is associated with a large number of single-node groups, whereas the strongly coupled network has only one big group through nearly all of the task, indicating complete synchronisation. Curiously, the critically coupled network alternates between these two extremes. The same behaviour is observed for Experiment 2, with the exception that the very strong coupled network desynchronises at the end of the task, as revealed by earlier analysis. These plots reinforce an important aspect raised in the Introduction and mentioned throughout the chapter: synchronisation dynamics modulate the assembly, collapse and reconfiguration of functional sub-networks. In our experiments, a higher diversity of such assemblies are present in the top performing agents, linking the adaptability of the agent to the flexibility of its functional connections.

The previous analysis is complemented by Figures 4.12(c) and 4.12(d), which present the dynamics of a metastability index λ and the Largest Lyapunov Exponent (LLE) for the chosen scenarios. λ (Equation 4.7) is calculated as the estimated variance of the synchronisation index r (Eq. 3.4) over all time points $t = 1 \ldots T$ and reflect the diversity of synchronisation states obtained for each coupling configuration of the network (Shanahan, 2010b).

$$\lambda = \frac{1}{T-1} \sum_{t=1}^{T} (r(t) - < r >_T)^2 \tag{4.7}$$

The Largest Lyapunov Exponent, calculated using the phase variables θ_i, $i = 1 \ldots N$ (Maistrenko et al., 2005), indicate how chaotic the phase dynamics - and hence our system - are. To obtain the LLE, we followed the method described in Rosenstein et al. (1993) which is specially designed to be robust and fast in small data sets.

In both experiments, we notice that the metastability decreases (as expected) as the coupling increases, showing that there is less variation in the synchronisation index. The dynamics of the number of groups relate to the metastability index, with the critically coupled network also appearing in an intermediate position. An interesting point for the critical coupling condition is to notice how the agent/environment interaction in the categorical perception task reduces the spontaneous

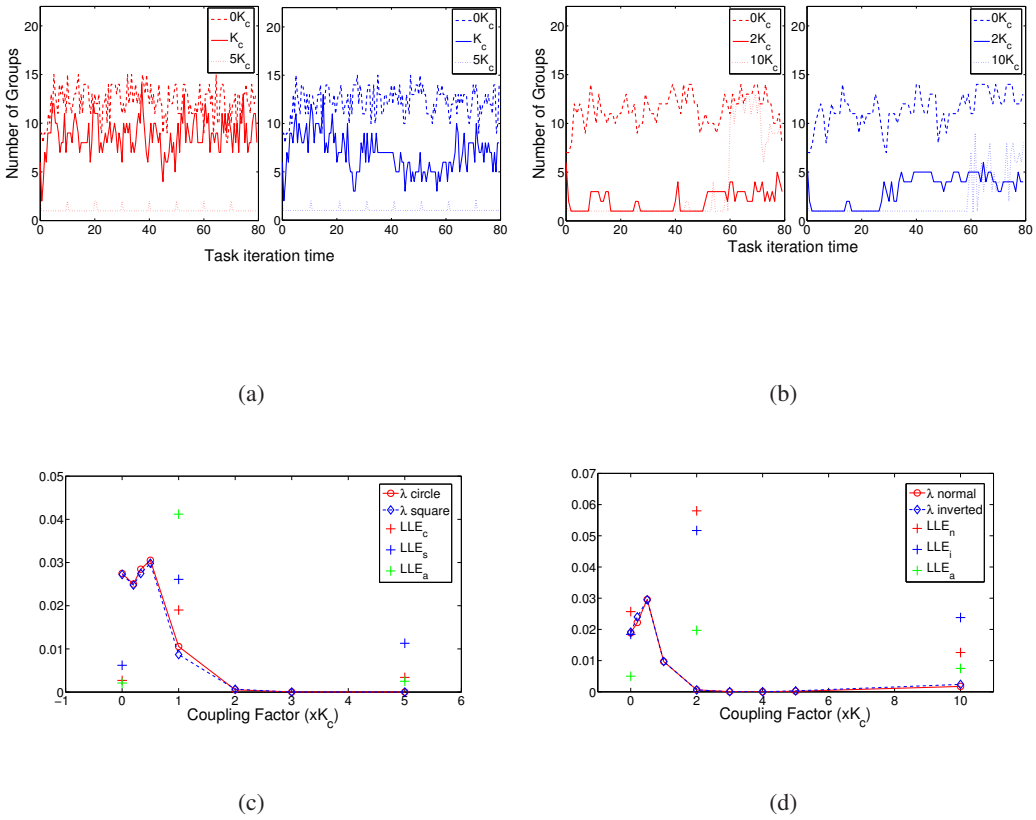

Figure 4.12: Clustering of oscillators and metastable states for different coupling conditions as the task progresses. (a) and (b): nodes that have similar frequencies and a phase shift below a small threshold are grouped. Values vary from 1 (single, giant cluster containing all the oscillators) to 15 (single-node clusters). (c): metastability index λ (Equation 4.7) superposed with the Largest Lyapunov Exponent (LLE) for the circle (LLE_c), square (LLE_s) and autonomous (LLE_a) configurations. Larger λ indicates a great diversity of synchronisation states in the network as the task progresses; LLE greater than 0 suggests chaotic dynamics. (d): same as (c), but for the normal vision, inverted vision and autonomous configurations. Figures (a) and (c) refer to Experiment 1 and Figures (b) and (d) refer to Experiment 2.

chaoticity level of the network (calculated for the autonomous network dynamics), whereas in the inverted vision scenario, near the critical coupling, chaotic behaviour is more prominent when the agent is engaged in the task than when under the influence of the autonomous network dynamics. Also, note that the Largest Lyapunov Exponent is close to zero in the uncoupled autonomous scenario for both tasks ($0K_c$). This is anticipated and due to the lack of external stimulus, which makes each node of the network oscillate independently in a quasiperiodic way. The sensorimotor coupling changes this behaviour (even without connections between nodes, coupling can be seen as occurring "indirectly" through the environment), and the network activity becomes more

chaotic. Therefore, the above observations reflect the adaptability and modulation of the network activity previously noticed in the information flow analysis. It also suggests that although neural synchronisation clearly plays an important role in the generation of behaviour in the fittest agents, other kinds of transient dynamics are also exploited (Santos et al., 2011).

In summary, this chapter explored the influence of synchronisation in behavioural performance and information dynamics in variations of a categorical perception task. The next chapter takes another perspective and investigates neural assembly computations in supervised and unsupervised learning tasks.

Chapter 5

Neural Assembly Computations

The dynamic formation of groups of neurons - neuronal assemblies - is believed to mediate cognitive phenomena at many levels, but their detailed operation and mechanisms of interaction are still to be uncovered. One hypothesis suggests that synchronised oscillations underpin their formation and functioning, with a focus on the temporal structure of neuronal signals. In this context, we investigate neuronal assembly dynamics in two complementary scenarios: the first, a supervised spike pattern classification task, in which noisy variations of a collection of spikes have to be correctly labelled; the second, an unsupervised, minimally cognitive evolutionary robotics tasks, in which an evolved agent has to cope with multiple, possibly conflicting objectives. In both cases, the more traditional dynamical analysis of the system's variables is paired with information theoretic techniques in order to get a broader picture of the ongoing interactions with and within the network. The neural network model allows one to fine tune the network synchronisation dynamics and assembly configuration. The experiments explore the computational power, redundancy, and the generalisation capability of neuronal circuits, demonstrating that performance depends nonlinearly on the number of assemblies and neurons in the network, and showing that the framework can be exploited to generate minimally cognitive behaviours, with dynamic assembly formation accounting for varying degrees of stimuli modulation of the sensorimotor interactions.

5.1 Introduction

Since Hebb's seminal work on brain activity (Hebb, 1949), the transient formation of neuronal groups or assemblies is increasingly linked to cognitive processes and behaviour. However, as stressed in Chapter 2, it is still unclear how neuronal groups form, organize, cooperate, and interact over time.

In this chapter we focus on a pragmatic investigation of three aspects of computations in neuronal assemblies. Given a computational task and a neural network model, comprised of many neurons that are organised in an arbitrary number of assemblies, (1) does increasing the number of neural assemblies improve performance? (2) Does the number of neurons per assembly affect performance? (3) Can dynamic assembly reorganization alone, leaving aside other plasticity mechanisms, be exploited to solve different tasks?

We approach these questions employing a neural network model based on the Kuramoto model of coupled phase oscillators (Section 3.3). In addition to modelling constraints (described in Section 5.2), the original Kuramoto model has limited spectral complexity compared to that of more biologically plausible neuronal models (Bhowmik & Shanahan, 2012); for this reason, recent extensions have been formulated to enhance its suitability to study a variety of neurobiological phenomena, incorporating e.g. spatially embedded couplings, transmission delays, and more complex phase response curves (Breakspear et al., 2010; Wildie & Shanahan, 2012). Nevertheless, it is possible to represent neurons as simple phase oscillators, model the spiking of individual cells, and results can still be of relevance. Indeed, this is exactly the objective, to avoid physiologically precise models that could make the analyses laborious and instead use a model that despite all the simplifications still presents complex and relevant spatiotemporal activity. One particular extension, presented in Orosz et al. (2009), allows one to fine tune the synchronisation regime, the number of assemblies, and the number of neurons per assembly, thus suiting our study, whilst also avoiding any problems in obtaining phase information (an issue in other models which consider frequency and amplitude dynamics (Pikovsky et al., 2001)). Hence the extended Kuramoto model is highly relevant, at a certain level of abstraction, to modelling neural mechanisms underlying adaptive and cognitive behaviours and is used in the studies presented here.

The experiments were set-up to encompass supervised and unsupervised learning scenarios (Dayan & Abbot, 2001). In supervised learning, there is an explicit target or supervisory signal mapping each set of inputs to expected outputs. In unsupervised learning, the system exploits the statistical structure of the set of inputs and operates as a self-organised, goal-oriented process. Although the latter is regarded as being more common in the brain, evidence suggests that both learning paradigms overlap and may be implemented by the same set of mechanisms (Knudsen, 1994; Dayan, 1999).

The first experiment, a supervised learning scenario, follows a method described in Maass et al. (2005) and Legenstein & Maass (2007) to assess computational performance in generic neuronal microcircuits. More specifically, we analyse the computational power and generalization capability of neuronal networks with diverse assembly configurations in a generic spike

pattern classification task. The method is specially suited to our goals because it proposes a measure to test the computational capability of neural microcircuits that is not exclusive to the task investigated here but to all computational tasks that only need to have in common which properties of the circuit input are relevant to the target outputs. In networks with the same number of neurons, we show that the performance of architectures constituted by many assemblies (and fewer neurons per assembly) is higher than the ones with fewer assemblies (and more neurons per assembly). We also show that in networks of varied size performance saturates as soon as a given number of assemblies is formed, and the addition of neurons in each assembly does not influence performance in the classification task. In both scenarios, an analysis of redundancy and synergy, based on concepts of information theory, supports and provides further insights into the properties of the system.

The pattern classification task mentioned above may reflect or mimic some of the computations that are actually carried on in a real-world cognitive scenario, nevertheless it does not capture the main task of cognition, which is the guidance of action. As pointed out in Engel et al. (2001), "the criterion for judging the success of cognitive operations is not the correct representation of environmental features, but the generation of actions that are optimally adapted to particular situations". Therefore, in the second experiment, an unsupervised learning scenario, we investigate evolved embodied cognitive behaviours in a simulated robotic agent. Following an Evolutionary Robotics approach, we show that the same network architecture of Experiment 1 can be used as a control system for a simulated robotic agent engaged in a minimally cognitive task, and that assembly reconfiguration can account for good performance in multiple, possibly conflicting tasks. The analysis is centred both on the system's variables dynamics, illustrating the interplay between dynamic assembly formation and the action being displayed by the robot, and the information dynamics between some components of the system, which complements the former analysis by quantifying and emphasising the non-linear relationships that are present in the brain-body-environment interactions.

As a consequence of approaching different learning paradigms, the analyses for the two experiments use distinct, but appropriate, tools. However, it is important to stress that the above experiments are conceptually connected by the emphasis on neuronal assembly dynamics and its impact on task performance. The methods employed to explore supervised learning tasks struggle to operate in unsupervised scenarios because the former rely on coordinated, time-specific perturbations and measurements, with a focus on precise classifications, whilst the latter are mainly concerned with the behaviour of the evolved robots. Notwithstanding, the first experiment provides insights into the system's dynamics which contribute to the comprehension of the more elaborated

second experiment. In this sense, the supervised and unsupervised learning tasks and the respective methods of investigation do not contradict but rather reinforce the flexibility of the framework in addressing diverse learning problems.

The chapter is organized as follows: Section 5.2 presents the neural network model, including the extension to the Kuramoto model which facilitates the study of assembly dynamics; Sections 5.3 and 5.4 contain task-specific analysis methods and the results of the first and second experiment, respectively; the chapter concludes in Section 5.5 by highlighting the main contributions and giving a general discussion of the results obtained.

5.2 Neural Network Model

Let us recall the original Kuramoto model (Equation 5.1), described in Section 3.3[1].

$$\dot{\theta}_n = \omega_n + \frac{K}{N}\sum_{m=1}^{N}\Gamma(\theta_n - \theta_m), n = 1, \ldots, N. \tag{5.1}$$

where θ_n is the phase of the *n*th oscillator, ω_n is the natural frequency of the *n*th oscillator, K is the coupling factor between the nodes of the network, $\Gamma(\theta_n - \theta_m) = sin(\theta_n - \theta_m)$ represents the interaction between nodes, and N is the total number of oscillators.

Ashwin et al. (2007) and Wordsworth & Ashwin (2008) showed, when adopting a specific Γ, that the model is able to display heteroclinic cycles, a fundamental mechanism of cognition according to some authors (Ashwin & Timme, 2005; Rabinovich et al., 2012). Additionally, Orosz and collaborators (Orosz et al., 2009) demonstrated how to design Γ so that the network organizes itself in an arbitrary number of stable clusters with a given phase relationship between clusters. These clusters, which emerge as an attractor of the system, remain stable up to a certain level of perturbations, applied in the form of inputs, above which a reorganization occurs, maintaining the same number of assemblies but with different membership configurations. Therefore, considering the aims of our study, this latter extension will be used in the subsequent experiments. Equation 5.2 describes the model for N oscillators (Orosz et al., 2009):

$$\dot{\theta}_n = \omega_n + \frac{K}{N}\sum_{m=1}^{N}\Gamma(\theta_n - \theta_m) + \epsilon_n I_n(t),\ n = 1, \ldots, N, \tag{5.2}$$

where $I_n(t)$ is an input scaled by a factor ϵ_n, and the PIF $\Gamma(\chi)$ has the form of Equation 5.3:

[1] In this chapter we used a different index notation compared to the one that was used in the previous chapters. This is to be consistent with the notation used in previous works that use some of the methods employed in this chapter. Therefore, two given oscillators θ_i and θ_j are referred to, in this chapter, as θ_n and θ_m.

$$\Gamma(\chi) = f_M(\chi) + f_M(\chi - \xi) \tag{5.3}$$

where $f_M(\chi) = -2tanh(Msin(\chi/2))sech^2(Msin(\chi/2))cos(\chi/2)$ and $\xi = 2\pi/M$.

This PIF is obtained by a suitable choice of Γ and its derivatives to ensure that a system with N oscillators will present M stable assemblies separated equally in phase, with oscillators grouped according to their initial phases (which will dictate their position in the attraction basin determined by the total number of assemblies and parameter M). Assembly membership, i.e. which oscillator belongs to which assembly, can be changed if one applies an input to a given oscillator with a minimum magnitude and length. These will depend on the number of oscillators and assemblies (parameter M) of the network. Nevertheless, small perturbations still affect the overall behaviour of the system.

Observe Figure 5.1, which illustrates the main properties of the model. In this example, the network is composed of 9 fully connected neuronal oscillators with unitary couple (without loss of generality, the PIF is assumed to capture any effect due to larger or smaller couplings). The initial phases are uniformly distributed in the interval $[0, 2\pi)$, and the oscillators organize in $M = 3$ different (but with equal number of members) assemblies after a settling period (Figure 5.1(c)). As the focus is on neuronal assembly in terms of phase relationships, we set the natural frequency w_n of all neurons to 1. In Figure 5.1(d), the raster plot shows the neuronal spikes that occur every time the phase of each oscillator reaches a given threshold (0 in the example, but any other marker is acceptable). Notice from both aforementioned figures the formation of three assemblies of three neurons each.

After a settling period the system stabilizes in M assemblies and presents a periodic firing behaviour. However, inputs to one or more neurons can change the network dynamics in two ways: it can modulate the ongoing activity in all assemblies without changing their organization or it can cause the assemblies to rearrange. Figure 5.1(e) illustrates the effect (see the caption for simulation parameters). At the beginning of the simulation, the initial phase values of each neuron will determine to which assembly each neuron will be associated. The number of assemblies (parameter M) determine the size of the attraction basin and hence the necessary input amplitude and length to cause a given node to switch assemblies. In the example, the phase of an oscillator has to be perturbed by an absolute value greater than $\pi/3$ to change to a different stable cluster. At time $t = 30$, an input of sufficient duration and magnitude is applied to one neuron causing it to "jump" and take part in a different assembly. At iteration $t = 50$, an input of the same duration but smaller amplitude than the one at $t = 30$ perturbs the overall dynamics of the network but does not result in a change in assembly membership. Lastly, at iteration 70 an input of the same

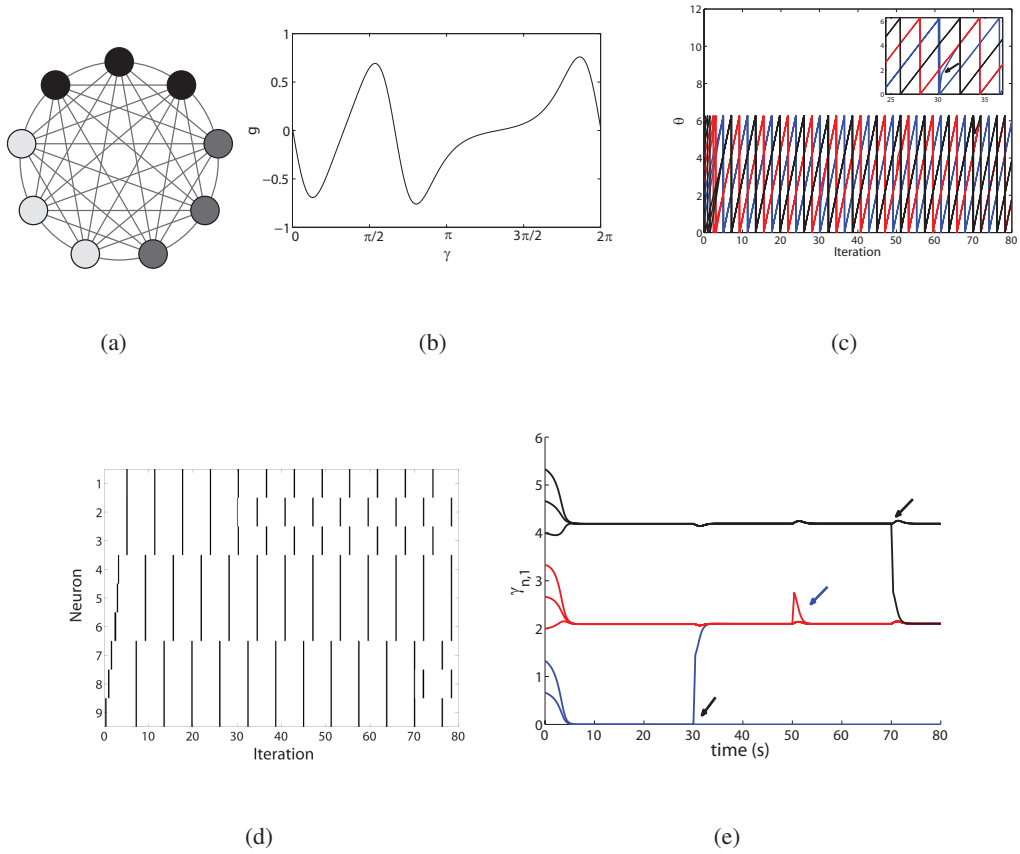

(a) (b) (c)

(d) (e)

Figure 5.1: Model simulation using the PIF described by Equation 5.3, with parameters $N = 9$, $M = 3$, $K = 1$ and $w_n = 1$. Oscillators form 3 clusters, and inputs to a given oscillator cause a transition to a different cluster, if the magnitude is high enough, or a modulation of the network behaviour, if the input is small enough. (a) Network topology model. (b) PIF diagram (Equation 5.3). (c) Phase dynamics of each oscillator. The initial phases are uniformly distributed in $[0, 2\pi)$, and as the simulation progresses the oscillators form $M = 3$ assemblies (assembly membership is represented by different colours in the plot). The small plot shows the moment ($t = 30$, see the black arrow) one oscillator moves from one assembly (blue) to another (red). (d) Raster plot showing the neuronal spikes that occur every time the phase of each oscillator reaches 0. (e) Effects of inputs on the system's dynamics, portrayed as the phase difference $\gamma_{n,1}$ of each node n to node 1: inputs can cause an oscillator to change assemblies (black arrows) or modulate its ongoing activity within the same assembly (blue arrow).

duration but opposite magnitude as the first causes the related neuron to jump to another assembly. Notice, in the insert plot of Figure 5.1(c) and in the raster plot in Figure 5.1(d) the changes in phase dynamics and spiking activity due to different forms of inputs.

5.3 Experiment 1

Maass et al. (2005) proposed a method to evaluate the computational power and generalization capability of neuronal microcircuits which is independent of the network set up. In this first experiment, the model described in the last section is used to analyse the computational performance of networks structured in various assembly sizes with diverse numbers of neurons per assembly. In all of the following analysis, different network configurations are obtained varying the value of M (Equation 5.2) and the initial phase of each neuron.

5.3.1 Methods

Classification Tasks, Computational Power, and Generalisation Capability

Maass et al. (2005) proposed the linear separation property as a quantitative measure for evaluating the computational power of a neuronal microcircuit. The premises are that the microcircuit consists of a pool of highly recurrently connected neurons and that the information encoded in their activity can be extracted by linear readout neurons able to learn via synaptic plasticity, with no influence from readout units to the microcircuit. In this way, the system resembles the Echo State Network (Jaeger, 2001) and the Liquid State Machine (Maass et al., 2002) frameworks, in which the dynamics of a highly connected and recurrent reservoir of neurons are captured by a readout unit (commonly linear); importantly, the readout unit is trained but the weights of the recurrent reservoir are fixed, which greatly simplifies the training problem by reducing it to a linear regression problem. Although these simplifying assumptions impact on the biological relevance of the results, they are still valid in face of the many uncertainties regarding electrochemical interactions in the brain and the nature of neural coding. In fact, literature in brain-machine interface (BMI) studies has been able to show that a relatively simple linear readout unit from a reduced number of neurons is able to extract the relevant neuronal activity that relates to the action being performed (Lebedev et al., 2005). Also, Buzsáki (2010) argues that cell assembly activity can be better understood from a "reader" perspective, able to produce outputs given the ongoing activity.

Consider the model described by Equation 5.2. Let us call the n size vector $\theta(t_0)$ the system state at time t_0. Now consider a neuronal microcircuit C and m different inputs $u_1, \ldots, u_m$ that are functions of time. One can build a $n \times m$ matrix M, in which each column consists of the states $\theta_{u_i}(t_0)$, i.e. each column consists of the phase value of each node n at time t_0 after the system has been perturbed by an input stream u_i. The rank $r \leq m$ of matrix M can then be considered as a measure of the computational power of circuit C. Based on linear algebra, the rationale is as follows: if M has rank m, a linear readout unit of microcircuit C can implement any of the 2^m

possible binary classifications of the m inputs, i.e. any given target output y_i at time t_0 resulting from the input u_i can be mapped by a linear readout unit (Maass et al., 2005).

Another important measure regarding a neuronal microcircuit is its ability to generalise a learnt computational function to new inputs. Consider a finite set S of s inputs consisting of many noisy variations of the same input signal. One can build a $n \times s$ matrix M whose columns are the state vectors $\theta_{u_s}(t_0)$ for all inputs u in S. An estimate of the generalisation capability of this circuit is then given by the rank r of matrix M. See Vapnik (1998) and Maass et al. (2005) for a more complete description of the method.

In the experiment, we evaluate oscillatory neuronal networks comprised of 80 ± 4 neurons organised in different assembly configurations. Ideally, for consistency in the comparisons between the measurements, the system should always have the same number of states across different trials; however, as we are interested in the gradient of performance when comparing different assemblies set up, we have used architectures with a few more or a few less states to allow for a broader set of configurations.

In this way, for a variety of possible architectures of microcircuits C, the task consists of classifying noisy variations u of 20 fixed spike patterns which were arbitrarily divided into two classes (0 or 1). For one randomly chosen classification task (there are 2^{20} possible classifications of the spike patterns), the objective is to train a linear readout unit to output at time $t = 4s$ the class of the spike pattern from which the noisy variation input had been generated. Each spike pattern u consisted of a Poisson spike train with a rate of $1Hz$ and a duration of $4s$. Inputs are always applied to node 2 of the network, according to Equation 5.2.

At the beginning of a simulation, 20 fixed spike patterns are generated. For each pattern, we produced 30 jittered spike trains by jittering each spike in each spike train by an amount drawn from a Gaussian distribution with zero mean and standard deviation of 5. Spikes which were outside the time interval of zero and $4s$ after jittering were rejected. 20 of the jittered sequences are used for training and 10 are used for testing the performance. Figure 5.2(a) shows some examples of input spike trains and the respective jittered versions. For each simulation, we randomly classified 10 spike patterns as belonging to class 1 and 10 to class 0 (recall that there are 2^{20} possible forms of classifying the patterns).

To calculate the computational power, we generated 76 different spike patterns in the same way as for the classification task described above. The state vectors of the neuronal circuit at time $t = 4s$ ($\theta(t_0 = 4)$) with one of the 76 spike patterns as input were stored in the matrix M, and its rank r was estimated by singular value decomposition. To calculate the generalisation performance, the procedure was similar to the one just described but instead of using 76 spike

patterns as inputs to the network we used 38 jittered versions of two different spike patterns, following the recommendation that the number of network states should be superior to the size of S (Legenstein & Maass, 2007).

Redundancy and Synergy

Another insight into the activity of neuronal assemblies can be given by measurements of redundancy and synergy (Reich et al., 2001; Schneidman et al., 2003; Narayanan et al., 2005). In a given network composed of many interacting neurons arranged in assemblies, if the information encoded by a given pair of neurons is greater than the sum of the information encoded by the individual neurons, we say that there is a synergistic interaction; if it is less, we say that the interaction is redundant.

Consider a neuronal network, with an activity set A_n of each individual neuron n composed of a states, and a finite set S of s inputs. The mutual information (in bits) between the stimuli and the responses, i.e. the reduction of uncertainty about the stimuli given that the neuronal activity A is known, is given by Equation 5.4:

$$I(S;A) = H(S) - H(S|A) = \sum_{s \in S} \sum_{a \in A} p(s,a) \log_2 \left[\frac{p(s,a)}{p(s)p(a)} \right] \tag{5.4}$$

The equation for a pair of neurons is thus:

$$I(S;A_1,A_2) = \sum_{s} \sum_{a_1,a_2} p(s,a_1,a_2) \log_2 \left[\frac{p(s,a_1,a_2)}{p(s)p(a_1,a_2)} \right] \tag{5.5}$$

Given the two equations above, the synergy between a pair of neurons is then defined as (Schneidman et al., 2003):

$$Syn(A_1,A_2) = \frac{I(S;A_1,A_2) - I(S;A_1) - I(S;A_2)}{I(S;A_1,A_2)} \tag{5.6}$$

Notice that if the mutual information between the two neurons is 0, i.e. if they have unrelated activity, Equation 5.5 reduces to $I(S;A_1,A_2) = I(S;A_1) + I(S;A_2)$, and the synergy value given by Equation 5.6 is 0. Synergy varies from -1, if the interaction between the neuronal pair is completely redundant, to 1, when the information conveyed by the pair activity is greater than the information conveyed individually by the neurons.

To estimate the synergy value, stimuli consisted of 8 noisy variations of 8 different spike patterns, lasting for 200 iterations and with the same characteristics as detailed before, and the neuronal activity A_n is the phase value of neuron n at the end of the simulation. We performed 20 experiments for each pair of neurons, and a total of 10 different randomly chosen pairs were

used. The results were then averaged. The sets S and A were discretised into 8 equiprobable states, which improves the robustness of the statistics (Marschinski & Kantz, 2002), and finally the joint probabilities associated to the information related measures were estimated using histograms (Lungarella et al., 2007a). In this way, at the end of each experiment, a table whose columns are all the possible combinations of $[a_1, a_2]$ and whose lines are all the possible stimuli $s_1, \ldots, s_8$ is formed, and each field of this table contains the probability $p(a_1, a_2|s_n)$, from which the synergy calculations were performed (Equations 5.4 to 5.6). An important point to stress is that ideally we should have tested all possible neuron pairs and assembly combinations, but that would have been computationally prohibitive. Nevertheless, considering the standard deviations observed in the experiments that follow, we believe the results are informative.

5.3.2 Results

Figure 5.2(b) shows the results for the classification performance, the computational power, and the generalisation capability of the system. Notice the increase in performance as one moves from networks with fewer assemblies (and more neurons per assembly) to architectures constituted by many assemblies (and few neurons per assembly). The computational power and the generalisation capability have the same values until a critical architecture is reached, after which they start to behave differently. Recall that both measures are based on calculations of matrices' ranks, which indicate the maximum number of linearly independent rows or columns (whichever is smaller). With just a few assemblies composed of several neurons, each assembly works as a single, large oscillator, and inter-assembly modulations due to external perturbations are minimum. The rank value, thus, is directly connected with the number of assemblies in the system. As the assemblies increase in number and decrease in size, inter-assemblies modulations become more prominent, and this is captured by the rank of the state matrix. The results indicate, therefore, that networks with more assemblies have the potential to classify a greater number of input patterns. In contrast, the greater the value of the rank of the state matrix M, the worse the generalisation of the circuit is likely to be, which means that small perturbations in spike times for a given spike pattern tend to be classified as belonging to a different spike pattern.

Maass et al. (2005) and Legenstein & Maass (2007) showed that, combined, the above two measures may provide a good estimate of the computational capabilities of a given neuronal microcircuit and may also be used to predict its performance in a classification task. There's no ultimate method for combining them both, but simply using the difference between the computational power and the generalisation performance can be a good indicator. Figure 5.2(b) shows the result. As explained in the previous paragraph, due to properties of the model the matrix ranks

calculated for each measure differ only for architectures with higher number of assemblies; the prediction of computational performance, therefore, is only applicable for a subset of all possible configurations of our model. Nevertheless, the prediction points at the correct region of possible architectures where performance is maximum.

Consider Figure 5.2(c), which shows the response of three different network configurations to variations in some simulation parameters: the number of different spike patterns presented to the network for classification, the frequency of the input spike trains, and the noise rate used to generate the jittered spike trains. Notice that increasing the value of the first or the latter results in a fall in performance, whilst the performance peaks at an intermediate value of the input frequency. This shows that classifying 60 different patterns (2^{60} possible classifications) is harder than classifying 20 using the same framework. Also, the relatively small variation in performance due to the input frequency indicates that the model has a good spike pattern discrimination time resolution.

Not surprisingly, noisier spike trains result in more classification mistakes, for an otherwise noisy train is now viewed as a different spike pattern, but notice that the drop in performance is sharper for networks composed of more assemblies (22.6% for a network with 40 assemblies in contrast with a 10% fall for a network with 10 assemblies), in agreement with what the generalisation analysis predicted. One of the reasons this might occur is illustrated in Figure 5.2(d). It shows the state separation of the system, a measure that captures how much the state $\theta(t)$ of one network reflects details of the input stream that occurred some time back in the past. Consider two input patterns u and v over 3000 iterations that differ only during the first 1000, with the same properties as described before. The state separation is given by $\|\theta_u(t) - \theta_v(t)\|$ for $t = 3000$. Notice that the architectures with fewer assemblies have a lower value of state separation than the ones with more assemblies, which means that perturbations caused by earlier input differences persist more in the latter configurations. For noisy spike trains, such amplified differences may impact on the overall pattern classification performance. The results also highlight that networks with more assemblies are affected more by inputs, which can be explained considering that in the latter case the network state $\theta(t)$ at a given time t is less influenced by the activity of a single neuron and more a product of the whole network interaction.

The synergy analysis confirms this last point (see Figure 5.2(d)). Notice that for architectures with fewer assemblies the level of redundancy is high ($Syn = -1$, Equation 5.6), but it reduces as the number of assemblies grow. The vast majority of networks with higher number of assemblies present information independence ($Syn = 0$), i.e., the information conveyed by the pair of neurons is the sum of the information they convey separately. Importantly, Schneidman et al. (2003) make the point that information independence may relate to neurons being responsive to

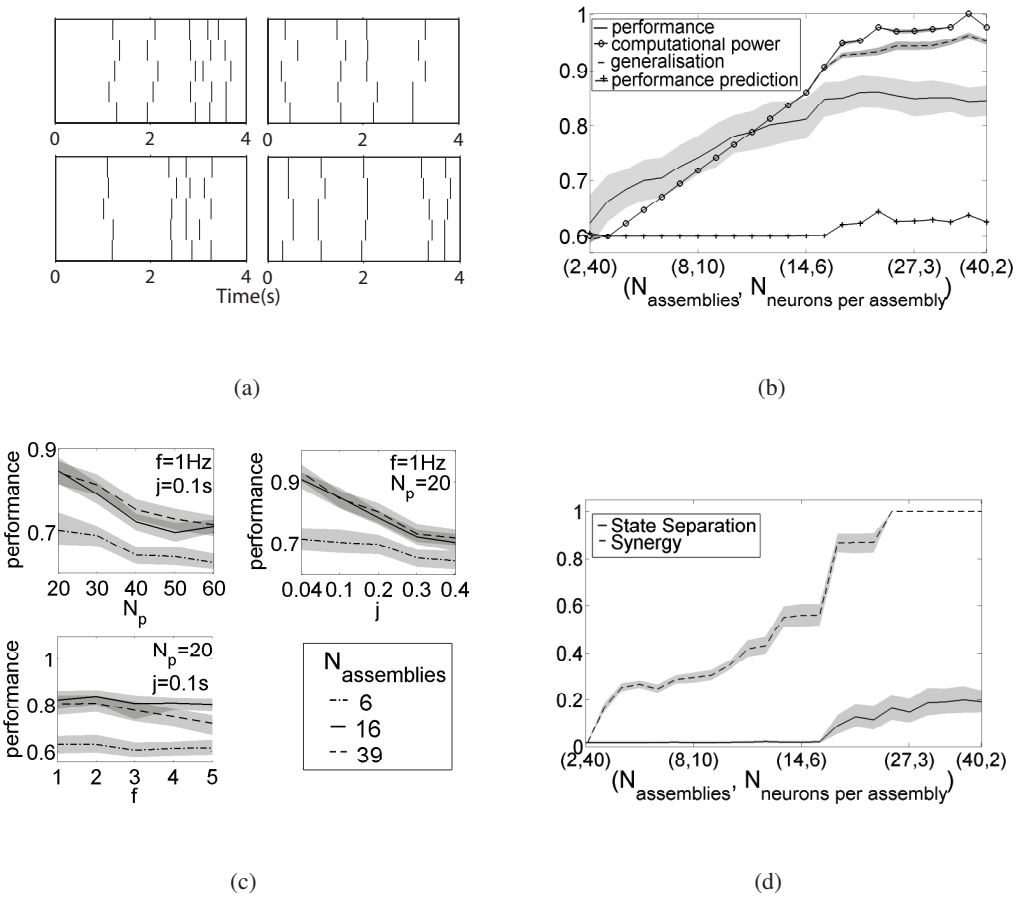

Figure 5.2: Results for Experiment 1. (a) Examples of spike trains used as inputs. In each of the four panels, five spike trains are presented: the original spike pattern (top train of each panel) and 4 respective jittered versions. (b) Classification performance (fraction of correct classifications) obtained by architectures of approximately 80 neurons arranged in diverse number of assemblies; computational power - the higher this values, the better a linear readout unit can discriminate between different input spike patterns (values are normalised between 0.6 and 1 to improve visualisation); generalisation capability - the smaller this values, the more likely the variations in a spike train will be interpreted as noise instead of consisting of a different spike train; performance prediction, calculated as the difference between the computational power and generalisation capability. (c) Impact on the classification performance of three different architectures (6, 16, and 39 assemblies composed of 13, 5, and 2 neurons, respectively) caused by variations in three parameters of the input spike train (each parameter is varied whilst keeping the other two constant): the standard deviation of the Gaussian jitter in the spike trains j, the spike firing rate f, and the number of patterns to classify N_p. (d) State separation and Synergy (rescaled to vary between 0 and 2 to improve visualisation). Higher values of the first indicate that the network state $\theta(t)$ reflects more details of the input stream that occurred some time in the past, higher values of the latter indicate a more synergistic system. All the previous results are mean values over 20 different simulations, and shaded areas are the 95% confidence interval.

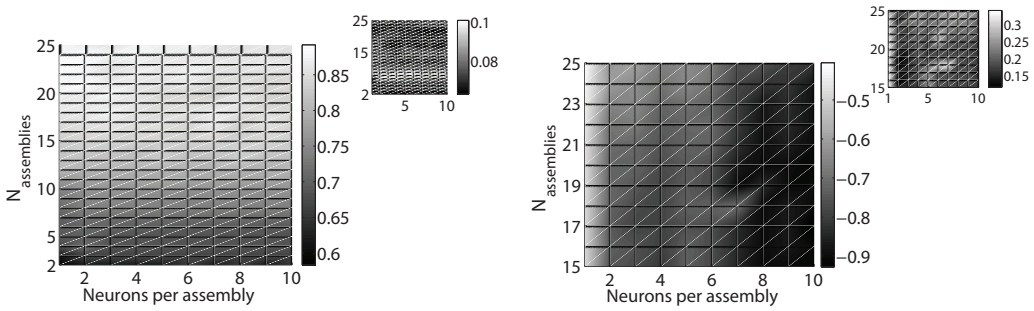

(a) (b)

Figure 5.3: Simulation results for Experiment 1. (a) Classification performance and (b) Synergy values (not normalised) for different network configurations. In contrast to Figure 5.2, in which all architectures had approximately 80 neurons, here the number of assemblies and neurons are varied independently. Results are mean values over 20 different simulations, and the small plot within each figure is the standard deviation.

different features of the stimulus, but the synergy measurement reflects an average over the whole set of stimuli S; for that reason, the neuronal pair may be redundant, synergistic, or independent for different subsets of S. Also, Reich et al. (2001) found neuronal pairs in nearby cortical neurons presenting varied forms of interactions - more specific, independent and redundant interactions. Thus, the measurements portrayed in the figure may be a result of averaging, not from independence, across the whole trial.

In the results above, we investigated networks with roughly the same number of states ($N_{assemblies} \times N_{neurons/assembly} \approx constant$). This constraint had to be imposed in order for the calculations of computational power and generalisation capability to hold. However, another interesting aspect of assembly computations is how performance and synergy change as one varies the number of neurons within each assembly for a given number of assemblies in the network. Figure 5.3 shows the results. Performance is predominantly higher in networks with more assemblies, regardless of the number of neurons within each. In other words, performance increases as the number of assemblies increases, but given a certain network with fixed number of assemblies, adding neurons to each assembly does not cause a salient increase in performance (e.g. networks with 2 assemblies with 1 or 5 neurons within each assembly have a classification performance of approximately 0.6 whereas networks with 20 assemblies with 1 or 5 neurons in each cluster have a classification performance of approximately 0.85). In contrast, the level of redundancy or independence is related mainly to the number of neurons within each assembly, regardless of the total number of assemblies (see Figure 5.3(b)). For example, neurons in a network with 20 assem-

blies with 1 neuron in each assembly present a much more independent activity than neurons in a network with 20 assemblies composed of 10 neurons each. This is in accordance with results obtained in motor cortex studies, which show that the synergistic or redundant interactions depend on the size of each neuronal assembly, and redundancy increases with the size of assemblies (Narayanan et al., 2005).

Recall that assemblies are formed by their phase relationship, i.e. two neurons belong to the same assembly only if they are synchronised with near zero phase lag. In this sense, the synchronisation properties of the network (dictated by the phase interaction function defined in Equation 5.3) make the dynamics of neurons constituting the same assembly similar and the dynamics of neurons constituting different assemblies dissimilar. Thus, increasing the number of assemblies, not the number of neurons, impact more on performance, and that is possibly due to an increase in entropy. However, the rationale is not simple because of nonlinear effects and the intrinsic dynamics of the network responding to inputs. Notably, the Kuramoto model presents second-order phase transitions and a given node can influence in different ways other nodes in the network, depending on the relationship between natural frequencies and on whether nodes are directly connected or not. Some of these effects may be in place, given the saturation in performance and the nonlinear impact on classification to adding assemblies or neurons to the network. In this sense, it is not trivial that adding neurons maximizes the classification performance because this is determined by the way these neurons are organised (assemblies) and limited by non-linear effects (highlighted by the saturations depicted in Figures 5.2(b) and 5.3(a)).

To conclude Experiment 1, we investigate whether the system can cope with multiple tasks by just relying on the phase dynamics, without any changes in the readout unit after training. This is performed by manipulating assembly membership, as described in Section 5.2, in order to solve opposite versions of a classification task. Changes in assembly membership (phase reorganisation) can be thought of as emulating attention mechanisms, which, according to experimental evidence (Steinmetz et al., 2000; Lakatos et al., 2008), can promote phase resetting and modulate the ongoing neuronal oscillations to respond differently to stimuli, thus justifying our approach. In the experiment that follows, the network architecture has been arbitrarily chosen to have 10 clusters of 8 neurons each, with similar results obtained for other configurations.

To begin with, we present to the network spike patterns that have to be classified. At the end of each pattern presentation, the network state $\theta(t)$ is stored, representing the system's response for this given input. After all the patterns are shown, the phase relationships in the network are reorganised (see Figure 5.4(a)). Then, we present the same spike patterns once more, the network state is stored, but the corresponding classification label (1 or 0) for each pattern is made exactly

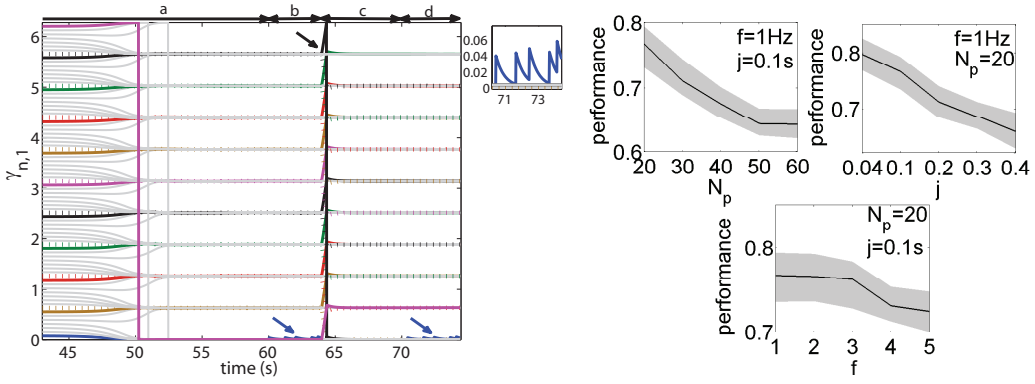

(a) (b)

Figure 5.4: Multiple classification task with dynamic network reconfiguration in an architecture of 10 assemblies with 8 neurons each. (a) Phase dynamics portrayed as the phase difference $\gamma_{n,1}$ of each node n to node 1. Coloured solid and dashed lines indicate nodes that change assembly membership (the black arrow shows the moment of change). The solid blue line depicts the phase behaviour of node 2, that has its ongoing phase dynamics modulated by the spike train input that has to be classified. Light solid grey lines relate to the remaining nodes. Phase "a'' shows the washout phase, when the phase relationships stabilize in 10 clusters of 8 neurons each, phase "b'' shows the dynamics during the classification task, phase "c'' comprises the reorganisation of the assemblies and phase "d'' shows the classification task (same input train, opposite classification labels). Assemblies are rearranged by perturbing the phase of a given node with an input of magnitude ± 1.7 for 20 iterations. Blue arrows point at the perturbation caused by the input in node 2 (detailed in the small plot). (b) Impact on the classification performance caused by variations in three parameters of the input spike train (notation similar to Figure 5.2(c)): the standard deviation of the Gaussian jitter in the spike trains j, the spike firing rate f, and the number of patterns to classify N_p.

the opposite from the ones previously used. Finally, an output readout unit is trained by linear regression using the network state and the desired classification label for each pattern. Essentially, the procedure replicates the previous experiment but with the classification task changing upon a reorganisation of the nodes' phase relationship.

Figure 5.4(a) presents the resulting network dynamics. First, the system goes through a washout phase (3000 iterations) and has its phase activity stabilized in 10 clusters of 8 neurons each. Then a spike train input to node 2, lasting 200 iterations, modulates the phase dynamics; at the end, the final network state is stored. In sequence, the phase relationships are rearranged by inputs to certain nodes, and the same classification procedure is executed, with the network state stored at the end. This process is performed for every spike pattern used for training, and finally the readout unit weights are calculated. Figure 5.4(b) shows the network performance obtained for different parameter configurations. Notice that the performance is comparable to the one obtained in the previous task (Figure 5.2(b)), which suggests that the phase reorganisation dynamics can be exploited to solve different tasks without the need for adaption or plasticity mechanisms at the readout unit level.

The results for experiment 1 suggest that neuronal assemblies and phase reorganisation dynamics can play a significant part in supervised classification tasks and, perhaps most relevant to cognition, can cope with multiple classification tasks without the need for additional adaptive mechanisms. However, the major part of (natural) neural and cognitive dynamics is bound up in the generation of unsupervised embodied behaviour. Hence, in order to explore the possible roles of neuronal assembly dynamics further, the properties of the model were investigated in a second experiment in which it was used in an unsupervised embodied learning scenario, as described in the next section.

5.4 Experiment 2

Plasticity mechanisms are a common feature in the brain and mediate many (if not all) cognitive processes during learning and development (Turrigiano & Nelson, 2004; Masquelier et al., 2009). There is a rich literature exploring models of artificial neuronal networks with some kind of synaptic plasticity in the context of real or simulated agents engaged in a behavioural task (Urzelai & Floreano, 2001; Sporns & Alexander, 2002; Di Paolo, 2003; Edelman, 2007; Wyeth & Milford, 2009; Shim & Husbands, 2012), but normally the techniques involve the modulation of the electric connections between nodes of the network as a response to the agent's actions and the environment. Here, we explore the way in which neurons and assemblies relate to each other, and how a modulation of this relationship alone, without other plasticity mechanisms, can

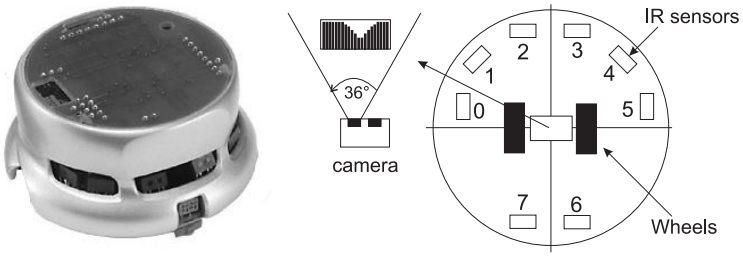

(a) (b)

Figure 5.5: (a) Real Khepera II robot and (b) its schematic representation, including the IR sensors and the camera.

be exploited to generate adaptive behaviour.

We conduct the analysis following an Evolutionary Robotics approach (ER) (Section 3.2), where an evolved simulated robotic agent controlled by a variation of the system investigated in Experiment 1 has to solve multiple tasks. In the following sections, we explain the robotic model used, the control system framework, the unsupervised learning task, and conclude with the outcomes of the experiment.

5.4.1 Methods

Robotic model

The robot is based on the Khepera II model (KTEAM, 2012). It has two wheels with independent electric motors, 8 infrared sensors and a camera (see Figure 5.5). The sensors measure the environmental luminosity (ranging from 65 to 450 - 65 being the highest luminosity that can be sensed) and the distance to nearby objects (ranging from 0 to 1023 - the latter value represents the closest distance to an object). The camera provides a 36 degrees, 64 pixels gray-scale horizontal image from its field of view. These 64 pixels are grouped into 3 mean inputs for the system: the mean value of pixels 0 - 13 representing the left reading, the mean value of pixels 24 - 39 representing the central reading and the mean value of pixels 48 - 63 representing the right reading. The readings range from 50 to 175 - the first value representing the maximum perception of a black stripe. In all experiments, a sensorimotor cycle (time between a sensory reading and a motor command) lasts $400ms$. The KiKS Khepera robot simulator, detailed in Appendix A, was used (Storm, 2004); it simulates with great fidelity motor commands and noisy sensory readings that are observed in the real robot.

Framework

The model studied in Experiment 1 was adapted so that it could be applied to control a simulated robotic agent. The framework, based on the general framework described in Section 3.3.1 and illustrated in Figure 5.2, is composed of 12 fully connected oscillators, with some nodes connected to the robot's noisy sensors (1 sensor per node). The rationale for a network with 12 nodes relates to richer dynamical behaviour in the Kuramoto Model with this number of nodes (Popovych et al., 2005). The frequency of each node is the sum of its natural frequency of oscillation, w_n, and the value of the sensory input related to that node (0 if there is no input), scaled by a factor ϵ_n.

At each iteration the phase differences γ from a node n to nodes $n-1$,$n = 2 \ldots 12$, are calculated following Equation 5.2. Then, the phase differences plus a bias term are linearly combined by a weight matrix W and fed into two nonlinear output units that have as activation function the sin function, which can be interpreted as two output neurons that capture the ongoing network activity - according to Pouget et al. (2008), nonlinear mappings (such as the one developed here) can be used as a comprehensive method to characterize a broad range of neuronal operations in sensorimotor contexts. The calculation results in two signals that will command the left and right motors of the agent (Equation 5.7):

$$\boldsymbol{M} = sin(\boldsymbol{W}^{'}\boldsymbol{\gamma}) \tag{5.7}$$

where $\boldsymbol{M} = [M_1, M_2]^T$ is the motor state space, with M_1 corresponding to the left motor command and M_2 to the right motor command.

Task

The robot described in Section 5.4.1 has two main objectives: it has to explore the environment whilst avoiding collisions (O_1) and it has to ensure that its battery level remains above a threshold (O_2), actively searching for the recharging area otherwise. The environment is a square arena with a recharging area represented by two light sources located next to a black stripe tag (Figure 5.7(b)). Whenever the robot's light sensory readings are below 100, it is considered to be inside the recharging area. The battery level BL dynamics is given by Equation 5.8:

$$BL(t+1) = \begin{cases} BL(t) - \alpha(BL(t) - Min(BL)), & \text{if ROCA} \\ BL(t) + \beta(Max(BL) - BL(t)), & \text{if RICA} \end{cases} \tag{5.8}$$

where α and β control the battery consumption and recharge rate, respectively, $Min(BL)$ and $Max(BL)$ are the lower and upper limit of BL (set here to 0 and 100, respectively), and $ROCA$ and $RICA$ stand for $Robot\ Outside\ Charging\ Area$ and $Robot\ Inside\ Charging\ Area$.

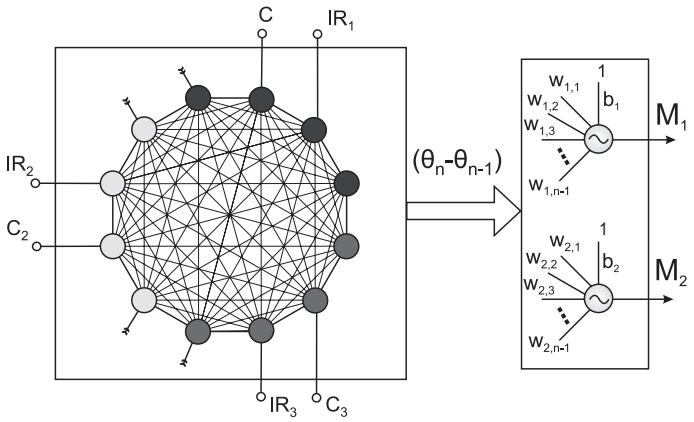

Figure 5.6: Framework for application in evolutionary robotics. The oscillatory network is composed of 12 fully connected neuronal oscillators, with nodes 2, 6 and 10 connected to the robot's infrared sensors and nodes 3, 7 and 11 connected to the visual sensors. Nodes 4, 5, 8 and 9 receive internal inputs only. The phase differences $\theta_n - \theta_{n-1}$, $n = 2 \ldots 12$, plus a bias term, are linearly combined by a weight matrix W and fed into two nonlinear output units that have as activation function the sin function, which can be interpreted as two output neurons that capture the ongoing network activity. The activation of each output neuron is used to command the motors M_1 and M_2.

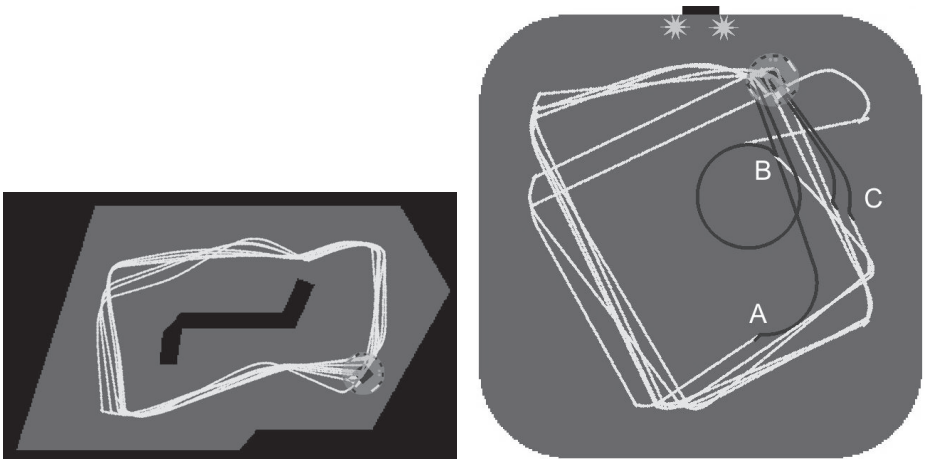

(a) (b)

Figure 5.7: Scenarios used in Experiment 2. (a) Obstacle avoidance training scenario and the behaviour displayed by a successfully evolved individual. (b) Task scenario. The arena has a recharging area represented by two light sources located next to a black stripe landmark (central top part of the figure). Light grey and black trajectories show the robot's behaviour when controlled by different assembly configurations.

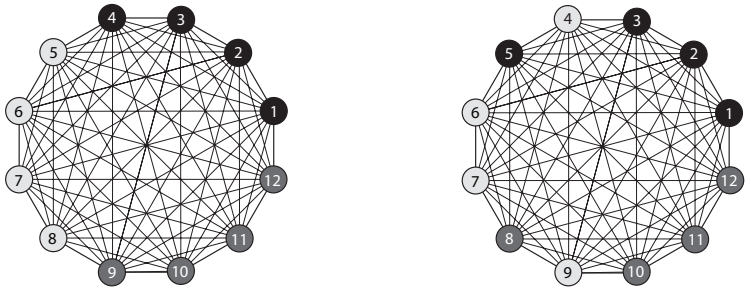

(a) (b)

Figure 5.8: Network assembly structure used in Experiment 2. Nodes with same colours are synchronised. (a) Configuration at the beginning of the experiment. (b) Configuration after an internal signal (caused by the drop of the battery level below 15) changes the assemblies set-up.

The network consists of $N = 12$ neurons with initial phases uniformly distributed in $[0, 2\pi)$. Nodes 2, 6 and 10 are connected to the robot's infrared distance sensors, and nodes 3, 7 and 11 are connected to the camera sensors. We set $\epsilon_n = 4$ for $n = 4, 8$ and $\epsilon_n = -4$ for $n = 5, 9$ (for $n = 2, 3, 6, 7, 10, 11$, ϵ_n is evolved, 0 otherwise, see the next section for details). We also adopted $M = 3$ (Equation 5.3), which leads to the formation of 3 assemblies with 4 neurons in each, denoted $(1, 2, 3, 4)$-$(5, 6, 7, 8)$-$(9, 10, 11, 12)$ (Figure 5.8(a)).

Whenever the battery level drops below 15 ($t = t_{low}$), an internal signal is generated which reorganizes the network in terms of neuronal synchronisation (Figure 5.8(b)). This signal consists of an input lasting $400ms$ (the same duration of a sensorimotor cycle) applied to nodes $4, 5, 8,$ and 9, i.e., considering Equation 5.2, $I_{4,5,8,9}(t) = 1$ for $t_{low} \leq t \leq t_{low} + 0.4$, 0 otherwise. Given the set up of the network described in the previous paragraph, this input shifts the phase of oscillators 4 and 8 and lags the phase of oscillators 5 and 9 enough to move them from their original basin of attraction to a neighbouring assembly. The network final configuration is thus $(1, 2, 3, 5)$-$(4, 6, 7, 9)$-$(8, 10, 11, 12)$. Whenever the battery level increases above 95 ($t = t_{high}$), an internal signal $I_{4,5,8,9}(t) = -1$ for $t_{high} \leq t \leq t_{high} + 0.4$, 0 otherwise, brings the network back to its original configuration (Figure 5.8(a)). Recall, from the task description in the previous paragraph, that the goal is to investigate if dynamic assembly formation can underpin the coordination of different, possibly conflicting behaviours in an autonomous agent.

Tasks are conflicting in the sense that the first (O_1) requires the agent to move and explore whilst minimizing sensory readings (and hence avoiding collisions), whereas in the latter (O_2) it has to approach a certain area of the environment, maximize the inputs from the light sensors (to recharge) whilst suppressing its movement to increase the time spent in the charging area (until the battery is recharged above the threshold).

Genetic Algorithm

We used a geographically distributed genetic algorithm with local selection and replacement (described in Section 3.1) to determine the parameters of the system: the input weights $\epsilon_n \in [-0.5, 0.5]$, $n = 2, 3, 6, 7, 10, 11$ and the two output neurons' weights $W_{N,a}$, $a = 1, 2$, with elements in the interval $[-5, 5]$, resulting in a genotype of length 30. The population size was 49, arranged in a 7×7 toroidal grid.

During evolution, we adopted a shaping technique (Dorigo & Colombetti, 1998; Bongard, 2011), in which the robot is required to execute and succeed in one task environment before proceeding to more complex scenarios. This technique has been shown to improve the evolvability of controllers in tasks that involve the accomplishment of many different objectives.

Therefore, considering the task previously described, the first phase of evolution, Phase 1, consists of 800 iterations of the algorithm where the fitness f is defined as the robot's ability to explore the environment whilst avoiding collisions with the environment walls and obstacles (Equation 5.9, based on Floreano & Mondada (1994)). Note that there is no influence of the battery level in this first stage of evolution. Figure 5.7(a) depicts the training scenario.

$$f = V(1 - \sqrt{\Delta v})(1 - i) \tag{5.9}$$

where V is the sum of the instantaneous rotation speed of the wheels (stimulating high speeds), Δv the absolute value of the algebraic difference between the speeds of the wheels (stimulating forward movement), and i is the normalized value of the distance sensor of highest activation (stimulating obstacle avoidance).

A generation is defined as 10 breeding events and the evolutionary algorithm runs for a maximum of 300 generations. If, at the end of this first evolutionary process, the agent attains a fitness above 0.4, it can proceed to the next phase.

During Phase 2 (scenario depicted in Figure 5.7(b)), robots are evaluated according to their ability to avoid collisions and the time they spend with the battery level below the threshold, i.e. if the battery level is above 15, fitness is scored following Equation 5.9, otherwise fitness is given by the fraction of time it took the robot to recharge its battery above 95. See Equation 5.10.

$$f = \begin{cases} V(1 - \sqrt{\Delta v})(1 - i), & \text{if } BL(t) \geq 15 \\ 1 - t_b/T, & \text{if } BL(t) < 15 \text{ and} \\ & BL(t + \tau) < 95 \end{cases} \tag{5.10}$$

where V, Δv and i, and BL, are as described in Equation 5.9 and 5.8, respectively; t_b is the number of iterations the robot spent with its battery level below 15 and T is the number of iterations

counting from the moment the battery dropped below 15 until it reached a level above 95.

At each iteration of the trial, the corresponding fitness value is calculated, and the final fitness is given by the mean fitness obtained across the whole trial. Notice that there is a selective pressure towards agents that reach the recharging area as fast as possible and remain in the area until the battery is recharged. Also, the learned behaviour in Phase 1 cannot be completely overwritten in Phase 2, as part of the evaluation function still accounts for the robot's ability to avoid collisions and explore the environment. Importantly, the second part of the fitness function described in Equation 5.10 does not reward a specific sequence of actions, only the final behaviour of the robot (reach the recharging area as fast as possible and remain there until recharged). There is no influence of the light or camera sensors in the calculations, thus the robot has to associate the distance sensors and vision information to find the area where recharge occurs.

5.4.2 Results

Robots successfully evolved to execute Phase 1 and Phase 2. Figure 5.7(a) portrays one of the evolved agents that navigates throughout the environment whilst avoiding collisions (Phase 1). Notice that because the agent is surrounded by walls and obstacles, sensory readings are nearly always present, thus the maximum fitness obtained is less than the maximum 1. Figure 5.7(b) shows the same agent after Phase 2 of evolution and Figure 5.9 shows the spiking activity (based on the phase dynamics) for every node of the network, the battery level, the distance and camera sensors, and the motor commands. The next paragraphs will explore in details the results of this latter phase.

At the beginning of the task, the agent wanders around the environment in straight lines, adjusting its trajectory only when faced by a wall. Notice from Figure 5.9 that both motor outputs are close to the maximum value of 10 and only change in response to the distance sensors' stimuli - the motors remain unresponsive to changes in the camera input (recall that the network receives input from all sensors at all times, and there are no ontogenetic plasticity mechanisms). Incidentally, the robot passes near the recharging area (black arrow near iteration 50), but because its battery level is still above the threshold the predominant behaviour remains "explore and avoid collisions".

However, near iteration 300 the battery level drops below 15 (point A in Figures 5.7(b) and 5.9), which triggers an internal signal that reorganizes the network configuration. The agent now should stop exploring the environment and drive towards the recharging area as fast as it can to maximize its fitness. Notice that at the moment this occurs, the robot is far from the recharging area so it has to use its visual information to orient and move towards the correct direction. The

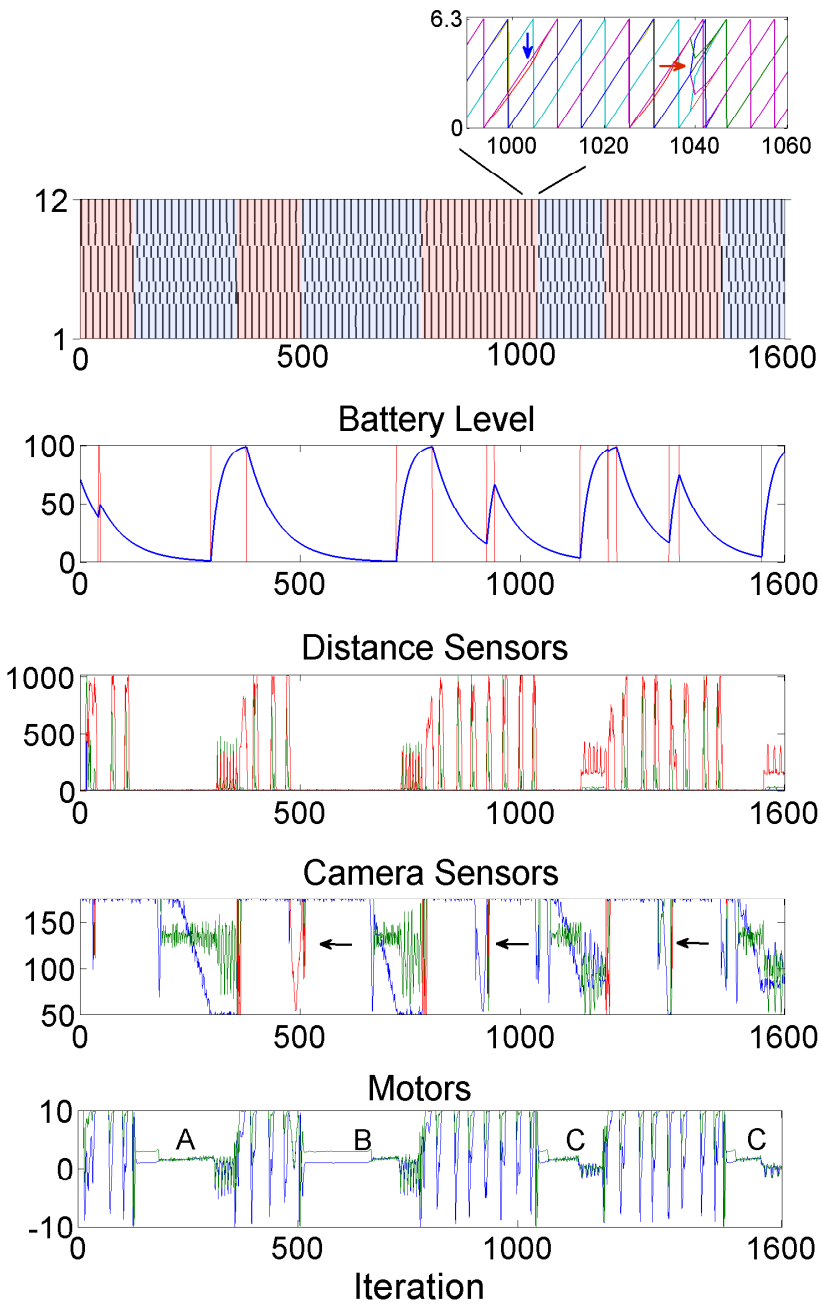

Figure 5.9: Experiment 2 variables dynamics. Downwards from the top: network raster plot (the red and blue shaded areas relate to different network configurations, the small plot shows details of the phase dynamics, the blue arrow shows how sensory stimulus modulate the ongoing dynamics, the red arrow points at a moment of assembly reorganisation); the battery level, with red lines indicating when the agent is within the recharging area (0 is outside, 100 is inside); the distance sensors (0 when there is no obstacle, 1023 if very close to one); the camera sensors (175 if no black stripe is seen, 50 if all the camera pixels detect black); and the motor commands (positive values indicate forward movement, backward movement otherwise). Letters A, B and C refer to the trajectories displayed in Figure 5.7(b).

adopted strategy is to move in circles until the visual stimulus (black landmark) is perceived, and then progress in a straight line towards it. This can be seen in Figure 5.9, with the consistent camera readings. As the robot approaches the landmark, the distance sensory readings increase but they don't cause the same response as before the network reorganization: the agent remains relatively still within the recharging area until the battery is recharged and does not display the characteristic turn around movement of obstacle avoidance. After the battery is above 95, another internal signal is triggered and assemblies are rearranged to their previous state. The robot hence returns to explore and avoid obstacles.

This same sequence of behaviour can be observed near iteration 500 (point B in Figures 5.7(b) and 5.9). The turning behaviour, brought about by differential wheel speeds, is much more noticeable here, and although the robot is closer to the recharging area, it does not have the visual stimulus at the time the battery drops below 15. When the first visual stimulus is perceived, the agent fixates on the landmark, and the sensory readings increase as it slowly moves towards the black stripe. A similar sequence of behaviour is displayed as the task continues, but the following moments when the battery drops below 15 occur when the agent has a visual stimulus, therefore there is no need to move in circles before heading towards the recharging area (points C).

Figure 5.10 depicts the activity of the assemblies during the task, represented by the phase difference $\gamma_{n,1}$ of each node n to node 1. The oscillators rapidly synchronise and form three neuronal assemblies equally spaced according to their phase differences (see Figure 5.8). Each assembly has inputs from one distance sensor and one camera sensor. This sensory stimuli modulate the ongoing network activity, causing small phase deviations from the respective assembly's mean phase (examples are indicated by blue arrows in Figure 5.10), yet all nodes remain within the basin of attraction of their respective cluster - they do not change their assembly membership. The small phase modulations of each cluster are captured by both output neurons and are responsible for adjusting the agent's motor commands and, consequently, its trajectory. Internal signals triggered by the battery level dynamics change the assemblies original arrangement (compare with Figure 5.9, top), and this new phase relationship, together with the sensory modulation, accounts for the change in the robot's behaviour.

The relationship between the assemblies rearrangement and the different behaviours displayed by the agent can be seen by plotting the network's phase differences together with the corresponding motor outputs at every sensorimotor time step. Because there are $\gamma_{i,i-1} = 11$ phase differences, we have to perform a dimension reduction to visualize the system's dynamics. This is done by projecting the original phase differences into the first two principal components calculated using a Principal Component Analysis (PCA) (Jolliffe, 2002). A single time series is

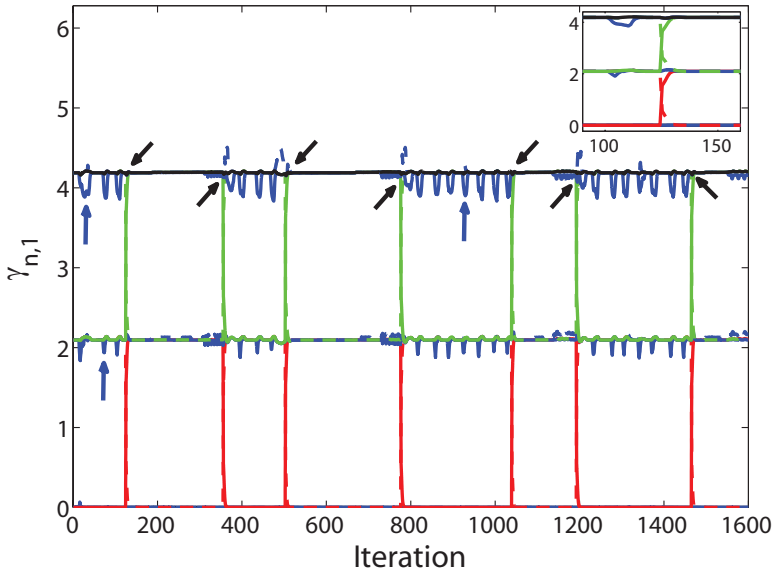

Figure 5.10: Phase dynamics portrayed as the phase difference $\gamma_{n,1}$ of each node n to node 1. The small plot shows the moment of an assembly reorganization (solid and dashed green and red lines show the change in assembly membership). Blue arrows point at examples of phase modulations due to sensory stimuli, black arrows indicate moments of assembly reorganisation. Notice how sensory stimuli modulate the ongoing dynamics in the whole network but ultimately do not cause an assembly change.

obtained from the two motor commands by subtracting the left from the right wheel commands. Figure 5.11(a) shows the results. Note that there are two clearly discernible regions in the state space, one comprising trial iterations $1-124$,$356-503$, $777-1039$, and $1194-1465$, and the other iterations $125-355$, $504-776$, $1040-1193$, and $1466-1600$. These regions relate to different assembly configurations (see Figure 5.9, top, and Figure 5.10), therefore rearranging the assemblies causes movement in the state space of the network-motor system, which has a direct correspondence with the behaviour of the robot.

As pointed out, the assembly reconfiguration is the main mechanism responsible for changing the way the robot behaves, there are no other plasticity mechanisms and both distance and visual sensors are always fed into the network. The effects of the inputs (or their relevance to the behaviour observed) vary depending on the assembly configuration. Observe the black arrows near iterations 900 and 1300 in the camera sensors panel in Figure 5.9. The battery level is above 15, the robot is exploring the environment and avoiding collisions (notice the distance sensors dynamics), but it also receives visual input. This input, however, does not affect the ongoing behaviour (see the motors dynamics). To highlight this effect, we conducted an information dynamics analysis, exploring how information flows from sensors to motors and from motors to sensors as the task

progresses.

Figure 5.11(b) shows the transfer entropy between the robot's distance and camera sensors and its motors for the duration of the trial, calculated according to Section 3.4. To obtain the time series, we adopted the same procedures for data collection and pre-processing described in Section 4.2.4, and we used a sliding window containing data from the past 200 iterations, therefore note that the results reflect a history of interactions and are not an instantaneous measurement of information flow. More specific, the sensors' time series (3 infrared sensors and 3 camera sensors) are submitted to a principal component analysis to perform a dimension reduction. The calculated principal component and the original time series of each sensor modality are used to create a single time series that captures the most significant features of the multidimensional input space. The motor commands are also combined to generate a single time series by subtracting the value of the left wheel command from the right wheel command. This data were then discretised into 6 equiprobable states and finally the Transfer Entropy is calculated. We performed a series of analyses with different parameter choices, and although there were differences in the values obtained, the overall qualitatively aspect of the curves was maintained.

In the top panel, the information flow from distance sensors to the motors (or, in other words, the causal influence from distance sensors to motor commands) oscillates throughout the task and has peaks between iterations $375 - 550$, $900 - 1075$ and $1300 - 1500$. In the bottom panel, the information flow from visual sensors to the motors also oscillates throughout the task and has peaks between iterations $375-550$, $700-900$ and $1100-1400$. Comparing these with Figure 5.9, one can see that there is a relationship between the distance and camera sensors, and the respective information flows. This relationship is due to complex brain-body-environment interactions and not only due to the presence of sensory stimulus, as e.g. one can verify observing iterations 500, 900 and 1350 in the camera sensors plot (Figure 5.9) and the respective information flow plot: although there are variations in the visual input, there is no corresponding increase in the transfer entropy values. Therefore, sensory inputs may or may not affect the motor commands, and the current assembly configuration will modulate this interaction.

The information flow dynamics offers another perspective in the robot's behaviour analysis. Notice that the information flow magnitude is nearly twice as much in the bottom panel as in the top panel. We saw in the previous dynamics and behaviour analyses that when the battery drops below 15, the robot moves towards the recharging area, but it doesn't display the otherwise natural obstacle avoidance behaviour when it eventually finds a wall. The transfer entropy analysis highlights that the visual information is the main source of behaviour modulation even though the distance sensors still have some influence. This is clear between iterations $1075-1250$: the visual

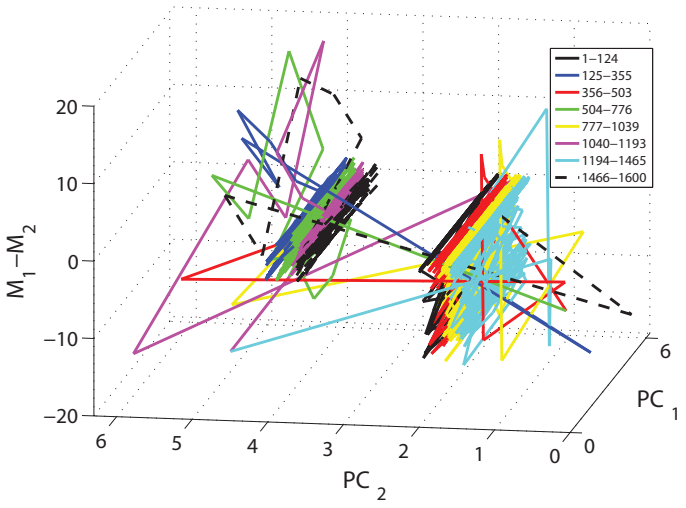

(a)

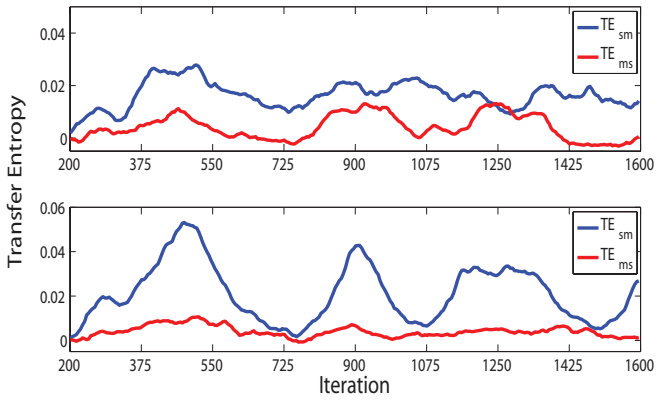

(b)

Figure 5.11: (a) System dynamics depicted by the projection of the 11 phase differences $\gamma_{i,i-1}$, $i = 2 \ldots 12$, of the 12 node network into their first two principal components (PC_1 and PC_2), and the motor output represented by the difference between the values of M_1 and M_2 (Equation 5.7). Different colours relate to different iteration intervals. Notice that, whenever there is an assembly rearrangement (Figures 5.9 and 5.10), there is a corresponding shift in the network-motor state space region, which relates to different behaviours displayed by the robot. (b) Transfer Entropy between the distance sensors time series and the motors time series (top panel), and between the camera sensors time series and the motors time series (bottom panel). A sliding window of length 200 iterations is used to obtain each time series at every iteration of the Transfer Entropy analysis. Results are smoothed using a low-pass filter with transfer function in the z-transform domain given by $1/(1 - 0.08z^{-1})$.

information flow (bottom panel) increases as the robot approaches the recharging area (higher visual input), and upon finding the wall there is an increase in the flow from motors to sensors in the top panel. This means that the robot's trajectory, mainly influenced by the visual inputs, determine the incoming sensory readings - the robot actively "produces" its inputs - whilst the information flow from distance sensors to motors decrease, meaning that there is little influence of the distance sensors in the robot's behaviour.

Finally, to stress the relevance of assembly reorganization in the evolutionary process, observe Figure 5.12. It shows the values at the end of Phase 1 and Phase 2 of evolution of the weights of the output unit neurons and of the input weights of nodes that have sensory input (see Figure 5.2). Notice that there are just minor adjustments in the value of a few parameters, most of them remain unchanged as evolution progress from one phase to another. This further supports the relevance and flexibility of dynamic assembly reorganization in multi-objective tasks.

5.5 Discussion

It is now established that synchronisation mechanisms and dynamic assembly formation in neuronal networks have a relationship with cognitive processes and behaviour; however, the underlying computational functions and interplay with behaviour are still to be uncovered. In this chapter, we conducted experiments both in supervised and unsupervised learning scenarios exploring concepts drawn from the "binding-by-synchrony" hypothesis, which considers neuronal assembly computations from a spike time perspective. In fact, there is a growing body of literature attesting that neuronal codes based solely on spike rates underperform or do not contribute in a variety of cognitive tasks (Borst & Theunissen, 1999; Carmena et al., 2003; Jacobs et al., 2009; Rabinovich et al., 2012).

The neuronal network model used is inspired by the Kuramoto model of coupled phase oscillators, and allows one to fine tune the network synchronisation dynamics and assembly configuration. The model has an intrinsic, ongoing oscillatory activity that can only be modulated - not determined - by external stimuli, in contrast with models which consider a static system with responses elicited only by stimulus onset. As reiterated throughout this thesis, cognitive processes unfold over time and therefore cannot rely only on external events. Also, by selectively choosing the value of parameter M (Equation 5.3) and the initial distribution of phases, one can precisely determine the number and constitution of assemblies. Although evidence points at assembly formation as a result of emergent processes, and several models capture this property (Izhikevich, 2006; Burwick, 2008; Ranhel, 2012), it is hard to foresee or design how the network will self-organise; hence, the model presented here contributes to studies which require a consistent emergent con-

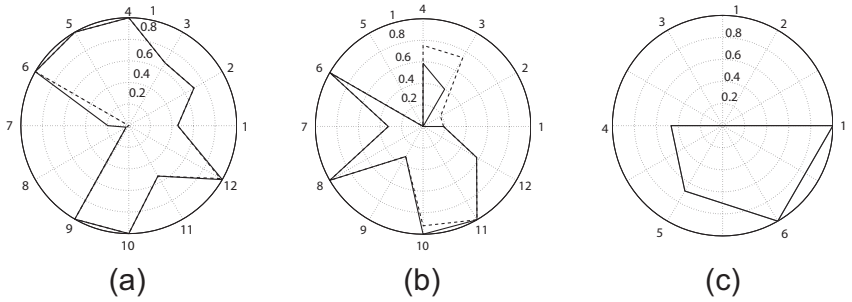

Figure 5.12: Values of the weights of the output unit neurons (panels (a) and (b)), and of the input weights ϵ_n of nodes that have sensory input (panel (c)), at the end of Phase 1 (solid black) and Phase 2 (dashed black) of evolution. Values are normalised between 0 and 1 to improve visualisation. See Figure 5.6 for details.

figuration and studies focused on a systematic exploration of different synchronisation regimes.

In Experiment 1, a supervised learning task, we studied the influence of the number and size of neuronal assemblies in a spike pattern classification task. The input spike patterns and the network phase dynamics both had roughly the same spike count across the task, similar to what has been observed in real cortical neuronal ensembles (Carmena et al., 2003), thus the discrimination had to rely on the precise timing of events. The analysis was based on the methods devised in Maass et al. (2005) and Legenstein & Maass (2007), which ensure that the results are not exclusive for the task investigated here but to all computational tasks that only have in common which properties of the circuit input are relevant to the target outputs. The main assumption of the method is that a linear readout unit generates the circuit outputs based on the state of the network nodes at a particular time, which resembles the approach adopted in brain-machine interface studies (Lebedev et al., 2005; Hatsopoulos & Donoghue, 2009) but is also suggested as a more appropriate form to understand assembly activity (Buzsáki, 2010). Although it is still not clear how the temporal relations in the brain are organized, and thus how reading the network state at a predetermined time could be justified, there are some possible solutions that may have evolved in natural brains: a redundancy in the circuitry may exist so that at any time an event occurs, or a classification task is required, an output is produced (Ranhel, 2012); there can be an interaction of the external rhythms with internally generated ones, forcing synchronised firing events to occur in strict time windows (Masquelier et al., 2009; Kopell et al., 2010); attention mechanisms may also interfere and promote phase resetting (Steinmetz et al., 2000; Lakatos et al., 2008).

Considering a network with a total number of neurons equal to 80 ± 4, our results show that performance increases as we raise the number of assemblies, and that increase can be predicted up to a certain extent by the computational power and generalisation capability of the system fol-

lowing the same procedure described in Legenstein & Maass (2007), although in our case simply using the difference between the computational power and the generalisation capability may not be the most appropriate form of combining them; this is an open problem which goes beyond the scope of this thesis. A further analysis, which varied the number and size of assemblies, revealed that the first impacts more on performance than the latter, a fact that can be attributed to the increased variability of possible network states due to a larger number of emergent clusters rather than fewer but larger assemblies. Also, the system presents a saturation in performance with respect to the number of clusters. Therefore, the results indicate that simply increasing the number of neurons or assemblies in the system does not necessarily originate a correspondent increase in performance. A similar phenomena is described in neuronal assembly physiology as "the neuronal mass principle" (Nicolelis & Lebedev, 2009), which states that a minimal number of neurons is needed in a neuronal population to stabilize its information capacity (captured by a readout unit) at a satisfactory level. Reducing the number of neurons causes an increasingly sharp drop in the information capacity of this population, whereas increasing the number of sampled neurons above a certain level does not increase the accuracy of predictions (Carmena et al., 2003; Lebedev et al., 2008).

Also, the results showed that, in our model, most of the neuronal architectures were highly redundant, most of the neurons in the higher performance configurations presented independent activity, and that increasing the number of neurons in a network with fixed number of assemblies increased the redundancy. All these findings resemble the results obtained in real cortical experiments, therefore a few remarks should be made: first, real neuronal ensembles are highly redundant, and that can be associated with resistance to error and natural mechanisms of probability distribution estimation (Barlow, 2001; Szczepanski et al., 2011); second, neuronal independence (as observed in our results) can be linked to code efficiency because the information capacity of individual neurons is not compromised by redundant scenarios (Schneidman et al., 2003); and third, there is still a lack of studies comparing the information flow dynamics due to neuronal interactions and due to single neurons alone - attesting the time-scales of the interactions as well as spurious effects such as averaging is still work in progress (Reich et al., 2001; Narayanan et al., 2005).

The computational power analysis emphasized that multiple readout units could be trained to perform different classification tasks based on the same network state. In contrast, to conclude Experiment 1, we investigated whether the system could cope with multiple classification tasks relying only on a manipulation of the phase dynamics by means of an internally generated signal, employing the same readout unit without any plasticity mechanisms. To support the approach,

there are clinical studies suggesting that intracortical electrical stimulation can induce cortical plasticity (Jackson et al., 2006), but functional plasticity can also be obtained faster as a result of attentional processes (Steinmetz et al., 2000; Lakatos et al., 2008; Schroeder & Lakatos, 2009). Our results show that the system can be trained in multiple classification tasks upon rearrangement of assembly configuration.

Although the results of the first experiment show that such temporal code carry information and suggest that it can be exploited in a variety of tasks, it is challenging to determine up to what extent the brain uses a temporal code. Moreover, there is evidence that the neuronal activity evoked by the body's sensorimotor interactions with the environment differs from the activity evoked by passive stimulus (Lungarella & Sporns, 2006; Eliades & Wang, 2008). Hence, research on temporal neuronal codes and assembly formation benefit if linked with behavioural studies (Engel, 2010; Panzeri et al., 2010); in this sense, evolutionary robotics (ER) emerges as a suitable technique to combine both approaches (Boden, 2006; Floreano et al., 2008; Floreano & Keller, 2010).

In Experiment 2, an ER unsupervised learning task, we evolved a simulated robotic agent, controlled by a variation of the system investigated in Experiment 1, to solve multiple tasks depending on its battery state. The results showed that the evolved framework together with the dynamic assembly formation can generate minimally cognitive behaviours. When working with increasingly complex tasks, the changes in the parameters of the system are relatively small, which indicate that the different assemblies formed dynamically also facilitate the evolutionary process. Finally, we highlighted the context-based neuronal dynamics showing that the phase space formed by the motors' readings and the nodes' phases have different orbits due to changes in assembly organisation, and an analysis of the information flow in the network reveals that such changes modulate the influence of the inputs in the robot's behaviour (determined by the motor commands).

Taken together, Experiments 1 and 2 employed information theory and decoding methods to provide further evidence that the dynamic formation of assemblies and the relative neuronal firing times can mediate processes involving the classification of spike patterns, and can selectively modulate the influence of external signals in the current network activity. Ultimately, there is no guarantee that the brain makes usage of a time-based decoding procedure, neither that it is able to exploit the information content revealed by the synergy analysis and the transfer entropy approach; nevertheless, it may shed light on aspects of brain-body-environment interactions and provide upper bounds on code efficiency when testing hypothesis (Quiroga & Panzeri, 2009; Jacobs et al., 2009).

Widespread noise is relevant to many neuronal and cognitive phenomena (Rolls & Deco,

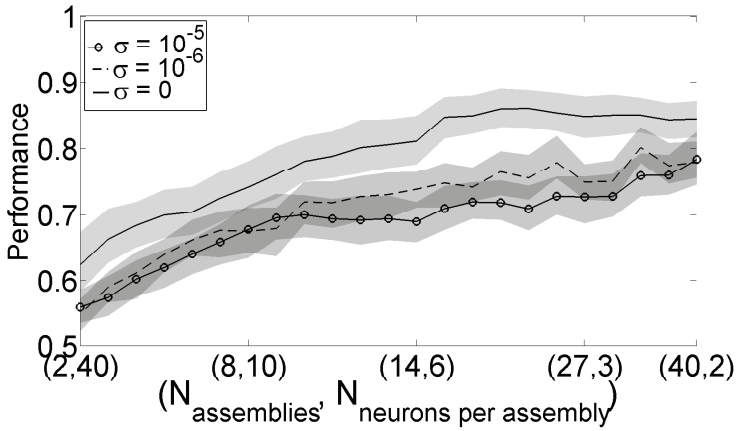

Figure 5.13: Effect of Gaussian noise of zero mean and standard deviation σ applied to all nodes of the network in the performance of the system. Results are mean values over 20 different simulations, and shaded areas are the 95% confidence interval.

2010). In the context of the study conducted in this chapter, it is common to construct the Kuramoto model (and its variations) having additive noise at the input level equivalent to noise applied at the network level (Acebrón et al., 2005). Based on Equation 5.2, the following equation shows the usual form of the Kuramoto model with inputs $I_n(t)$ and noise $\chi_n(t)$:

$$\dot{\theta}_n = \omega_n + \frac{K}{N}\sum_{m=1}^{N} g(\theta_n - \theta_m) + I_n(t) + \chi_n(t),\ n = 1, \ldots, N, \tag{5.11}$$

In this sense, Experiments 1 and 2 had a subset of noisy neurons (only neurons that had inputs). As a preliminary study, we have run two further simulations of Experiment 1 adding Gaussian noise of zero mean and standard deviation σ to all nodes of the network. The results are presented in Figure 5.13. Notice that classification performance falls with increasing noise magnitude (an effect also present in Figures 5.2(c) and 5.4(b)), but the trend observed in our original results is kept and higher performance levels are obtained in architectures with more assemblies. Thus, at least for this experiment, noise applied to all neurons alters the classification performance in a quantitative rather than a qualitatively way.

How would additive noise affect measures of redundancy and synergy? The intuition that noisy scenarios are better tackled with redundant architectures is justified - there are works showing that cortical circuits, which operate in an intrinsically noisy environment, are highly redundant (Narayanan et al., 2005; Szczepanski et al., 2011). However, there is criticism regarding the interpretation of information theoretical measurements such as redundancy (Schneidman et al., 2003; Latham & Nirenberg, 2005), as well as findings showing predominantly synergistic or independent activity in neuronal circuits, instead of redundancy, depending on factors such as which area and which neurons are recorded or which kind of task is performed (Reich et al., 2001). Additionally,

as shown by Szczepanski et al. (2011), neurons can dynamically switch their interactions during the execution of the task, thus synergetic, independent, or redundant activity may be masked by averaging processes. Finally, redundancy and synergy are found to be largely influenced by the network architecture and the decoding unit used (Schneidman et al., 2003). The conclusion is that redundancy is not necessary for good performance in noisy scenarios, but mostly important it depends largely on the experimental paradigm used.

One limitation encountered in the methods used in Experiment 1, chosen for their ability to assess computational performance in generic neuronal microcircuits independently of task paradigm, is that in some circumstances noisy neurons may make the computational power and generalization capability analyses inconclusive due to state matrices having complete rank most of the time (Legenstein & Maass, 2007). This was not an issue in previous works that used these methods (e.g. (Maass et al., 2005; Legenstein & Maass, 2007)) because emergent properties of the neural architecture resulted in highly silent networks with dynamics that were marginally affected by noise; conversely, the model in this article is composed of self-sustained oscillators which are always active. Considering that silence in the brain is still a point of much controversy (Shoham & Segev, 2006), the applicability of the methods used in Experiment 1 to a variety of problems and neural architectures remains an open question.

To conclude, implementing the methods or the experiments described in this chapter in a biological network is impractical at the moment for limitations in both recording and stimulation technologies: the best technologies are able to record and stimulate a limited number of neurons. However, more important than trying to implement the methods or experiments in a biological network are the insights and future work opportunities we gain. There are many open questions in neuroscience regarding neural assemblies, their properties, and relationship with behaviour. This very simple model, based on a model that is being increasingly applied to study neuroscience problems (the Kuramoto model), has shown promising results in supervised and unsupervised learning tasks. The point to stress is not solely performance levels - support vector machines, for instance, would surely excel in Experiment 1, attaining far better results than our approach - but the ability to solve relatively complex tasks mimicking mechanisms that current research suggests is exploited by the brain, namely neuronal assembly dynamics. Therefore, a better comprehension of the framework, its limitations and possible extensions, and ultimately understanding of the computational properties of neuronal assembly dynamics, whether at solving data mining tasks or as part of novel behaviour generation mechanisms, should precede biological implementations.

In this chapter, we investigated neural assembly computations in supervised and unsupervised learning tasks. In the next chapter, the final chapter of experiments, we modify the original Kur-

amoto model to obtain a more biologically plausible centre-surround connection pattern between neurons and investigate whether such spatially structured configuration, which may lead to travelling waves or synchronised dynamics, facilitate or are advantageous to promote the different behaviours required by a sequential, associative learning task.

Chapter 6

Travelling Waves and Synchronised Dynamics in an Associative Sensorimotor Learning Task

In this chapter, we investigate whether spatially structured connections, which may lead to travelling waves or synchronised dynamics, facilitate or are advantageous to promote the different behaviours required by a sequential, associative learning task. The Kuramoto model is extended with a wavelet-like spatial kernel to obtain a centre-surround connection pattern between neurons, which supports the emergence of both waves and synchronisation in the network. The results show that agents with higher performance present higher neuronal synchronisation without sensory stimulation and that in the presence of sensory readings the network is less synchronised. Also, the transfer entropy analysis highlights the context-dependent influence of each sensory modality in the motor commands. Finally, the simulated pseudo-field potential envelope, which captures the global dynamics of the system, is shown to contain relevant sensory and motor information, paving the way for future studies and more advanced frameworks.

6.1 Introduction

In this chapter, we investigate whether or not spatially modulated oscillatory activity, which impacts on synchronisation phenomena, might be useful for generating minimally cognitive behaviours. First, we extend the Kuramoto model substituting the global connectivity pattern present in the original model by spatial patterns of influence, which can lead to the emergence of travelling waves and synchronised dynamics; then, we evolve simulated robots to perform a sequential task where different sensory modalities have to be associated with multiple, possibly conflicting

behaviours, in order to maximize fitness.

The global (all-to-all) connectivity pattern of the original Kuramoto model (Section 3.3) may account for the dynamics of a few neurons densely connected, but becomes less biologically plausible for large groups of neurons because transmission delays and spatially dependent coupling strengths are present (Cumin & Unsworth, 2007; Breakspear et al., 2010). Thus, a more realistic configuration would restrict the connectivity of the otherwise fully connected network and include excitatory and inhibitory couplings. Specific to the Kuramoto model, Breakspear et al. (2010) and Heitmann et al. (2012) showed that this can be achieved using a spatial kernel convoluted with the sin function, which leads to a wavelet-like modulation of the phase interaction function. A consequence of using this phase interaction function, which includes more complex interactions than that captured by the sin function alone, is the emergence of patterns of activity characterised by distance-dependent phase differences between nodes - travelling waves - in addition to global synchronisation dynamics (Ermentrout & Kleinfeld, 2001; Ermentrout, 2005). In this way, we extend our framework (Section 3.3.1) to obtain flexible spatio-temporal phenomenon in the form of travelling waves and synchronisation.

There is evidence that the interplay between travelling waves and synchronisation is a fundamental property in cognitive processes (Gong & van Leeuwen, 2009). Waves are a widespread spatio-temporal phenomena, capable of modulating the membrane properties of neurons and consequently their spiking activity. Also, they can be sensorily evoked or result from attentional processes (Wu et al., 2008), thereby affecting transient assembly formation and possibly mediating cognitive acts. For instance, Rubino et al. (2006) showed that synchronisation between ongoing neuronal oscillations and sensory stimulus generates waves that carry task-related relevant information in an experiment with primates; Zheng & Yao (2012) found that visual stimulation in the cat visual cortex modulate the propagation of waves in specific directions, but because this modulation was independent of stimulus features, they speculate that waves have a role in communication rather than in coding; Cabral et al. (2011) showed, using a realistic computational model, that spatio-temporal fluctuations occur in the resting-state network and correlate with functional connectivity. In addition, waves have been observed in hippocampus (Lubenov & Siapas, 2009), in the sensorimotor cortex of mices (Ferezou et al., 2007), in the turtle olfactory bulb (Lam et al., 2000), and in a great variety of in vitro and in vivo systems (Wu et al., 2008). The consensus, however, is that the functional significance of travelling waves and synchronisation is far from being understood.

Regarding sensorimotor processes, there is a divergence about the interplay between waves and synchrony: Ermentrout & Kleinfeld (2001) associated travelling waves to periods of behavioural

choice and synchrony to stimulus attendance, whereas Heitmann et al. (2012) suggested that wave patterns encode motor actions and synchrony is observed during resting states. The latter grounded their findings in the cortical idling hypothesis (Pfurtscheller et al., 1996), which states that parts of the motor cortex shift from activated to a resting state upon termination of motor activity. Nevertheless, both approaches agree that wave-synchrony switching dynamics may constitute a fundamental aspect of neural computations.

The experiments in this chapter address this debate and evolve networks able to display both waves and synchrony. The task entails sensorimotor behaviours, such as obstacle avoidance and phototaxis, that have to be performed in a particular sequence in an associative learning scenario. This task is particularly interesting because it requires non-trivial solutions and the rewards are implicit, i.e., sensory readings that are relevant for obtaining good performance in the task are not part of the fitness function. Also, the parameters of the framework are free to evolve over a broad dynamical range. In this way, the model is suitable to investigate whether spatial phenomena (travelling waves) or synchrony facilitate or are advantageous to promote the different behaviours required by the task.

The evolved behaviours are studied by the dynamical analysis of the system's variables and the directed flow of information between the different sensory modalities and the motors. We show that robots with good performance display a high level of synchronisation throughout the task, but travelling waves solutions could not be obtained. Therefore, at least for this task, spatially structured connections, which support the formation of waves, don't seem to be helpful, but fully synchronised networks are and these are easily found with larger values for the coupling strength between nodes and the suppression of inhibitory connections. The information flow dynamics demonstrate the diverse influence of camera, light, and distance sensors in motor commands depending on the task sequence and the robot's behaviour. To conclude, we simulate the pseudo local field potential generated by the network and conduct a mutual information analysis to show that sensory and motor information can be extracted from the global dynamics of the system.

This chapter is organised as follows: the next section presents the methods, including the extension to the Kuramoto model to support travelling waves and synchrony, the ER framework, the details of the sequential associative learning task, and the genetic algorithm (based on the algorithm described in Section 3.1); Section 6.3 presents the results; Section 6.4 closes the chapter with a discussion about the results obtained.

6.2 Methods

6.2.1 Kuramoto model with wavelet-like spatial kernel

Recall, from Section 3.3, the original Kuramoto model (rewritten here as Equation 6.1 for clarity).

$$\frac{d\theta_i}{dt} = \omega_i + \frac{K}{N}\sum_{j=1}^{N} sin(\theta_j - \theta_i), i = 1, \ldots, N. \tag{6.1}$$

where θ_i is the phase of the *i*th oscillator, ω_i is the natural frequency of the *i*th oscillator, and K is the coupling strength between the N oscillators.

The original model assumes all-to-all isotropic connectivity, thus suppressing any dynamics due to spatial embedding effects. This can be tackled by incorporating a finite width spatial kernel $W(j, i)$ to the model (Breakspear et al., 2010), which results in a wavelet-like modulation of the phase interaction function given by Equation 6.2.

$$\frac{d\theta_i}{dt} = \omega_i + \frac{K}{N}\sum_{j=1}^{N} W(j,i) sin(\theta_j - \theta_i), i = 1, \ldots, N. \tag{6.2}$$

The properties of the function $W(j, i)$ will impact directly on the dynamics observed in the network. For instance, Ermentrout & Kleinfeld (2001) argue that networks in which short-range excitatory connections and long-range inhibitory connections predominate present both traveling waves and synchronised dynamics as possible patterns of activity. Another biologically plausible connection topology found to elicit travelling waves and synchronised dynamics in networks of coupled oscillators is the centre-surround, in which the form of the excitatory/inhibitory surround modulates the emergence of waves and synchrony (Ermentrout, 1998; Breakspear et al., 2010). A possible function with such properties is presented in Equation 6.3, formed by a Gaussian function and its fourth derivative (Heitmann et al., 2012).

$$W(j,i) = e^{-bd_{ji}^2} + 4he^{-bd_{ji}^2}(\frac{1}{3}b^2d_{ji}^4 - bd_{ji}^2) \tag{6.3}$$

where b regulates the slope of the Gaussian, h modulates the inhibitory surround, and d_{ji} is the distance between nodes j and i.

Notice that if $h = 0$, the coupling reduces to a purely Gaussian coupling with only excitatory connections of magnitudes determined by parameters b and d_{ji}. If $h = 1$, the function assumes the form of the 4th derivative of a Gaussian, presenting inhibitory short-distance connections and excitatory couplings which fade out with distance. Figure 6.2.1 illustrate the effect.

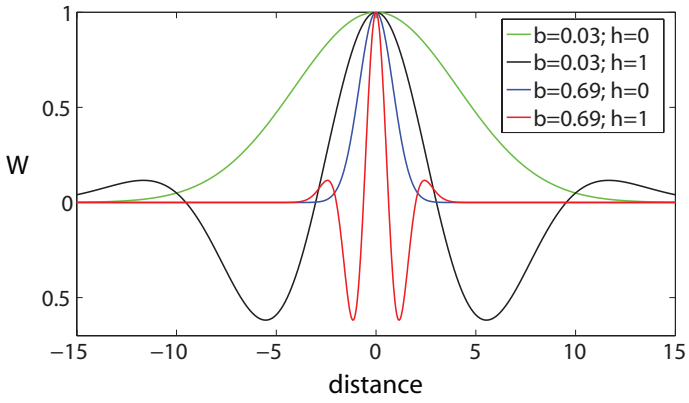

Figure 6.1: (a) Centre-surround coupling kernel. The excitatory/inhibitory couplings are modulated by parameters b and h (Equation 6.3).

Intermediate values modulate the shape and extent of the inhibitory/excitatory connections, which in turn influence the emergence of waves or synchronised solutions. More specifically, Heitmann et al. (2012) showed that waves are observed only if $h > 0.59$, which leads to a strong inhibitory surround; synchronisation is obtained only if the inhibitory surroundings are weak ($h < 0.49$); the intermediate region characterised by $0.41 \leq h \leq 0.59$ presents bi-stable solutions. Therefore, by systematically tunning the coupling function, one can obtain systems that present waves, synchrony, or both. Importantly, the existence of bi-stable solutions under the same coupling configuration supports the investigation of distinct functional networks that emerge out of fixed structural connections.

For simplicity, instead of using a 2-dimensional grid, we opted for a network structured as an array with periodic boundaries - a ring. Although apparently trivial, this architecture supports a diversity of dynamical phenomena and is found in biological systems e.g. the slug olfactory lobe (Kazanci & Ermentrout, 2007). In this structure, the distance between two nodes is not obvious because there are two paths following opposing directions from a node j to a node i. In this sense, we will use the metric presented in Zanette (2000) for it fulfills the requirements that define a well-behaved metric. See Equation 6.4.

$$d_{ji} = \frac{L}{N} min\left\{|j-i|, N-|j-i|\right\} \tag{6.4}$$

where L is the linear size of the ring and N is the total number of nodes in the network.

Figure 6.2(a) illustrates the synchronisation dynamics of the extended model for different sets of parameters, and Figures 6.2(b) and 6.2(c) show examples of solutions composed of waves and synchrony, respectively, obtained by a suitable choice of parameters K, b, and h. Notice that in networks with strong inhibitory surroundings ($h = 1$) the synchronisation dynamics vary as

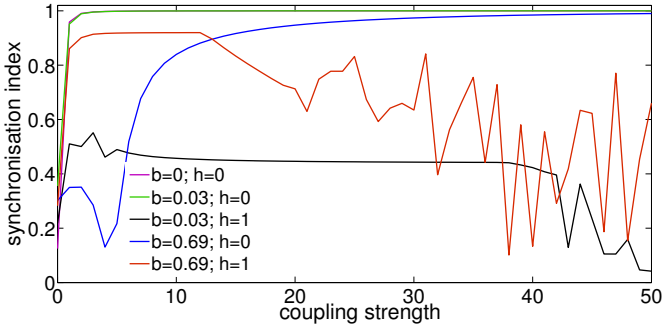

(a)

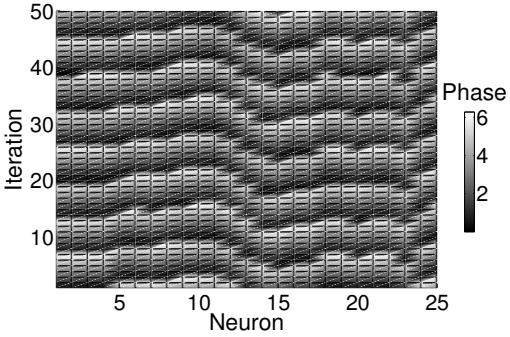

(b)

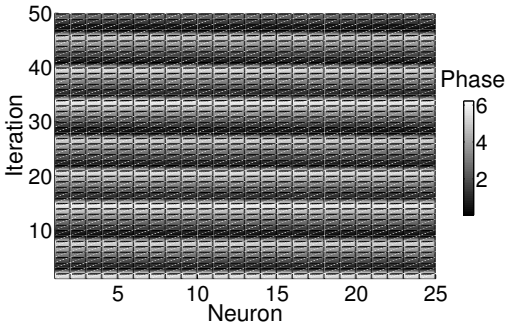

(c)

Figure 6.2: Dynamics of the extended Kuramoto model for different values of K, b, and h (Equation 6.2). (a) Synchronisation dynamics. The synchronisation index (Equation 3.4) is calculated after 500 iterations for each coupling strength K. (b) Travelling waves emerge for $K = 1$, $b = 0.03$, and $h = 1$. (c) Synchronised dynamics for $K = 10$, $b = 0.03$, and $h = 0$.

the coupling strength increases; also, patterns of travelling waves emerge and develop over time. In networks with only excitatory couplings ($h = 0$), increasing the coupling K leads to full synchronisation, where every oscillator has roughly the same phase dynamics of its neighbours over time.

6.2.2 Robotic model and framework

The robotic model and the framework used in the experiments of this chapter are essentially the same as described in Section 5.4.1. The experiments are performed using the Evorobot* simulator, described in Section A.2.

The framework, based on the general framework described in Section 3.3.1 and illustrated in Figure 6.3, is composed of 25 fully connected oscillators arranged in a ring of linear size 25, with

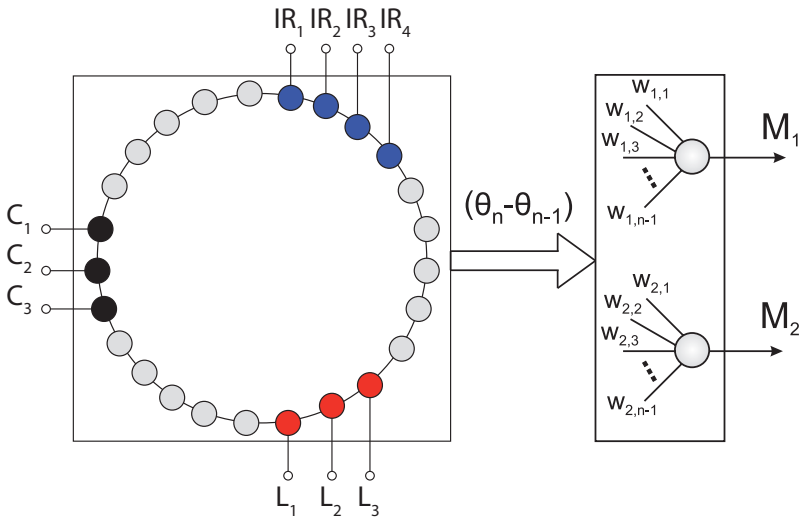

Figure 6.3: Framework for application in evolutionary robotics. The oscillatory network is a ring composed of 25 fully connected neuronal oscillators, with 4 nodes connected to the robot's infrared sensors (IR), 3 nodes connected to the light sensors (L), and 3 nodes connected to the visual sensors (C). The phase differences $\theta_n - \theta_{n-1}$, $n = 2 \ldots 25$, are linearly combined by a weight matrix W, producing the commands to the motors M_1 and M_2.

some nodes connected to the robot's sensors (each sensor is attached to a single node and no more than one sensor is attached to any given node). Each sensor group (4 distance sensors, 3 light sensors, and 3 camera sensors) are displaced in the ring with 5 independent nodes (without sensor connection) between each group. The frequency of each node is the sum of its natural frequency of oscillation, w_i, and the value of the sensory input $I_i(t)$ related to that node (0 if there is no input), scaled by a factor z_i (Equation 6.5).

$$\frac{d\theta_i}{dt} = (\omega_i + z_i I_i(t)) + \frac{K}{N}\sum_{j=1}^{N} W(j,i) sin(\theta_j - \theta_i) \tag{6.5}$$

At each iteration the phase differences γ from a node n to nodes $n-1$,$n = 2 \ldots 25$, are calculated following Equation 6.5. Then, the phase differences are linearly combined by a weight matrix W. The calculation results in two signals that will command the left and right motors of the agent. Complying with the simulator's requirements, signals are allowed to vary between $[0, 1]$ - magnitudes above 1 and below 0 are clamped (Equation 6.6):

$$\boldsymbol{M} = min\left[1, max(0, \boldsymbol{W}'\boldsymbol{\gamma})\right] \tag{6.6}$$

where $\boldsymbol{M} = [M_1, M_2]^T$ is the motor state space, with M_1 corresponding to the left motor command and M_2 to the right motor command.

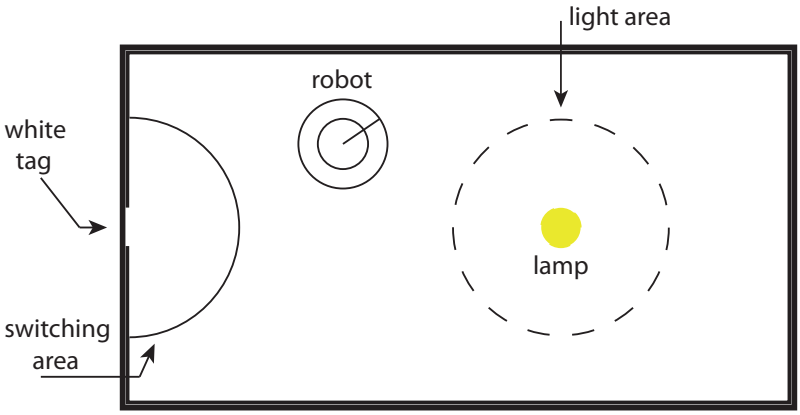

Figure 6.4: Task set-up. The robot is placed in a rectangular arena with black walls and two distinct circular areas: in the leftmost part, a "switching area", with a white tag attached on the wall; in the centre, a "light area", in which a lamp is placed. The objective of the robot is to spend as much time as possible within the area surrounding the lamp when the lamp is on. The lamp is normally off but it can be switched on by entering the "switching area".

6.2.3 Task

The task consists of a sequential, associative learning task (Urzelai & Floreano, 2001) (Figure 6.4). The robot is placed in a 500×250 rectangular arena with black walls and two distinct circular areas (of radii 80): in the leftmost part, a "switching area", with a 40 units long white tag attached on the wall; in the centre, a "light area", in which a lamp is placed (at coordinates 400×125). The objective of the robot is to spend as much time as possible within the area surrounding the lamp when the lamp is on. At the beginning of the task, the lamp is off but it can be switched on by entering the "switching area". Therefore, to solve the task, the robot has to quickly turn on the light, and then move as fast as possible towards the "light area", where it has to stand. The task is associative in the sense that the robot has to learn to associate visual and light informations to correctly display the sequence of actions that will lead to the appropriate behaviour (reward is based solely on the time spent in the light area, and there is no extra reward based on sensory readings).

Notice that a successful robot should use the white tag information, detected by its cameras, to find the "switching area", and once the lamp is on, it should use the light information, detected by its light sensors, to find and stand within the "light area". Additionally, any collisions would cause a delay in the sequence of actions, hence they should be avoided.

6.2.4 Genetic algorithm

A variation of a steady state genetic algorithm (described in Section 3.1) is used to determine the parameters of the system: the frequency of each of the 25 nodes, $w_i \in [7.8, 8]$ Hz, the 10 input weights $z_i \in [-5, 5]$, the matrix $W_{N-1,a}$ with $24 \times 2 = 48$ elements in the interval $[-1, 1]$, a motor output weight $s \in [0, 100]$, the coupling between units $K \in [0, 50]$, and the spatial kernel parameters $b \in [0.03, 0.69]$ and $h \in [0, 1]$, resulting in a genotype of length 87 for a network with $N = 25$. The population size was 100 and the evolutionary algorithm runs for a maximum of 300 generations. The parameters ranges were empirically chosen; experiments with different intervals obtained similar results.

At the beginning of each generation, agents are randomly placed in the environment. A task is comprised of 500 iterations (an iteration corresponds to a $380ms$ sensorimotor cycle). Fitness (described below) is scored at every iteration, and the average score is the task fitness. To avoid biases due to initial conditions, the final fitness of each agent is given by the average of three task simulations with random initial positions.

The fitness function is composed of two terms, A and B, calculated according to Equation 6.7.

$$f = \overbrace{V(1 - \sqrt{\Delta v})(1 - i)}^{A} + \overbrace{\frac{t}{T}}^{B} \tag{6.7}$$

where V is the sum of the instantaneous rotation speed of the wheels (stimulating high speeds), Δv is the absolute value of the algebraic difference between the speeds of the wheels (stimulating forward movement), i is the normalized value of the distance sensor of highest activation (stimulating obstacle avoidance), t is the time spent in the "light area" when the lamp is on, and T is the total number of task iterations.

Notice that part A of the fitness encourages obstacle avoidance whereas part B scores for the time spent inside the "light area" when the lamp is on. Each part has a minimum value of 0 and a maximum value of 1, therefore the maximum fitness the robot could attain is 2. However, this is never the case because the robot constantly finds and averts walls, and the sequence of actions to switch the lamp on consumes time.

Finally, neither the camera information nor the light readings participate in the fitness function. Therefore, the task objective is implicit, and the robot has to learn to associate visual and light informations to correctly display the sequence of actions that will lead to higher fitnesses. In fact, part A of the fitness is redundant because a robot that keeps colliding scores less in part B, however its inclusion in the fitness function facilitates the evolutionary process. As we perform a great number of evolutionary runs, we opted for including it.

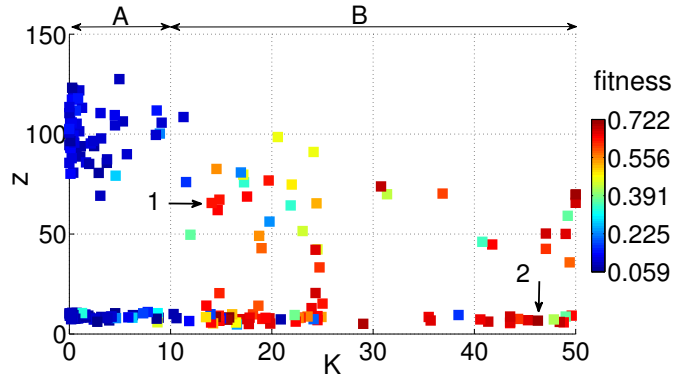

(a)

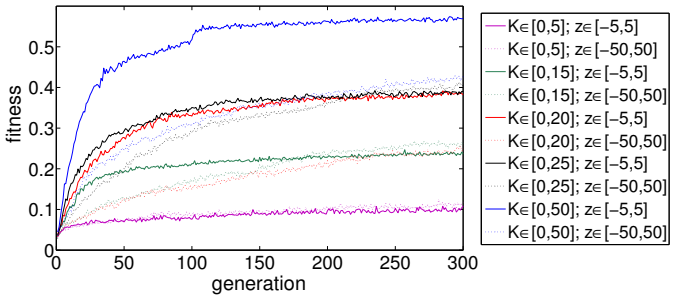

(b)

Figure 6.5: (a)Final fitness obtained in each of the 200 evolutionary runs as a function of the Euclidean distance of evolved weights z_i with respect to the origin and the coupling strength K. Individuals 1 and 2 were chosen for detailed analysis. (b) Mean evolution of the fitness obtained in each of the 20 evolutionary runs for each of the 10 possible $\{K, z\}$ intervals.

6.3 Results

The objective of the chapter is to investigate the functional roles of spatially structured connections, which can promote travelling waves or synchronisation, in the behaviour of an agent engaged in a minimally cognitive task. To this end, the first step was to evolve the framework in the task described in the previous section.

Agents with good fitness were obtained, but after a detailed inspection into the variables' dynamics we found that they were in the vast majority highly synchronised solutions. Based on that, before progressing with the analysis we opted to conduct another set of evolutions with more limited intervals in which the coupling parameter K and the input weights z_i are allowed to vary (all of the other intervals remained as described in Section 6.2.4). Together with parameters b

and h (Equation 6.2), K and z_i have a direct impact on the synchronisation dynamics; therefore, with this strategy, we attenuate the effects of a possibly irregular fitness landscape and reinforce that the good solutions found by the evolutionary process in the different parameters intervals, if existent, support travelling waves or strong synchronisation. We performed 10 series of evolutions (comprised of 20 runs each) with different $\{K, z\}$ interval combinations. Figure 6.5 shows the evolution results.

The first observation from Figure 6.5(a) is that individuals with low K (region A) have very low fitnesses, regardless of input weights. In contrast, individuals with higher K (region B) have higher fitnesses. In region B, 44% of individuals evolved with $z \in [-5, 5]$ obtained fitness greater than 0.5, but only nearly half of that number, 23%, attained this fitness when evolving with $z \in [-50, 50]$. The remaining 33% had final fitness below 0.5. Also, notice from Figure 6.5(b) that individuals with high K evolved faster with small input weights (blue and red curves), but individuals with low K evolved faster with high input weights (green and magenta curves). Based on that, we chose two individuals to conduct the analysis (individuals 1 and 2 in the figure, both with fitnesses above 0.6): individual 1 (henceforth named R1) from a region of lower K and higher z, and individual 2 (henceforth named R2) from a region of higher K and lower z.

Figure 6.6(a) depicts the fitness evolution of both robots. Notice that R2 attains a high fitness much faster than R1 - for instance, around generation 50 (out of 300), R2 already has a fitness comparable to its final fitness whereas R1 scores half of it. This was found to be the case for most of the individuals with high fitness.

R1 coupling strength (parameter K) is almost 4 times smaller than the coupling strength from R2. In this way, we can expect R1 to be less synchronised than R2. An important factor to observe to determine the existence of travelling waves, before looking into the dynamics, is the shape of the spatial kernel. Recall from Section 6.2.1 that kernels with strong lateral inhibition are mandatory for the existence of waves. Figure 6.6(b) shows the dynamics of the spatial kernel obtained for R1 and R2 after evolution. Notice that both robots have no lateral inhibition, they present only excitatory connections that fade away with distance. In fact, none of the individuals portrayed in Figure 6.5(a) presented kernels with lateral inhibition. Based on that, we run another series of evolution tunning parameters b and h (Equation 6.3) so that any good solution obtained would present lateral inhibition and hence support the existence of waves. However, no good solutions were obtained. Therefore, the first conclusion is that only individuals that present synchronised solutions could successfully solve the task.

We proceed with the analysis by investigating the behaviours of R1 and R2. Figure 6.7 shows the results. The first and third rows correspond to the behaviour of the robots when starting from

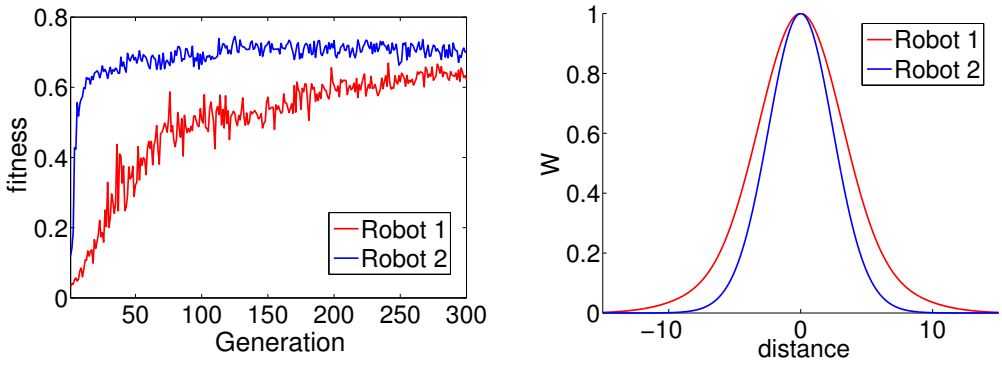

(a) (b)

Figure 6.6: Fitness obtained in each iteration of evolution (a) and coupling kernel evolved (b) for robots R1 and R2.

three different positions in the environment (Figures 6.7(a), 6.7(b), and 6.7(c) for R1 and Figures 6.7(g), 6.7(h), and 6.7(i) for R2). Both R1 and R2 successfully solve the task: they start by locating the light switching area, indicated by the white tag on the wall, then they move towards it; once the light is on, they turn and move towards the lamp, displaying a phototaxis-like behaviour.

To solve the task successfully the robots need to perform a sequence of actions. In this sense, we conducted three analyses disrupting the original environmental set-up to understand the basic behaviour primitives that drive the agents. To support the behavioural analysis, we included information flow measurements between the robot's sensors and motors (Table 6.1). This helps to highlight the influence of each sensor modality in the behaviour displayed.

In the first analysis, we removed the white tag from the wall. With this disruption, it is possible to observe whether the robots are actively using the visual information to move towards the area or if this behaviour derives from the environment configuration and passive exploration. Figures 6.7(d) and 6.7(j) show the results for R1 and R2, respectively. Notice that R1 moves erratically in the environment whereas R2 spins without covering much ground, which can be considered as a good strategy to find a landmark in an unknown environment. Therefore, both behaviours reveal that the robots actively search for the white tag at the beginning of the task. Also, because there are no sensory readings from R1 or R2, the transfer entropy values are all null and the behaviour displayed is the autonomous behaviour (i.e. the behaviour in the absence of external stimuli).

In the second analysis, we keep the lamp off during the whole duration of the task. In this way, we investigate the behaviour of agents after they reach the light switching area but without the subsequent presence of light. Figures 6.7(e) and 6.7(k) show the results for R1 and R2, respectively. R1 moves towards the white tag, reaching the light switching area, and continues to move

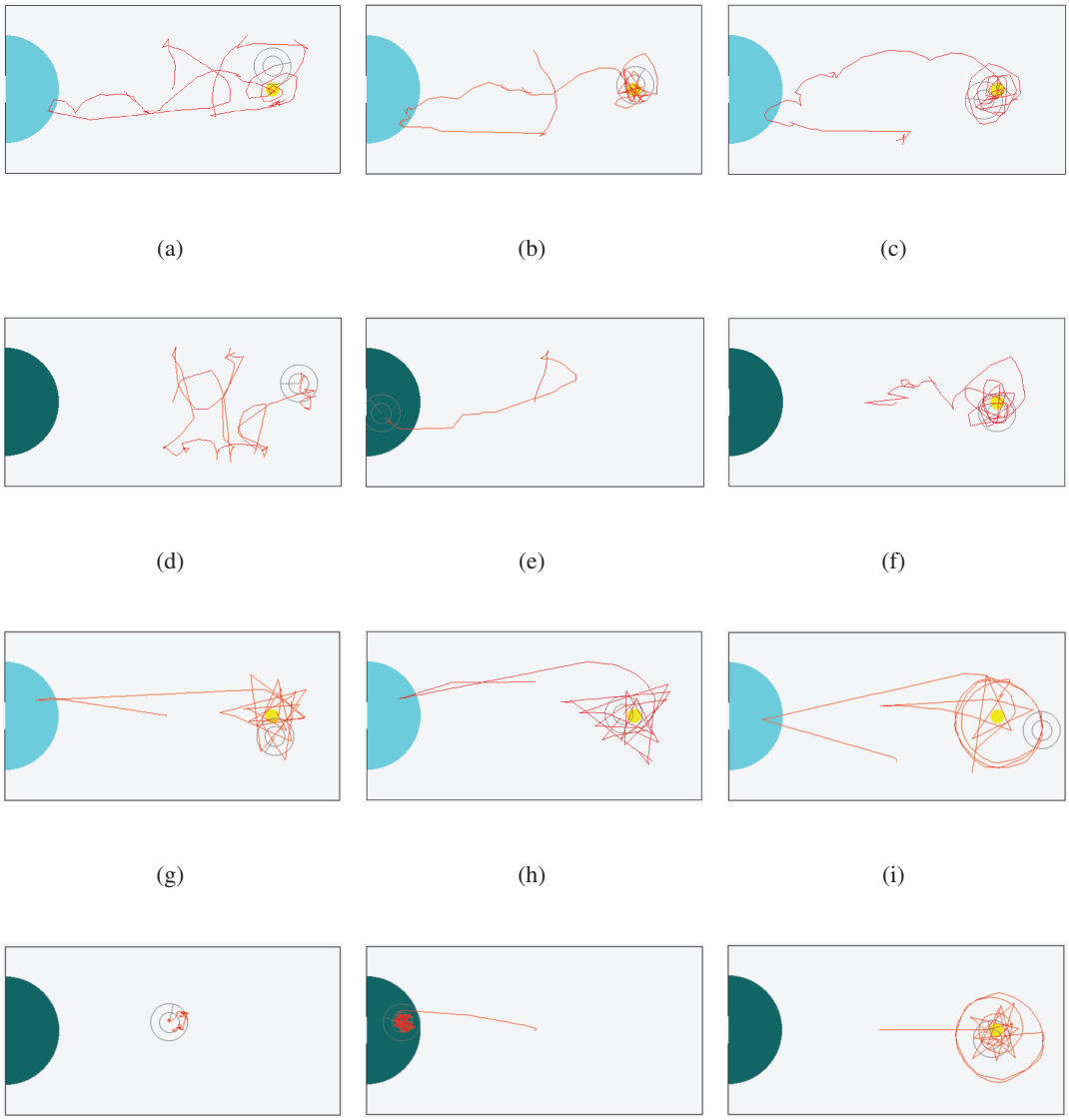

Figure 6.7: Evolved behaviours displayed by R1 (a-c) and R2 (g-i) from different initial positions. Panels (d-f) and (j-l) show the behaviours displayed in task disruptions for R1 and R2, respectively: in the situation depicted by (d,j) there is no white tag on the wall; in (e,k) the lamp is kept off; in (f,l) the lamp is always on.

Table 6.1: Transfer Entropy between the distance (TED), light (TEL), and camera (TEC) sensors time series and the motors time series for R1 and R2 (subscript sm indicates the flow from sensors to motors, and subscript ms indicates the flow from motors to sensors). In both cases a sliding window of length 500 iterations is used to obtain each time series.

R1						
	TED_{sm}	TED_{ms}	TEL_{sm}	TEL_{ms}	TEC_{sm}	TEC_{ms}
normal	0	0	0.03	0.01	0	0
no tag	0	0	0	0	0	0
no light	0.01	0	0	0	0.01	0
light always	0	0	0.02	0.02	0.01	0

R2						
	TED_{sm}	TED_{ms}	TEL_{sm}	TEL_{ms}	TEC_{sm}	TEC_{ms}
normal	0	0	0.03	0.02	0	0
no tag	0	0	0	0	0	0
no light	0.03	0.01	0	0	0.01	0.01
light always	0.01	0	0.05	0.01	0	0

uninterruptedly until it crashes against the wall. This shows that R1 is using the visual information but ignoring the distance sensors. R2, on the other hand, moves towards the tag but once close to the wall it starts to spin, displaying a behaviour similar to that observed in the absence of the white tag. Notice, from the transfer entropy analysis, that there is a flow of information from distance and visual sensors to the motors, but these are minimal and of equal magnitude in R1. In comparison, the flow observed in R2 from distance sensors to motors is three times higher, which indicates that the distance readings are influencing the motor commands more in R2 than in R1 - indeed, R2, as opposed to R1, does not collide with the wall. Also, in R2 there is a flow from motors to distance and light sensors, which corresponds to the counter-intuitive fact that motor activity is producing the sensory readings, e.g. by avoiding collisions and spinning, R2 receives visual information but this does not affect its motor outputs at that time, the "move towards the white tag" behaviour is suppressed by the "avoid collisions" strategy.

Finally, in the third analysis the lamp is kept on during the whole duration of the task, regardless of the robots entering the light switching area. Figures 6.7(f) and 6.7(l) show the results for R1 and R2, respectively. Notice that both robots move towards the light, performing phototaxis

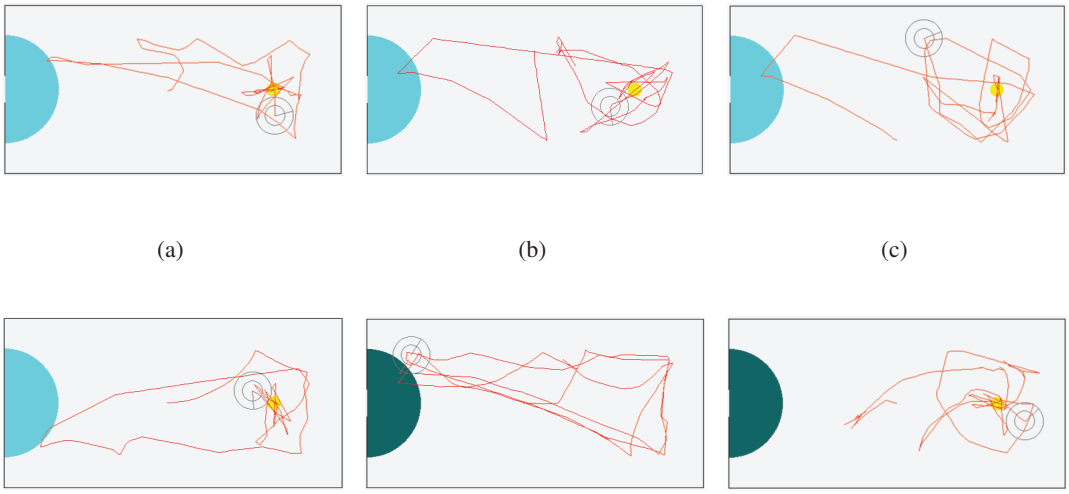

(a) (b) (c)

(d) (e) (f)

Figure 6.8: Evolved behaviours displayed by a robot with high fitness but that does not use all of the sensory information to solve it. (a-c) behaviours displayed from different initial positions. (d-f) behaviours displayed in task disruptions: in (d) there is no white tag on the wall; in (e) the lamp is kept off; in (f) the lamp is always on.

and ignoring the presence of the white tag. The experiment is also characterised by a higher flow due to the light sensors in comparison with the distance or the camera sensors.

Combined, the behavioural and information dynamics analyses show that although both agents perform well during evolution and the task behaviour is similar, the robots have a different behaviour repertoire. Both actively search for the white tag and present as primary and most fundamental behaviour phototaxis, that is, in the presence of light all other behaviours are suppressed. This demonstrates that they learn to associate the visual and light stimuli to the reward (recall that neither is explicitly present in the fitness function). However, R2 is able to avoid collisions if the light is not presented after entering the switching area, and its trajectories are neater than the trajectories of R1.

To conclude the behavioural analysis, we present in Figure 6.8 an agent that obtained high fitness during evolution but solves the task by exploiting the environmental configuration. This is to stress that the task could be solved by robots that have not learned how to associate all of the sensory stimuli with the rewards. Indeed, many individuals presented the behaviour we describe in the following paragraph, and that reinforces the importance of performing a behavioural analysis prior to looking at the variables' dynamics or more sophisticated investigations of information flow.

Consider Figures 6.8(a), 6.8(b), and 6.8(c), which show the behaviour of this robot when

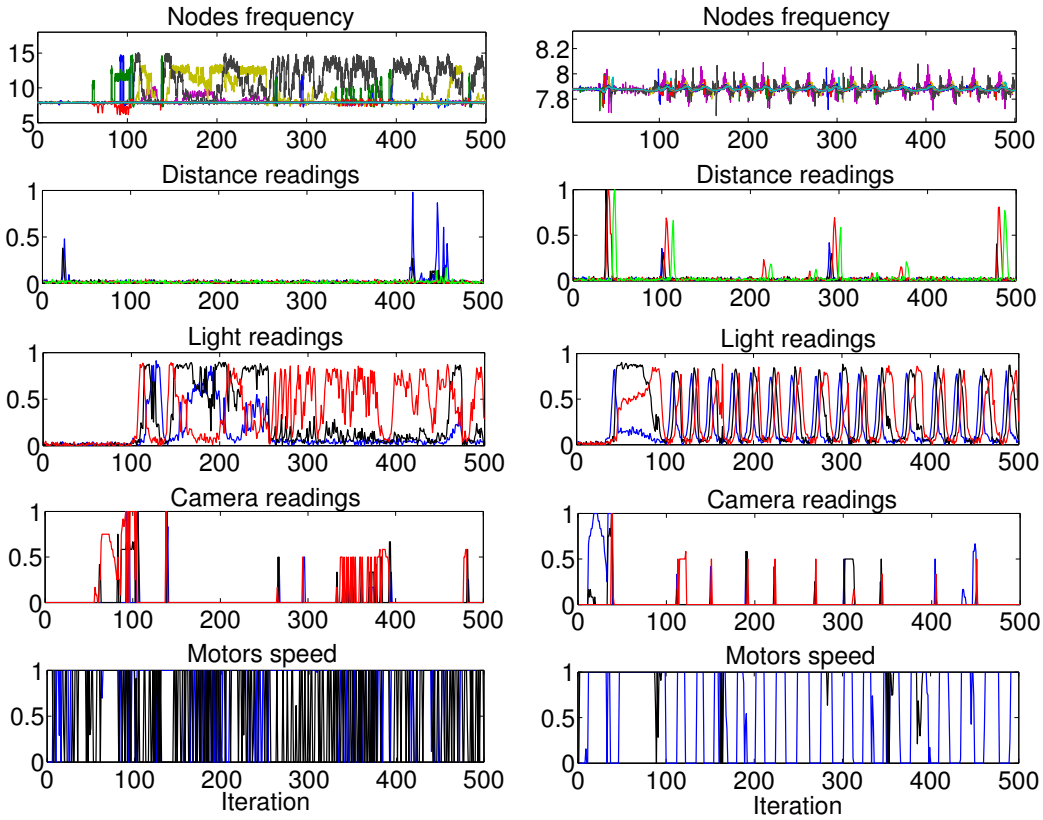

(a) (b)

Figure 6.9: Variables dynamics from R1 (a) and R2 (b) during the execution of the task. Downwards from the top: frequency (Hz) of each node; distance sensors (0 when there is no obstacle, 1 if very close to one); light sensors (0 if completely dark, 1 if very close to the light source); camera sensors (0 if no white stripe is seen, 1 if all the camera pixels detect white); and the motor commands (values higher than 0.5 indicate forward movement, backward movement otherwise).

starting from three different positions in the environment. Notice that it succeeds in solving the task: it starts by moving towards the light switching area and then it performs phototaxis once the light is on. However, after performing the disruptions described previously, we found that the robot managed to switch the light on without relying on the white tag (Figure 6.8(d)). After running the simulation without the light (Figure 6.8(e)), we note that the agent simply moves around the environment, avoiding collisions, but due to the reduced size of the arena it finds the light switching area eventually and by chance. Although the phototaxis behaviour is present, as shown by Figure 6.8(f), the strategy adopted by this individual is to explore the environment until the light is on and from that point the robot moves towards the light.

After exploring the behaviours of R1 and R2, we continue by analysing the dynamics of some

variables of the system. Figure 6.9 shows the frequency of each node, the distance, light, and camera readings, and the motors' speed over time for the behaviours portrayed in Figures 6.7(a) and 6.7(g). The most prominent difference between R1 and R2 are the nodes' frequency: whereas in the first we observe wide deviations from the narrow natural frequencies evolved ($w_i \in [7.8, 8]$), in the latter the network remains much more synchronised throughout the task. This is due to different values of inputs weights z_i and coupling strength K between nodes (see Figure 6.5), R1 has larger z_i and smaller K than R2.

The sensory dynamics are similar for both robots and relate to the behaviours observed. At the beginning of the task all readings are null, thus the robots present their autonomous behaviour (R1 moving erratically and R2 spinning). When the white tag is seen, which corresponds to an increase in the camera readings, the robots move towards the light switching area, causing a progressive increase in the visual inputs. Once inside the area, the lamp is on and that increases the light sensors readings. The robots then move towards the lamp and start performing phototaxis, causing oscillations in the measurements from the light sensors. Incidentally, distance readings are observed as the robots get closer to walls due to the proximity of the light area.

There are two main differences between R1 and R2's variables dynamics worth stressing. The first are the motor commands, which in R1 vary with higher frequency than in R2 and therefore explain why the trajectories of R2 are neater. The second occurs between iterations $[300, 400]$ in R1: notice that there are significant visual readings, which indicate that at that moment the predominant phototaxis behaviour is strongly modulated by the presence of the white tag.

The TE analysis offers another perspective. Figures 6.10(a) and 6.10(b) show the transfer entropy between the light and camera sensors, and the motor commands of R1 and R2, respectively. To obtain the time series, we adopted the same procedures for data collection and pre-processing described in Section 4.2.4, and we used a sliding window containing data from the past 70 iterations.

For R1, the first measurements of TE from camera sensors to motors show 2 peaks, one between iterations $[80, 100]$, and the other, more noticeable, between iterations $[300, 400]$. The TE from light sensors to motors varies constantly but there are more noticeable readings between iterations $[100, 250]$ and $[300, 400]$. Comparing with the sensory dynamics (Figure 6.9), the information flow measurements can be explained as follows: at the beginning, the robot moves towards the white tag (visual stimulus) but there is no light, hence the higher readings in the flow from camera to motors and the negligible flow from light sensors to motors. Once the lamp is on, this is reverted, and a more expressive flow from light sensors to motors is justified by the robot pursuing the lamp. The higher flow due to visual information observed around iteration 350

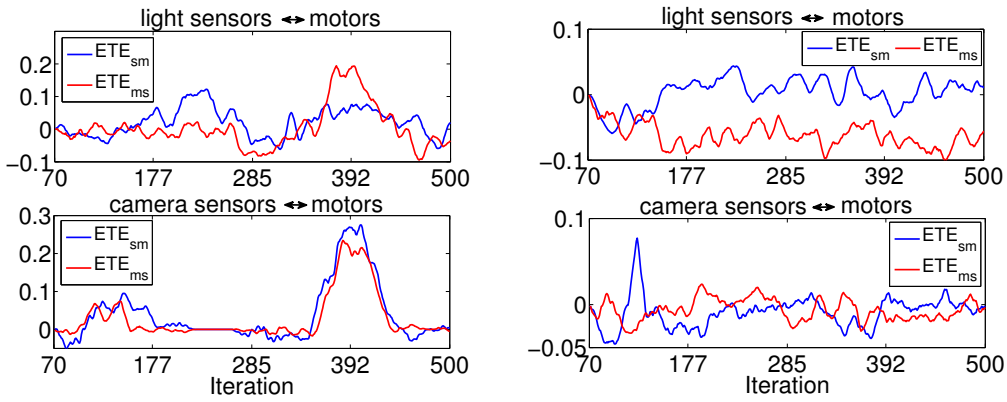

(a) (b)

Figure 6.10: (a) Transfer Entropy between the light sensors time series and the motors time series (top panel), and between the camera sensors time series and the motors time series (bottom panel) for R1. (b) Same as (a), but for robot R2. In both cases a sliding window of length 70 iterations is used to obtain each time series at every iteration of the Transfer Entropy analysis. Results are smoothed using a low-pass filter with transfer function in the z-transform domain given by $1/(1-0.5z^{-1})$.

corresponds to the modulation of the phototaxis behaviour due to the sight of the white tag, described two paragraphs above. The interesting point to note is the higher flow from motors to light sensors, measured during this behaviour modulation. R1 is attracted by the white tag, thus the motor commands are mainly influenced by the visual information and the light readings are more of a "passive" consequence; in other words, the motor commands influence the light readings, but the opposite is less salient.

For R2 (Figure 6.10(b)) the rationale is similar, but the neater behaviour presented by this robot finds correspondence in the information flow. At the beginning of the task, around iteration 80, there is a peak in the flow from camera sensors to motors, which corresponds to the behaviour of actively seeking and moving towards the white tag. Once the light switching area is reached, the visual flow reduces and the flow from light sensors to motors increases and oscillates as the robot moves around the lamp performing phototaxis. Also, notice that the flow from motors to light sensors remains lower than the flow from light sensors to motors, which indicates that it is the light information that is driving the robot.

The previous analyses focused on the dynamics and information flow between sensors and actuators of the robot. To conclude the analysis of results, we investigate the relationship between the network activity and the sensors and motors' activity. To this end, we calculate the field potential (FP) generated by the network and relate its dynamics with that of the different sensor

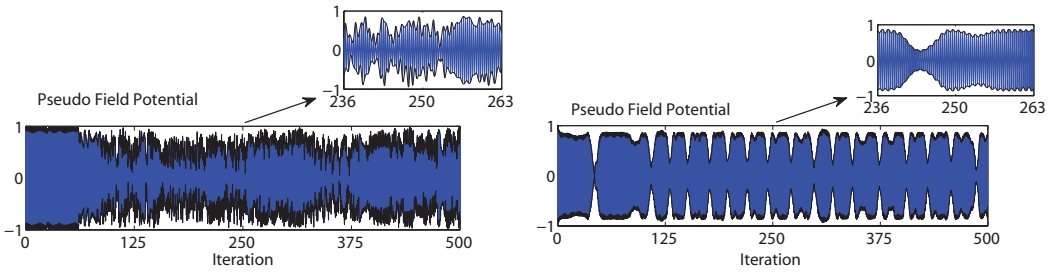

(a) (b)

Figure 6.11: (a) Pseudo-field potential (PFP) of robot R1 during task execution, calculated according to Equation 6.8. The black line highlights the PFP envelope (PFPe). (b) Same as (a), but for R2.

modalities. To obtain the FP, we used the methods described in Heitmann et al. (2012) to calculate a gross approximation of the mean electric field generated by a group of neurons. The pseudo-FP (PFP) is given by Equation 6.8.

$$PFP(t) = r(t)cos(\Psi(t)) \tag{6.8}$$

where $r(t)$ and $\Psi(t)$ are the synchronisation index and the mean phase of the network at time t, respectively, calculated according to Equation 3.4.

This equation calculates the PFP by approximating the neurons' membrane potential by the cosine components of the oscillators' phases. This leads to a high-frequency signal whose amplitude is modulated by the coherence between oscillators in a way that the higher the synchronisation level, the higher the amplitude of the PFP. In this sense, the PFP highlights the common action of neurons.

The envelope dynamics of the PFP signal (PFPe) was shown to contain behaviourally relevant information in systems where travelling waves and synchronised solutions manifest (Boonstra et al., 2007; Heitmann et al., 2012). To give explicit emphasis on the dynamics of the signal envelope rather than on the absolute values of the magnitudes alone, we re-scaled the signal $r(t)$ so that the minimum value of $r(t)$ corresponds to 0 and the maximum value of $r(t)$ corresponds to 1. Figure 6.11 shows the results.

The PFPe from R1 (Figure 6.11(a)) has a high amplitude at the beginning of the task because the absence of sensory readings leads to nodes oscillating with almost the same frequency (see Figure 6.9(a)). With the robot approaching the white tag and later engaging in phototaxis, the sensory readings disturb the natural frequencies which in turn modulate the mean synchronisation index and phase, causing variations in the PFP dynamics. The explanation for the PFPe from

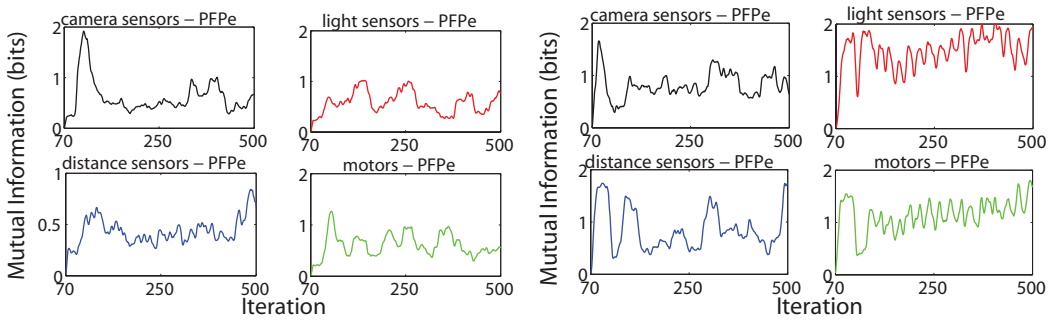

Figure 6.12: (a) Mutual information between the motors, the distance, light, and camera sensors time series, and the pseudo-field potential envelope time series for R1. (b) Same as (a), but for robot R2. In both cases a sliding window of length 70 iterations is used to obtain each time series at every iteration of the MI analysis. Results are smoothed using a low-pass filter with transfer function in the z-transform domain given by $1/(1 - 0.5z^{-1})$.

R2 is very much alike that of R1, but notice that the dynamics have a lower frequency and have a straight-forward behavioural correspondence: the PFPe is high at the beginning for there is little sensory stimulation which promotes widespread synchronisation, then it decays due to the increasing visual inputs as the robot moves towards the white tag; in sequence, the PFPe increases as the robot moves towards the lamp and from that point its dynamics follows that of the light sensors readings and motor commands (Figure 6.9(b)).

To establish a relationship between the PFPe, which represents the global network activity, and the sensors and motors, we calculated the mutual information (MI) between these variables. MI was estimated according to Equation 2.11 and following the same procedures for data collection and pre-processing described in Section 4.2.4. A sliding window containing data from the past 70 iterations was used.

Figures 6.12(a) and 6.12(b) show the results for R1 and R2, respectively. The results can be explained following a similar reasoning used to describe the PFP or the TE dynamics. Briefly, the information flow between the PFPe and each sensor modality peaks or oscillates according to the corresponding sensory reading, which vary as the robot performs different behaviours to solve the sequential task. The interesting fact to note is that the MI curve is different for each sensor modality and for the motor commands, which suggests that once the system is evolved it is possible to use the PFPe information to control the robot instead of using the phase dynamics of every node of the network. That could greatly simplify the system, specially when scaling up, because the number of free parameters in readout units based on PFPe dynamics would not

increase with the addition of nodes in the network, whereas in the current architecture each node inserted leads to two additional output weights (see Figure 6.3).

6.4 Discussion

In this chapter, we applied an extended version of the Kuramoto model of coupled phase oscillators to study whether spatially structured connections, which may lead to travelling waves or synchronised dynamics, facilitate or are advantageous to promote the different behaviours required by a sequential, associative learning task. The diversity in the model dynamics was obtained by incorporating a wavelet-like spatial kernel to obtain a centre-surround connection pattern between neurons.

In the experiment, the robot had to develop a particular sequence of actions in order to score more fitness points. The framework, based on the general architecture described in Section 3.3.1, has linear output units, a ring topology, and natural frequencies varying in a narrow range around 8 Hz (8-13 Hz rhythms in the motor cortex are modulated during action execution and movement (Muthukumaraswamy et al., 2004; Lepage & Theoret, 2006)). The values of the spatial kernel parameters, determined by evolution, were allowed to vary in a wide range that supports the emergence of waves and synchrony.

After a comprehensive collection of experiments, which explored different ranges of parameters, the results showed that robots with good performance had predominantly synchronised networks, characterised by bigger coupling strength between nodes and without inhibitory connections. Spatially structured connections, which support the formation of waves, did not generate good solutions. To rule out the hypothesis that travelling waves were not observed due to limitations of the genetic algorithm and properties of the fitness landscape, we conducted longer evolutions forcing the parameters to vary in a range that would necessarily lead to solutions displaying travelling waves. Once more, robots with good performance were not found. Also, more synchronised solutions evolved faster than less synchronised networks. Larger input weights generated robots with longer fitness convergence and lower performance (although this is probably due to the genetic algorithm producing fine-grained weights when they varied between $[-5, 5]$ and coarse-grained weights when they varied between $[-50, 50]$).

A question that immediately arises is whether the original Kuramoto model, which under weak coupling and narrow natural frequency bands presents a propensity for synchronisation (Acebrón et al., 2005), has good performance on this task or the incorporation of the spatial kernel produces some effect to make evolution more successful. In Figure 6.13, we show the mean fitness evolution of two experiments using the framework described in Section 6.2 but with global

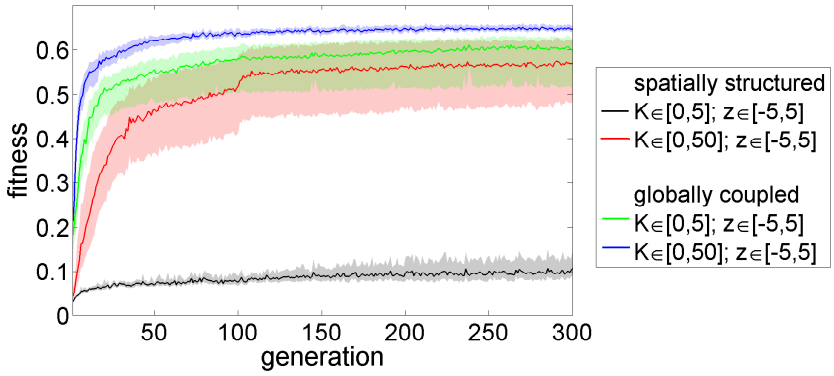

Figure 6.13: Mean evolution of the fitness obtained in each of the 20 evolutionary runs for networks with global connectivity (original Kuramoto model) and networks with spatially structured connectivity (results reproduced from Figure 6.5(b)). The figure shows the results for two coupling scenarios: weak coupling ($K \in [0, 5]$) and strong coupling ($K \in [0, 50]$). Shaded areas correspond to the 95% confidence interval.

connectivity (i.e., removing the effects of the spatial kernel), and compare it with the respective architectures whose results are portrayed in Figure 6.5(b). The original model performance overcomes that of the model with spatially structured connections, and there is a more noticeable difference in the weak coupling configuration. The conclusion is that, at least for this task, networks with more propensity for synchronisation obtain better results than networks with spatially structured connections, which are either less synchronised or present travelling waves solutions.

The strategy of altering the input weights z_i, despite impacting on stimulus modulation of natural frequencies and thereby on the synchronisation dynamics of the network, could have promoted more elaborated effects. In a series of works, Tass showed that strong perturbations to the natural frequencies in a network of phase oscillators can synchronise or desynchronise the population (Tass, 1999, 2001a,b, 2003). However, perturbations need to be coordinated, of specific frequencies, amplitudes, and durations, and have to be delivered at precise epochs of the phase dynamics. Heitmann et al. (2012) also found that carefully delivered perturbations succeed in eliciting transitions between travelling waves and synchrony. It is still unclear how these techniques could be extended to an agent-environment system, where stimulus-evoked perturbations depend on emergent behaviours, occur at varied times, and with different magnitudes.

Based on the above, it is hard to determine whether the predominance of synchronised solutions is a by-product of the framework used or if this type of solution is intrinsically advantageous for the robot (in particular, Rubino et al. (2006) point out that synchronised activity is widespread in the motor cortex, with limited occurrence of spatio-temporal patterns). To begin with, the 1-

dimensional ring topology has certainly simpler dynamics than its 2- or 3-dimensional networks counterparts, which are a better representative of real neuronal circuits. However, they are much more complex to simulate and analyse. Considering that there are interesting biological circuits whose dynamics are captured by 1-dimensional structures (Kazanci & Ermentrout, 2007), and that under some conditions the dynamics of a 2-dimensional sheet can be decomposed into a set of 1-dimensional problems (Ermentrout et al., 1998, 2001), the original experiments presented in this chapter are informative. A crucial aspect is how to extract from the network activity motor commands that generate stable behaviours. In our model, the linear output units benefit from synchronisation because synchronised oscillators present stable phase differences that lead to balanced motor commands, but that is not to say that the dynamics of the network need to be fully entrained with zero phase-lag between nodes during the whole duration of the task. For instance, Steingrube et al. (2010) and Shim & Husbands (2012) showed that transient stable phase-locked states can be obtained from chaotic dynamics and generate coordinated motor behaviour. Also, Ashwin & Timme (2005) and Rabinovich et al. (2012) argued that computations based on stable heteroclinic cycles (a sequence of successive metastable states) have several advantages over computations that rely on stable state dynamics. Therefore, the key issue is how to decode information present in spatio-temporal patterns of neuronal activity. Promising models have been developed e.g. by studying odour discrimination in the olfactory system of insects (Nowotny et al., 2003; Krofczik et al., 2009; Assisi et al., 2011), but it is still unclear whether these models, or models that are able to generate more intuitive periodic locomotion behaviours, could account for, or be extended to, scenarios that require more complex sensorimotor interactions. Additionally, other architectures such as neurons with different axon lengths arranged in bi- or tri-dimensional lattices, as opposed to an isotropic ring structure, could possibly originate other forms of interactions. In this sense, Heitmann et al. (2012) argue that cortical pyramidal neurons are a plausible alternative to decode spatio-temporal patterns given that the dendritic tree of pyramidal neurons can detect and discriminate temporal synaptic sequences (Branco et al., 2010). Therefore, a possible future extension would be to incorporate e.g. the Traub model for pyramidal neurons (Traub et al., 1991) to the framework presented in this chapter.

The dynamical analysis of the system's variables of two evolved robots, R1 and R2, showed that they present higher neuronal synchronisation without sensory stimulation and that in the presence of sensory readings the network becomes less synchronised. Also, the behavioural trajectories of R2, who has a high level of synchronisation throughout the task and small input weights, were neater than the trajectories of R1, who has a lower level of synchronisation throughout the task and larger input weights. These results are in agreement with the "cortical idling hypothesis"

(Pfurtscheller et al., 1996), which states that synchrony is observed outside periods of sensory stimulation and wave patterns encode motor action states. However, this hypothesis contrasts with that posed by Ermentrout & Kleinfeld (2001), who stated that synchrony is related to the presence of a sensory stimulus and waves are present in the absence of stimulation. As with many other phenomena in the brain, it is most likely that both proposed explanations hold. Nevertheless, we note that Churchland et al. (2010) reported that neuronal variability is reduced in the presence of sensory stimulation or attentional processes, and that would be a general network property. Recent extensions to these findings show that across trial neuronal activity variability is generated by fluctuations between multistable attractors and that the presence of stimuli stabilises one specific attractor (Deco & Hugues, 2012); this suppression of neural variability depends on properties of the stimuli and the ongoing neural state (White et al., 2012), and on network architecture (Litwin-Kumar & Doiron, 2012). More specific to our study, the best evolved networks converge to fully synchronised states in the absence of sensory stimuli, which also means that they display less variation in neuronal activity across trials and that, according to the aforementioned works, may be useful for noise suppression, sensory processing, and information encoding.

The transfer entropy analysis emphasised the time-dependent influence of each sensor modality along the task, adding a complementary perspective to the dynamical analysis of the system's variables. The results showed that the information flow from sensors to motors, associated to behaviourally relevant sensory information, and the flow from motors to sensors, associated to passive sensory readings that occur as a consequence of motor behaviour, are asymmetric and vary over time depending on the sequence of actions. In this sense, the behavioural sequence that leads to higher fitnesses - quickly finding the light switching area and standing closer to the lamp once it is on - has a correspondence in the information flow dynamics and allows one to gain further insights into the robot's decisions upon facing conflicting behavioural choices. However, the results from information theoretical measurements should be appreciated with care. As stressed in Section 3.4, data from agent-environment systems pose extra challenges for sensible analyses. Likewise Chapters 4 and 5, we used the extensions suggested by Marschinski & Kantz (2002) to alleviate some of the limitations, together with a window length for data collection small enough to contain behaviourally relevant information but also large enough to include a minimum number of points to facilitate the estimation of probabilities and the reduction of biases. Although negative values of transfer entropy are observed in some periods of the task, which is an indicative that the bias in the data during those periods was particularly high, we believe that the qualitative aspect of the curves contribute to the conclusions.

The final part of the results presented the calculations of the pseudo field potential (PFP)

and the mutual information (MI) between the PFP envelope (PFPe), the different sensor modalities (distance, camera, light), and the motors. For that, we used a method that estimates the PFP based on the average membrane voltage potential of the neurons (Heitmann et al., 2012), although evidence points at synaptic activity as the variable fundamentally linked to the LFP production (Mazzoni et al., 2008). The MI analysis showed that sensory and motor information are present in the PFPe, with distinct dynamics following the behavioural act being performed. The extent to which LFPs from cortical circuits encode sensory stimuli is still unclear, but there is evidence that its activity contains information about inputs and subsequent cortical processing (Belitski et al., 2008). Indeed, researchers from the field of brain-machine interfaces were capable of decoding motor intentions based on the LFP activity of primates using a relatively simple linear decoder (Carmena et al., 2003; Lebedev et al., 2005); moreover, it has been shown that LFP dynamics contains information about target direction, trajectory, and velocity in reach and grasp tasks (Bansal et al., 2011). This suggests that a possible extension to the work reported in this chapter would be to use the PFPe information to establish the motor commands of robot, which could facilitate the scaling up process. In conclusion, this novel approach combining evolutionary robotics and methods of PFP analysis may contribute to experiment predictions and hypothesis testing regarding LFPs and their relationship with cognitive processes.

Finally, in the analysis of results we showed that some agents solved the task without associating the visual stimulus with the light switching area; rather, they exploited the environmental configuration to incidentally enter the region and thereby turn the lamp on. This strategy, although successful, does not score as many fitness points as R1 or R2's strategy, and would underperform in different environment configurations. A possible solution would be to increase the number of task simulations per robot before scoring the final fitness (in the experiments we used 3) or use environments with wider dimensions, thus reducing the chance of obtaining a good performance without actively associating each stimulus with a specific behavioural sequence. However, one must be aware that these modifications would inevitably lead to an increase in the evolution time.

Chapter 7

Summary of conclusions and future work

7.1 Summary

This thesis has been primarily concerned with better understanding the role of neuronal oscillations and information dynamics towards the generation of embodied cognitive behaviours and with investigating the efficacy of such systems as practical robot controllers. We developed a novel model based on the Kuramoto model of coupled phase oscillators and performed three minimally cognitive evolutionary robotics experiments. The analyses focused both on a behavioural level description, investigating the robot's trajectories, and on a mechanism level description, exploring the variables' dynamics and the information transfer properties within and between the agent's body and the environment.

The first experiment demonstrated that in an active categorical perception task under normal and inverted vision, networks with a definite, but not too strong, propensity for synchronisation are more able to reconfigure, to organise themselves functionally, and to adapt to different behavioural conditions. The second experiment related assembly constitution and phase reorganisation dynamics to performance in supervised and unsupervised learning tasks. We demonstrated that assembly dynamics facilitate the evolutionary process, can account for varying degrees of stimuli modulation of the sensorimotor interactions, and can contribute to solving different tasks leaving aside other plasticity mechanisms. The third experiment explored an associative learning task considering a more realistic connectivity pattern between neurons. We demonstrated that networks with travelling waves as a default solution perform poorly compared to networks that are normally

synchronised in the absence of stimuli.

Overall, this thesis showed that neural synchronisation dynamics, when suitably flexible and reconfigurable, produce an asymmetric flow of information and can generate minimally cognitive embodied behaviours.

The next section recapitulates the experimental work conducted and stresses the main results obtained; Section 7.3 explores possible directions for future works; finally, Section 7.4 closes the thesis by presenting the final remarks.

7.2 Contributions

The primary contribution of this thesis is a novel model to study neuronal synchronisation phenomena in different benchmark evolutionary robotics tasks. We show that, at a certain level of abstraction, the framework is biologically plausible and flexible enough to encompass a variety of open problems in neuroscience and cognitive science. This is demonstrated in three different minimally cognitive tasks, focusing on diverse aspects of neuronal synchronisation dynamics. More specifically, in the behavioural tasks studied:

- *We demonstrate that neural synchronisation dynamics, when suitably flexible and reconfigurable, can generate minimally cognitive embodied behaviour and can be used as practical robot controllers*

We succeeded in evolving simulated robots in a variety of tasks. For instance, the first experiment investigates the role of synchronisation in the performance of a simulated robotic agent during the execution of active categorical perception under normal and inverted vision; the second experiment analyses dynamic assembly formation in a supervised spike pattern classification task and in an unsupervised robotics task, in which an evolved robot has to cope with multiple, possibly conflicting objectives; the third experiment evolves a robotic agent in a sequential, associative learning task using a more realistic centre-surround connectivity pattern between neurons to explore the functional roles of travelling waves and neural synchronisation in a behavioural task.

- *We demonstrate that performances are directly linked with the synchronisation regime of the network*

In particular, the results from Chapter 4 indicate that networks with a definite, but not too strong, propensity for synchronisation are more able to reconfigure, to organise themselves functionally, and to adapt to different behavioural conditions. The results from Chapter 5 show that dynamic assembly formation facilitates the evolutionary process and accounts for varying degrees of stimuli

modulation of the sensorimotor interactions, i.e. we show that synchronisation selectively modulates the influence of external signals in the current network activity. Finally, in Chapter 6 we show that networks that present travelling waves as a default solution have a far worst performance than networks that are normally synchronised in the absence of stimuli, which further supports the cortical idling hypothesis.

- *We demonstrate that neuronal assemblies and phase reorganisation dynamics can play a significant part in supervised classification tasks and, perhaps most relevant to cognition, can cope with multiple classification tasks without the need for additional adaptive mechanisms.*

The results show that performance depends nonlinearly on the number of assemblies and neurons in the network, and is predominantly higher in networks with more assemblies, regardless of the number of neurons within each. We also show that redundancy is widely present across different architectures and is directly proportional to the number of neurons in a network with fixed number of assemblies; synergy, on the contrary, is higher in architectures with fewer neurons within each assembly, regardless of the total number of assemblies. All these findings resemble the results obtained in real cortical experiments.

- *We demonstrate the asymmetry of information flow and its behavioural correspondence*

We pair the more traditional dynamical analysis of the system's variables with information theoretic techniques in order to get a broader picture of the ongoing interactions with and within the network, reinforcing the asymmetry of information flow and its behavioural correspondence. The results systematically show that the combined approach, in the context of evolved robots, provides a complementary form of analyses. In Chapter 4, we show that even though the network is fully connected, the information flow is not symmetric, and the higher performance of the critical coupled network can be linked to its flexible ongoing dynamics which can be modulated by the environmental context; also, the normal and inverted vision conditions elicit a difference in the information flow at specific points of the agent's trajectory, and with no explicit plasticity mechanisms, it can respond and adapt to conflicting sensory conditions and obtain good performance on the task. In Chapters 5 and 6, the transfer entropy analysis emphasised the time-dependent influence of each sensor modality along the task, i.e. the information flow from sensors to motors, associated to behavioural relevant sensory information, and the flow from motors to sensors, associated to passive sensory readings that occur as a consequence of motor behaviour, are asymmetric and vary over time depending on the sequence of actions. In particular, in Chapter 5 the dynamical analysis of the phase space formed by the motors readings and the nodes' phases reveal different

orbits that are due to changes in assembly organisation, and an analysis of the information flow in the network reveals that such changes modulate the influence of the inputs in the robot's behaviour (determined by the motor commands). In Chapter 6, the dynamics of the pseudo-field potential envelope is shown to contain behavioural relevant information, similar to what has been found in diverse animal experiments. This emphasizes the potential of the framework in experiment predictions and hypothesis testing regarding large scale neuronal activity and its relationship with cognitive processes.

7.3 Limitations and Future Work

Despite solid evidence that synchronisation mechanisms underpin cognitive processes, the underlying mechanisms of neural dynamics are far from being understood. Even the most established principles, such as the number of nervous cells in the human brain, have been challenged (Lent et al., 2011). In this sense, the limitations and future work directions suggested in the following paragraphs focus on technical details that limit the framework and the significance of results presented throughout the thesis.

Starting with the network model, the original formulation of the Kuramoto model does not take into account important properties of real nervous systems (e.g. spatial distribution of units, transmission delays, asymmetrical interactions), therefore an important step towards more biologically plausible architectures would be to implement extended versions of the model which tackle some of these constraints (Tass, 1999; Cumin & Unsworth, 2007; Breakspear et al., 2010). A special emphasis should be put into spatially distributed patterns of connectivity and different forms of interactions. In particular, Kazanci & Ermentrout (2007) showed that the interplay between chemical and electrical synapses in a network of coupled oscillators elicit a great variety of dynamical patterns (including travelling waves and synchrony). Moreover, neural networks with freely diffusing gaseous neuromodulators - GasNets - improved evolvability of robotic agents engaged in sensorimotor tasks (Husbands et al., 1998; Philippides et al., 2005). Also, more elaborate neuronal architectures, such as small-world structured networks or modular communities, unfold more complex, metastable dynamics which are intrinsically connected to dynamic pattern formation in brain activity and hence are fundamental to adaptive behaviour (Omel'chenko et al., 2008; Tognoli & Kelso, 2009; Chialvo, 2010; Shanahan, 2010b; Wildie & Shanahan, 2012). A great limitation towards this latter point was the lack of rigorous mathematical formulations establishing the conditions to obtain specific synchronisation regimes in arbitrary network topologies using the Kuramoto model - this result was known for fully-connected networks only. However, a recent work from Dorfler and collaborators (Dorfler et al., 2013) has established the synchron-

isation conditions for almost all possible network topologies, hence an immediate extension to the work presented here would be to perform the experiments of Chapter 4, which were constrained to the fully connected architecture in order to permit the network tuning on specific synchronisation regimes, using more complex networks.

The model employed in Chapter 6 is a step towards this direction for it includes a spatial kernel that promotes asymmetrical interactions and supports travelling waves and synchrony. A possible extension would be to use more biologically plausible connectivity schemes such as that implemented by Cabral et al. (2011), who used an empirically defined structural connectivity map of 66 regions of the human brain to build a Kuramoto inspired model, or to incorporate time delays (Yeung & Strogatz, 1999). Considering the model presented in Chapter 5, future extensions should accommodate more biologically plausible aspects of neuronal assemblies, such as noise or multiple assembly membership (i.e. entitle a given neuron to participate simultaneously in two or more assemblies). The first has been shown to provide a substrate for many neuronal and cognitive phenomena (Rolls & Deco, 2010), the latter to enhance the computational power of a neuronal circuit (Izhikevich, 2006). Another possible extension to the model would be to substitute the continuously coupled oscillators used in this thesis with pulse-coupled oscillators, which are not only a more biologically plausible abstraction of neuronal synaptic activity, but also present rich metastable dynamics that can be exploited to compute arbitrary logic operations (Neves & Timme, 2008, 2012; Wildie & Shanahan, 2012). However, the network cluster states in the works just cited are emergent processes found numerically (despite the switching dynamics being controllable), whilst the model studied in this work can be systematically tuned into predefined assembly configurations. Finally, Ashwin et al. (2007) showed that if the phase interaction function includes more than the first Fourier mode only, the system supports stable heteroclinic cycles. This extension should be explored in future works, given the evidence that this sort of dynamics is a fundamental brain operation (Rabinovich et al., 2010, 2012).

As for the task scenarios, the experiments were conducted following an evolutionary robotics approach which, despite all the advantages mentioned throughout the thesis, suffers from high computational cost for fitness assessments which can be a limitation in scaling up to more complex tasks. To tackle this problem, Bongard (2011) offers an encouraging technique that stops the evolution of inferior phenotypes independently of the fitness function used, which reduces the evolution time complexity from polynomial to sublinear time. Also, simulated experiments have to be carefully set-up to avoid undesirable gaps when transferring to real world scenarios. In this sense, the addition of noise during simulations is essential to obtain good cross-platform performance (Jakobi, 1998). Another useful approach would be to incorporate ontogenetic plasticity

mechanisms to the robot's controller, which are shown to greatly increase adaptability to sensory disruptions and dynamic environments (Urzelai & Floreano, 2001). Finally, a central extension to progress with the understanding of neural synchronisation and cognitive processes and to developing better robotic controllers is to consider more complex robotic bodies (Pfeifer & Bongard, 2006). Cognition is an emergent process from brain-body-environment interactions, therefore more complex bodies may facilitate more complex cognitive acts without increasing the complexity of the underlying neural architecture. Nevertheless, ER is a promising approach to testing hypotheses which have not been extensively explored yet in the context of the relationship between neural synchronisation and behaviour.

The transfer entropy analysis, in common with other information theoretic tools, relies on the proper choice of parameters, on accurate probability density estimations, and require large numbers of data points for robust estimations. Using the extensions to the original TE measure suggested in Marschinski & Kantz (2002), we reduced some of the undesirable effects caused by small data sets. Likewise, further work should consider varying the orders of the Markov processes (parameters m and n in Eq. 3.10) for they influence the estimated value of transfer entropy and may be used to reveal time dependences since motor, sensors, and nodes may operate at different time scales (Lungarella & Sporns, 2006; Gourévitch & Eggermont, 2007). Also, in addition to dividing data into short segments (windows), future investigations should consider the permutation techniques devised by Barrett et al. (2012) to alleviate bias and non-stationarity problems. Finally, the joint probability distributions, here estimated using histograms, could benefit from other methods such as neighborhood (Verdes, 2005; Hlaváčková-Schindler et al., 2007) or kernel estimation (Kantz & Schreiber, 1997) methods.

7.4 Final remarks

Neuronal activity is complex, transient, emerges and varies over space and time, therefore it is hard to establish whether synchronisation is behaviourally relevant or an epiphenomenon. To mention but two recent findings that put into perspective widely accepted concepts mentioned throughout the chapters: Rolls et al. (2012) demonstrated that information transmission in connected neuronal systems can occur without synchronisation, which opposes the communication-through-coherence hypothesis; Díaz et al. (2007) showed that the neuronal activity measured by local field potentials may be generated by asynchronous oscillators. Nevertheless, it is the consensus that synchronisation mediates cognitive processes and is an effective mechanism for sensorimotor coordination. In this sense, we believe that future work exploring dynamical models of neuronal activity, specially in embodied and Evolutionary Robotics contexts, is amongst the most promising approaches to

unveil the functional roles of neural synchronisation.

Our contribution is a novel framework, based on coupled phase oscillators, to further understand the relationship between neuronal synchronisation, information dynamics, and behaviour. Although there has been much work on coupled oscillator based control of complex motor behaviours, particularly locomotion, to date there has been very little research on the wider issues of neuronal synchronisation and phase information in the generation of embodied cognitive behaviours. The experiments demonstrated that different aspects of neuronal synchronisation dynamics can be exploited to generate minimally cognitive embodied behaviour and can be used as practical robot controllers, with emphasis on the asymmetry of information flow and its behavioural correspondence. Therefore, the work presented in this thesis reinforces that exploring a simulated brain-body-environment system, in addition to the existing methods, could contribute to unveiling important mechanisms of the neural system which may not be easily identifiable in living organisms and that could inspire the design of new robotic controllers.

Bibliography

Abbott, L. (1999). Lapicque's introduction of the integrate-and-fire model neuron. *Brain Research Bulletin*, 50(5-6), 303–304. 4

Abeles, M. (1988). Neural codes for higher brain functions. *In: Markowitsch HJ, editor. Information processing by the brain, Stuttgart*. 25

Acebrón, J. A., Bonilla, L. L., Pérez Vicente, C. J., Ritort, F., & Spigler, R. (2005). The Kuramoto model: A simple paradigm for synchronization phenomena. *Reviews of Modern Physics*, 77(1), 137–185. 79, 121, 144

Adrian, E. D. (1928). *The basis of sensations*. Norton. 36

Adrian, E. D. (1950). The electrical activity of the mammalian olfactory bulb. *Electroencephalogr. Clin. Neurophysiol.*, 2, 377–388. 24

Adrian, E. D. & Zotterman, Y. (1926). The impulses produced by sensory nerve-endings, part ii: The response of a single end-organ. *J. Physiol.*, 61(2), 151–171. 36

Akam, T. & Kullmann, D. M. (2010). Oscillations and filtering networks support flexible routing of information. *Neuron*, 67(2), 308–20. 30

Andersen, R. A. & Cui, H. (2009). Intention, action planning, and decision making in parietal-frontal circuits. *Neuron*, 63, 568–583. 34

Applegate, D. L., Bixby, R. E., Chvtal, V., & Cook, W. J. (2006). *The Traveling Salesman Problem: A Computational Study*. Princeton University Press. 48

Arthuis, M., Valton, L., Régis, J., Chauvel, P., Wendling, F., Naccache, L., Bernard, C., & Bartolomei, F. (2009). Impaired consciousness during temporal lobe seizures is related to increased long-distance cortical-subcortical synchronization. *Brain*, 132, 2091-2101. 6

Ashwin, P. & Timme, M. (2005). When instability makes sense. *Nature*, 404, 36–37. 93, 146

Ashwin, P., Wordsworth, J., & Townley, S. (2007). Dynamics on networks of cluster states for globally coupled phase oscillators. *SIAM J. Applied Dynamical Systems 6, no. 4 728-758*. 93, 153

Assisi, C., Stopfer, M., & Bazhenov, M. (2011). Using the structure of inhibitory networks to unravel mechanisms of spatiotemporal patterning. *Neuron*, 69, 373–386. 146

Attneave, F. (1954). Some information aspects of visual perception. *Psychological Review*, 61, 183–193. 40

Attwell, D. & Laughlin, S. B. (2001). An energy budget for signaling in the grey matter of the brain. *Journal of Cerebral Blood Flow and Metabolism*, 21(10), 1133–45. 5

Averbeck, B. B. & Lee, D. (2004). Coding and transmission of information by neural ensembles. *Trends in neurosciences*, 27(4), 225–30. 5, 26

Bäck, T., Fogel, D. B., & Michalewicz, Z., Eds. (2000a). *Evolutionary Computation 1: Basic Algorithms and Operators*. Bristol, UK: Institute of Physics Publishing. 48, 49

Bäck, T., Fogel, D. B., & Michalewicz, Z., Eds. (2000b). *Evolutionary Computation 2: Advanced Algorithms and Operators*. Bristol, UK: Institute of Physics Publishing. 48, 49

Bak, P., Tang, C., & Wiesenfeld, K. (1987). Self-organized criticality. *Phys. Rev. A*, 38(1), 364–374. 24

Bansal, A. K., Vargas-Irwin, C. E., Truccolo, W., & Donoghue, J. P. (2011). Relationships among low-frequency local field potentials, spiking activity, and three-dimensional reach and grasp kinematics in primary motor and ventral premotor cortices. *Journal of neurophysiology*, 105(4), 1603–19. 148

Barlow, H. (2001). Redundancy reduction revisited. *Network: Comput. Neural Syst.*, 12(3), 241–53. 119

Barlow, H. B. (1961). Possible principles underlying the transformation of sensory messages. In W. A. Rosenblith (Ed.), *Sensory communications*: MIT Press, Cambridge, MA. 40

Barnett, L., Barrett, A. B., & Seth, A. K. (2009). Granger causality and transfer entropy are equivalent for gaussian variables. *Phys. Rev. Lett.*, 103(23). 42

Barrett, A. B., Murphy, M., Bruno, M., Noirhomme, Q., Boly, M., Laureys, S., & Seth, A. K. (2012). Granger causality analysis of steady-state electroencephalographic signals during propofol-induced anaesthesia. *PLoS ONE*, 7(1):e29072. 43, 154

Beer, R. (2003). The dynamics of active categorical perception in an evolved model agent. *Adaptive Behavior*, 11(4), 209–243. 8, 10, 51, 52, 62, 64

Beggs, J. (2008). The criticality hypothesis: how local cortical networks might optimize information processing. *Phil. Trans. of the Royal Society, Series A*, 366(1864), 329-43. 55, 85

Belitski, A., Gretton, A., Magri, C., Murayama, Y., Montemurro, M., Logothetis, N. K., & Panzeri, S. (2008). Low-frequency local field potentials and spikes in primary visual cortex convey independent visual information. *The Journal of neuroscience*, 28(22), 5696–709. 148

Berger, H. (1929). Uber das elektrenkephalogramm des menschen. *Arch. Psychiat. Nervenkr.*, 87, 527–570. 3, 4

Bhowmik, D. & Shanahan, M. (2012). How well do oscillator models capture the behaviour of biological neurons? *IJCNN'12, Proc. of the IEEE 2012 Int. Joint Conf. on Neural Networks*, (pp. 1–8). 56, 91

Bigge, B. & Harvey, I. (2010). Evolvable mechanics: Hardware tools for evolutionary robotics. In *2010 IEEE Congress on Evolutionary Computation (CEC)* (pp. 1–7). 33

Boden, M. A. (2006). *Mind as machine: a history of Cognitive Science*. Vol. I and II, Oxford Univ. Press., UK. 8, 120

Bongard, J. C. (2011). Innocent until proven guilty: Reducing robot shaping from polynomial to linear time. *IEEE Trans. Evolutionary Computation*, 15(4), 571–585. 110, 153

Boonstra, T., Daffertshofer, A., Breakspear, M., & Beek, P. (2007). Multivariate time-frequency analysis of electromagnetic brain activity during bimanual motor learning. *Neuroimage*, 36, 370–377. 142

Borst, A. & Theunissen, F. E. (1999). Information theory and neural coding. *Nature Neurosci.*, 2(11), 947–57. 40, 42, 59, 117

Branco, T., Clark, B., & Hausser, M. (2010). Dendritic discrimination of temporal input sequences in cortical neurons. *Science*, 329, 1671–1675. 146

Breakspear, M., Heitmann, S., & Daffertshofer, A. (2010). Generative models of cortical oscillations: neurobiological implications of the Kuramoto model. *Front. Hum. Neurosci.*, 4. 11, 56, 91, 125, 127, 152

Brooks, R. A. (1991a). Intelligence without reason. *Proceedings of the 12th International Joint Conference on Artificial Intelligence (IJCAI-91)*, (pp. 569–595). 8, 32

Brooks, R. A. (1991b). Intelligence without representation. *Artificial Intelligence*, 47(1-3), 139–160. 8

Brown, P. (2003). Oscillatory nature of human basal ganglia activity: relationship to the pathophysiology of Parkinson's disease. *Mov. Disord.*, 18, 357–63. 6

Brunel, N. & van Rossum, M. C. W. (2007). Lapicque's 1907 paper: from frogs to integrate-and-fire. *Biological Cybernetics*, 97(5-6), 337–9. 4, 19

Buehlmann, A. & Deco, G. (2010). Optimal information transfer in the cortex through synchronization. *PLoS Comput. Biol.*, 6(9). 43, 59

Bullmore, E. & Sporns, O. (2009). Complex brain networks: graph theoretical analysis of structural and functional systems. *Nature Reviews Neurosci.*, 10(3), 186–98. 28

Burwick, T. (2006). Oscillatory networks: pattern recognition without a superposition catastrophe. *Neural computation*, 18(2). 29, 30

Burwick, T. (2008). Temporal coding: Assembly formation through constructive interference. *Neural Computation*, 20(7), 1796–1820. 26, 29, 117

Burwick, T. (2009). On the relevance of local synchronization for establishing a winner-take-all functionality of the gamma cycle. *Neurocomputing*, 72(7-9), 1525–1533. 30

Buzsáki, G. (2006). *Rhythms of the Brain*. Oxford University Press. 4, 5, 14, 16, 26, 27, 31, 56

Buzsáki, G. (2010). Neural syntax: Cell assemblies, synapsembles, and readers. *Neuron*, 68. 16, 27, 38, 96, 118

Buzsáki, G. & Draguhn, A. (2004). Neuronal oscillations in cortical networks. *Science*, 304, 1926–1929. 14, 24

Buzsáki, G., Geisler, C., Henze, D. A., & Wang, X. J. (2004). Interneuron diversity series: Circuit complexity and axon wiring economy of cortical interneurons. *Trends Neurosci.*, 27(4), 186–93. 5

Cabral, J., Hugues, E., Sporns, O., & Deco, G. (2011). Role of local network oscillations in resting-state functional connectivity. *NeuroImage*, 57(1), 130–9. 125, 153

Canolty, R. T., Cadieu, C. F., Koepsell, K., Ganguly, K., Knight, R. T., & Carmena, J. M. (2012). Detecting event-related changes of multivariate phase coupling in dynamic brain networks. *Journal of Neurophysiology*, 107(7), 2020–31. 16, 27

Cantero, J. L. & Atienza, M. (2005). Role of neural synchronization in the emergence of cognition across the wake-sleep cycle. *Reviews in the Neurosciences*, 16, 69–83. 31

Carmena, J. M., Lebedev, M., Crist, R. E., ODoherty, J. E., Santucci, D. M., Dimitrov, D. F., Patil, P. G., Henriquez, C. S., & Nicolelis, M. A. L. (2003). Learning to control a brain-machine interface for reaching and grasping by primates. *PLoS Biology*, 1(2), 193–208. 39, 58, 117, 118, 119, 148

Chialvo, D. R. (2010). Emergent complex neural dynamics. *Nature Physics*, 6(10), 744–750. 7, 152

Churchland, M., Yu, B., Cunningham, J., Sugrue, L., Cohen, M., Corrado, G., Newsome, W., Clark, A., Hosseini, P., Scott, B., Bradley, D., Smith, M., Kohn, A., Movshon, J., Armstrong, K., Moore, T., Chang, S., Snyder, L., Lisberger, S., Priebe, N., Finn, I., Ferster, D.and Ryu, S., Santhanam, G., Sahani, M., & Shenoy, K. (2010). Stimulus onset quenches neural variability: a widespread cortical phenomenon. *Nature Neurosci.*, 13(3), 369–78. 25, 34, 147

Clark, A. (1997). *Being There: Putting brain, body, and world together again*. Cambridge, MA: The MIT Press. 8, 32

Cohen, A. H., Holmes, P. J., & Rand, R. H. (1982). The nature of the coupling between segmental oscillators of the lamprey spinal generator for locomotion: a mathematical model. *J. Math. Biology*, 13, 345–369. 22

Cohen, I. & Miles, R. (2000). Contributions of intrinsic and synaptic activities to the generation of neuronal discharges in in vitro hippocampus. *J. Physiol.*, 524(2), 485–502. 16

Cohen, M. R. & Maunsell, J. H. R. (2009). Attention improves performance primarily by reducing interneuronal correlations. *Nat. Neurosci.*, 12, 1594–1600. 25

Colombetti, G. (2010). Enaction, sense-making, and emotion. *in Stewart, Gapenne and Di Paolo (Eds.). Enaction: Toward a New Paradigm for Cognitive Science*. 7

Cover, T. & Thomas, J. (1991). *Elements of Information Theory.* John Wiley (New York). 41

Csicsvari, J., Jamieson, B., Wise, K. D., & Buzsáki, G. (2003). Mechanisms of gamma oscillations in the hippocampus of the behaving rat. *Neuron*, 37(2), 311–22. 24

Cumin, D. & Unsworth, C. (2007). Generalising the Kuramoto model for the study of neuronal synchronisation in the brain. *Physica D*, 226(2), 181–196. 58, 125, 152

da Rocha, A., Rocha, F., & Massad, E. (2011). The brain as a distributed intelligent processing system: An EEG study. *PLoS ONE*, 6(3), e17355. 5

Dale, K. & Husbands, P. (2010). The evolution of reaction-diffusion controllers for minimally cognitive agents. *Artificial Life*, 16(1), 1–19. 10, 33, 62

Darwin, C. (1859). *On the Origin of Species by Means of Natural Selection, or the Preservation of Favoured Races in the Struggle for Life*. London, UK: John Murray. 46

Dayan, P. (1999). Unsupervised learning. *in Wilson, R. A. and Keil, F., editors. The MIT Encyclopedia of the Cognitive Sciences.* 91

Dayan, P. & Abbot, L. F. (2001). *Theoretical Neuroscience: Computational and Mathematical Modelling of Neural Systems*. MIT Press. 91

De Oliveira, S. C., Thiele, A., & Hoffmann, K. P. (1997). Synchronization of neuronal activity during stimulus expectation in a direction discrimination task. *J. Neurosci.*, 17, 9248–9260. 34

Deco, G., Buehlmann, A., Masquelier, T., & Hugues, E. (2011). The role of rhythmic neural synchronization in rest and task conditions. *Front. Hum. Neurosci.*, 5:4. 84

Deco, G. & Hugues, E. (2012). Neural network mechanisms underlying stimulus driven variability reduction. *PLoS computational biology*, 8(3), e1002395. 34, 147

Dennett, D. & Kinsbourne, M. (1991). Time and the observer: the where and when of time in the brain. *Behav. Brain Sci.*, 15, 183–247. 26

Destexhe, A. & Sejnowski, T. J. (2009). The Wilson-Cowan model, 36 years later. *Biol. Cybern.*, 101(1), 1–2. 21

Di Paolo, E. (2003). Evolving spike-timing-dependent plasticity for single-trial learning in robots. *Phil. Trans. of the Royal Society A*, 361(1811), 2299–319. 52, 105

Di Paolo, E. A. (2000). Homeostatic adaptation to inversion of the visual field and other sensorimotor disruptions. *From Animals to Animals, Proc. Sixth Int. Conf. Sim. of Adaptive Behavior, Paris, J-A. Meyer, A. Berthoz, D. Floreano, H. Roitblat and S W. Wilson (eds)*, (pp. 440–449). 65

Díaz, J., Razeto-Barry, P., Letelier, J., Caprio, J., & Bacigalupo, J. (2007). Amplitude modulation patterns of local field potentials reveal asynchronous neuronal populations. *The Journal of neuroscience*, 27(34), 9238–45. 16, 154

Dimitrov, A., Lazar, A., & Victor, J. D. (2011). Information theory in neuroscience. *J. Comput. Neurosci.*, 30, 1–5. 40, 42

Doesburg, S. M., Green, J. J., McDonald, J. J., & Ward, L. M. (2009). Rhythms of consciousness: binocular rivalry reveals large-scale oscillatory network dynamics mediating visual perception. *PLoS ONE*, 4:e0006142. 6

Donoghue, J. P., Nurmikko, A., Black, M., & Hochberg, L. R. (2007). Assistive technology and robotic control using motor cortex ensemble-based neural interface systems in humans with tetraplegia. *J. Physiol.*, 579(3), 603–611. 39

Dorfler, F., Chertkov, M., & Bullo, F. (2013). Synchronization in complex oscillator networks and smart grids. *Proc. Natl. Acad. Sci. USA*, 110 (6), 2005–2010. 152

Dorigo, M. & Colombetti, M. (1998). *Robot Shaping: An Experiment in Behavior Engineering*. Cambridge, MA: MIT Press. 110

Dreyfus, H. L. (1991). Being-in-the-world: A commentary on Heideggers being and time, division 1. 8

Eagleman, S. L. & Dragoi, V. (2012). Image sequence reactivation in awake V4 networks. *Proc. Natl. Acad. Sci. USA*. 33

Eckhorn, R. (1992). Information processing in the cortex. *(ed. Aertsen, A.), Springer, Berlin*, (pp. 385–420). 24

Eckhorn, R., Bauer, R., Jordan, W., Brosch, M., Kruse, W., Munk, M., & Reitboeck, H. J. (1988). Coherent oscillations: a mechanism of feature linking in the visual cortex? multiple electrode and correlation analyses in the cat. *Biol. Cybern.*, 60(2), 121–30. 5, 24

Edelman, G. M. (2007). Learning in and from brain-based devices. *Science*, 318(5853), 1103–5. 105

Egbert, M. D., Barandiaran, X. E., & Di Paolo, E. A. (2010). A minimal model of metabolism based chemotaxis. *PLoS Comput. Biol.*, 6(12), e1001004. 52

Eliades, S. J. & Wang, X. (2008). Neural substrates of vocalization feedback monitoring in primate auditory cortex. *Nature*, 453(7198), 1102–6. 120

Engel, A. (2010). Directive minds: How dynamics shapes cognition. *in Stewart, Gapenne and Di Paolo (Eds.). Enaction: Toward a New Paradigm for Cognitive Science*. 8, 29, 33, 51, 120

Engel, A., Fries, P., & Singer, W. (2001). Dynamic predictions: oscillations and synchrony in top-down processing. *Nat. Rev. Neurosci.*, 2(10), 704–716. 5, 6, 8, 25, 33, 34, 84, 92

Engel, A. K. & Fries, P. (2010). Beta-band oscillations - signalling the status quo? *Current Opinion in Neurobiology*, 20, 156–165. 31

Engel, A. K., Konig, P., Kreiter, A. K., & Singer, W. (1991). Stimulus-dependent neuronal oscillations in cat visual cortex: inter-columnar interactions as determined by cross-correlation analysis. *Eur. J. Neurosci.*, 2, 588–606. 24

Ermentrout, B. (1998). Neural networks as spatio-temporal pattern-forming systems. *Rep. Prog. Phys.*, 61, 353–430. 127

Ermentrout, B. (2005). Waves and oscillations in networks of coupled neurons. *Dynamics of Coupled Map Lattices and of Related Spatially Extended Systems, Lecture Notes in Physics, Springer-Verlag Berlin/Heidelberg*. 125

Ermentrout, B., Wang, J. W., Flores, J., & Gelperin, A. (1998). Monotonicity of phaselocked solutions in chains and arrays of nearest-neighbor coupled oscillators. *SIAM J. MATH. ANAL.*, 29 (1), 208–234. 146

Ermentrout, B., Wang, J. W., Flores, J., & Gelperin, A. (2001). Model for olfactory discrimination and learning in limax procerebrum incorporating oscillatory dynamics and wave propagation. *Journal of Neurophysiology*, 85 (4), 1444–52. 146

Ermentrout, G. B. (1985). Losing amplitude and saving phase. *In Othmer H. G. (ed) Nonlinear Oscillations in Biology and Chemistry. Springer-Verlag.* 22

Ermentrout, G. B. (1991). An adaptive model for synchrony in the firefly pteroptyx malaccae. *J. Math. Biol.*, 29, 571–585. 2

Ermentrout, G. B. & Carson, C. C. (2002). Modeling neural oscillations. *Physiology and Behavior*, 77, 629–633. 15, 16, 23

Ermentrout, G. B. & Kleinfeld, D. (2001). Traveling electrical waves in cortex: Insights from phase dynamics and speculation on a computational role. *Neuron*, 29, 33–44. 11, 125, 127, 147

Ermentrout, G. B. & Kopell, N. (1984). Frequency plateaus in a chain of weakly coupled oscillators. *SIAM Journal on Applied Mathematics*, 15, 215–237. 22

Ermentrout, G. B. & Kopell, N. (1994). Inhibition-produced patterning in chains of coupled nonlinear oscillators. *SIAM Journal on Applied Mathematics*, 54, 478–507. 23

Ernst, U. A. & Eurich, C. W. (2002). Cortical population dynamics and psychophysics. *The Handbook of Brain Theory and Neural Networks, 2nd edition, MIT Press, Cambridge MA*, (pp. 294–300). 21

Ferezou, I., Haiss, F., Gentet, L. J., Aronoff, R., Weber, B., & Petersen, C. (2007). Spatiotemporal dynamics of cortical sensorimotor integration in behaving mice. *Neuron*, 56, 907–923. 125

FitzHugh, R. (1961). Impulses and physiological states in theoretical models of nerve membrane. *Biophysical J.*, 1, 445–466. 5, 20

FitzHugh, R. & Izhikevich, E. M. (2006). Fitzhugh-Nagumo model. *Scholarpedia*, 1(9), 1349. 20

Flanders, M. (2011). What is the biological basis of sensorimotor integration? *Biol. Cybern.*, 104, 1–8. 84

Fleischer, J. G., Gally, J., Edelman, G. M., & Krichmar, J. L. (2007). Retrospective and prospective responses arising in a modeled hippocampus during maze navigation by a brain-based device. *Proc. Natl. Acad. Sci. USA*, 104(9), 3556–61. 33

Floreano, D., Husbands, P., & Nolfi, S. (2008). Evolutionary robotics. *In Siciliano and Khatib (Eds.) Springer Handbook of Robotics*, (pp. 1423–1451). 8, 33, 51, 120

Floreano, D. & Keller, L. (2010). Evolution of adaptive behaviour in robots by means of Darwinian selection. *PLoS Biology*, 8(1). 8, 51, 120

Floreano, D. & Mattiussi, C. (2008). *Bio-Inspired Artificial Intelligence*. MIT Press. 8, 51

Floreano, D. & Mondada, F. (1994). Automatic creation of an autonomous agent: Genetic evolution of a neural-network driven robot. *In D. Cliff, P. Husbands, J. Meyer, and S. W. Wilson, editors, From Animals to Animats III: Proc. of the Third Int. Conf. on Simulation of Adaptive Behavior*, (pp. 402–410). 110

Fodor, J. A. (1975). *The Language of Thought*. Cambridge, MA: Harvard University Press. 8

Fogel, D. B. (1994). An introduction to simulated evolutionary computation. *IEEE Transactions on Neural Networks*, 5(1), 3–14. 48

Fogel, L. J. (1962). Autonomous automata. *Industrial Research, vol. 4*, (pp. 14–19). 47

Fries, P. (2005). A mechanism for cognitive dynamics: neuronal communication through neuronal coherence. *Trends in Cognitive Sciences*, 9(10), 47480. 5, 6, 25, 26

Fries, P. (2009). Neuronal gamma-band synchronization as a fundamental process in cortical computation. *Annu. Rev. Neurosci.*, 32, 209–224. 6

Fries, P., Reynolds, J. H., Rorie, A. E., & Desimone, R. (1996). Modulation of oscillatory neuronal synchronization by selective visual attention. *Science*, 291(5508), 1560. 34

Gallagher, S. (2005). *How the Body Shapes the Mind.* New York, NY: Oxford University Press. 8

Gawne, T., Kjaer, T. W., & Richmond, B. J. (1996). Latency: another potential code for feature binding in striate cortex. *J. Neurophysiol.*, 76, 1356–1360. 37

Gerstein, G., Bedenbaugh, P., & Aertsen, M. (1989). Neuronal assemblies. *IEEE Trans. Biomedical Engineering*, 36(1), 4–14. 25

Gerstner, W. & Kistler, W. M. (2002). *Spiking Neuron Models - Single Neurons, Populations, Plasticity*. Cambridge University Press. 36, 37

Gerstner, W., Kreiter, K., Markram, H., & Herz, V. (1997). Neural codes: firing rates and beyond. *Proc. Natl. Acad. Sci. USA*, 94(24), 12740–1. 6

Gigliotta, O. & Nolfi, S. (2008). On the coupling between agent internal and agent/environmental dynamics: development of spatial representations in evolving autonomous robots. *Adaptive Behavior*, 16, 148–165. 52

Girard, P., Hupé, J.-M., & Bullier, J. (2001). Feedforward and feedback connections between areas V1 and V2 of the monkey have similar rapid conduction velocities. *J. Neurophysiol.*, 85, 1328–1331. 27

Glass, L. (2001). Rhythmic processes in physiology. *Nature 410 277-284*. 3, 6, 18

Glass, L. & Mackey, M. C. (1988). *From Clocks to Chaos: The Rhythms of Life.* Princeton University Press. 3

Goldberg, D. E. (1989). *Genetic Algorithms in Search, Optimization, and Machine Learning*. New York: Addison-Wesley. 46

Gong, P. & van Leeuwen, C. (2009). Distributed dynamical computation in neural circuits with propagating coherent activity patterns. *PLoS Comput. Biol.*, 5:e1000611. 125

Gourévitch, B. & Eggermont, J. (2007). Evaluating information transfer between auditory cortical neurons. *J. Neurophysiol.*, 97, 2533–2543. 43, 59, 154

Granger, C. (1969). Investigating causal relations by econometric models and cross-spectral methods. *Econometrica*, 37(3), 424–438. 42

Gray, C. M., Koenig, P., Engel, A. K., & Singer, W. (1989). Oscillatory responses in cat visual cortex exhibit inter-columnar synchronization which reflects global stimulus properties. *Nature*, 23, 334–337. 24

Gross, T. & Blasius, B. (2008). Adaptive coevolutionary networks: a review. *J. R. Soc. Interface*, 5, 259–271. 28

Hagmann, P., Cammoun, L., Gigandet, X., Meuli, R., Honey, C. J., Wedeen, V., & Sporns, O. (2008). Mapping the structural core of human cerebral cortex. *PLoS Biol.*, 6, e159. 28

Hagmann, P., Kurant, M., Gigandet, X., Thiran, P., Wedeen, V. J., Meuli, R., & Thiran, J.-P. (2007). Mapping human whole-brain structural networks with diffusion MRI. *PLoS One*, 2, e597. 28

Halliday, D., Resnick, R., & Walker, J. (2004). *Fundamentals of Physics*. John Wiley & Sons, 7th edition. 3

Hansel, D., Mato, G., & Meunier, C. (1995). Synchrony in excitatory neural networks. *Neural Computation*. 22, 56

Harnad, S. (1990). The symbol grounding problem. *Physica D*, 42, 335–346. 8

Harnad, S. e. (1987). *Categorical Perception: The Groundwork of Cognition.* Cambridge University Press. 10, 63

Harris, K. D., Barthó, P., Zugaro, M. B., Moncoduit, L., Marguet, S., & Buzsáki, G. (2003). Neocortical population patterns during EEG activation: Waking, REM, and anesthetised states. *Society for Neuroscience Meeting, Washington DC*. 16

Harvey, I. (2001). Artificial evolution: A continuing SAGA. *In Evolutionary Robotics: From Intelligent Robots to Artificial Life, Takashi Gomi (ed.), Proc. of 8th Intl. Symposium on Evolutionary Robotics (ER2001) Springer-Verlag Lecture Notes in Computer Science LNCS 2217*. 49

Harvey, I., Di Paolo, E., Wood, R., Quinn, M., & Tuci, E. (2005). Evolutionary robotics: A new scientific tool for studying cognition. *Artificial Life*, 11(1-2), 79–98. 8, 51

Hatsopoulos, N., Ojakangas, C., Paninski, L., & Donoghue, J. (1998). Information about movement direction obtained from synchronous activity of motor cortical neurons. *Proc. Natl. Acad. Sci. USA*, 95, 15706–15711. 5, 41

Hatsopoulos, N. G. & Donoghue, J. P. (2009). The science of neural interface systems. *Annual Review of Neurosci.*, 32, 249–66. 39, 118

Hebb, D. (1949). *The Organization of Behavior*. Wiley, New York. 5, 25, 90

Heitmann, S., Gong, P., & Breakspear, M. (2012). A computational role for bistability and traveling waves in motor cortex. *Front. in Comput. Neurosci.*, 6, 1–15. 11, 125, 126, 127, 128, 142, 145, 146, 148

Héliot, R., Orsborn, A. L., Ganguly, K., & Carmena, J. M. (2010). System architecture for stiffness control in brainmachine interfaces. *IEEE Transactions on Systems, Man, and Cybernetics A*, 40(4), 732–742. 39

Hill, A. V. (1936). Excitation and accommodation in nerve. *Proc. Roy. Soc. B*, 119, 305–355. 5

Hipp, J. F., Engel, A. K., & Siegel, M. (2011). Oscillatory synchronization in large-scale cortical networks predicts perception. *Neuron*, 69(2), 387–96. 30

Hlaváčková-Schindler, K., Paluš, M., Vejmelka, M., & Bhattacharya, J. (2007). Causality detection based on information-theoretic approaches in time series analysis. *Physics Reports*, 441(1), 1–46. 154

Hodgkin, A. L. (1948). The local changes associated with repetitive action in a non-medulated axon. *J. Physiol.*, 107, 165–81. 18

Hodgkin, A. L. & Huxley, A. F. (1952). A quantitative description of membrane current and its application to conduction and excitation in nerve. *J. Physiol.*, 117, 500–544. 5, 20

Hoffmann, M. & Pfeifer, R. (2011). *The implications of embodiment for behavior and cognition: animal and robotic case studies.*, (pp. 31–58). Exeter: Imprint Academic. 33

Holland, J. H. (1975). *Adaptation in Natural and Artificial Systems*. Ann Arbor: University of Michigan Press. 46, 47, 48, 49

Honey, C., Kotter, R., Breakspear, M., & Sporns, O. (2007). Network structure of cerebral cortex shapes functional connectivity on multiple time scales. *Proc. Natl. Acad. Sci. USA*, 104, 10240–10245. 43

Honey, C. & Sporns, O. (2008). Dynamical consequences of lesions in cortical networks. *Human brain mapping*, 29(7), 8029. 43

Hoppensteadt, F. & Izhikevich, E. (1997). *Weakly Connected Neural Networks*. Springer. 22

Hoppensteadt, F. & Izhikevich, E. (2000). Pattern recognition via synchronization in phase-locked loop neural networks. *IEEE Trans. Neural Networks*, 11(3), 734–738. 2

Hoppensteadt, F. C. & Izhikevich, E. M. (1998). Thalamo-cortical interactions modeled by weakly connected oscillators: could the brain use FM radio principles? *Biosystems*, 48, 85–94. 22, 24

Husbands, P. (2009). Never mind the iguana, what about the tortoise? Models in adaptive behaviour. *Adaptive Behavior*, 17(4), 320–324. 52

Husbands, P., Smith, T., Jakobi, N., & O Shea, M. (1998). Better living through chemistry: Evolving GasNets for robot control. *Connection Science*, 10, 185–210. 33, 50, 152

Huygens, C. (1673). *Horologium Oscillatorium.* Apud F. Muguet, Parisiis, France English translation: The Pendulum Clock, Iowa State University Press, Ames, 1986. 1

Ijspeert, A., Crespi, A., Ryczko, D., & Cabelguen, J. (2005). From swimming to walking with a salamander robot driven by a spinal cord model. *Science*, 315(5817), 1416–1420. 9, 33

Ito, S., Hansen, M. E., Heiland, R., Lumsdaine, A., Litke, A. M., & Beggs, J. M. (2011). Extending transfer entropy improves identification of effective connectivity in a spiking cortical network model. *PLoS ONE*, 6(11):e27431. 43

Izhikevich, E. (1999). Weakly pulse-coupled oscillators, FM interactions, synchronization, and oscillatory associative memory. *IEEE Trans. Neural Networks*, 10(3), 508–526. 6

Izhikevich, E. (2006). Polychronization: Computation with spikes. *Neural Computation*, 282, 245–282. 117, 153

Izhikevich, E. M. (2004). Which model to use for cortical spiking neurons? *IEEE Trans. Neural Networks*, 15(5), 1063–1070. 17, 19, 21

Izhikevich, E. M. (2007). *Dynamical Systems in Neuroscience: The Geometry of Excitability and Bursting.* The MIT Press. 16, 18, 22

Izquierdo, E. (2008). *The dynamics of learning behaviour: a situated, embodied, and dynamical systems approach*. PhD thesis, CCNR, University of Sussex. 10, 33, 52, 62, 64, 65

Jackson, A., Gee, V., Baker, S., & Lemon, R. (2003). Synchrony between neurons with similar muscle fields in monkey motor cortex. *Neuron*, 38, 115–125. 5

Jackson, A., Mavoori, J., & Fetz, E. E. (2006). Long-term motor cortex plasticity induced by an electronic neural implant. *Nature*, 444(7115), 56–60. 120

Jacobs, A. L., Fridman, G., Douglas, R. M., Alam, N. M., Latham, P. E., Prusky, G. T., & Nirenberg, S. (2009). Ruling out and ruling in neural codes. *Proc. Natl. Acad. Sci. USA*, 106(14), 5936–41. 37, 38, 39, 40, 117, 120

Jaeger, H. (2001). The echo state approach to analyzing and training recurrent neural networks. *Tech. Rep. No. 148 Bremen: German National Research Center for Information Technology.* 96

Jakobi, N. (1998). *Minimal Simulations for Evolutionary Robotics*. PhD thesis, University of Sussex. 153

Jirsa, V. K. & Haken, H. (1997). A derivation of a macroscopic field theory of the brain from the quasimicroscopic neural dynamics. *Physica D*, 99, 503–526. 21

Jolliffe, I. T. (2002). *Principal Component Analysis*. Springer-Verlag New York. 68, 113

Kahana, M. J., Seelig, D., & Madsen, J. R. (2001). Theta returns. *Current opinion in neurobiology*, 11(6), 739–744. 25, 31

Kantz, H. & Schreiber, T. (1997). *Nonlinear Time Series Analysis*. Cambridge University Press, Cambridge, MA. 154

Katz, P. E. (1999). *Beyond Neurotransmission: Neuromodulation and its Importance for Information Processing.* Oxford University Press. 7

Kayser, C., Montemurro, M. A., Logothetis, N. K., & Panzeri, S. (2009). Spike-phase coding boosts and stabilizes information carried by spatial and temporal spike patterns. *Neuron*, 61(4), 597608. 6, 37

Kazanci, F. G. & Ermentrout, B. (2007). Pattern formation in an array of oscillators with electrical and chemical coupling. *SIAM J. Appl. Math.*, 67(2), 512–529. 128, 146, 152

Kim, S.-P., Sanchez, J. C., Rao, Y. N., Erdogmus, D., Carmena, J. M., Lebedev, M., Nicolelis, M. A. L., & Principe, J. C. (2006). A comparison of optimal mimo linear and nonlinear models for brain-machine interfaces. *Journal of Neural Engineering*, 3(2), 14561. 39, 58

Kitzbichler, M., Smith, M., Christensen, S., & Bullmore, E. (2009). Broadband criticality of human brain network synchronization. *PLoS Comput. Biol.*, 5(3). 55, 56, 85

Klimesch, W. (1999). EEG alpha and theta oscillations reflect cognitive and memory performance: a review and analysis. *Brain Research Reviews*, 29, 169–195. 31

Knight, B. (1972). Dynamics of encoding in a population of neurons. *J. Gen. Physiol.*, 59, 734–766. 5, 19

Knudsen, E. I. (1994). Supervised learning in the brain. *The Journal of Neuroscience*, 14(7), 3985–3997. 91

Konig, P., Engel, A., & Singer, W. (1996). Integrator or coincidence detector? The role of the cortical neuron revisited. *Trends in Neurosciences*, 19, 130–137. 6

Kopell, N. (1995). Chains of coupled oscillators. *In Arbib M.A. (Ed) Brain Theory and Neural Networks, The MIT press, Cambridge, MA*. 22

Kopell, N., Kramer, M., Malerba, P., & Whittington, M. (2010). Are different rhythms good for different functions? *Front. Hum. Neurosci.*, 4 (187). 6, 16, 18, 27, 31, 118

Kopell, N., Whittington, M. A., & Kramer, M. A. (2011). Neuronal assembly dynamics in the beta1 frequency range permits short-term memory. *Proc. Natl. Acad. Sci. USA*, 108(9), 3779–3784. 6, 16, 18, 27

Koza, J. R. (1992). *Genetic Programming: On the Programming of computers by Means of Natural Selection*. MIT Press. 47

Kreiter, A. K. & Singer, W. (1996). Stimulus-dependent synchronization of neuronal responses in the visual cortex of the awake macaque monkey. *J. Neurosci.*, 16, 2381–2396. 25

Krofczik, S., Menzel, R., & Nawrot, M. P. (2009). Rapid odor processing in the honeybee antennal lobe network. *Front. Comput. Neurosci.*, 2:9. 146

Krupa, D. J., Wiest, M. C., Shuler, M. G., Laubach, M., & Nicolelis, M. A. (2004). Layer-specific somatosensory cortical activation during active tactile discrimination. *Science*, 304, 1989–1992. 34

KTEAM (2012). http://www.k-team.com. 106

Kullback, S. (1959). *Information Theory and Statistics*. Wiley, New York. 59

Kunyosi, M. & Monteiro, L. (2009). Recognition of noisy images by PLL networks. *Signal Processing*, 89. 6

Kuramoto, Y. (1984). *Chemical Oscillation, Waves, and Turbulence*. Springer, New York. 5, 53

Kurthen, M. (2007). *From mind to action: The return of the body in cognitive science.*, (pp. 129–143). Heidelberg: Winter Verlag. 32

Lakatos, P. (2005). An oscillatory hierarchy controlling neuronal excitability and stimulus processing in the auditory cortex. *J. Neurophysiol.*, 94, 1904–1911. 16

Lakatos, P., Karmos, G., Mehta, A. D., Ulbert, I., & Schroeder, C. E. (2008). Entrainment of neuronal oscillations as a mechanism of attentional selection. *Science*, 320(5872), 110–3. 103, 118, 120

Lam, Y. W., Cohen, L. B., Wachowiak, M., & Zochowski, M. R. (2000). Odors elicit three different oscillations in the turtle olfactory bulb. *J. Neurosci.*, 20, 749–762. 125

Landau, A. N. & Fries, P. (2012). Attention samples stimuli rhythmically. *Current Biology*, 22(11), 1000–1004. 34

Lapicque, L. (1907). Recherches quantitatives sur lexcitation électrique des nerfs traitée comme une polarization. *J. Physiol. Pathol. Gen.*, 9, 620–635. 3, 4, 19

Latham, P. E. & Nirenberg, S. (2005). Synergy, redundancy, and independence in population codes, revisited. *The Journal of Neuroscience*, 25(21), 5195–5206. 121

Lebedev, M., Carmena, J. M., ODoherty, J. E., Zacksenhouse, M., Henriquez, C. S., Principe, J. C., & Nicolelis, M. A. L. (2005). Cortical ensemble adaptation to represent velocity of an artificial actuator controlled by a brain-machine interface. *The Journal of Neuroscience*, 25(19), 4681–93. 39, 58, 96, 118, 148

Lebedev, M. A., ODoherty, J. E., & Nicolelis, M. A. L. (2008). Decoding of temporal intervals from cortical ensemble activity. *Journal of Neurophysiology*, 99(1), 166–86. 119

Ledberg, A., Montagnini, A., Coppola, R., & Bressler, S. L. (2012). Reduced variability of ongoing and evoked cortical activity leads to improved behavioral performance. *PloS one*, 7(8), e43166. 25

Legenstein, R. & Maass, W. (2007). Edge of chaos and prediction of computational performance for neural circuit models. *Neural Networks*, 20(3), 323–334. 91, 98, 99, 118, 119, 122

Lent, R., Azevedo, F. A. C., Andrade-Moraes, C. H., & Pinto, A. V. O. (2011). How many neurons do you have? Some dogmas of quantitative neuroscience under revision. *European Journal of Neurosci.*, (pp. 1–9). 152

Lepage, J. & Theoret, H. (2006). EEG evidence for the presence of an action observation- execution system in children. *European Journal of Neurosci.*, 23, 2505–2510. 144

Li, Z. & Hopfield, J. (1989). Modeling the olfactory bulb and its neural oscillatory processings. *Biol. Cybern.*, 61(5). 6

Lima, B., Singer, W., & Neuenschwander, S. (2011). Gamma responses correlate with temporal expectation in monkey primary visual cortex. *The Journal of Neuroscience*, 31(44), 15919–15931. 34

Litwin-Kumar, A. & Doiron, B. (2012). Slow dynamics and high variability in balanced cortical networks with clustered connections. *Nature Neurosci.*, 15(11), 1498–1507. 147

Llinas, R. & Ribary, U. (1993). Coherent 40 Hz oscillation characterizes dream state in humans. *Proc. Natl. Acad. Sci. USA*, 90, 2078–2081. 31

Llinás, R. R. (1988). The intrinsic electrophysiological properties of mammalian neurons: insights into central nervous system function. *Science*, 242(4886), 1654–64. 15

Lopes dos Santos, V., Conde-Ocazionez, S., Nicolelis, M., Ribeiro, S. T., & Tort, A. B. L. (2011). Neuronal assembly detection and cell membership specification by principal component analysis. *PloS One*, 6(6), 20996. 16, 27

Lubenov, E. & Siapas, A. (2009). Hippocampal theta oscillations are travelling waves. *Nature*, 459, 534–539. 125

Lundstrom, B. N. & Fairhall, A. L. (2006). Decoding stimulus variance from a distributional neural code of interspike intervals. *The Journal of Neuroscience*, 26(35), 9030–9037. 37

Lungarella, M., Ishiguro, K., Kuniyoshi, Y., & Otsu, N. (2007a). Methods for quantifying the causal structure of bivariate time series. *Int. J. of Bifurcation and Chaos*, 17(3):903-921. 59, 60, 99

Lungarella, M., Pegors, T., Bulwinkle, D., & Sporns, O. (2005). Methods for quantifying the informational structure of sensory and motor data. *Neuroinformatics*, 3 (3), pp. 243-262. 61, 68

Lungarella, M., Pitti, A., & Kuniyoshi, Y. (2007b). Information transfer at multiple scales. *Phys. Rev. E*, 056117. 59

Lungarella, M. & Sporns, O. (2006). Mapping information flow in sensorimotor networks. *PLoS Comput. Biol.*, 2(10):e144. 33, 41, 43, 120, 154

Maass, W., Legenstein, R., & Bertschinger, N. (2005). Methods for estimating the computational power and generalization capability of neural microcircuits. *In L. K. Saul, Y. Weiss, and L. Bottou, editors, Advances in Neural Information Processing Systems, MIT Press*, 17, 865–872. 91, 96, 97, 99, 118, 122

Maass, W., Natschlager, T., & Markram, H. (2002). Real-time computing without stable states: A new framework for neural computation based on perturbations. *Neural Computation*, 14(11), 2531–2560. 96

MacKay, D. M. & McCulloch, W. S. (1952). The limiting information capacity of a neuronal link. *Bulletin of Mathematical Biophysics*, 14, 127–135. 40

Magee, J. C. & Johnston, D. (1997). A synaptically controlled, associative signal for hebbian plasticity in hippocampal neurons. *Science*, 5297, 209–213. 16

Maistrenko, Y. L., Popovych, O. V., & Tass, P. A. (2005). Chaotic attractor in the Kuramoto model. *Int. J. of Bifurcation and Chaos*, 15(11), 3457–3466. 58, 66, 83, 87

Majewska, A. K. & Sur, M. (2006). Plasticity and specificity of cortical processing networks. *Trends in Neurosciences*, 29, 323–329. 33

Manyakov, N. V. & Van Hulle, M. M. (2008). Synchronization in monkey visual cortex analyzed with an information-theoretic measure. *Chaos*, 18:037130. 41

Marocco, D., Cangelosi, A., & Nolfi, S. (2002). The role of social and cognitive abilities in the emergence of communication: Experiments in evolutionary robotics. *EPSRC/BBSRC International Workshop Biologically-Inspired Robotics Bristol*, (pp. 174–181). 33

Marschinski, R. & Kantz, H. (2002). Analysing the information flow between financial time series: An improved estimator for transfer entropy. *The European Physical Journal B*, 30 (2), p.275-281. 60, 61, 68, 99, 147, 154

Masquelier, T., Hugues, E., Deco, G., & Thorpe, S. (2009). Oscillations, phase-of-firing coding, and spike timing-dependent plasticity: an efficient learning scheme. *The Journal of Neuroscience*, 29(43), 13484–93. 6, 105, 118

Massey, J. (1990). Causality, feedback and directed information. In *Proc. Intl. Symp. Information Theory Applications (ISITA-90)* (pp. 303–305). 42

Mazzoni, A., Panzeri, S., Logothetis, N. K., & Brunel, N. (2008). Encoding of naturalistic stimuli by local field potential spectra in networks of excitatory and inhibitory neurons. *PLoS Comput. Biol.*, 4(12). 42, 84, 148

McCarthy, J. & Hayes, P. J. (1969). Some philosophical problems from the standpoint of artificial intelligence. *in B. Meltzer & D. Michie (eds.), Machine Intelligence 4, Edinburgh, UK: Edinburgh University Press*, (pp. 463–502). 8

McDonnell, M., Ikeda, S., & Manton, J. (2011). An introductory review of information theory in the context of computational neuroscience. *Biol. Cybern.*, 105, 55–70. 59

Melloni, L., Molina, C., Pena, M., Torres, D., Singer, W., & Rodriguez, E. (2007). Synchronization of neural activity across cortical areas correlates with conscious perception. *J. Neurosci.*, (pp. 2858–2865). 25, 31

Merleau-Ponty, M. (1945). *Phenomnologie de la perception.* Paris: Gallimard. 7

Michalewicz, Z. (1996). Genetic algorithms + data structures = evolution programs. *Springer*. 46, 48

Michalewicz, Z. & Fogel, D. B. (2000). *How to solve It: Modern Heuristics*. Springer. 47

Milenkovic, O., Alterovitz, G., Battail, G., Coleman, T. P., Hagenauer, J., Meyn, S. P., Price, N., Ramoni, M. F., Shmulevich, I., & Szpankowski, W. (2010). Introduction to the special issue on information theory in molecular biology and neuroscience. *IEEE Transactions on Information Theory - Special issue on information theory in molecular biology and neuroscience*, 56(2), 649–652. 40, 42

Miller, B. L. & Goldberg, D. E. (1996). Genetic algorithms, tournament selection, and the effect of noise. *Complex Systems, vol. 9, pp. 193–212*. 48

Mirollo, R. E. & Strogatz, S. H. (2004). Synchronization of pulse-coupled biological oscillators. *SIAM Journal on Applied Mathematics*, 50(6), 1645–1662. 5

Mitri, S., Wischmann, S., Floreano, D., & Keller, L. (2012). Using robots to understand social behaviour. *Biological Reviews*, (pp. 1–9). 33

Moioli, R., Vargas, P. A., & Husbands, P. (2009). A multiple hormone approach to the homeostatic control of conflicting behaviours in an autonomous mobile robot. *IEEE Congress on Evolutionary Computation 2009, CEC 2009, Trondheim, Norway*. iii

Moioli, R., Vargas, P. A., & Husbands, P. (2010a). The dynamics of a neural network of coupled phase oscillators with synaptic plasticity controlling a minimally cognitive agent. *In: Diamantaras, K.;Duch, W.;Iliadis, L.. (Org.). ICANN'10 Proceedings of the 20th international*

conference on Artificial neural networks: Part II. 1ed.: Springer Berlin Heidelberg, 6353, 245–255. iii, 58

Moioli, R., Vargas, P. A., & Husbands, P. (2010b). Exploring the Kuramoto model of coupled oscillators in minimally cognitive evolutionary robotics tasks. *2010 IEEE Congress on Evolutionary Computation (CEC), Barcelona, Spain*, (pp. 2483–2490). iii, 58

Moioli, R. C., Vargas, P. A., & Husbands, P. (2012). Synchronisation effects on the behavioural performance and information dynamics of a simulated minimally cognitive robotic agent. *Biol. Cybern.*, 106, 407–427. iii, 43

Mondada, F., Bonani, M., Raemy, X., Pugh, J., Cianci, C., Klaptocz, A., Magnenat, S., Zufferey, J.-C., Floreano, D., & Martinoli, A. (2009). The e-puck, a robot designed for education in engineering. *Proc. of the 9th Conf. on Autonomous Robot Systems and Competitions*, 1(1), 59–65. 188

Monteiro, L., Canto, N., & Orsatti, F.and Piqueira, J. (2003). Global and partial synchronism in phase-locked loop networks. *IEEE Transactions on Neural Networks*, 14(6). 55

Munte, T. F., Altenmuller, E., & Jancke, L. (2002). The musicians brain as a model of neuroplasticity. *Nature Reviews Neurosci.*, 3, 473–478. 33

Murray, J. D. (1989). *Mathematical Biology: An Introduction*. Springer-Verlag Berlin Heidelber. 4

Muthukumaraswamy, S., Johnson, B., & McNair, N. (2004). Mu rhythm modulation during observation of an object-directed grasp. *Cognitive Brain Research*, 19, 195–201. 144

Nadasdy, Z. (2009). Information encoding and reconstruction from the phase of action potentials. *Front. Syst. Neurosci.*, 3:6. 37

Nadasdy, Z. (2010). Binding by asynchrony: the neuronal phase code. *Front. Neurosci.*, 4(51). 37

Nagumo, J., Arimoto, S., & Yoshizawa, S. (1962). An active pulse transmission line simulating nerve axon. *Proc. IRE.*, 50, 20612070. 5, 20

Narayanan, N. S., Kimchi, E. Y., & Laubach, M. (2005). Redundancy and synergy of neuronal ensembles in motor cortex. *The Journal of Neuroscience*, 25(17), 4207–16. 98, 103, 119, 121

Neuenschwander, S., Engel, A. K., Konig, P., Singer, W., & Varela, F. J. (1996). Synchronization of neuronal responses in the optic tectum of awake pigeons. *Vis. Neurosci.*, 13, 575–584. 25

Neves, F. S. & Timme, M. (2008). Controlled perturbation-induced switching in pulse-coupled oscillator networks. *J. Phys. A: Math. Theor.*, 42:345103. 153

Neves, F. S. & Timme, M. (2012). Computation by switching in complex networks of states. *Phys. Rev. Lett.*, 109:018701. 153

Neymotin, S., Jacobs, K. M., Fenton, A., & Lytton, W. W. (2010). Synaptic information transfer in computer models of neocortical columns. *Journal of computational neuroscience*, 30(1), 69–84. 43

Nicolelis, M. A. L., Fanselow, E. E., & Ghazanfar, A. A. (1997). Hebbs dream: The resurgence of cell assemblies. *Neuron*, 19, 219–22. 25

Nicolelis, M. A. L. & Lebedev, M. A. (2009). Principles of neural ensemble physiology underlying the operation of brain-machine interfaces. *Nature Reviews Neurosci.*, 10(7), 530–40. 5, 26, 119

Nikonov, A. A., Parker, J. M., & Caprio, J. (2002). Odorant-induced olfactory receptor neural oscillations and their modulation of olfactory bulbar responses in the channel catfish. *J. Neurosci.*, 22, 2352–2362. 16

Nöe, A. (2004). *Action in perception.* Cambridge, MA: MIT Press. 8, 51

Nolfi, S. & Floreano, D. (2000). *Evolutionary Robotics: The Biology, Intelligence, and Technology of Self-Organizing Machines*. MIT Press. 187

Nowotny, T., Rabinovich, M., Huerta, R., & Abarbanel, H. (2003). Decoding temporal information through slow lateral excitation in the olfactory system of insects. *Journal of Computational Neuroscience*, 15, 271–281. 146

Omel'chenko, O., Maistrenko, Y., & Tass, P. (2008). Chimera states: The natural link between coherence and incoherence. *Phys. Rev. Lett.*, 100, 044105. 152

Oram, M. W., Foldiák, P., Perrett, D. I., & Sengpiel, F. (1998). The ideal homunculus: decoding neural population signals. *Trends in neurosciences*, 21(6), 259–65. 38

O'Regan, J. K. & Nöe, A. (2001). A sensorimotor account of vision and visual consciousness. *Behavioral and Brain Sciences*, 24(5), 939–1031. 8, 32

Orosz, G., Moehlis, J., & Ashwin, P. (2009). Designing the dynamics of globally coupled oscillators. *Progress of Theoretical Physics 122, no. 3 611-630.* 91, 93

Paisley, A. C. & Summerlee, A. J. (1984). Relationship between behavioral states and activity of the cerebral cortex. *Prog. Neurobiol.*, 22, 155–184. 25

Panzeri, S., Brunel, N., Logothetis, N. K., & Kayser, C. (2010). Sensory neural codes using multiplexed temporal scales. *Trends in Neurosciences*, 33(3), 111–20. 35, 36, 37, 38, 120

Passingham, R. E., Stephan, K. E., & Kotter, R. (2002). The anatomical basis of functional localization in the cortex. *Nature Rev. Neurosci.*, 3, 606–616. 28

Penttonen, M. & Buzsáki, G. (2003). Natural logarithmic relationship between brain oscillators. *Thalamus and Related Systems*, 2(2), 145–152. 24

Pérez, T., G. G. C. E. V. M. V. R. P. G. & Mirasso, C. (2011). Effect of the topology and delayed interactions in neuronal networks synchronization. *PloS one*, 6(5):e19900. 6

Pfeifer, R. & Bongard, J. (2006). *How the body shapes the way we think: a new view of intelligence*. MIT Press. 8, 32, 154

Pfeifer, R., Lungarella, M., & Iida, F. (2007). Self-organization, embodiment, and biologically inspired robotics. *Science*, 318, 1088–1093. 51

Pfeifer, R. & Scheier, C. (1999). *Understanding Intelligence*. MIT Press. 8, 32

Pfurtscheller, G., Stancak, A., & Neuper, C. (1996). Post-movement beta synchronization. a correlate of an idling motor area? *Electroencephalogr. Clin. Neurophysiol.*, 98, 281–293. 11, 126, 147

Philippides, A., Husbands, P., Smith, T., & O'Shea, M. (2005). Flexible couplings: Diffusing neuromodulators and adaptive robotics. *Artificial Life*, 11(1-2), 139–160. 33, 152

Pikovsky, A., Rosenblum, M., & Kurths, J. (2001). *Synchronization: A Universal Concept in Nonlinear Sciences*. Cambridge University Press. 1, 3, 22, 23, 91

Pinsky, P. F. & Rinzel, J. (1994). Intrinsic and network rhythmogenesis in a reduced traub model for ca3 neurons. *J. Comput. Neurosci.*, 1, 39–60. 16

Pitti, A. (2007). *Phase Synchronization Between Internal and Body Dynamics for Exploration, Memory, and Control of Embodied Behavior*. PhD thesis, University of Tokyo. 33

Pitti, A., Lungarella, M., & Kuniyoshi, Y. (2009). Generating spatiotemporal joint torque patterns from dynamical synchronization of distributed pattern generators. *Front. NeuroRobotics*, 3:2, 1–14. 9, 33, 40

Pitti, A., Niiyama, R., & Kuniyoshi, Y. (2010). Creating and modulating rhythms by controlling the physics of the body. *Autonomous Robots*, 28:3, pp. 317-329. 33, 40

Popovych, O., Maistrenko, Y., & Tass, P. (2005). Phase chaos in coupled oscillators. *Phys. Rev. E*, 71(6), 3–6. 58, 66, 107

Pouget, A., Dayan, P., & Zemel, R. (2008). Information processing with population codes. *Nature Reviews Neurosci.*, 1(2), 125–32. 38, 107

Quinn, M., Smith, L., Mayley, G., & Husbands, P. (2003). Evolving controllers for a homogeneous system of physical robots: structured cooperation with minimal sensors. *Philos. Trans. Phys. Sci. Eng.*, 361, 2321–2344. 33, 52

Quiroga, R. Q. & Panzeri, S. (2009). Extracting information from neuronal populations: information theory and decoding approaches. *Nature Reviews Neurosci.*, 10(3), 173–85. 39, 42, 120

Rabinovich, M., Afraimovich, V., Bick, C., & Varona, P. (2012). Information flow dynamics in the brain. *Physics of life reviews 9, no. 1 51-73*. 93, 117, 146, 153

Rabinovich, M., Afraimovich, V., & Varona, P. (2010). Heteroclinic binding. *Dynamical Systems*, 25(3), 433–442. 153

Ranhel, J. (2012). Neural assembly computing. *IEEE Transactions on Neural Networks and Learning Systems*, 23(6), 916–927. 117, 118

Rapoport, A. & Horvath, W. J. (1960). The theoretical channel capacity of a single neuron as determined by various coding systems. *Information and Control*, 3(4), 335–350. 40

Rechenberg, I. (1973). *Evolutionsstrategie: Optimierung technischer Systeme nach Prinzipien der biologischen Evolution*. Frommann-Holzboog. 47

Reich, D. S., Mechler, F., Purpura, K. P., & Victor, J. D. (2000). Interspike intervals, receptive fields, and information encoding in primary visual cortex. *J. Neurosci.*, 20, 1964–1974. 37

Reich, D. S., Mechler, F., & Victor, J. D. (2001). Independent and redundant information in nearby cortical neurons. *Science*, 294(5551), 2566–8. 98, 102, 119, 121

Reil, T. & Husbands, P. (2002). Evolution of central pattern generators for bipedal walking in real-time physics environments. *IEEE Trans. Evolutionary Computation*, 6(2), 159–168. 33

Riehle, A., Gruen, S., Diesmann, M., & Aertsen, A. (1997). Spike synchronization and rate modulation differentially involved in motor cortical function. *Science*, 278, 1950–1953. 34

Rieke, F., Warland, D., van Steveninck, R. R., & Bialek, W. (1997). *Spikes: Exploring the Neural Code*. Bradford Book - MIT Press, Cambridge MA. 36, 84

Rohde, M. (2008). *Evolutionary Robotics Simulation Models in the Study of Human Behaviour and Cognition.* PhD thesis, CCNR, University of Sussex. xi, 52

Rolls, E. T. & Deco, G. (2010). *The Noisy Brain - Stochastic Dynamics as a Principle of Brain Function.* Oxford University Press. 120, 153

Rolls, E. T., Franco, L., Aggelopoulos, N. C., & Reece, S. (2003). An information theoretic approach to the contributions of the firing rates and the correlations between the firing of neurons. *J. Neurophysiol.*, 89, 2810–2822. 41

Rolls, E. T., Webb, T. J., & Deco, G. (2012). Communication before coherence. *European Journal of Neurosci.*, 36, 2689–2709. 154

Rosenberg-Katz, K., Jamshy, S., Singer, N., Podlipsky, I., Kipervasser, S., Andelman, F., Neufeld, M., Intrator, N., Fried, I., & Hendler, T. (2012). Enhanced functional synchronization of medial and lateral pfc underlies internally-guided action planning. *Front. Hum. Neurosci.*, 6:79. 34

Rosenstein, M., Collins, J., & Deluca, C. (1993). A practical method for calculating largest Lyapunov exponents from small data sets. *Physica D: Nonlinear Phenomena*, 65(1-2), 117–134. 87

Rubino, D., Robbins, K. A., & Hatsopoulos, N. G. (2006). Propagating waves mediate information transfer in the motor cortex. *Nature Neurosci.*, 9(12), 1549–1557. 125, 145

Runge, J., Heitzig, J., Petoukhov, V., & Kurths, J. (2012). Escaping the curse of dimensionality in estimating multivariate transfer entropy. *Phys. Rev. Lett.*, 108, 258701–5. 43

Sakurai, Y. (1999). How do cell assemblies encode information in the brain? *Neuroscience and Biobehavioral Reviews*, 23, 785–796. 26

Saleh, M., Reimer, J., Penn, R., Ojakangas, C. L., & Hatsopoulos, N. G. (2010). Fast and slow oscillations in human primary motor cortex predict oncoming behaviorally relevant cues. *Neuron*, 65(4), 461–471. 34

Santos, B., Barandiaran, X., & Husbands, P. (2011). Metastable dynamical regimes in an oscillatory network modulated by an agent's sensorimotor loop. *Proc. IEEE Symposium on Artificial Life (SSCI)*. 89

Schneidman, E., Bialek, W., & Berry II, M. J. (2003). Synergy, redundancy, and independence in population codes. *The Journal of Neuroscience*, 25(21), 5195–206. 98, 100, 119, 121, 122

Schreiber, T. (2000). Measuring information transfer. *Phys. Rev. Lett.*, 85, 461464. 42, 59, 60

Schroeder, C. E. & Lakatos, P. (2009). Low-frequency neuronal oscillations as instruments of sensory selection. *Trends in Neurosciences*, 32(1), 9–18. 120

Schwefel, H.-P. (1965). *Kybernetische Evolution als Strategie der experimentellen Forschung in der Stromungstechnik*. PhD thesis, Technische Universit at Berlin. 47

Schwefel, H.-P. (1981). *Numerical Optimization for Computer Models*. John Wiley. 46

Schyns, P. G., Thut, G., & Gross, J. (2011). Cracking the code of oscillatory activity. *PLoS Biology*, 9(5), e1001064. 40

Seth, A. (2007). Granger causality. *Scholarpedia*, 2(7):1667. 42

Seth, A., McKinstry, J., Edelman, G., & Krichmar, J. (2004). Visual binding through reentrant connectivity and dynamic synchronization in a brain-based device. *Cerebral Cortex*, 14. 8

Shanahan, M. (2010a). *Embodiment and the Inner Life: Cognition and Consciousness in the Space of Possible Minds.* Oxford University Press. 6

Shanahan, M. (2010b). Metastable chimera states in community-structured oscillator networks. *Chaos*, 20, 013108. 87, 152

Shanahan, M. (2012). The brain's connective core and its role in animal cognition. *Phil. Trans. of the Royal Society B*, 367(1603), 2704–2714. 26

Shannon, C. (1948). A mathematical theory of communication. *Bell System Technical Journal 27, pp. 379423*. 40, 41

Shim, Y. & Husbands, P. (2012). Chaotic exploration and learning of locomotion behaviours. *Neural Computation*, 24(8), 2185–2222. 105, 146

Shoham, S., O. D. H. & Segev, R. (2006). How silent is the brain: is there a "dark matter" problem in neuroscience? *J. Comp. Physiol. A*, 192, 777–784. 122

Siegel, M., Donner, T. H., & Engel, A. K. (2012). Spectral fingerprints of large-scale neuronal interactions. *Nature reviews Neurosci.*, 13(2), 121–34. 5, 32

Silverman, B. (1998). *Density Estimation for Statistics and Data Analysis*. London: Chapman and Hall. 55

Singer, W. (1993). Synchronization of cortical activity and its putative role in information processing and learning. *Annu. Rev. Physiology*, 55, 349–374. 5, 6, 30

Singer, W. (1999). Neuronal synchrony: a versatile code for the definition of relations? *Neuron*, 24(1), 49–65. 5, 6, 26, 29, 38

Singer, W. (2009). The brain, a complex self-organizing system. *European Review*, 17(02), 321–329. 5, 26

Singer, W. & Gray, C. M. (1995). Integration and the temporal correlation hypothesis. *Annu. Rev. Neurosci.*, 18, 555–586. 5

Sporns, O. (2011). *Networks of the Brain*. MIT Press. 28

Sporns, O. & Alexander, W. (2002). Neuromodulation and plasticity in an autonomous robot. *Neural Networks*, 15, 761–774. 105

Staniek, M. & Lehnertz, K. (2008). Symbolic transfer entropy. *Phys. Rev. Lett.*, 100 (15). 43, 68, 77

Stapleton, J. R., Lavine, M. L., Nicolelis, M. A., & Simon, S. A. (2007). Ensembles of gustatory cortical neurons anticipate and discriminate between tastants in a single lick. *Front. Neurosci.*, 1, 161–174. 34

Stein, R. (1965). A theoretical analysis of neuronal variability. *Biophys. J.*, 5, 173–194. 19

Steingrube, S., Timme, M., Wrgtter, F., & Manoonpong, P. (2010). Self-organized adaptation of a simple neural circuit enables complex robot behaviour. *Nature Physics 6, no. 3 224-230.* 146

Steinmetz, P. N., Roy, A., Fitzgerald, P. J., Hsiao, S. S., & Johnson, K. O. (2000). Attention modulates synchronized neuronal firing in primate somatosensory cortex. *Nature*, 436, 187–190. 34, 103, 118, 120

Steriade, H., Jones, E. G., & Llinás, R. (1990). *Thalamic Oscillations and Signalling*. John Wiley & Sons, New York. 5

Steriade, M., McCormick, D. A., & Sejnowski, T. J. (1993). Thalamocortical oscillations in the sleeping and aroused brain. *Science*, 262(5134), 679–85. 25

Stewart, J., Gapenne, O., & Di Paolo, E. E. (2010). *Enaction: Toward a New Paradigm for Cognitive Science.* MIT Press. 7, 8, 32

Storm, T. (2004). KiKS, a Khepera simulator for Matlab 5.3 and 6.0. http://theodor.zoomin.se/index/2866.html. 106, 187, 188

Strogatz, S. (2000). From Kuramoto to Crawford: exploring the onset of synchronization in populations of coupled oscillators. *Physica D*, 143. 55

Szczepanski, J., Arnold, M., Wajnryb, E., Amigo, J. M., & Sanchez-Vives, M. V. (2011). Mutual information and redundancy in spontaneous communication between cortical neurons. *Biol. Cybern.*, 104, 161–174. 41, 68, 119, 121, 122

Taga, G. (1994). Emergence of bipedal locomotion through entrainment among the neuro-musculo-skeletal system and the environment. *Physica D*, 75(1-3), 190–208. 9

Tallon-Baudry, C. (2009). The roles of gamma-band oscillatory synchrony in human visual cognition. *Front. Biosci.*, 14, 321–332. 25

Tass, P. A. (1999). *Phase resetting in medicine and biology: stochastic modelling and data analysis*. Springer 2006. 5, 25, 145, 152

Tass, P. A. (2001a). Effective desynchronization by means of double- pulse phase resetting. *Europhys. Lett.*, 53(1), 15–21. 145

Tass, P. A. (2001b). Effective desynchronization with bipolar double pulse stimulation. *Phys. Rev. E*, 66:036226. 145

Tass, P. A. (2003). A model of desynchronizing deep brain stimulation with a demand-controlled coordinated reset of neural subpopulations. *Biol. Cybern.*, 89(2), 81–8. 145

Tessone, C. J. & Zanette, D. H. (2012). Synchronised firing induced by network dynamics in excitable systems. *Europhysics Lett.*, 99, 68006. 56

Thorpe, S., Fize, D., & Marlot, C. (1996). Speed of processing in the human visual system. *Nature*, 381, 520–522. 37

Tognoli, E. & Kelso, J. A. S. (2009). Brain coordination dynamics: True and false faces of phase synchrony and metastability. *Prog. Neurobiol.*, 87(1), 31–40. 152

Tononi, G., Sporns, O., & Edelman, G. (1992). Reentry and the problem of integrating multiple cortical areas: Simulation of dynamic integration in the visual system. *Cerebral Cortex*, 2, 310–335. 24, 30

Tort, A. B. L., Kramer, M., Thorn, C., Gibson, D. J., Kubota, Y., Graybiel, A. M., & Kopell, N. J. (2008). Dynamic cross-frequency couplings of local field potential oscillations in rat striatum and hippocampus during performance of a t-maze task. *Proc. Natl. Acad. Sci. USA*, 105(51), 20517–22. 34

Tovee, M. J. & Rolls, E. T. (1995). Information encoding in short firing rate epochs by single neurons in the primate temporal visual cortex. *Vis. Cognit.*, 2(1), 35–58. 37

Toyama, K., Kimura, M., & Tanaka, K. (1981). Cross-correlational analysis of interneuronal connectivity in cat visual cortex. *J. Neurophysiol.*, 46, 191–201. 25

Traub, R. D., Wong, R. K., Miles, R., & Michelson, H. (1991). A model of a CA3 hippocampal pyramidal neuron incorporating voltage-clamp data on intrinsic conductances. *J Neurophysiol.*, 66(2), 635–50. 146

Tsodyks, M. V., Skaggs, W. E., Sejnowski, T. J., & McNaughton, B. L. (1997). Paradoxical effects of external modulation of inhibitory interneurons. *J. Neurosci.*, 17, 4382–4388. 21

Tsukada, M., Ichinose, N., Aihara, K., Ito, H., & Fujii, H. (1996). Dynamical cell assembly hypothesis - theoretical possibility of spatio-temporal coding in the cortex. *Neural networks*, 9(8), 1303–1350. 27

Turrigiano, G. & Nelson, S. (2004). Homeostatic plasticity in the developing nervous system. *Nature Reviews Neurosci.*, 5(2), 97–107. 105

Uhlhaas, P. J., Pipa, G., Lima, B., Melloni, L., Neuenschwander, S., Nikolic, D., & Singer, W. (2009). Neural synchrony in cortical networks: history, concept and current status. *Front. in Integrative Neurosci.*, 3(17), 1–19. 6, 25

Uhlhaas, P. J., Roux, F., Rodriguez, E., Rotarska-Jagiela, A., & Singer, W. (2010). Neural synchrony and the development of cortical networks. *Trends in Cognitive Sciences*, 14(2), 72–80. 5

Urzelai, J. & Floreano, D. (2001). Evolution of adaptive synapses: Robots with fast adaptive behavior in new environments. *Evol. Comput.*, 9(4), 495–524. 11, 105, 131, 154

van der Pol, B. (1926). On relaxation oscillation. *Phil. Mag.*, 2, 978992. 3

Van Der Werf, J., Jensen, O., Fries, P., & Medendorp, W. P. (2010). Neuronal synchronization in human posterior parietal cortex during reach planning. *Journal of Neuroscience*, 30(4), 1402–1412. 34

Vapnik, V. N. (1998). *Statistical Learning Theory.* John Wiley (New York). 97

Varela, F., Lachaux, J., Rodriguez, E., & Martinerie, J. (2001). The brainweb: phase synchronization and large-scale integration. *Nat. Rev. Neurosci.*, 2(4). 5, 6, 14, 25, 26, 27, 84

Varela, F. J. (1995). Resonant cell assemblies: a new approach to cognitive functions and neuronal synchrony. *Biol. Res.*, 28, 81–95. 26

Varela, F. J., Thompson, E., & Rosch, E. (1991). *The Embodied Mind: Cognitive Science and Human Experience.* Cambridge, MA: The MIT Press. 8, 32

Verdes, P. F. (2005). Assessing causality from multivariate time series. *Phys. Rev. E*, 72, 026222. 154

Viana, R. L., Batista, A. M., Batista, C. A. S., de Pontes, J. C. A., Silva, F. A. D. S., & Lopes, S. R. (2012). Bursting synchronization in networks with long-range coupling mediated by a diffusing chemical substance. *Communications in Nonlinear Science and Numerical Simulation*, 17(7), 2924–2942. 4, 25

Vicente, R., G. L. L. M. C. R. F. I. & Pipa, G. (2008). Dynamical relaying can yield zero time lag neuronal synchrony despite long conduction delays. *Proc. Nat. Acad. Sci. USA*, 105(44), 17157–62. 6

Vicente, R., Wibral, M., Lindner, M., & Pipa, G. (2011). Transfer entropy: a model-free measure of effective connectivity for the neurosciences. *J. Comput. Neurosci.*, 30, 4567. 42, 43, 59

von der Malsburg, C. (1981). The correlation theory of the brain. *Internal report. Max-Planck-Institute for Biophysical Chemistry, Gottingen, Germany*. 5, 26, 29

von der Malsburg, C. (1986). Am I thinking assemblies ? In G. Palm & A. Aertsen (Eds.), *Proceedings of the Trieste Meeting on Brain Theory,October 1984* (pp. 161–176). Berlin, Heidelberg: Springer. 29

von Ehrenfels, C. (1890). Uber gestaltqualitaten. *Vierteljahrsschrift für wissenschaftliche Philosophie*, (pp. 249–292). 7

Von Stein, A., Chiang, C., & Konig, P. (2000). Topdown processing mediated by interareal synchronization. *Proc. Natl. Acad. Sci. USA*, 97, 14748–14753. 34

von Uexkull, J. (1940). *Kompositionslehre der Natur. Biologie als undogmatische Naturwissenschaft.* Frankfurt a. M.: Ullstein. 7

Ward, L. M. (2003). Synchronous neural oscillations and cognitive processes. *Trends in Cognitive Sciences*, 7(12), 553–559. 25, 31, 34

White, B., Abbott, L. F., & Fiser, J. (2012). Suppression of cortical neural variability is stimulus- and state-dependent. *J. Neurophysiol.*, 108(9), 2383–92. 147

Whitley, D. & Kauth, J. (1988). Genitor: A different genetic algorithm. In *Proc. of the Rocky Mountain Conf. on Artificial Intelligence, Denver*. 50

Whittington, M. A. & Traub, R. (2003). Interneuron diversity series: Inhibitory interneurons and network oscillations in vitro. *Trends Neurosci.*, 26, 676–682. 5

Wickelgren, W. A. (1992). Webs, cell assemblies, and chunking in neural nets. *Concepts Neurosci.*, 1, 1–53. 26

Wiener, N. (1956). *The theory of prediction.* McGraw-Hill, New York. 42

Wildie, M. & Shanahan, M. (2012). Metastability and chimera states in modular delay and pulse-coupled oscillator networks. *Chaos*, 22:043131. 91, 152, 153

Williams, P. & Beer, R. (2010). Information dynamics of evolved agents. *From Animals to Animals, Proc. 11th Int. Conf. Sim. of Adaptive Behavior, S. Doncieux, B. Girard, A. Guillot, J. Hallam, J.-A. Meyer and J-B. Mouret (eds)*, (pp. 38–49). 41, 43

Williams, P. L. & Beer, R. D. (2011). Generalized measures of information transfer. *arXiv:1102.1507*. 43

Wilson, H. (1999). *Spikes, decisions, and actions. Dynamical foundations of neuroscience.* Oxford University Press. 22, 23

Wilson, H. & Cowan, J. (1972). Excitatory and inhibitory interactions in localized populations of model neurons. *Biophys. J.*, 12, 124. 5, 21

Wilson, H. & Cowan, J. (1973). A mathematical theory of the functional dynamics of nervous tissue. *Kybernetik*, 13, 55–80. 5, 21

Winfree, A. (1980). *The geometry of biological time*. Springer-Verlag. 3, 5, 53

Wischmann, S., Floreano, D., & Keller, L. (2012). Historical contingency affects signaling strategies and competitive abilities in evolving populations of simulated robots. *Proc. Natl. Acad. Sci. USA*, 109(3), 864–868. 33

Womelsdorf, T., Schoffelen, J., Oostenveld, R., Singer, W., Desimone, R., Engel, A., & Fries, P. (2007). Modulation of neuronal interactions through neuronal synchronization. *Science*, 316(5831), 1609–1612. 5, 6, 84

Wordsworth, J. & Ashwin, P. (2008). Spatiotemporal coding of inputs for a system of globally coupled phase oscillators. *Phys. Rev. E*, 78(6), 1–10. 93

Wu, J.-Y., Huang, X., & Zhang, C. (2008). Propagating waves of activity in the neocortex: what they are, what they do. *The Neuroscientist*, 14(5), 487–502. 125

Wyeth, G. & Milford, M. (2009). Spatial cognition for robots: Robot navigation from biological inspiration. *IEEE Robotics and Automation Magazine*, 16(3), 24–32. 105

Yeung, M. K. S. & Strogatz, S. H. (1999). Time delay in the Kuramoto model of coupled oscillators. *Phys. Rev. Lett.*, 1, 1–4. 153

Zanette, D. (2000). Propagating structures in globally coupled systems with time delays. *Phys. Rev. E*, 62(3), 3167–72. 128

Zhang, Y., Chen, Y., Bressler, S. L., & Ding, M. (2008). Response preparation and inhibition: The role of the cortical sensorimotor beta rhythm. *Neuroscience*, 156(1), 238–246. 31

Zheng, L. & Yao, H. (2012). Stimulus-entrained oscillatory activity propagates as waves from area 18 to 17 in cat visual cortex. *PLoS ONE*, 7(7), e41960. 125

Appendix A

Appendix A: Simulators

Thanks to recent developments in computing technology, mathematical modelling and computational simulation of robotic system are advancing. Simulated robots and environments contribute to flexibility and to reducing the time to perform an experiment. For example, Nolfi & Floreano (2000) conducted an experiment that required circa 66 hours in real robots whilst the same experiment required 1 hour of computer simulation.

The next sections briefly detail the two simulators used in this thesis: KIKS simulator, used in Chapter 5, and Evorobot* simulator, used in Chapter 6.

A.1 KiKS Simulator

The KiKS simulator has been developed by Storm (2004) and is illustrated in Figure A.1. The simulator runs under Matlab® using a Khepera robot toolbox, developed by K-Team, named kMatlab (the toolbox is freely available from `http://www.k-team.com/mobile-robotics-products/khepera-ii`).

The simulator's main screen contains an arena, a robot, and a control panel. One can add lamps and objects of varied shapes in the environment and change the original size of the arena. Also, predefined or user-defined environments can be saved and loaded. The simulation can be distributed or locally run, with adjustable speeds, and using one or more robots. The light, camera, and distance sensors can be monitored on the run; light sensors vary from 65 (maximum luminosity) to 450 (absence of light), distance sensors vary from 0 to 1023 (obstacle very far and very close, respectively), and camera sensors vary from 50 to 175 (black and white pixels detected, respectively). There are predefined functions to control the speed of each wheel and read sensory data. Finally, the simulation incorporates noise and uses realistic sensory and motor dynamics.

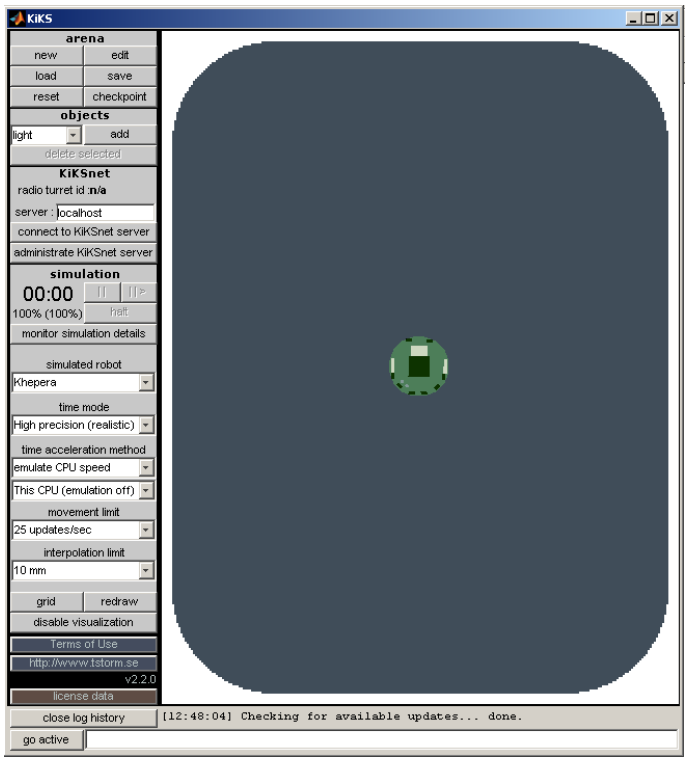

Figure A.1: KiKS simulator main screen.

For a complete description of all functionalities, the manual is available from Storm (2004).

A.2 Evorobot* Simulator

The Evorobot* simulator (freely available at `http://laral.istc.cnr.it/evorobotstar/`) has been developed by Stefano Nolfi and Onofrio Gigliotta as an extension of the Evorobot simulator and is depicted in Figure A.2. Like KiKS, Evorobot simulates a Khepera robot; Evorobot*, however, is based on the e-puck robotic platform (Mondada et al., 2009). E-puck robots share many features with the Khepera line (in fact, both have been developed by the same team), including sensory and motor configurations, but with focus on educational applications, portability, and reduced costs.

Evorobot* has been specifically developed for Evolutionary Robotics studies, providing a number of tools to facilitate the experiments: single or multiple robots compatibility; inbuilt genetic algorithm and neural network controllers; lamps, cylinders, and other objects of varied shapes and sizes; easily configurable environments; predefined functions to control the speed of each wheel and read sensory data. The graphic interface permits the user to visualise the environment and the robots' trajectories, the fitness evolution over time, and to change the simulation parameters on the run. If enhanced simulation speed is necessary, the graphic inter-

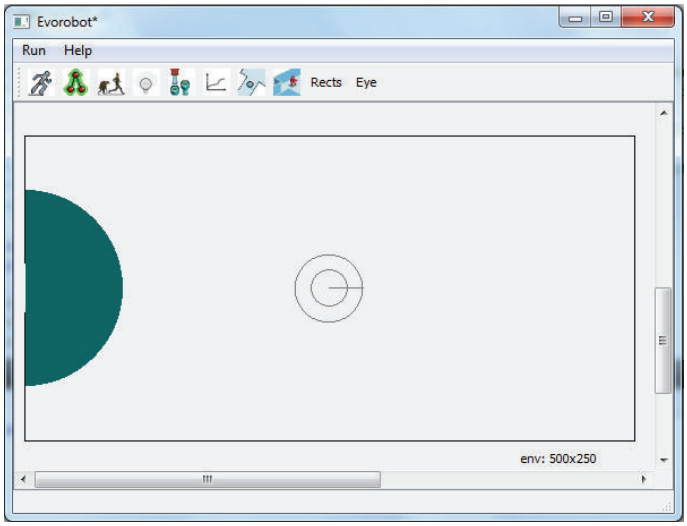

Figure A.2: Evorobot* simulator main screen.

face can be turned off. The program must be written in C or C++, and there are versions compatible with Windows or Linux platforms. Finally, the simulation incorporates noise and uses realistic sensory and motor dynamics. For further details, the manual is available from `http://laral.istc.cnr.it/evorobotstar/`.